LBL-34541
CONF-9306201
UC-411

Advanced Light Source

Soft X-Ray Interferometry

Report of the Workshop

Lawrence Berkeley Laboratory
June 25, 1993

Lawrence Berkeley Laboratory
University of California
Berkeley, California 94720

September 1993

Prepared for the U.S. Department of Energy under Contract No. DE-AC03-76SF00098

DISCLAIMER

Soft X-Ray Interferometry

Report of the Workshop

at

Lawrence Berkeley Laboratory

June 25, 1993

Organized by:

Malcolm Howells and Zahid Hussain

Lawrence Berkeley Laboratory
University of California
Berkeley, California 94720

This work was supported by the Director, Office of Energy Research, Office of Basic Energy Sciences, Materials Sciences Division, of the U.S. Department of Energy under Contract No. DE-AC03-76SF00098

Contents

ALS WORKSHOP ON SOFT X-RAY INTERFEROMETRY

PRELIMINARY PROGRAM

June 25, 1993

Building 2, Room 100B

AGENDA

CHAIR: Malcolm Howells		
8:00 - 9:00 a.m.	COFFEE	
9:00 - 9:10	Welcome on behalf of the ALS	Brian Kincaid
9:10 - 9:20	Introductory Remarks	Malcolm Howells
9:20 - 10:00	The Scientific Origins of the LBL Soft X-Ray Interferometer Project	David Shirley
10:00 - 10:40	Fourier Transform Spectroscopy: A Sketch Map to Lyman Alpha and Beyond	Anne Thorne
10:40 - 11:00	COFFEE BREAK	
11:00 - 11:30	High Resolution Fourier Spectroscopy at Wisconsin	Fredrick Roesler
11:30 - 12:10 p.m.	Fourier Transform Spectroscopy Using Synchrotron Radiation	Dieter Möller
12:10 - 1:30	WORKING LUNCH	
CHAIR: Zahid Hussain		
*1:30 - 2:00	Technical Proposals for a 10-100eV Fourier Transform Spectrometer at ALS	Malcolm Howells
*2:00 - 2:30	Some Technical Issues in Implementing the ALS Fourier Transform Spectrometer	Zahid Hussain
*2:30 - 3:00	Discussion of Engineering	
3:00 - 3:20	COFFEE BREAK	
3:20 - 3:50	Application of Hard X-ray Interferometry	Wenbing Yun
3:50 - 4:55	"Open Microphone" for ideas surfacing during the day	
4:55 - 5:00	Closing Remarks	David Shirley
5:00	Adjourned	
6:00	Reception at Malcolm's House	
7:00	Walk around to dinner somewhere on Solano Avenue	

*indicates the session when engineering aspects of the proposed ALS program will be discussed.

Rev. June 23, 1993 (sf)

Workshop on Soft X-ray Interferometry

June 25, 1993
Lawrence Berkeley Laboratory
Berkeley, CA

Roger G. Carr
Stanford Synchrotron Rad. Lab
SLAC/Bin 69
P.O. Box 4349
Stanford, CA 94309-0210

Ben Feinberg
Lawrence Berkeley Laboratory
1 Cyclotron Road, 80-101
Berkeley, CA 94720

Keith Franck
Lawrence Berkeley Laboratory
1 Cyclotron Road, 25-123
Berkeley, CA 94720

Eric Gullikson
Lawrence Berkeley Laboratory
1 Cyclotron Road, 2-400
Berkeley, CA 94720

Phil Heimann
Lawrence Berkeley Laboratory
1 Cyclotron Road, 2-400
Berkeley, CA 94720

Malcolm Howells
Lawrence Berkeley Laboratory
1 Cyclotron Road, 2-400
Berkeley, CA 94720

Eric Hudson
Lawrence Berkeley Laboratory
1 Cyclotron Road, 2-300
Berkeley, CA 94720

Tony Huff
Lawrence Berkeley Laboratory
1 Cyclotron Road, 2-300
Berkeley, CA 94720

Zahid Hussain
Lawrence Berkeley Laboratory
1 Cyclotron Road, 2-300
Berkeley, CA 94720

Scott Kellar
Lawrence Berkeley Laboratory
1 Cyclotron Road, 2-300
Berkeley, CA 94720

Kwang Je Kim
Lawrence Berkeley Laboratory
1 Cyclotron Road, 71-259
Berkeley, CA 94720

Brian Kincaid
Lawrence Berkeley Laboratory
1 Cyclotron Road, 80-101
Berkeley, CA 94720

Ted Lauritzen
Lawrence Berkeley Laboratory
1 Cyclotron Road, 46-161
Berkeley, CA 94720

Robert Madden
NIST
Bldg. 245, Room B119
Physics A257
Gaithersburg, MD 20899

Wayne McKinney
Lawrence Berkeley Laboratory
1 Cyclotron Road, 2-400
Berkeley, CA 94720

Eddie Moler
Lawrence Berkeley Laboratory
1 Cyclotron Road, 2-300
Berkeley, CA 94720

Dieter Möller
Fairleigh Dickenson University
1000 River Rd.
Teaneck, NY 07666

Howard Padmore
Lawrence Berkeley Laboratory
1 Cyclotron Road, 2-400
Berkeley, CA 94720

Barry Petersen
Lawrence Berkeley Laboratory
1 Cyclotron Road, 2-300
Berkeley, CA 94720

Alan Ramsey
Princeton University
Plasma Physics Laboratory
P.O. Box 451
Princeton, NJ 08543

Fred Roesler
Univ. of Wisconsin-Madison
1150 University Ave.
Madison, WI 53706

David Shirley
Pennsylvania State University
Kern Graduate Building, 114
University Park, PA 16802

Gary Sommargren
Lawrence Livermore Laboratory
L-395
P.O. Box 5511
Livermore, CA 94551

Anne Thorne
Physics Dept., Imperial College
of Science and Technology
United Kingdom

Simonetta Turek
Lawrence Berkeley Laboratory
1 Cyclotron Road, 2-400
Berkeley, CA 94720

Wenbling Yun
Argonne National Laboratory
APS, Bldg. 360
9700 South Cass Avenue
Argonne, IL 60439

Executive Summary

The purpose of the soft x-ray interferometry workshop held at Lawrence Berkeley Laboratory was to discuss with the scientific community the proposed technical design of the soft x-ray Fourier-transform spectrometer being developed at the ALS. Different design strategies for the instrument's components were discussed, as well as detection methods, signal processing issues, and how to meet the manufacturing tolerances that are necessary for the instrument to achieve the desired levels of performance. Workshop participants were encouraged to report on their experiences in the field of Fourier transform spectroscopy.

There are a number of problems in the physics of atoms and small molecules that challenge the resolution of the diffraction grating spectrometers that are traditionally used for vacuum-ultraviolet (VUV) and soft x-ray experiments at synchrotron radiation facilities. An interesting example is the helium absorption spectrum in the region from 60 to 80 eV near the double ionization threshold. Helium is the archetypal electron-exchange and three-body system and its spectrum exhibits many Rydberg series that correspond to the possible two-electron excitations with both negative and positive parity states involved. Fundamental studies of photoabsorption processes in helium go back to the 1960's.[1] Using the monochromators of today, however, scientists can only resolve about twenty of the infinite number of members of the double-excitation Rydberg series below the N=2 threshold of He^+. Furthermore, the transitions from the negative parity states can hardly be seen because of very small natural line widths even though they are believed to have very high oscillator strength. Although the present technology has been pushed to the limit [2,3] (resolving power ≅ 16000), it has allowed only limited studies of the interactions between the Rydberg series that should show an interesting transition to chaotic states at sufficiently high values of the principal quantum number. Similarly, the study of the lowest-order negative-parity states, which are predicted to have widths in the microvolt range or lower, has been severely restricted by present day monochromator performance. The information from these studies is needed for comparison with the many theoretical analyses of the helium spectrum.

To address the types of problems described above, the ALS is developing a Fourier transform spectrometer that is intended to operate up to 100 eV. The motivation is solely improved resolution and not the throughput (Jaquinot) or multiplex (Fellgett) advantage, neither of which apply for the sources and detectors used in this spectral range. Our proposed implementation of this is via a Mach-Zehnder geometry that has been (1) distorted from a square to a rhombus to get grazing incidence of a suitable angle for 100 eV and (2) provided with a mirror-motion system to make the path difference between the interfering beams tunable. The experiment consists of measuring the emergent light intensity ($I(x)$) as a function of the path difference (x). The resolving power of the system is limited by the amount of path difference obtainable that is 1 cm (one million half-waves at 200Å wavelength) in our design thus allowing a resolving power of one million. The free spectral range of the system is limited by the closeness with which the function $I(x)$ is sampled. We propose to illuminate a helium absorption cell with roughly 1%-band-width light from a monochromator thus allowing one hundred aliases without spectral overlap even for sampling of $I(x)$ at one hundredth of the Nyquist frequency.

References:

1. P. Madden, K. Codling, "New Autoionizing Atomic Energy Levels in He, Ne, and Ar," Phys. Rev. Lett. **10**, 516-8 (1963).

2. Domke, C. Xue, A. Puschmann, T. Mandel, E. Hudson, D. A. Shirley, G. Kaindl, C. H. Greene, H. R. Sadeghpour, "Extensive Double-Excitation States in Atomic Helium," Phys. Rev. Lett., **66**, 1306-9 (1991).

3. Domke, G. Remmers, G. Kaindl, "Observation of the (2*p*, *nd*) $^1P^0$ Double-Excitation Rydberg Series of Helium," Phys. Rev. Lett., **69**, 1171-4 (1992).

Discussion Notes:

Mirrors and Beam Splitters. Anne Thorne asked if beam dispersion had been considered. Malcolm Howells replied that a milliradian is ok and typical of synchrotron radiation. A question arose about the thickness of the mirrors. Howells pointed out that molybdenum is only used as the optical coating, while the material used for the substrate must be thick enough to polish. Madden asked if the phase changes of the light upon reflection had been considered. Wenbing Yun replied that theta-critical is such that phase changes are small.

Anne Thorne reported that they originally used two separate pieces for beam splitters. Then they tried a solid piece of silicon which worked as both beam splitters—this worked well. When they tried a solid piece of magnesium fluoride, they had problems because of inhomogeneity. Now they are back to using two separate pieces with the drift of the system requiring adjustments every few hours. The moral of the story being that the beam splitters should be adjustable so that they can be realigned easily.

Flex Hinges. Robert Madden suggested considering vertical design as an alternative. One drawback of this is that second order terms become important. Dave Shirley brought up the possibility of making the translation system three-dimensional (3D). This provides improved stability for motion along one dimension. Anne Thorne suggested making the optical system 3D by adding a roof to the structure to reduce the influence of pitch.

Inchworm Drive. Roger Carr said with inchworm drives the thermal drift is quite high and the creep can reach 10% per second. Robert Madden reported that the space-based VUV systems had abandoned the use of inchworm drives because of creep. Anne Thorne said that a magnetic drive doesn't jerk and has very smooth motion.

Position Indexing. Someone pointed out that you can expect [(1.25 nm) x ("n" factor)] resolution at the lower limit, but polarization alignments must be done very carefully or non-linearities will drive the value of "n" way up.

Data Sampling. Anne Thorne said one must measure the amplitude and phase and "both" sides of the interferogram because absorption lines are not symmetric.

Post-Workshop Comments from Anne Thorne

Two problems discussed—how to avoid pitch error on the moving mirrors and how to keep the beam splitter and recombiner aligned to within the micro-radian tolerance—are obviously crucial. Interestingly, the microradian alignment tolerance is almost identical with ours, since we have 10 times the beam diameter at 10 times the wavelength. But we do have the advantage that our two beam-splitter elements are immediately adjacent.

As regards scanning and sampling, I do think you will have to get a laser reference beam through your interferometer somehow, close to and parallel to the signal beam so that it sees exactly the same path differences. Sub-dividing the laser fringes to the required accuracy I do not see as an enormous problem. I think it will turn out to be not very different from what we already do, although the sampling tolerance does depend on the signal to noise ratio you are aiming to achieve. I suggest that you consider continuous scanning so that you can put your signal frequency where you want it, within limits, and make yourself a nice sanitary digital filter to eliminate the out-of-alias noise. You can then make up your time integration by co-adding, with the laser fringes as reference. Admittedly you lose the "fly-back" time, but you save on settling-down time, and most importantly you do not rely on everything staying in perfect alignment with perfect performance for hours on end. If something goes wrong or breaks down you can save the pile you already have, start again next day, and co-add the spectra, whereas if the same thing happens 5 hours through a 6 hour scan you lose everything. The criterion for continuous scanning is a smooth scan velocity—it does not have to be very constant. I think you should look at the possibility of a magnetic drive. We have found that linear motors work well.

The Scientific Origins of the LBL Soft X-Ray Interferometer Project

David Shirley

Pennsylvania State University

SCIENTIFIC ORIGINS OF THE LBL SOFT X-RAY INTERFEROMETER PROJECT (DAVID A. SHIRLEY)

OUTLINE

I. $E/\Delta E$ vs. E : Is high-res. necessary?

II. History of our interest in high-res.

III. Achieving $E/\Delta E = 10^4$ with

A. SGM [Mostly N_2 π^*]

B. PGM [Mostly molecules, and He^{**}]

C. TGM [At BL 8-1, SSRL]

IV. More on He^{**} : on to $E/\Delta E = 10^6$!

I. $E/\Delta E$ Vs. E:

≤ 10 eV (lasers)	≤ 30 eV Norm. Inc. Optics	$30\text{eV} < E < 1000\text{eV}$ Graging Inc. Optics
$E/\Delta E \rightsquigarrow 10^7$	$\sim 10^5$	$\sim 10^3$ until recently

For soft X-rays) — Is high resolution necessary?

[ANSWER: YES!]

↘ Study doubly-excited systems in the continuum:

⇒ $\bar{e}$-$\bar{e}$ correlations

II. History of our interest in high-resolution: photoelectron satellites

[The improvement of $E/\Delta E$ with time]

PHOTOELECTRON SATELLITES

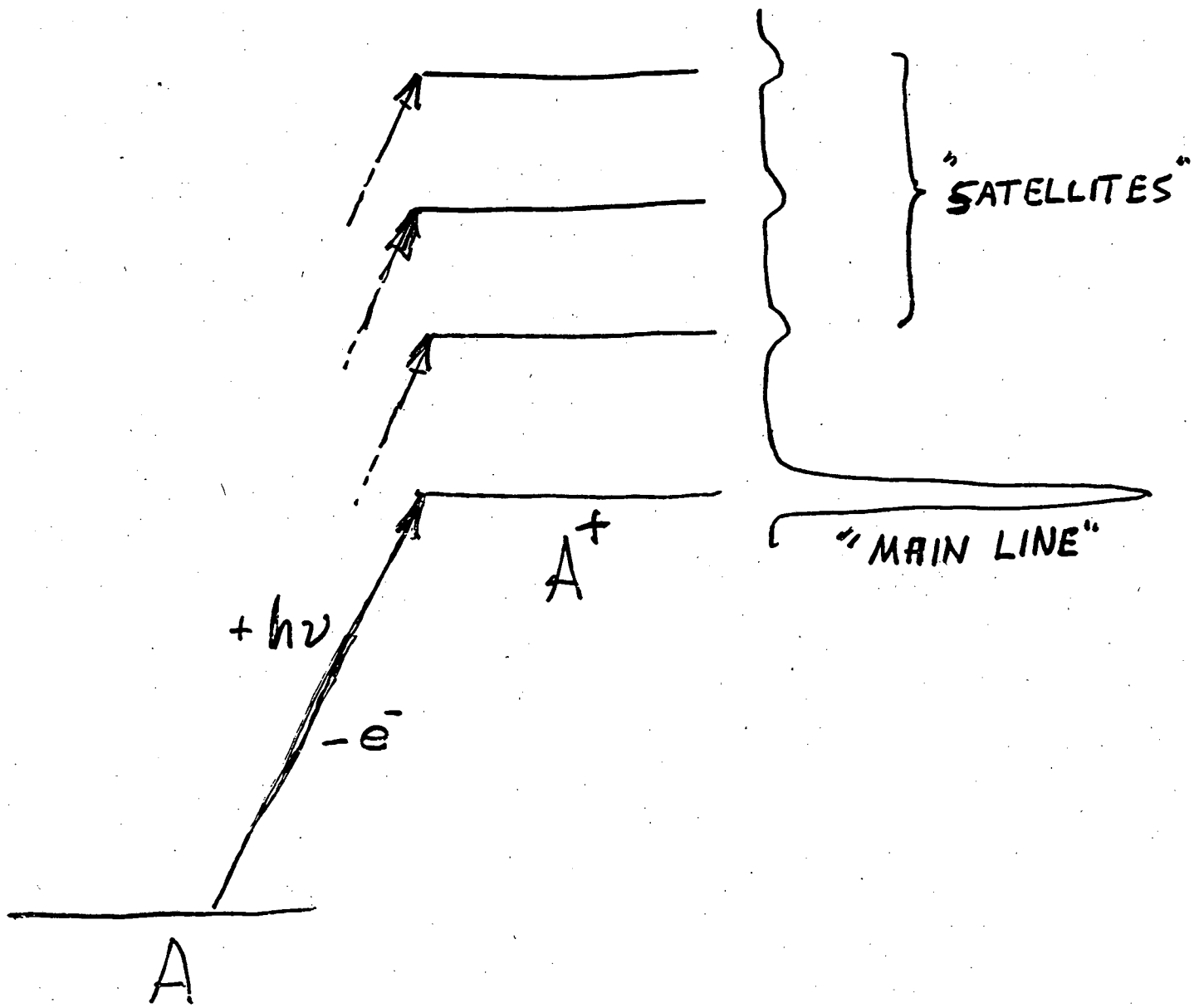

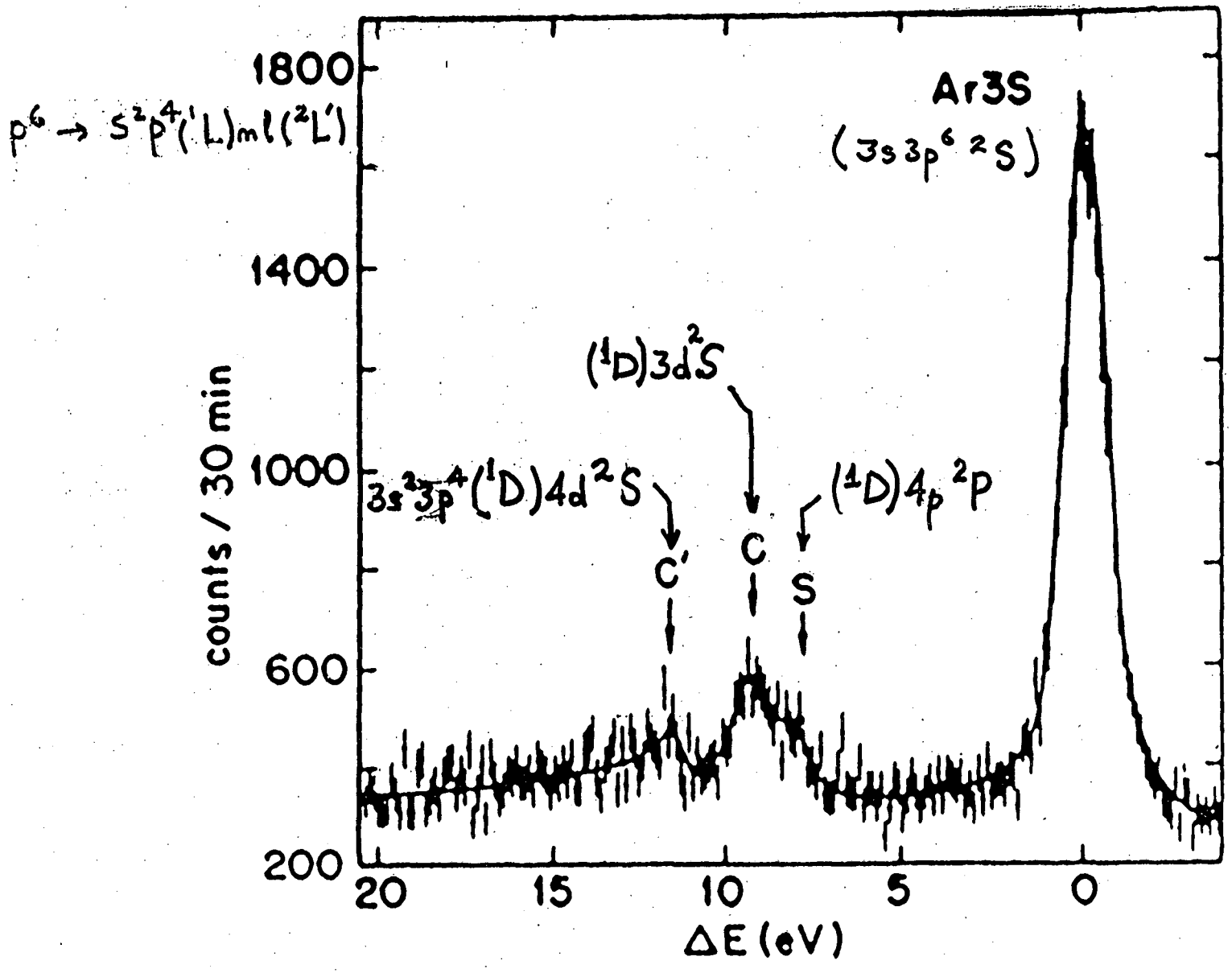

From D.P. Spears, H.J. Fischbeck, and T.A. Carlson
Phys. Rev. A 9, 1603 (1974)

From H. Kossmann, B. Krässig, V. Schmidt and J.E. Hansen

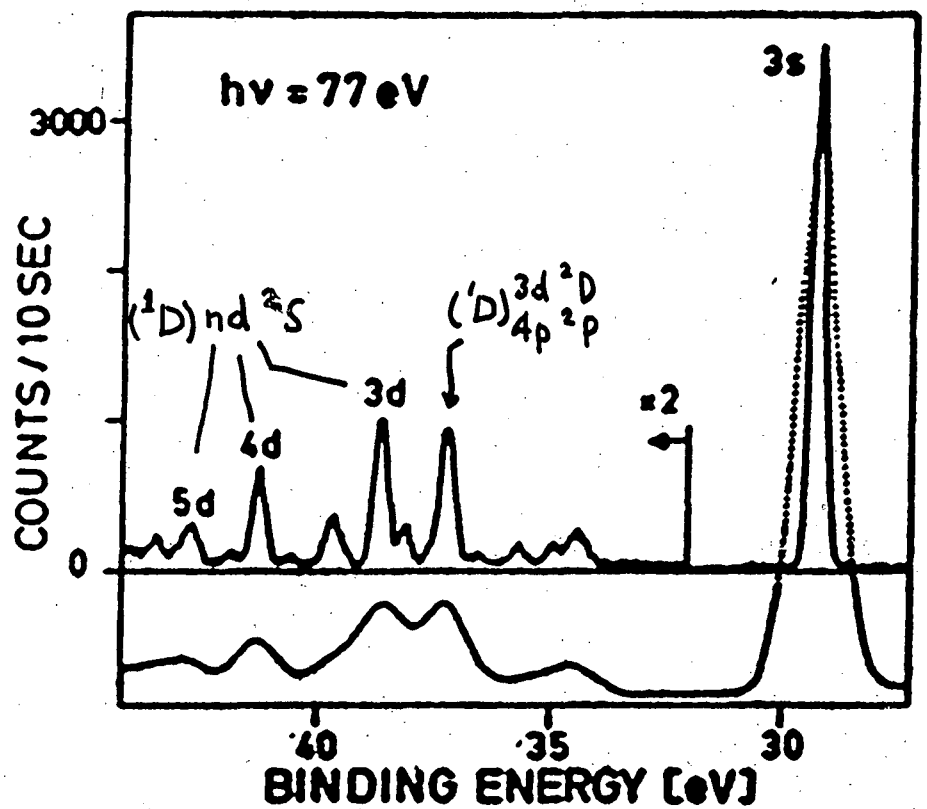

FIG. 2. Satellite lines of argon measured at the quasimagic angle. Upper part: Experimental spectrum obtained in this work. Lower part: Same spectrum convoluted by a Gaussian distribution with 1 eV FWHM.

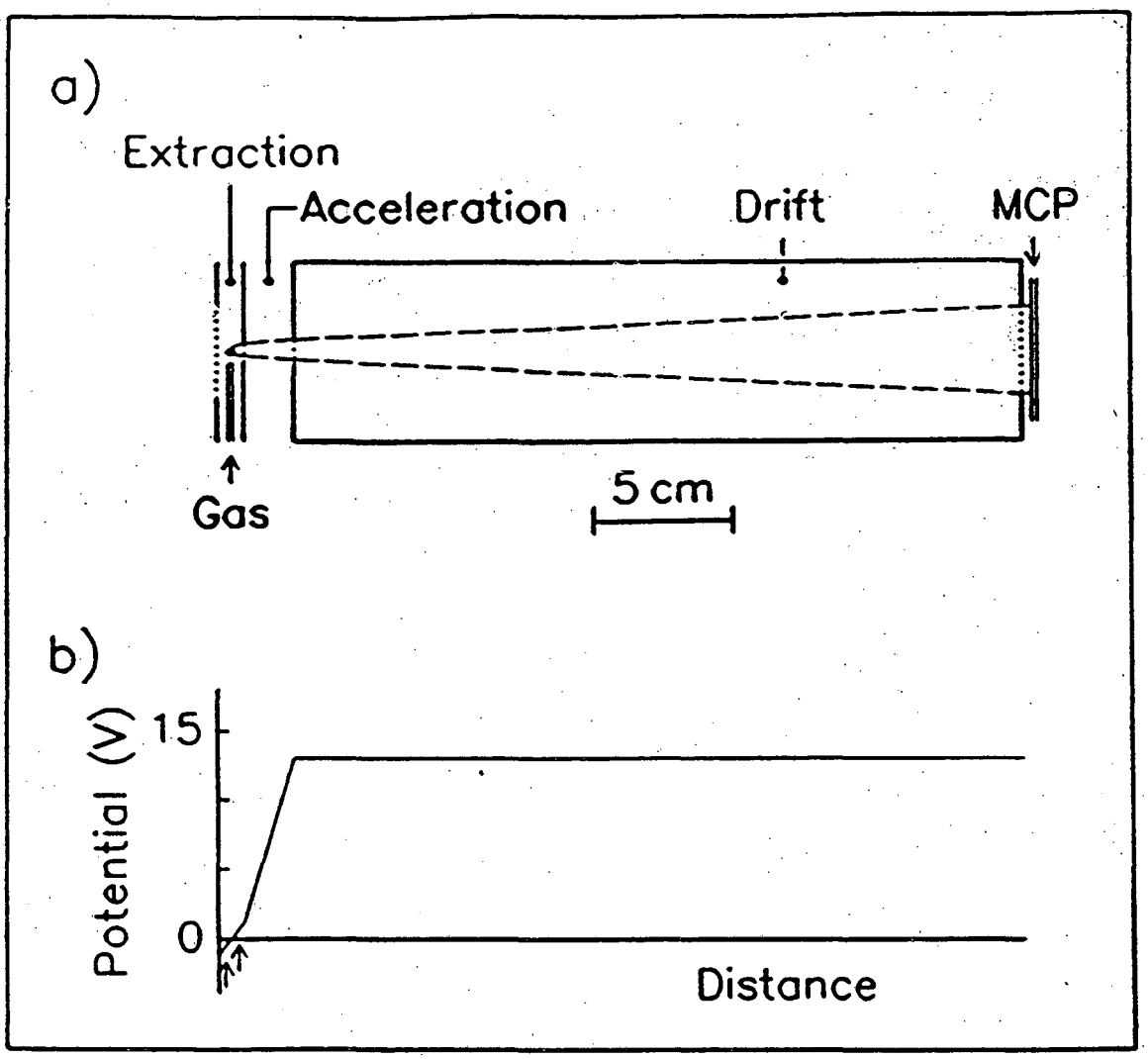

XBL 866-2147

P.A. Heimann, U. Becker, H.G. Kerkhoff, B. Langer, D, Szostak, R. Wehlitz, D.W. Lindle, T.A. Ferrett, and D.A. Shirley Phys. Rev. A 34, 3782 (1986)

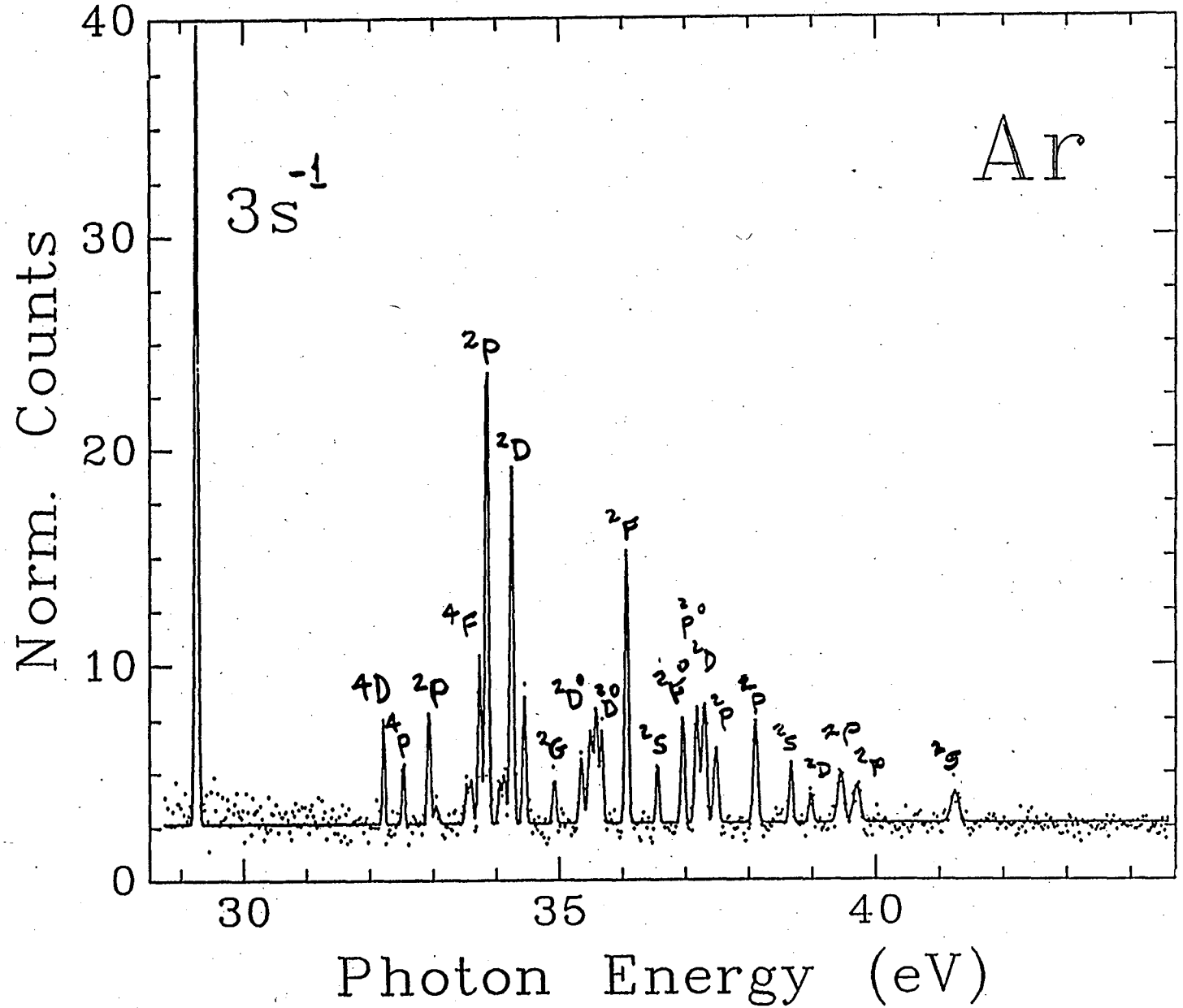
Ar
3s⁻¹
Norm. Counts
Photon Energy (eV)
0
10
20
30
40
30
35
40
4D
4P
2P
4F
2P
2D
2G
2D°
2D°
2F
2S
2P°
2P°
2D
2P
2P
2S
2D
2P
2P
2G

- XBL 881-276 -

Intensity (arb. units.)
0.0
0.5
1.0
32
34
36
38
Photon Energy (eV)
Ar+ 3s2 3p4 nl
(3P)3d(4D)
(3P)4s(4P)
(3P)4s(2P)
(3P)3d(4F)
(3P)3d(2P)
(3P)3d(4P)
(1D)4s(2D)
(3P)3d(2F)
(3P)3d(2D)
(1D)3d(2G)
(3P)4p(4P°)
(3P)4p(4D°)
(3P)4p(2D°)
(3P)4p(2P°)
(3P)4p(4S), (3P)4p(2S)
(1D)3d(2F)
(1S)4s(2S)
(1D)4p(2F°)
(1D)4p(2P°), (1D)3d(2D)
(1D)4p(2D°)
(1D)3d(2P)

III. Achieving $E/\Delta E = 10^4$ with

A. SGM's

[Some spectra, mostly $N_2\,\pi^*$]

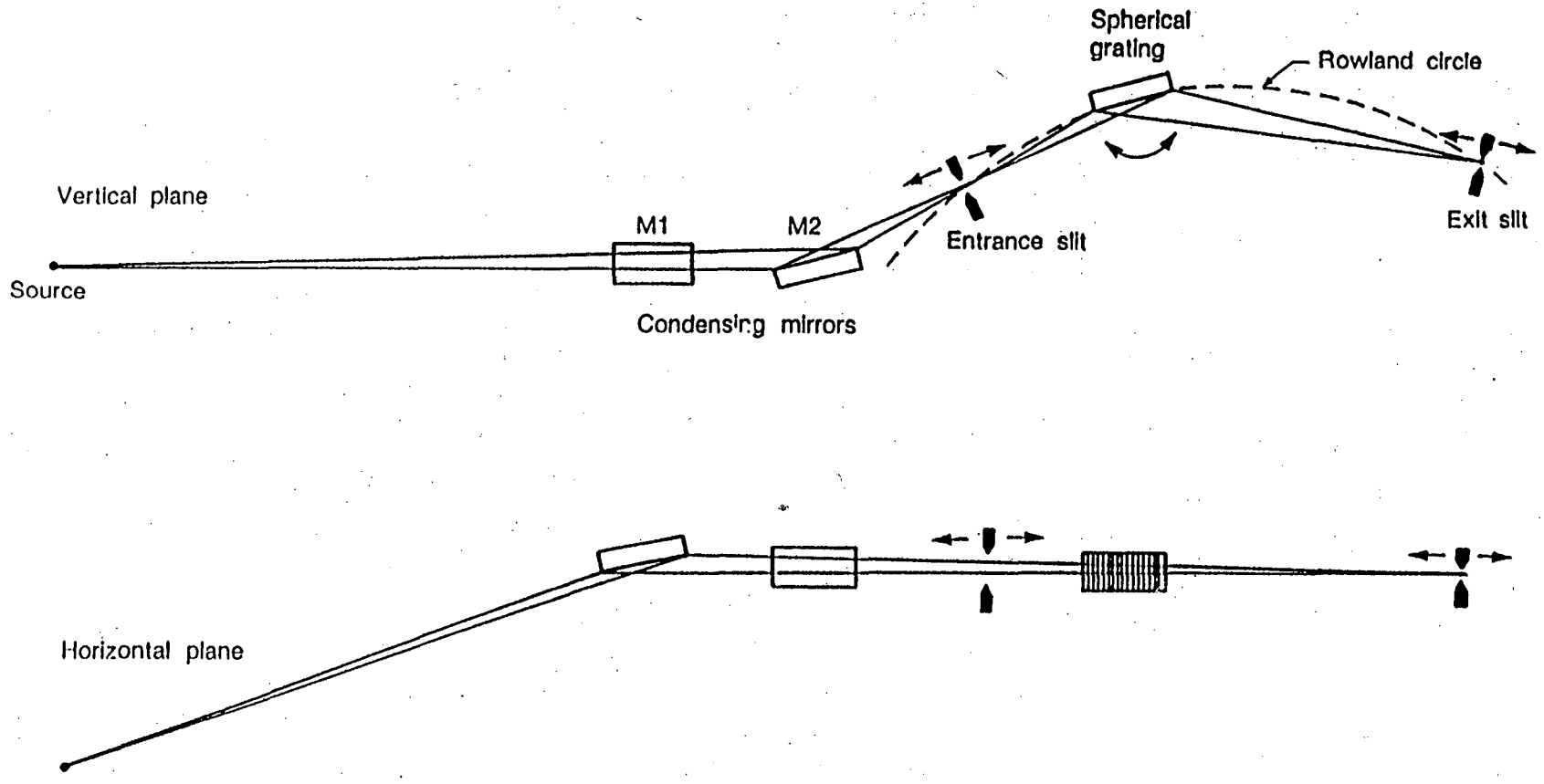

Schematic of the Rense and Violett spherical grating monochromator system. The condensing mirrors M1 and M2 are designed so that M1 focuses in the horizontal plane to the exit slit, and M2 focuses in the vertical plane to the entrance slit. Each mirror has essentially zero focusing effect in its sagittal direction.

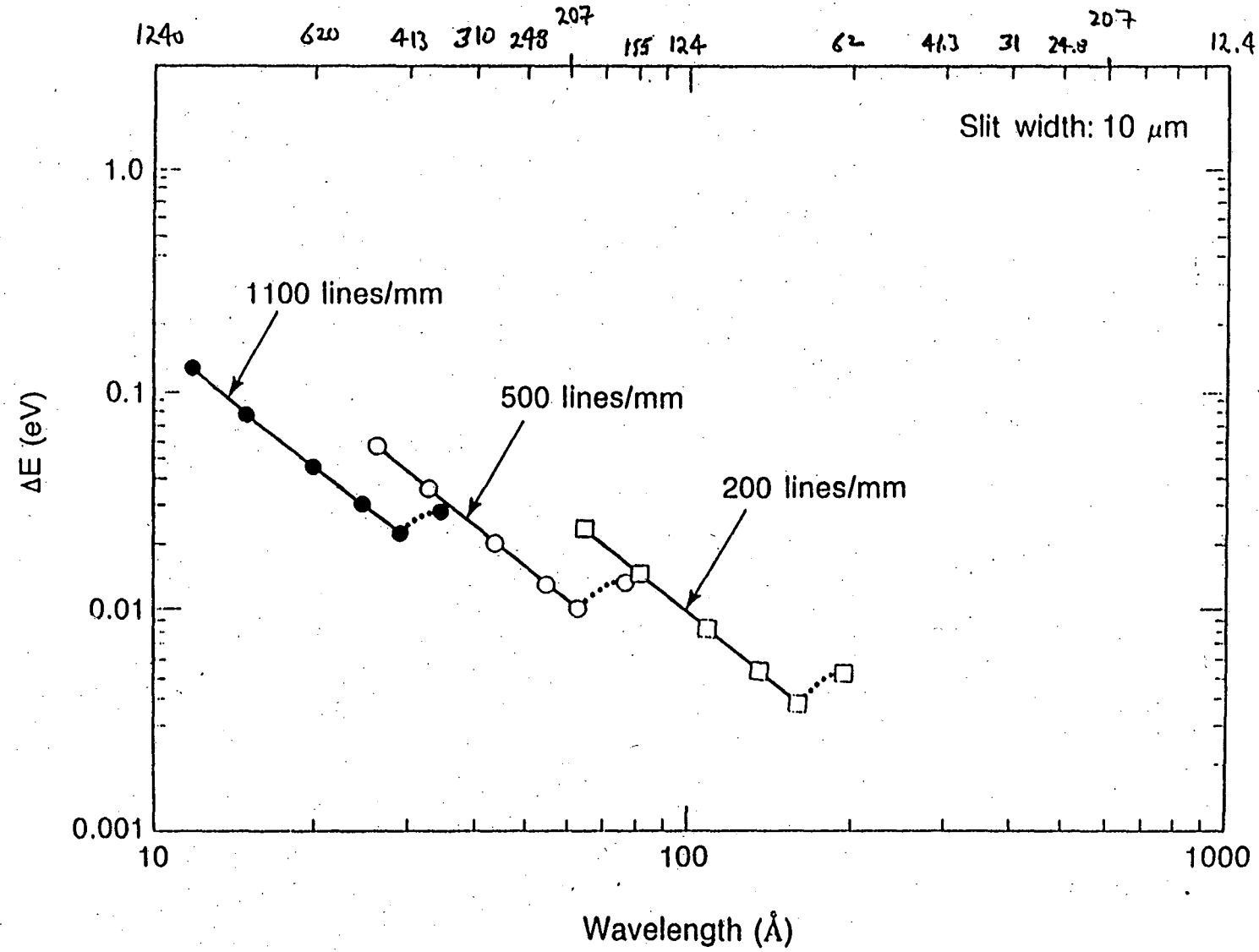

Detailed plots of the resolution of the 3° spherical grating monochromator of Beam Line C. The plots are for 10-μm slits and are derived from computer ray traces of the whole beam line. The solid lines correspond to regions where the Rowland condition is exactly satisfied and where resolution

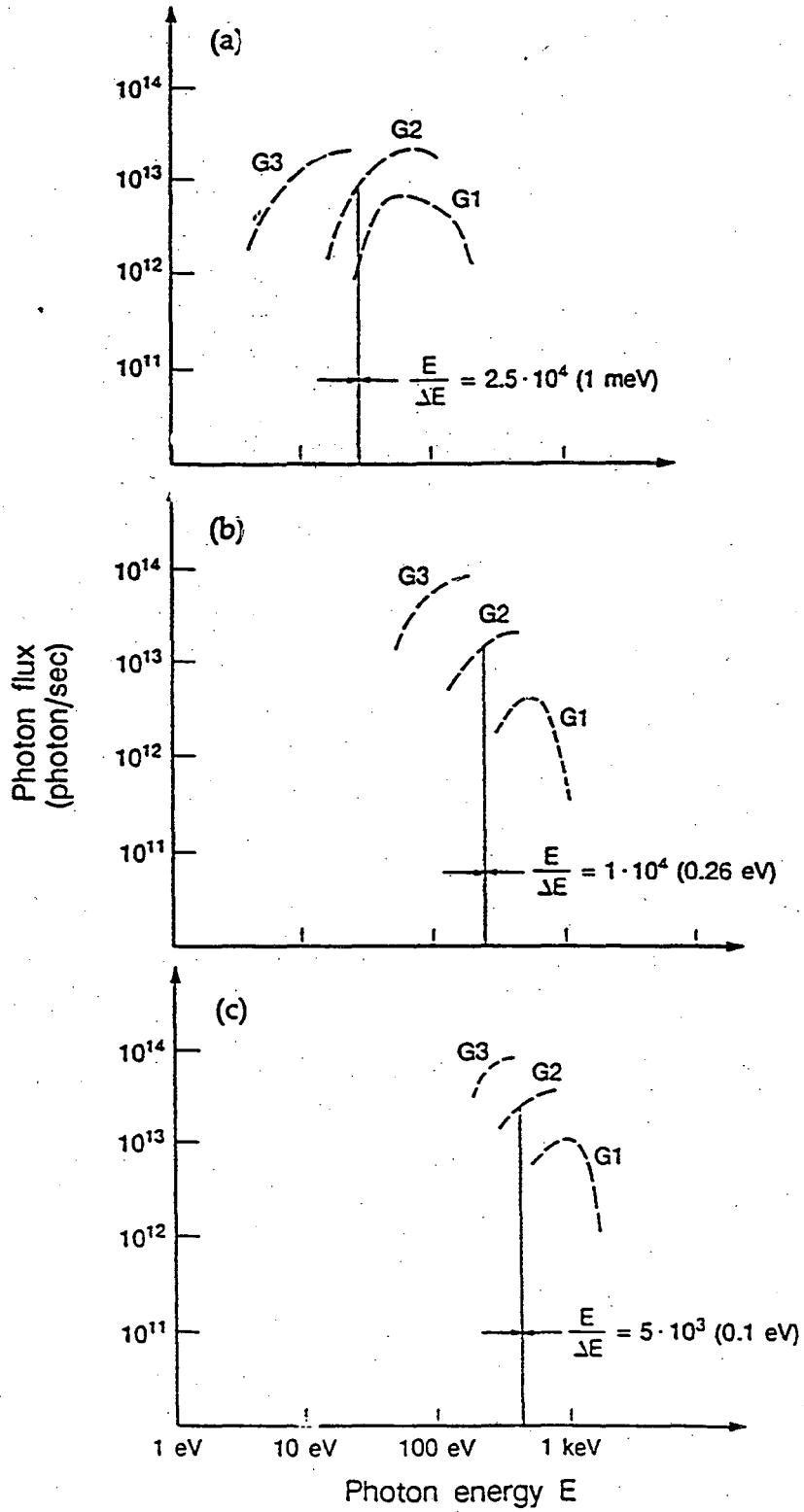

Fig. 4-5. Photon flux from (a) a 10° spherical grating monochromator, in conjunction with undulator U9.0; (b) a 3° SGM, in conjunction with undulator U5.0; and (c) a 2° SGM, in conjunction with undulator U3.65. For each, more detailed parameters appear in Tables 4-2 and 4-3. The curves shown here assume that the monochromators are set for best resolution.

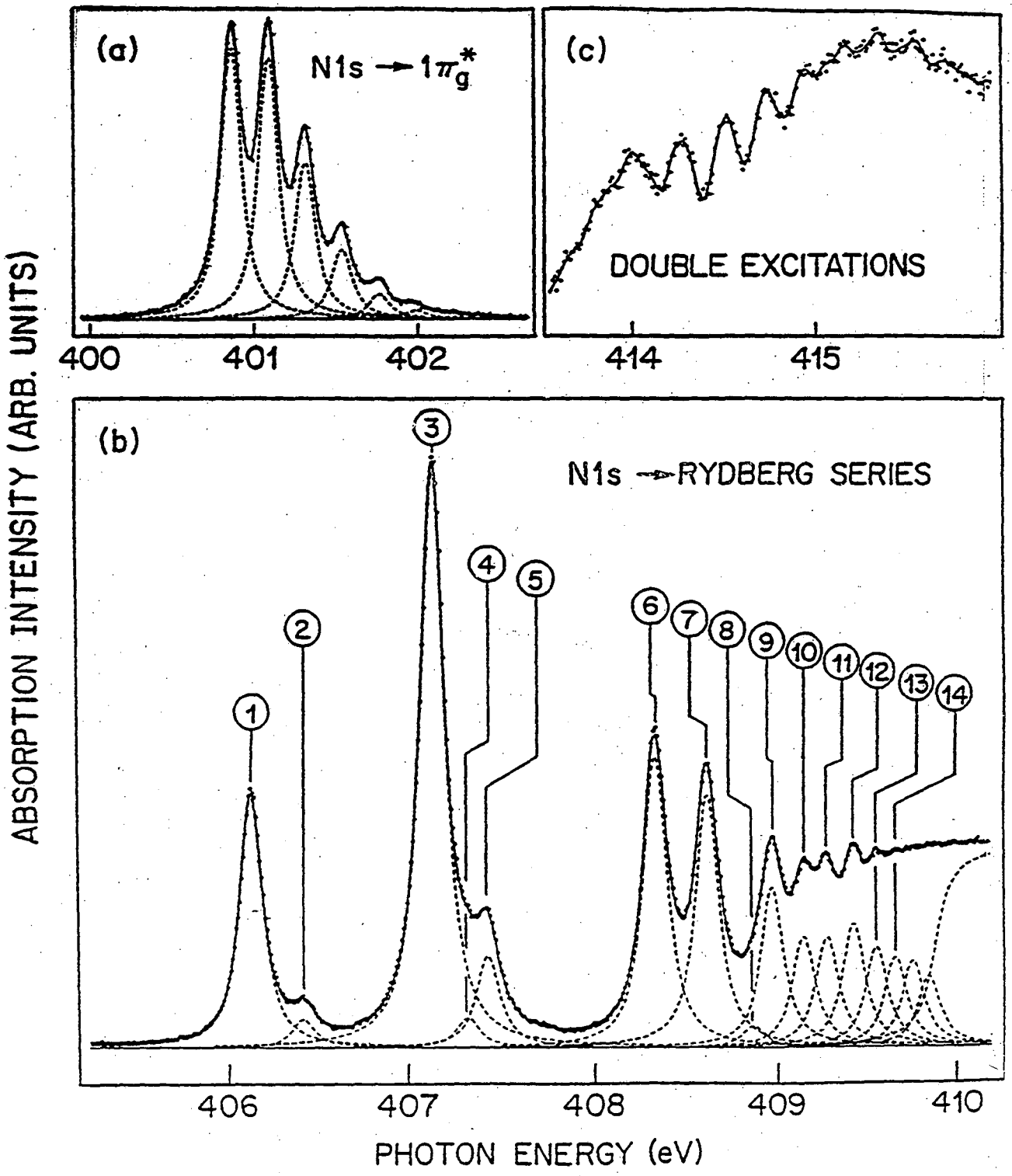
(a)
N1s → 1πg*
(c)
DOUBLE EXCITATIONS
400
401
402
414
415
(b)
N1s → RYDBERG SERIES
1
2
3
4
5
6
7
8
9
10
11
12
13
14
406
407
408
409
410
ABSORPTION INTENSITY (ARB. UNITS)
PHOTON ENERGY (eV)

Fig. 2

(From P.A. Heimann, et al, VUV-9 Proc.)

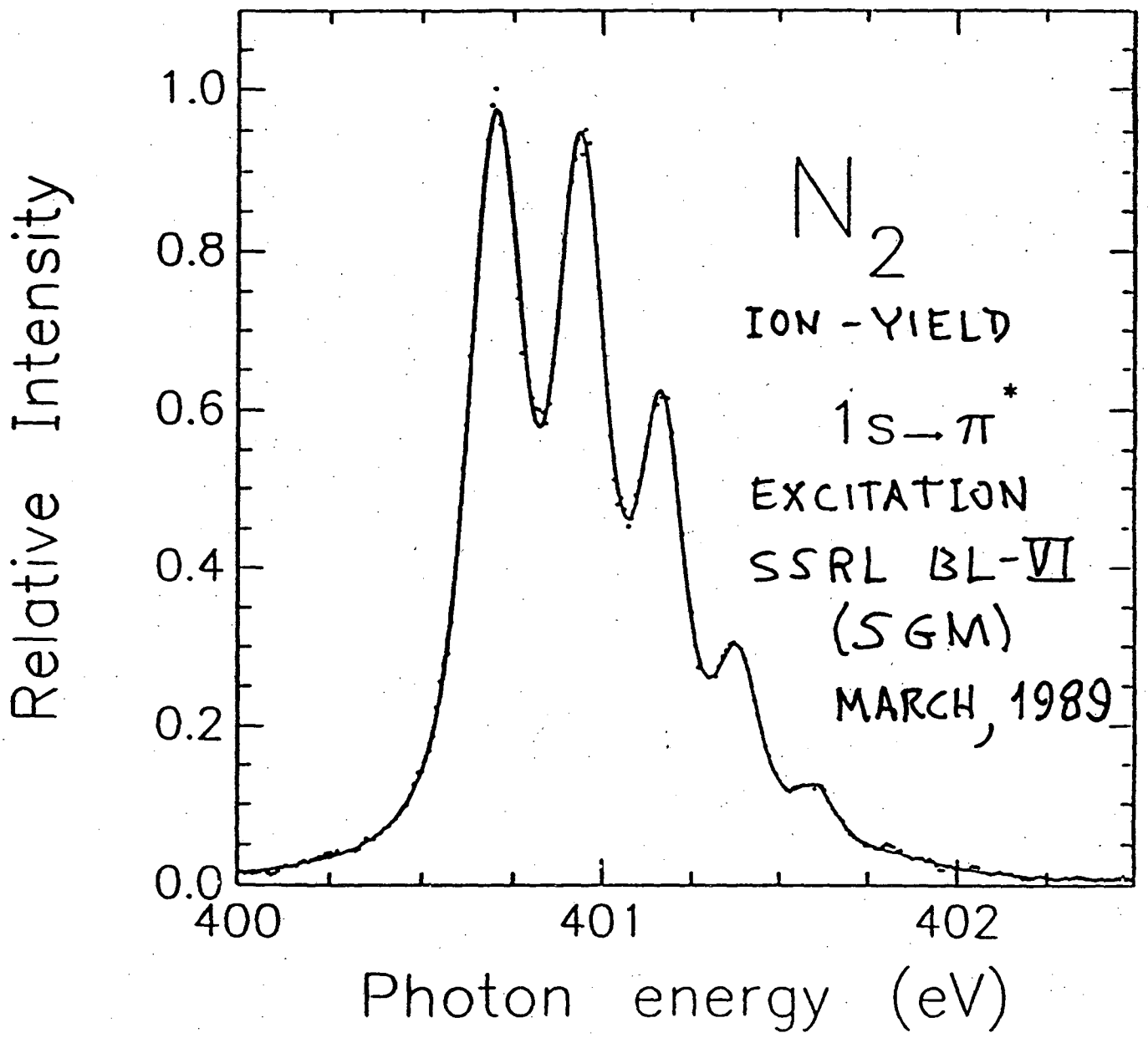

N2: 1s -> 1πg*
0-0
0-1
0-2
0-3
0-4
0-5
0-6
0-7
0-8
0-9
401.5
402.0
402.5
403.0
400
401
402
403
Photon Energy [ev]

N_2 1s -> $1\pi_g^*$

$\hbar\omega$: 236.5 $\pm$ .9 meV

$\hbar\omega_x$: 2.8 $\pm$ .3 meV

r_o: 1.186 $\pm$ .003 Å

Γ: 125 $\pm$ 5 meV

III. B. $E/\Delta E = 10^4$ with a PGM

(SX-700 II @ BESSY)

M. Domke, G. Kaindl, E. Hudson, ...

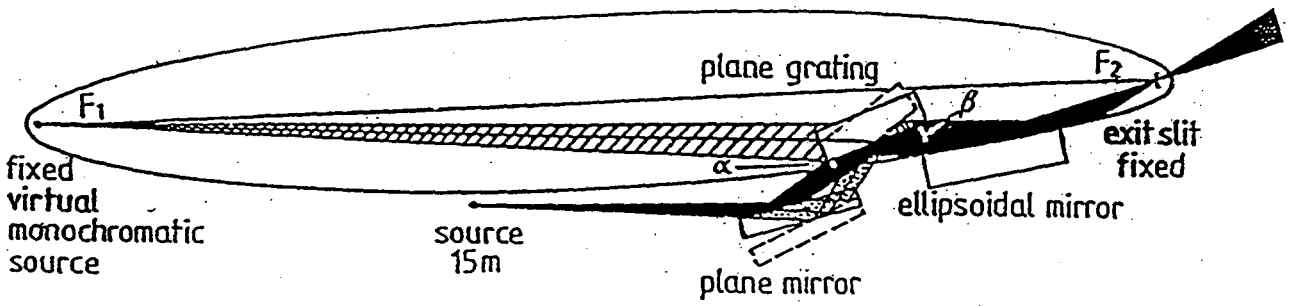
plane grating
F2
F1
β
α
exit slit
fixed
fixed
virtual
monochromatic
source
source
15m
ellipsoidal mirror
plane mirror

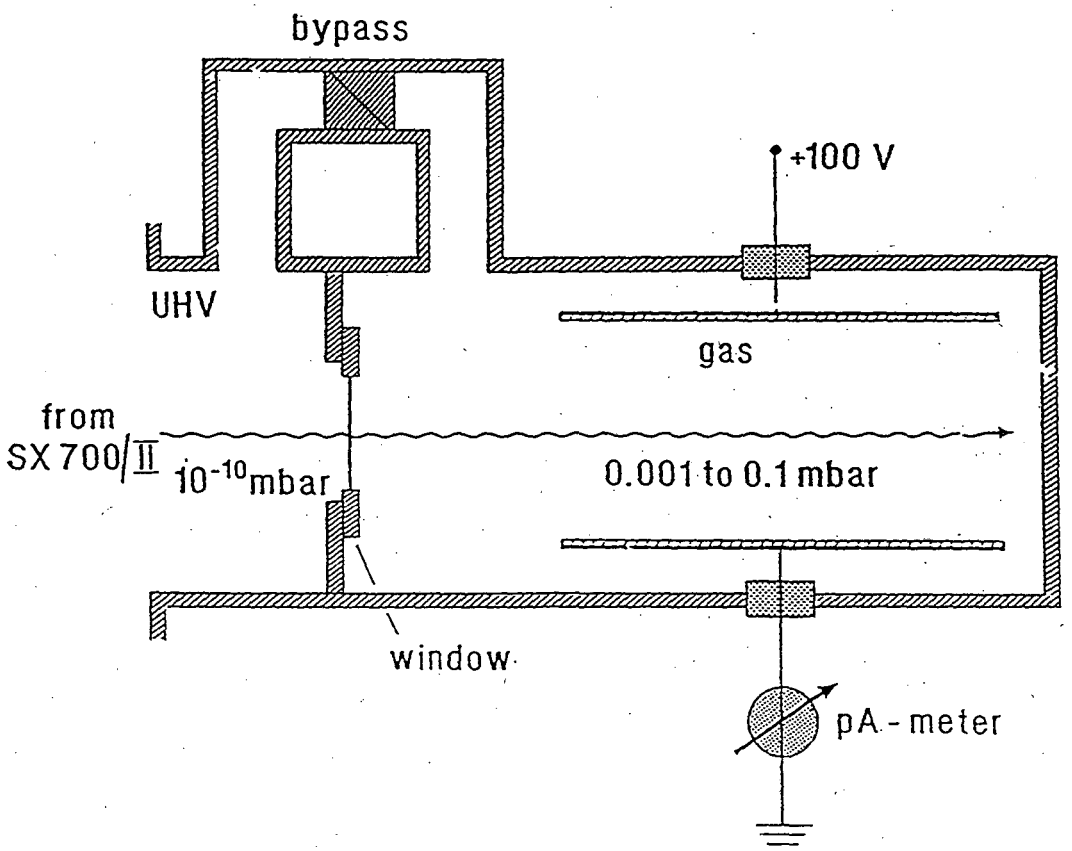
bypass
+100 V
UHV
gas
from
SX 700/II
10-10mbar
0.001 to 0.1 mbar
window
pA - meter

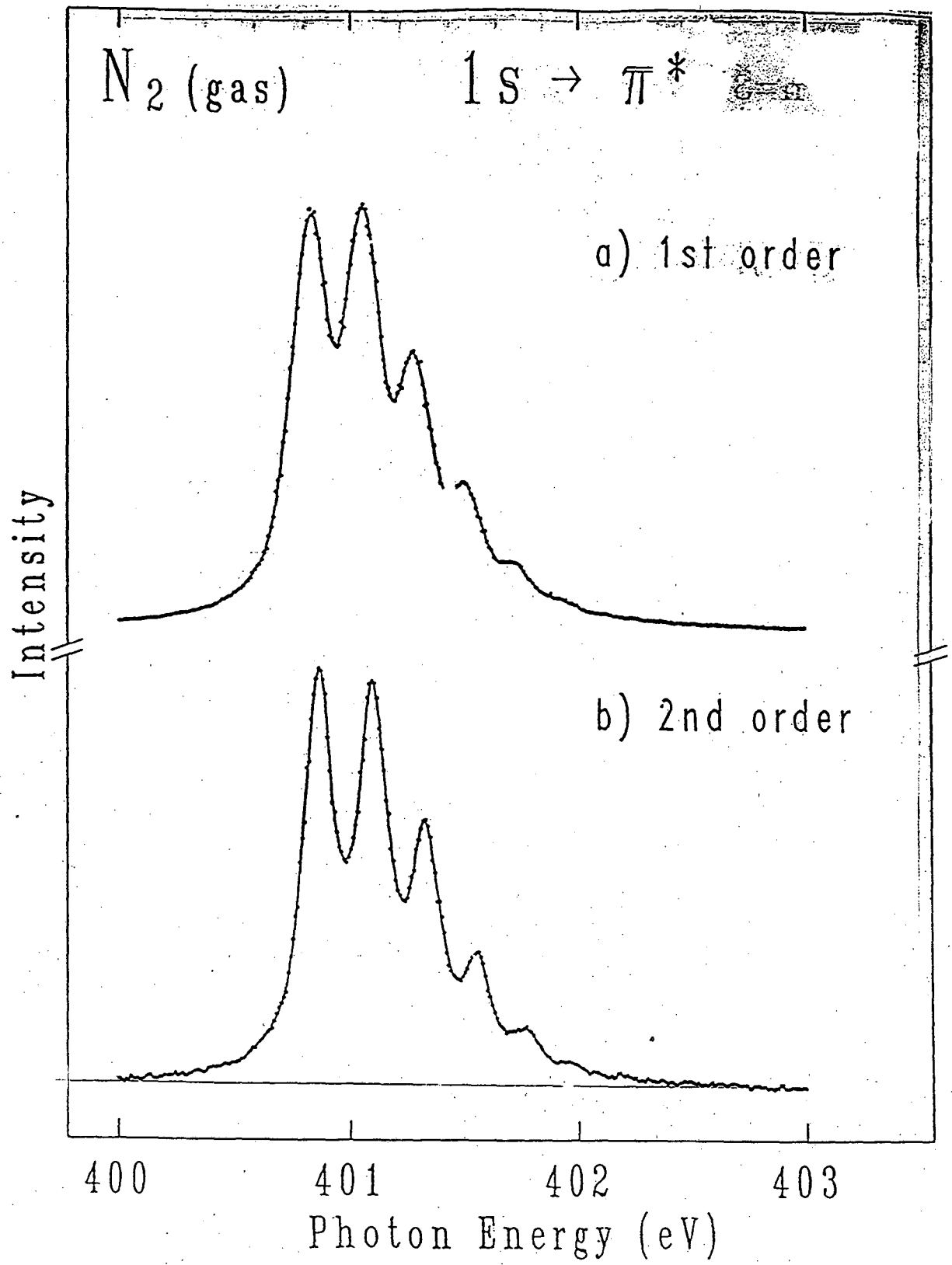
N2 (gas)
1s → π*
a) 1st order
b) 2nd order
Intensity
400
401
402
403
Photon Energy (eV)

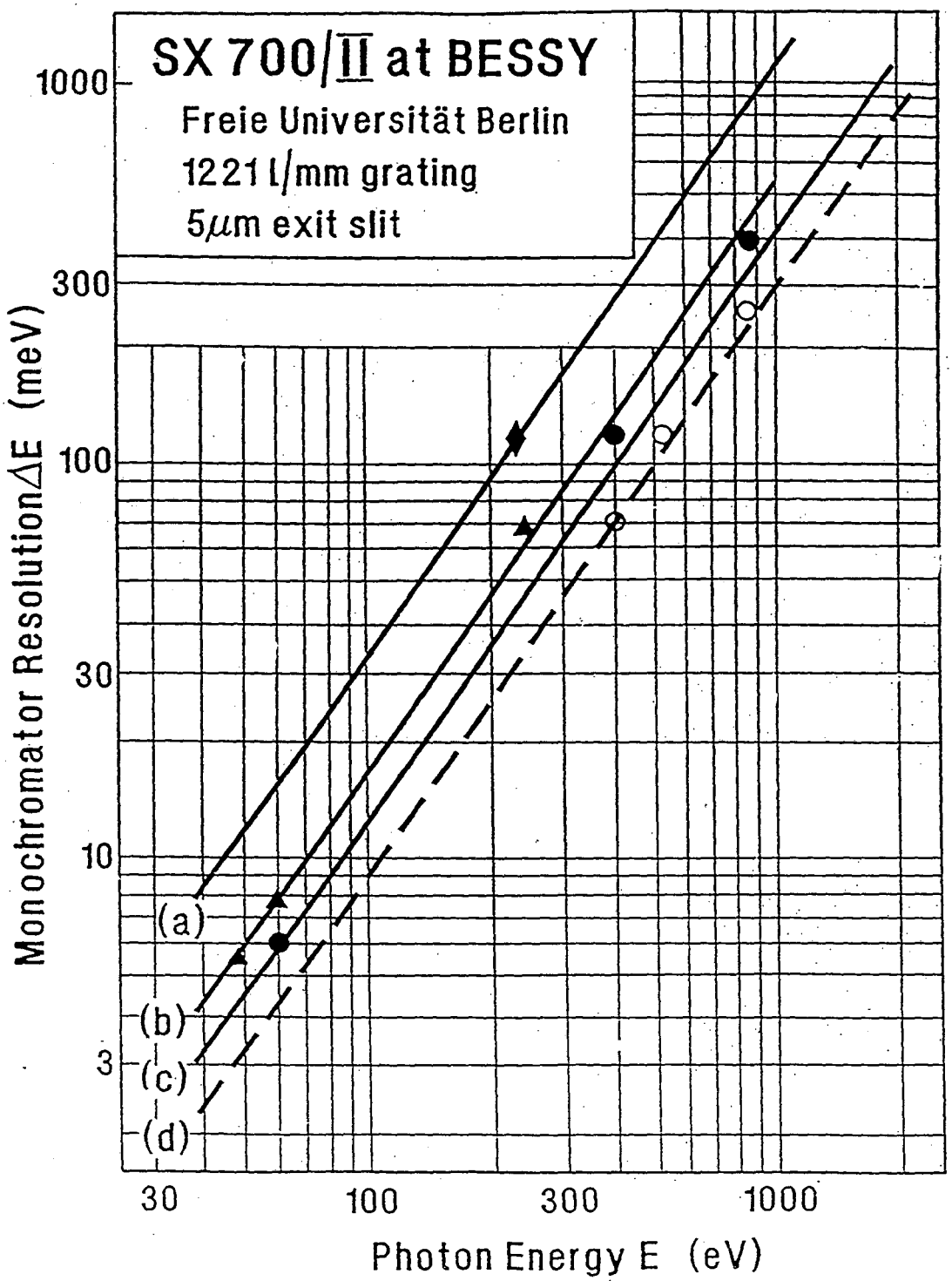
SX 700/II at BESSY
Freie Universität Berlin
1221 l/mm grating
5μm exit slit
1000
300
100
30
10
3
Monochromator Resolution ΔE (meV)
(a)
(b)
(c)
(d)
30
100
300
1000
Photon Energy E (eV)

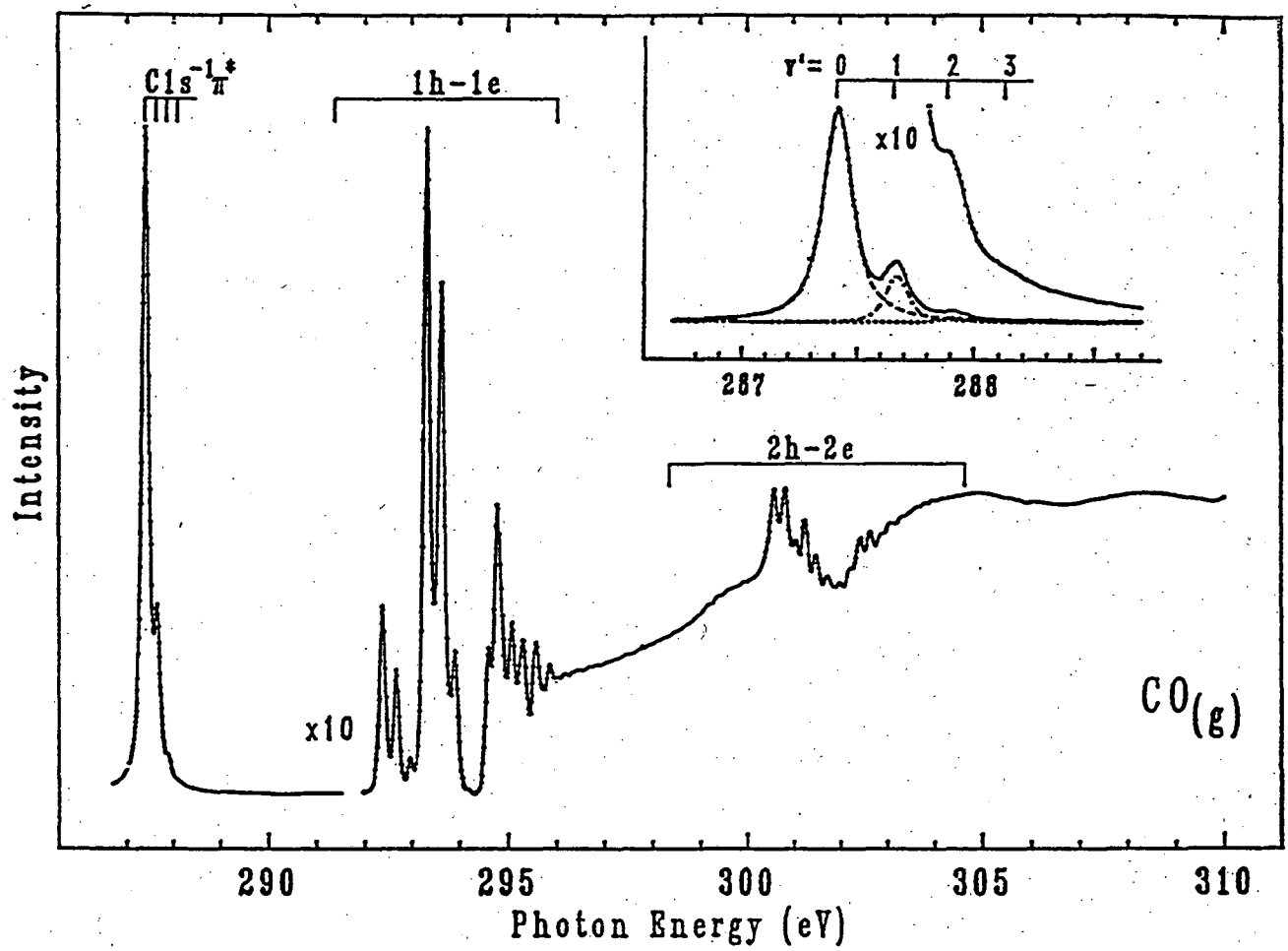
C1s$^{-1}\pi^*$
1h-1e
2h-2e
v'= 0 1 2 3
x10
287
288
x10
Intensity
CO(g)
290
295
300
305
310
Photon Energy (eV)

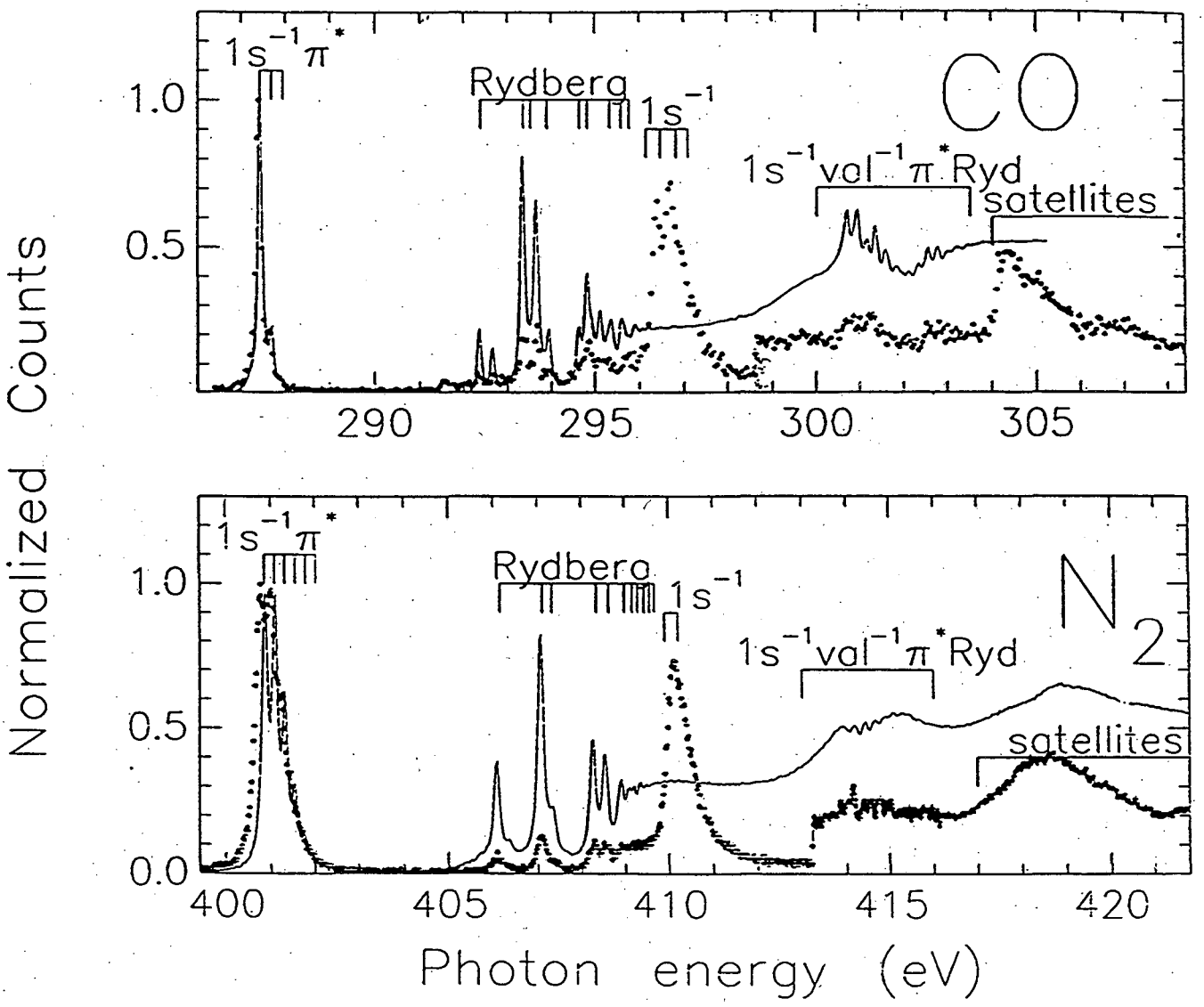
Normalized Counts
1s⁻¹π*
Rydberg
1s⁻¹
CO
1s⁻¹val⁻¹π*Ryd
satellites
1.0
0.5
290
295
300
305
1s⁻¹π*
Rydberg
1s⁻¹
N2
1s⁻¹val⁻¹π*Ryd
satellites
1.0
0.5
0.0
400
405
410
415
420
Photon energy (eV)

XBL 911-129

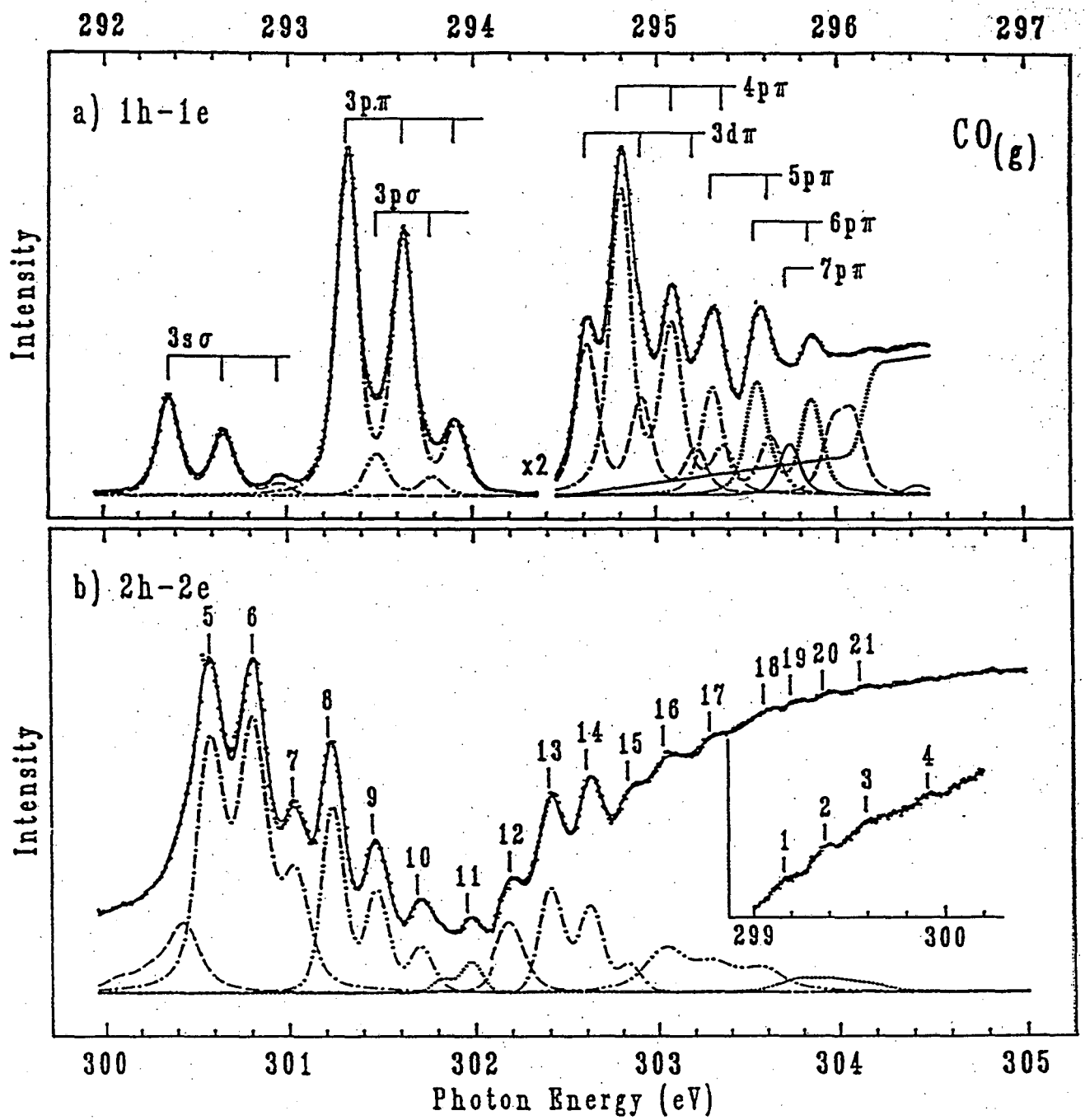
292
293
294
295
296
297
a) 1h-1e
3pπ
3pσ
4pπ
3dπ
5pπ
6pπ
7pπ
3sσ
CO(g)
x2
Intensity
b) 2h-2e
5
6
8
7
9
10
11
12
13
14
15
16
17
18
19
20
21
1
2
3
4
299
300
Intensity
300
301
302
303
304
305
Photon Energy (eV)

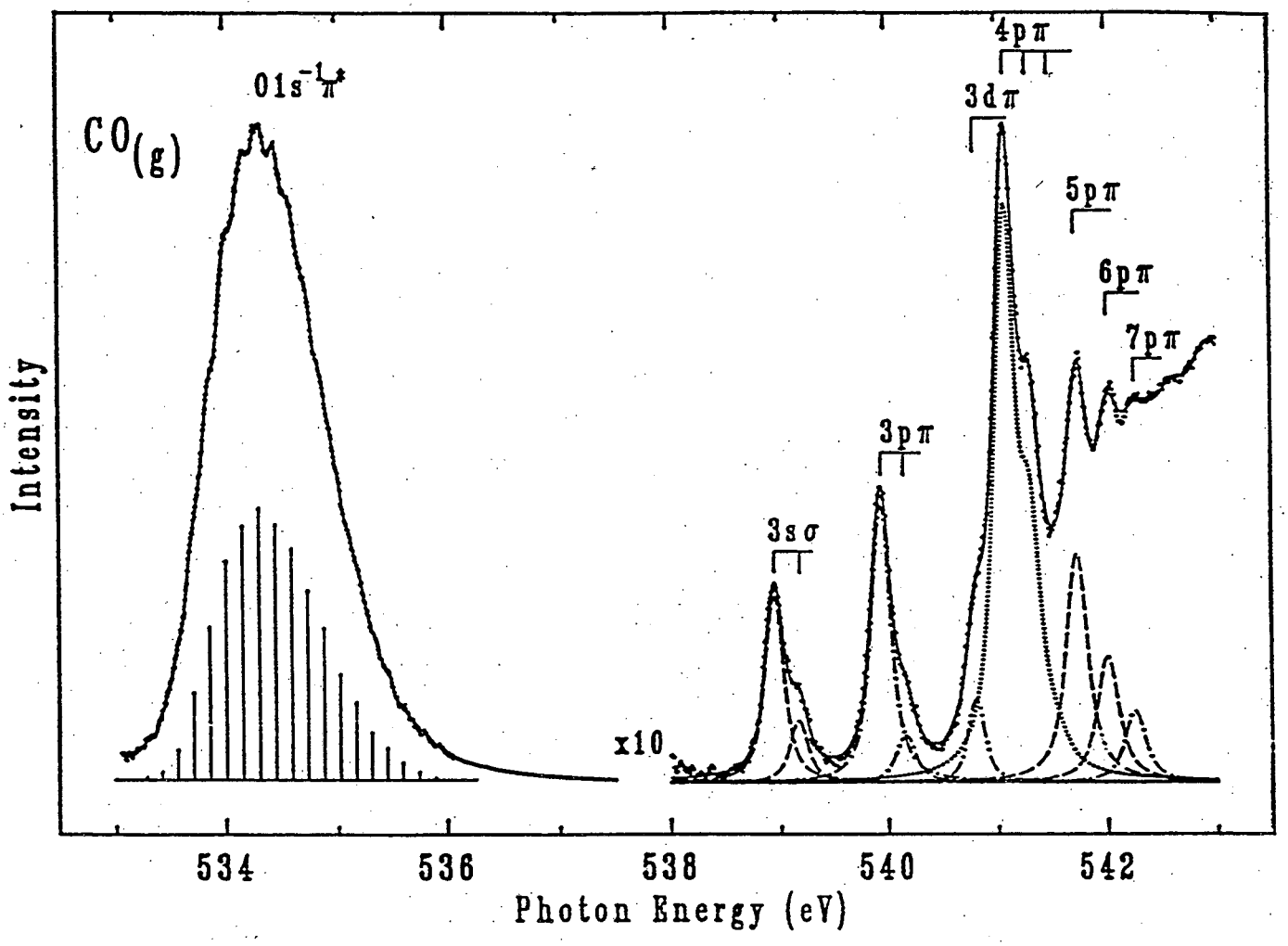
CO(g)
01s⁻¹π*
4pπ
3dπ
5pπ
6pπ
7pπ
3pπ
3sσ
x10
Intensity
534
536
538
540
542
Photon Energy (eV)

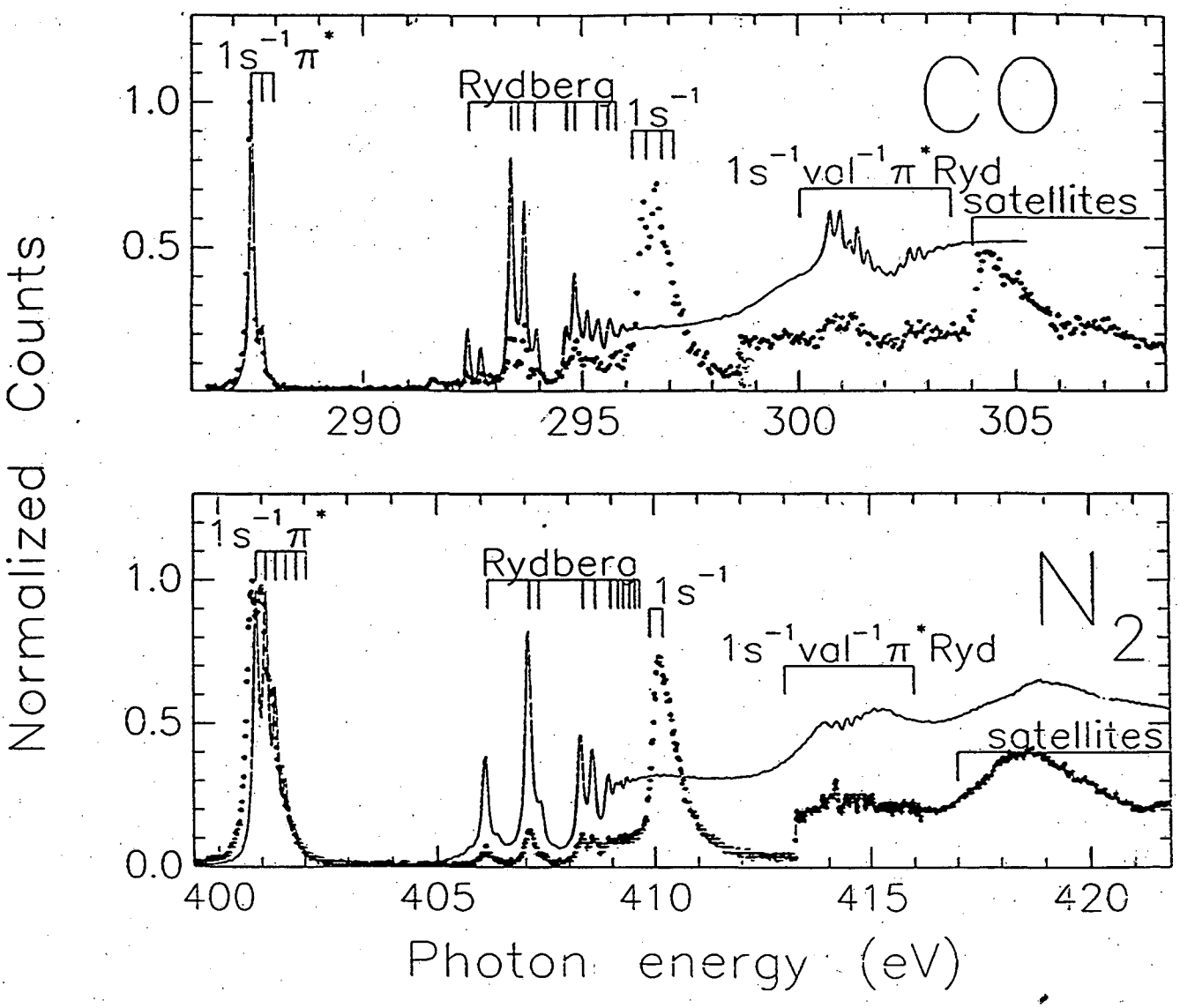
Normalized Counts
1s⁻¹π*
Rydberg
1s⁻¹
CO
1s⁻¹val⁻¹π*Ryd
satellites
1.0
0.5
290
295
300
305
1s⁻¹π*
Rydberg
1s⁻¹
N2
1s⁻¹val⁻¹π*Ryd
satellites
1.0
0.5
0.0
400
405
410
415
420
Photon energy (eV)

XBL 911-129

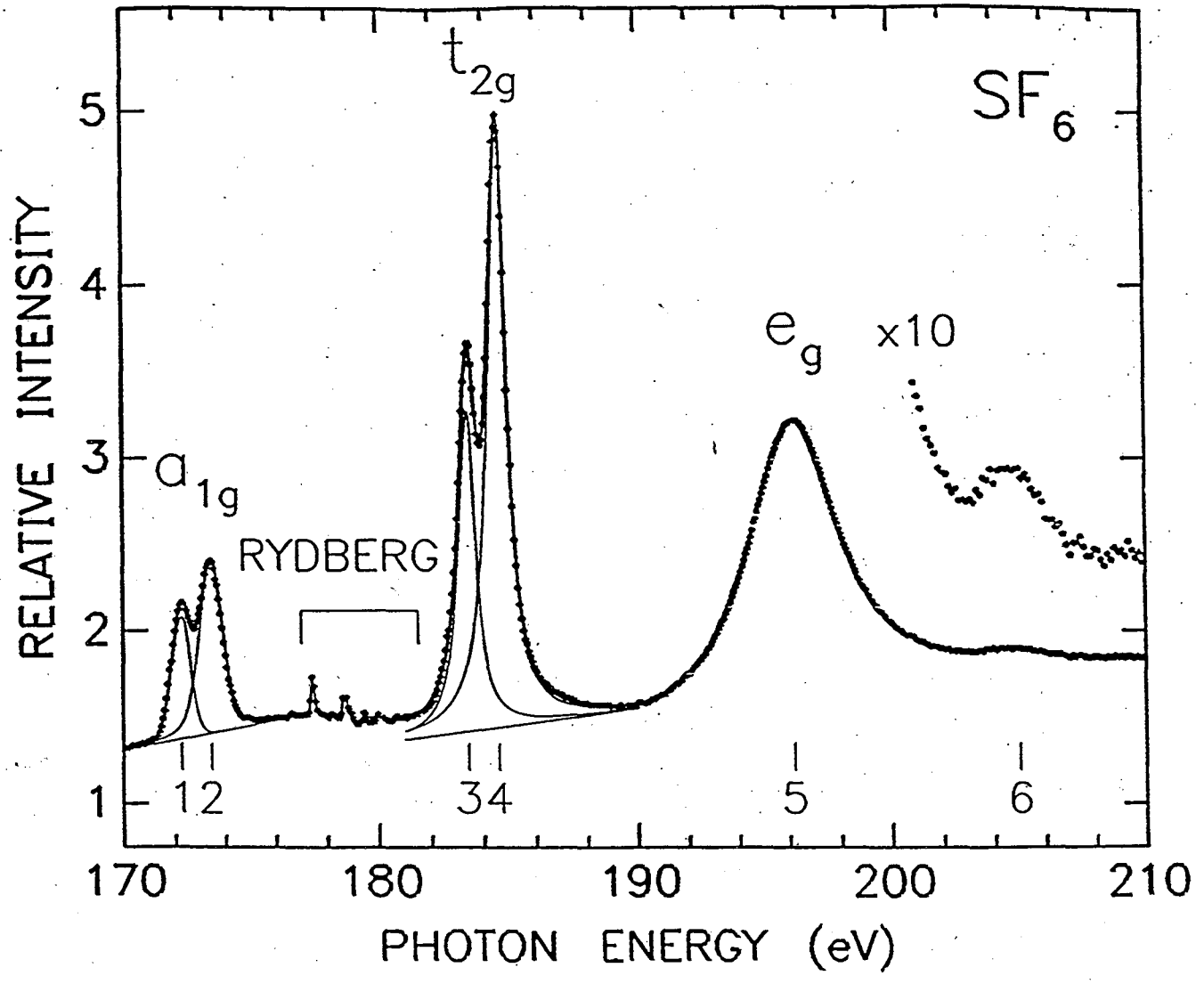
t_{2g}
SF_6
e_g
x10
a_{1g}
RYDBERG
1 2
3 4
5
6
RELATIVE INTENSITY
PHOTON ENERGY (eV)
1
2
3
4
5
170
180
190
200
210

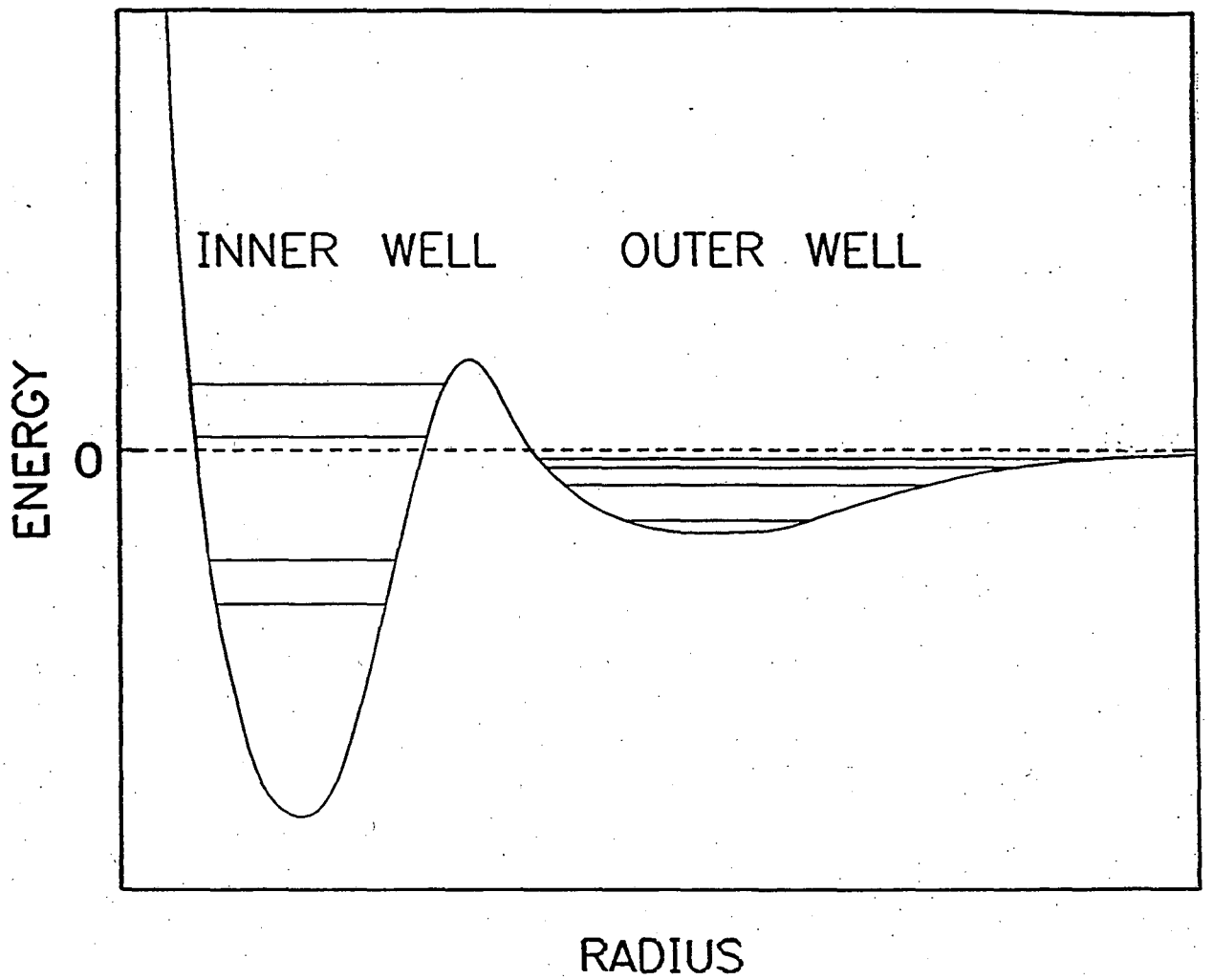
INNER WELL
OUTER WELL
ENERGY
0
RADIUS

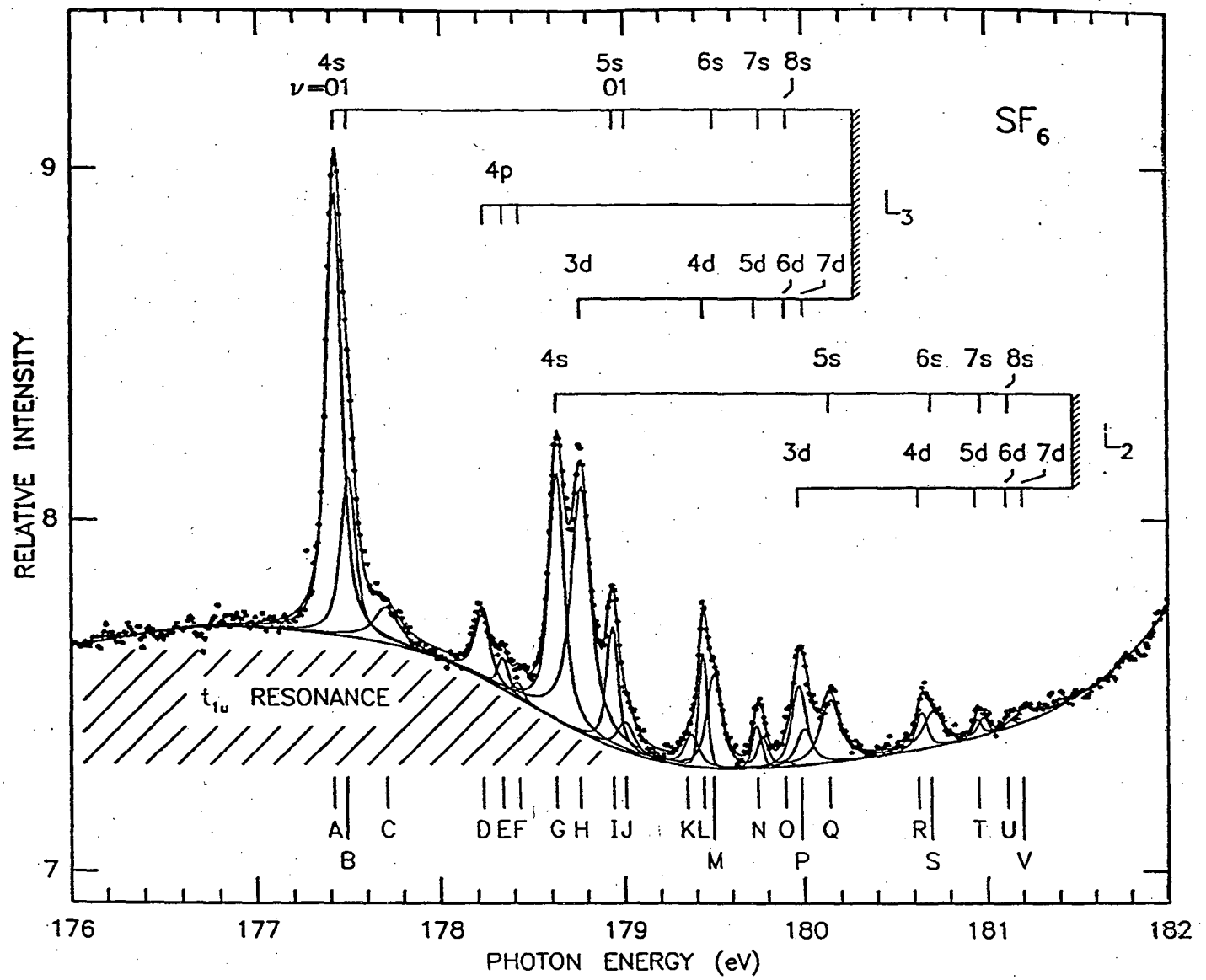
4s
ν=01
5s
01
6s 7s 8s
SF6
4p
L3
3d
4d 5d 6d 7d
4s
5s
6s 7s 8s
3d
4d 5d 6d 7d
L2
t1u RESONANCE
A
B
C
D E F
G H
I J
K L
M
N O
P
Q
R
S
T U
V
RELATIVE INTENSITY
9
8
7
176
177
178
179
180
181
182
PHOTON ENERGY (eV)

BESSY

Berliner Elektronenspeicherring-Gesellschaft
für Synchrotronstrahlung mbH

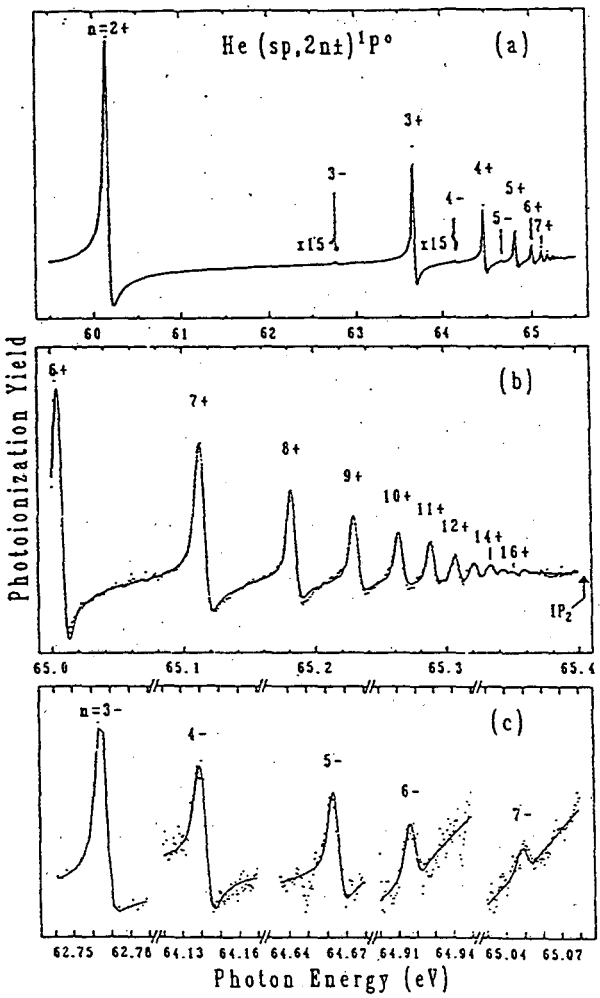

Jahresbericht 1990

III. C. $E/\Delta E \approx 10^4$ with a TGM

(M. Howells, Z. Hussain, T. Reich, ...)

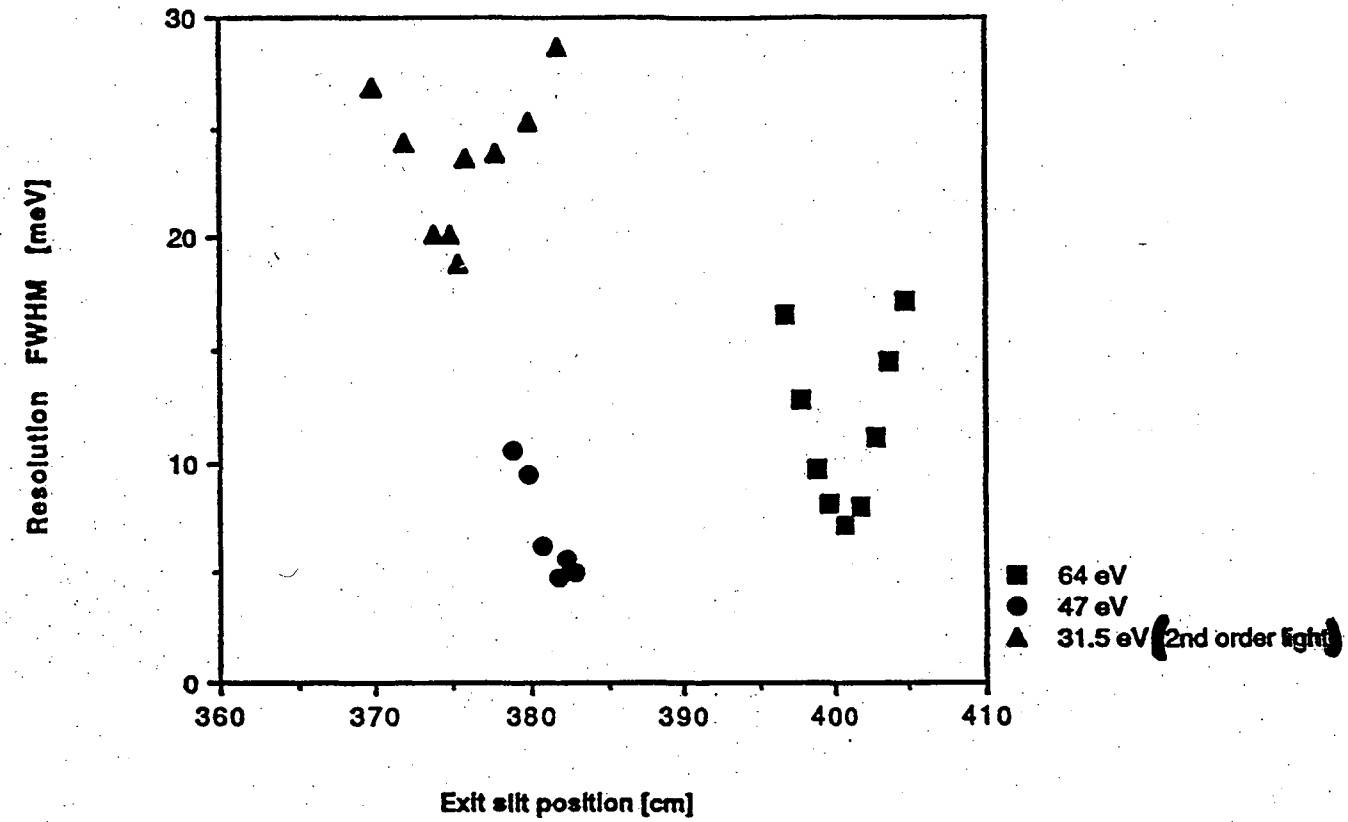
Resolution FWHM [meV]
30
20
10
0
360
370
380
390
400
410
Exit slit position [cm]
64 eV
47 eV
31.5 eV (2nd order light)

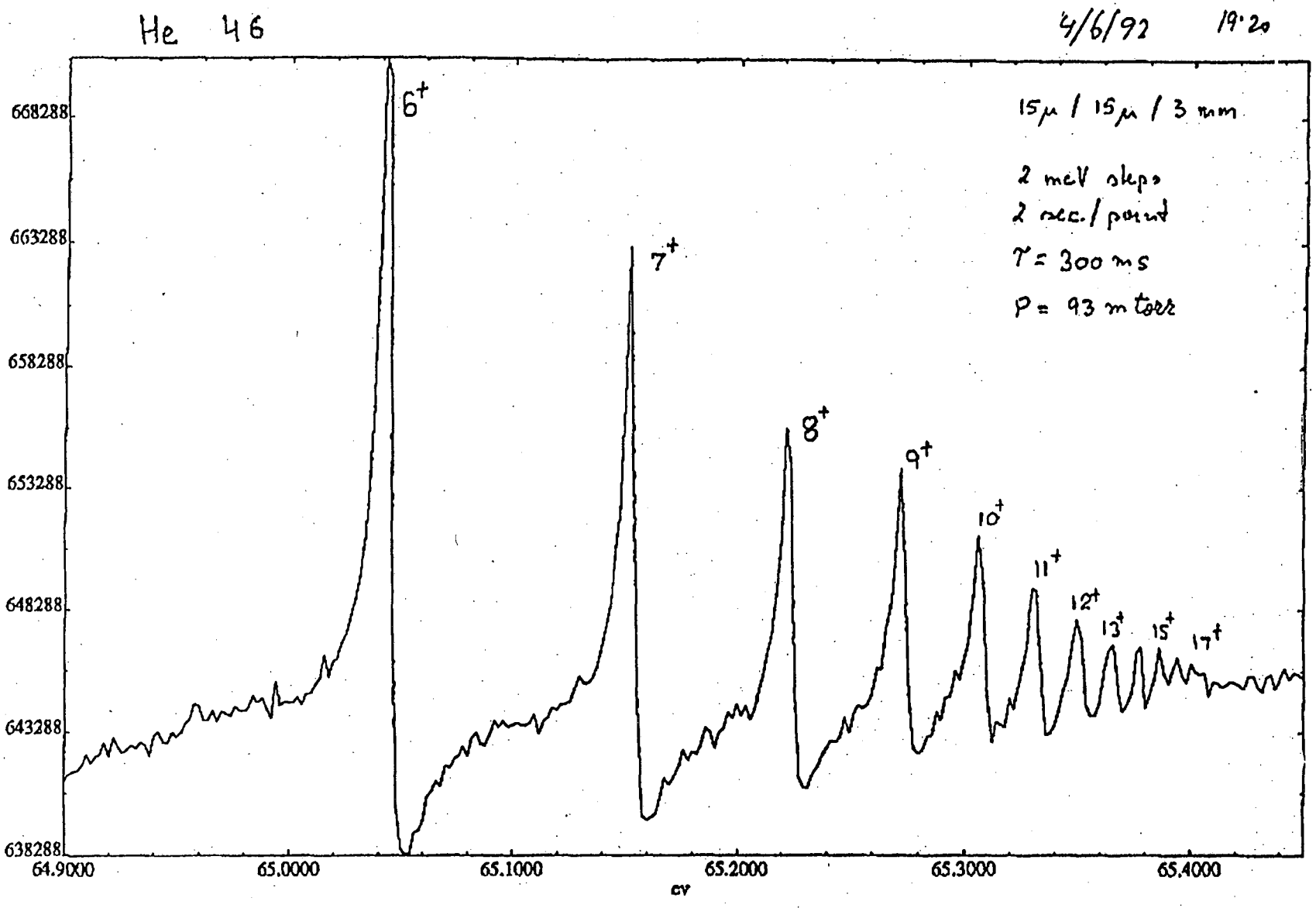
He 46
4/6/92 19:20
15μ / 15μ / 3 mm
2 meV steps
2 sec./point
τ = 300 ms
P = 93 m torr
6+
7+
8+
9+
10+
11+
12+
13+
15+
17+
668288
663288
658288
653288
648288
643288
638288
64.9000
65.0000
65.1000
65.2000
65.3000
65.4000
cv
I_TOTAL

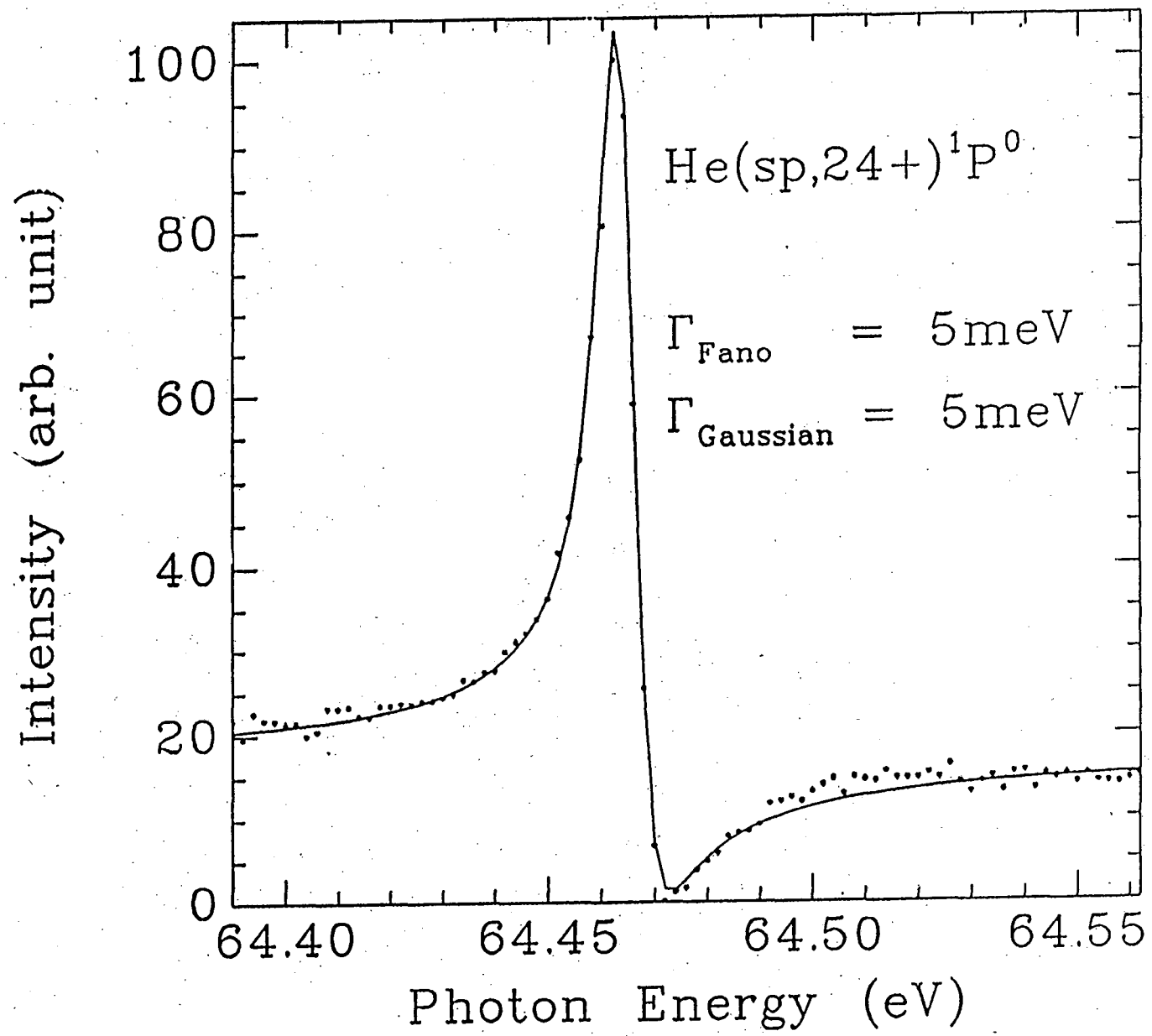
100
80
60
40
20
0
64.40
64.45
64.50
64.55
Intensity (arb. unit)
Photon Energy (eV)
He(sp,24+)$^1P^0$
Γ_{Fano} = 5meV
$\Gamma_{Gaussian}$ = 5meV

IV. More on He^{**}, and on to 10^6!

Excited States of Helium

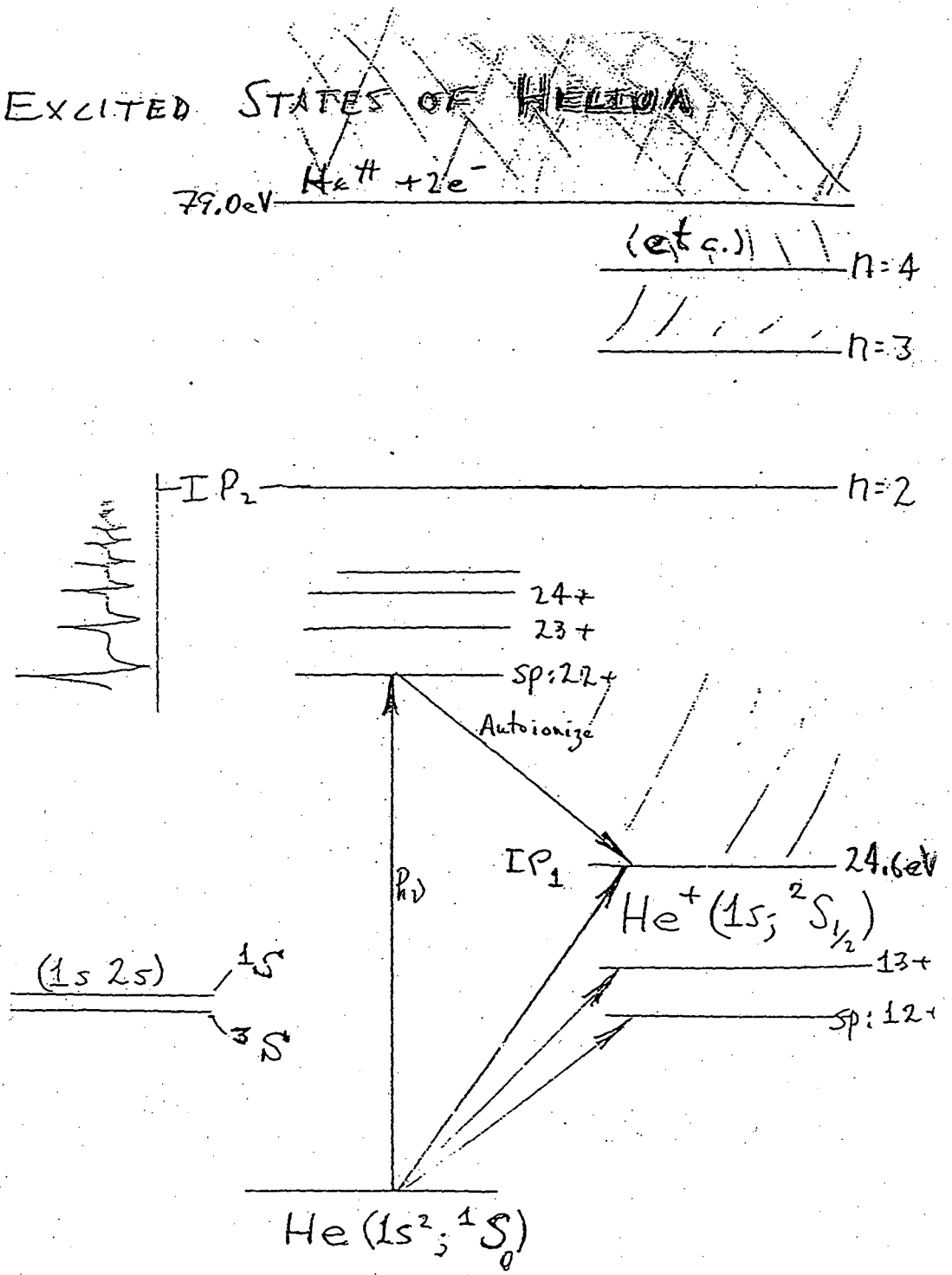

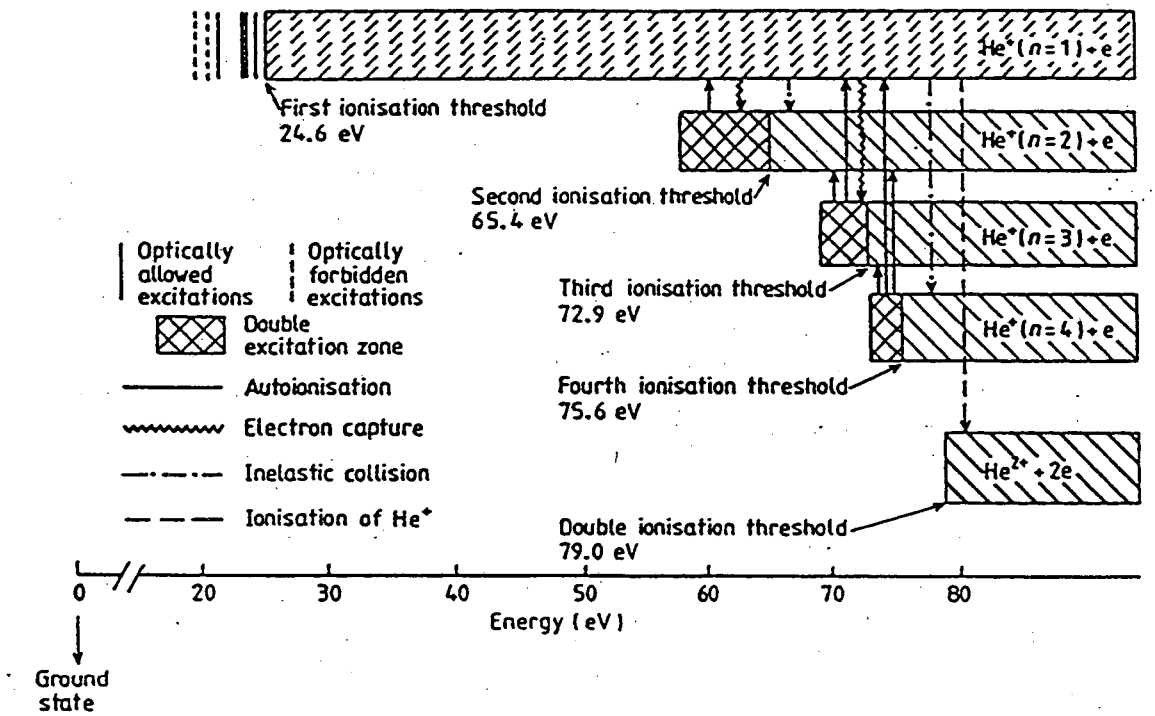

Figure 1. Diagram showing increasing number of channels in the spectrum of helium and their interconnection by autoionisation and other processes (Fano 1969).

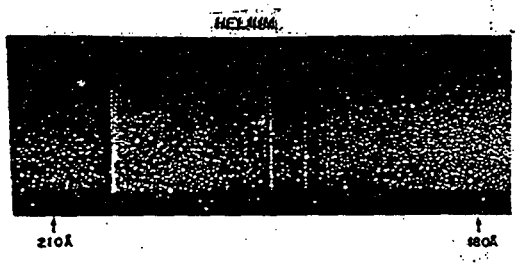
HELIUM
210Å
180Å

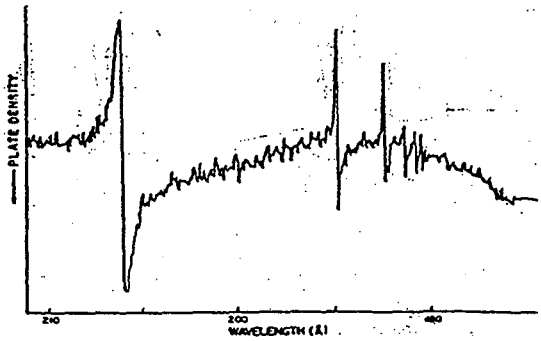
PLATE DENSITY
WAVELENGTH (Å)

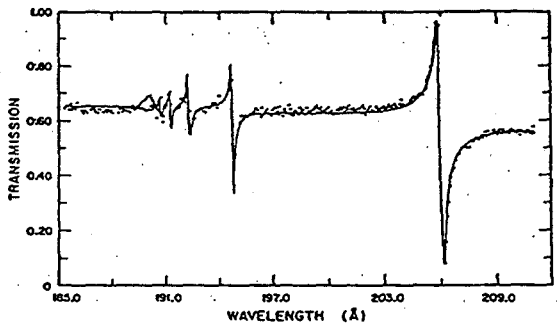
TRANSMISSION
WAVELENGTH (Å)

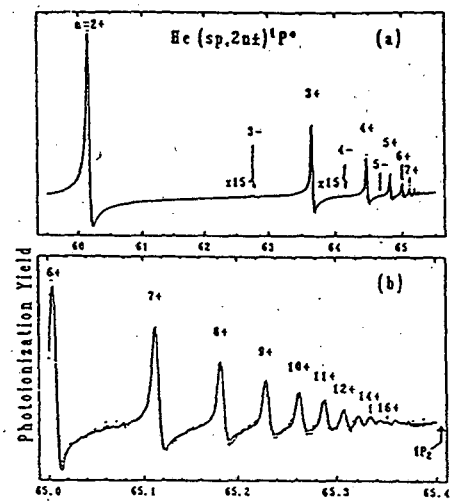
He (sp,2nℓ)¹P°
(a)
(b)
Photoionization Yield

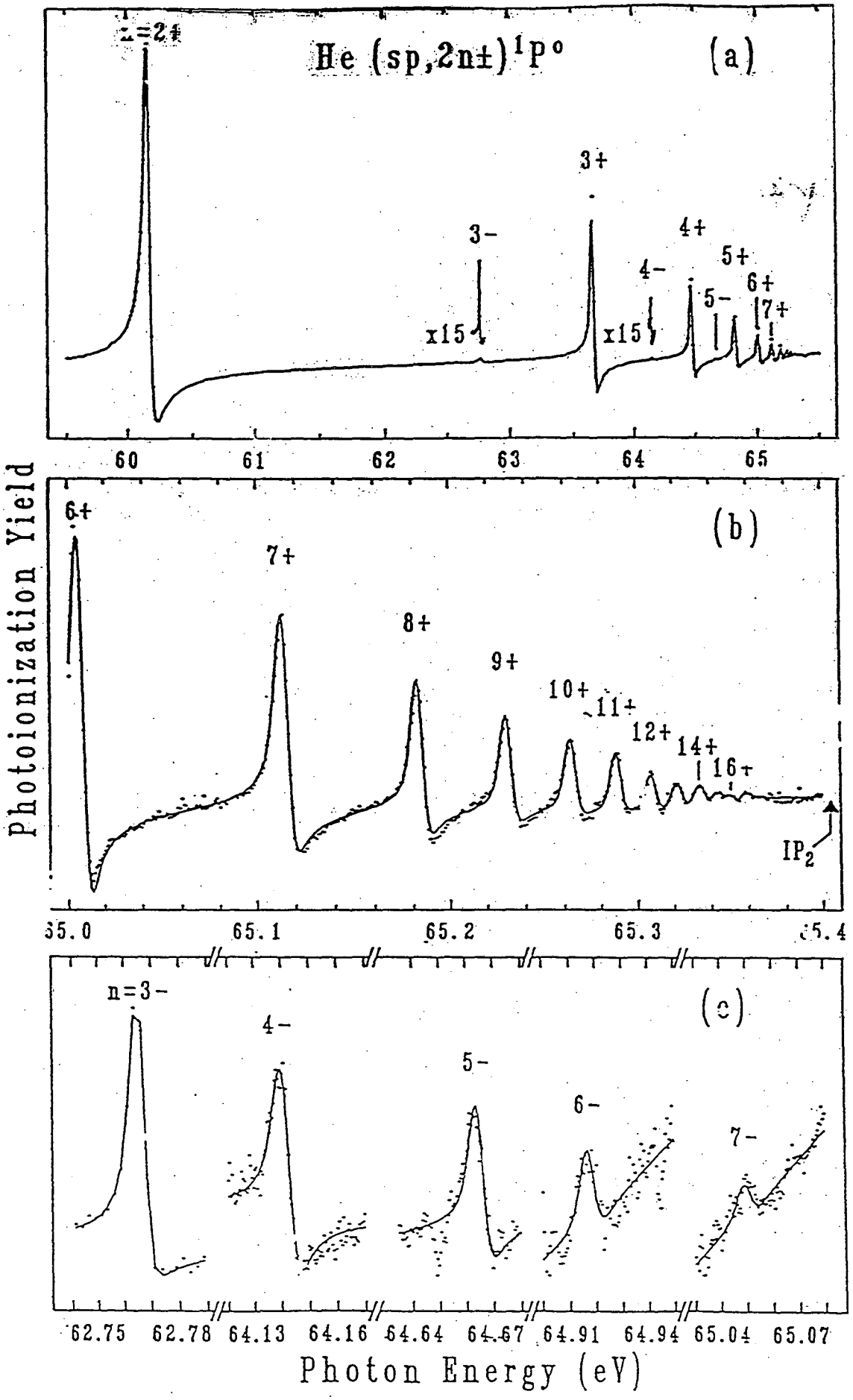
He (sp,2n±)¹P°
(a)
n=2+
3+
3-
4+
4-
5+
5-
6+
7+
x15
x15
60
61
62
63
64
65
(b)
6+
7+
8+
9+
10+
11+
12+
14+
16+
IP2
65.0
65.1
65.2
65.3
(c)
n=3-
4-
5-
6-
7-
62.75
62.78
64.13
64.16
64.64
64.67
64.91
64.94
65.04
65.07
Photoionization Yield
Photon Energy (eV)

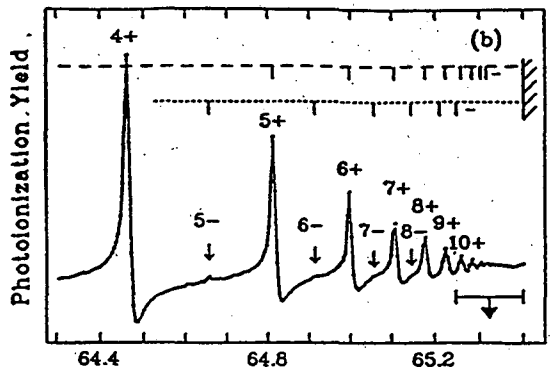
Photolonization Yield
(b)
4+
5+
6+
7+
8+
9+
10+
5−
6−
7−
8−
64.4
64.8
65.2

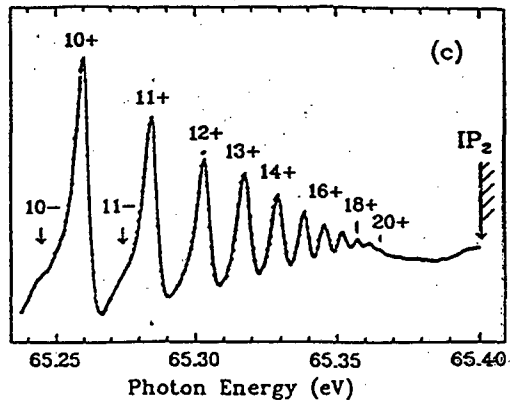
(c)
10+
11+
12+
13+
14+
16+
18+
20+
IP2
10−
11−
65.25
65.30
65.35
65.40
Photon Energy (eV)

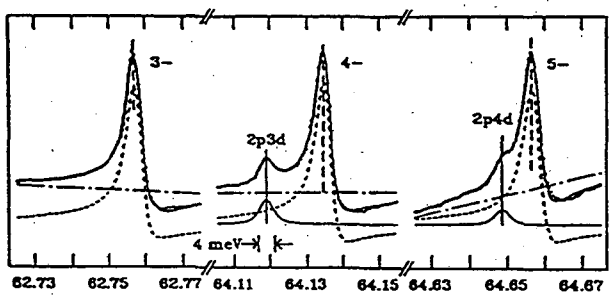
3−
4−
5−
2p3d
2p4d
4 meV
62.73
62.75
62.77
64.11
64.13
64.15
64.63
64.65
64.67

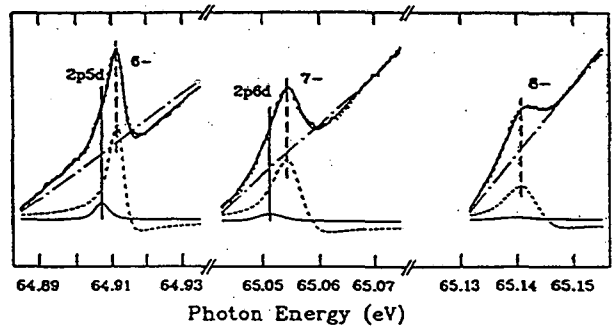
2p5d
6−
2p6d
7−
8−
64.89
64.91
64.93
65.05
65.06
65.07
65.13
65.14
65.15
Photon Energy (eV)

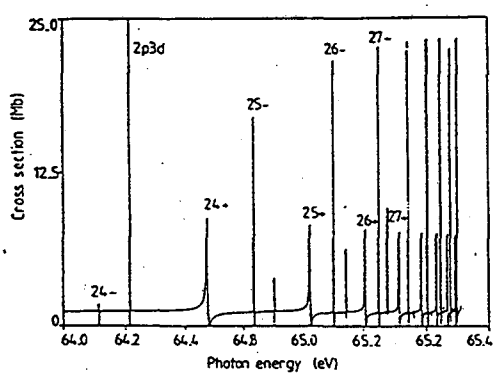
25.0
12.5
0
Cross section (Mb)
2p3d
24−
24+
25−
25+
26−
27−
64.0
64.2
64.4
64.8
65.0
65.2
65.2
65.4
Photon energy (eV)

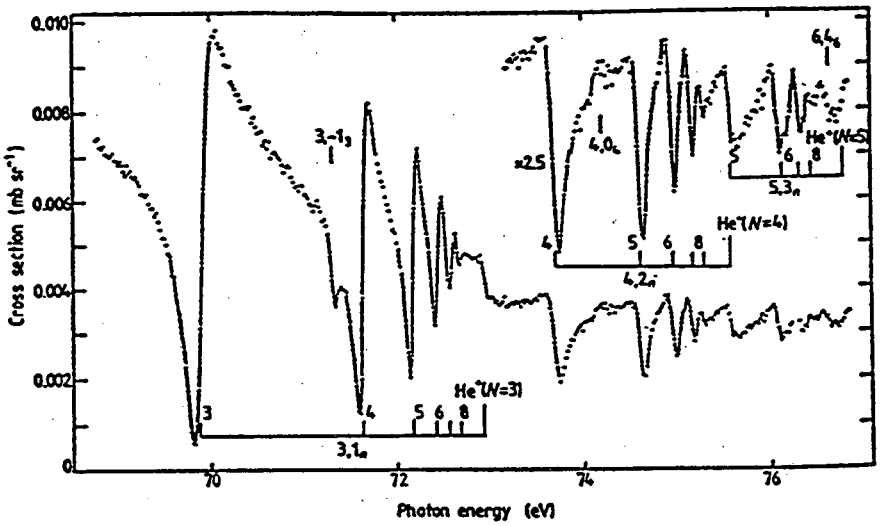
Cross section (mb sr⁻¹)
Photon energy (eV)
He⁺(N=3)
He⁺(N=4)
He⁺(N=5)
×2.5

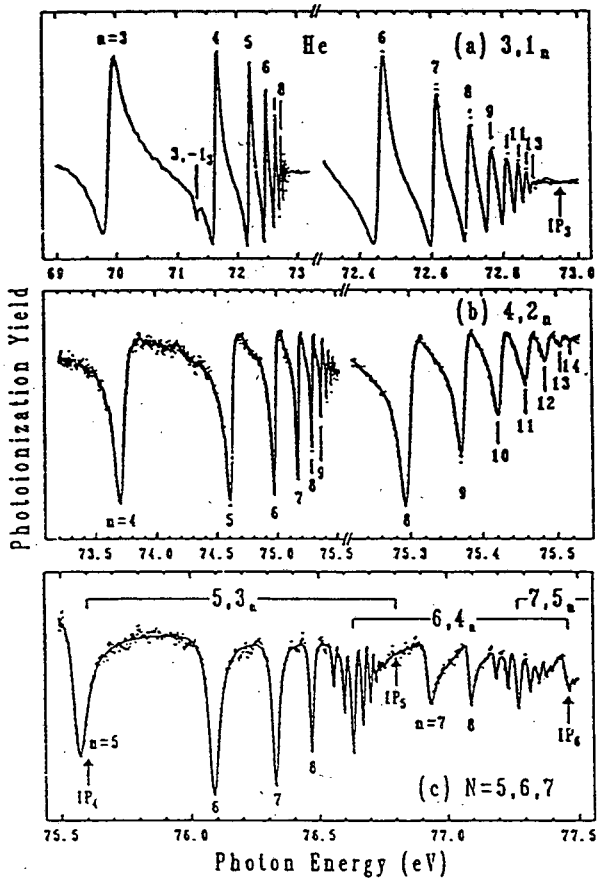
He
(a) 3,1n
(b) 4,2n
(c) N=5,6,7
Photoionization Yield
Photon Energy (eV)

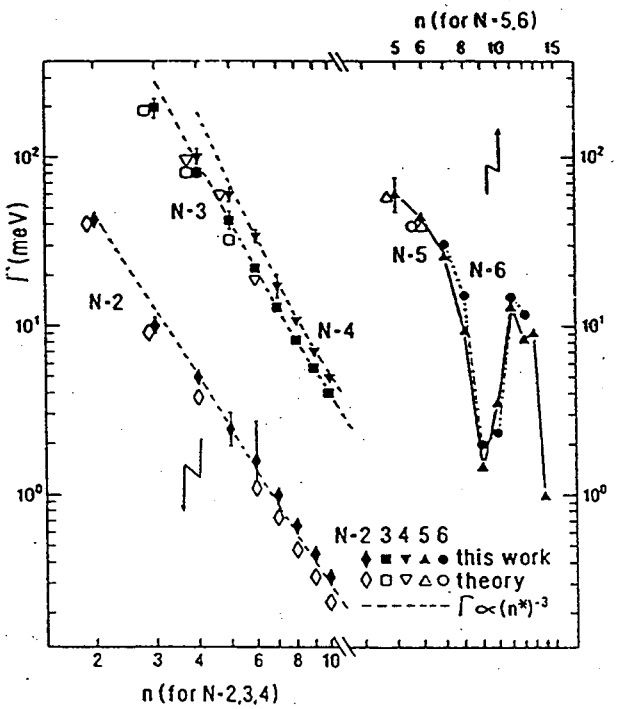
n (for N-5,6)
n (for N-2,3,4)
Γ (meV)
N-2
N-3
N-4
N-5
N-6
N-2 3 4 5 6
this work
theory
Γ∝(n*)⁻³

ever, the upper entries in the families remain physically meaningful—identified, in fact, by an experimental arrangement that detects the electron at infinity together with the state of excitation of the residue—whereas the lower entries are now no longer eigenstates. The difference lies in that, for the top entries, the two electrons are separated to infinity where e^2/r_{12} vanishes, whereas for the bottom entries r_{12} is finite, thus invalidating the independent electron labels. Bottom entries drawn from different families in Eq. 2 that share the same {S, L, J, π} but differ only in N and n are mixed by the electron-electron interaction with the result that the physical eigenstates are linear combinations of various independent particle configurations. (Incidentally, only the nonseparable portion of the interaction is responsible for this mixing and therefore for the contrast between top and bottom entries.) Turning to the quark families, we see again that the top members are unchanged (this is a standard choice), only the bottom ones getting mixed as in Eq. 3 upon the superposition of electroweak and strong interactions. The analogy may suggest a dynamical explanation in terms of an underlying substructure of quarks ("ur-quarks"?). Suppose, as in the atomic example of three charged particles, the quarks themselves are composites of three ur-quarks. A distinction can then be made between two types of composites of the three ur-quarks, depending on whether one pair of relative distances vanishes (recall an inversion in the nature of chromodynamics relative to electrodynamics, that the interaction vanishes when distances go to zero rather than to infinity). One type, with a pair of ur-quarks having zero separation, would correspond to the u, c, and t, while a second, in which all pairs are finitely separated, to the d, s, and b. In the language of atomic physics, the switching on of interactions between the ur-quarks causes "configuration mixing" of the d, s, and b as given by the KM matrix in Eq. 3.

Experimental Data on Doubly Excited Atoms

This section gives a brief review of experiments on doubly excited states over the last 20 years. It is designed to highlight those key features of the data that will be picked up in the next section to draw lessons on the family structure and on the hierarchical coupling between families of states of the three-body atomic system.

Excitation by photons. The simple sketch in Fig. 1 of two-electron states also shows how they may be excited and observed in the laboratory. One method is photoabsorption from the ground state of H^-, or He, in an energy range below the detachment or ionization thresholds H(N) or $He^+(N)$. Against the background of the absorption into the one-electron continuum of the first family, structures appear in the absorption cross section at specific energies marking the positions of doubly excited states. The first doubly excited states in atoms were observed in this way in He (*13*), utilizing synchrotron light from electron synchrotrons that provide photons of the requisite energy (≈60 eV or 20 nm). States of $^1P_1^o$ symmetry of the $N = 2$ family in Eq. 2 were observed as a Rydberg sequence of resonances converging to the $He^+(N = 2)$ limit, which lies $24.6 + 54.4(1 - 1/4) = 65.4$ eV above the ground state of He. Experiments with synchrotron light in many other atoms have since been designed to study such sequences of doubly excited states, typically with relatively small values of N (*14*). The most recent data (*15*) through $N = 6$ are shown in Fig. 3. States of much larger N have not been observed. This is not because of any lack of photon energy in synchrotron sources but more a reflection of the weakness of excitation to such N as will be discussed.

Lasers provide much higher resolution, and stepwise absorption of multiple laser photons has reached doubly excited states in more complex atoms, particularly in the alkaline earths such as barium. However, the lowest quasi-bound states within a family when N is large have remained out of reach. As typical examples, when N is 4 or 5, the states observed can be attributed to principal quantum numbers n larger than 10 for the second electron (*16*), or, when N is 20, the values of n are 40 or larger (*17*). That is, the doubly excited states of high excitation that have been studied through multiple laser photoabsorption have a very unequal energy sharing between the two electrons. States in which the two electrons have comparable radial excitation, which are the lowest members of each column in Eq. 2 or in Fig. 1, have remained elusive to such laser experimental searches, the best results being those in (*18*).

The longest sequence of comparably excited states seen in photoabsorption is from a very recent study on H^- at LAMPF (*3*, *4*). (In such particle physics laboratories, H^- is often the initial charged species that is accelerated. Later, upon stripping of the two electrons, proton beams and subsidiary meson or neutrino beams are generated.) In a very innovative use of the relativistic beam of H^- (≈800 MeV) for atomic physics studies, Howard Bryant and his colleagues have studied various aspects of this atomic negative ion (*19*). The recent ex-

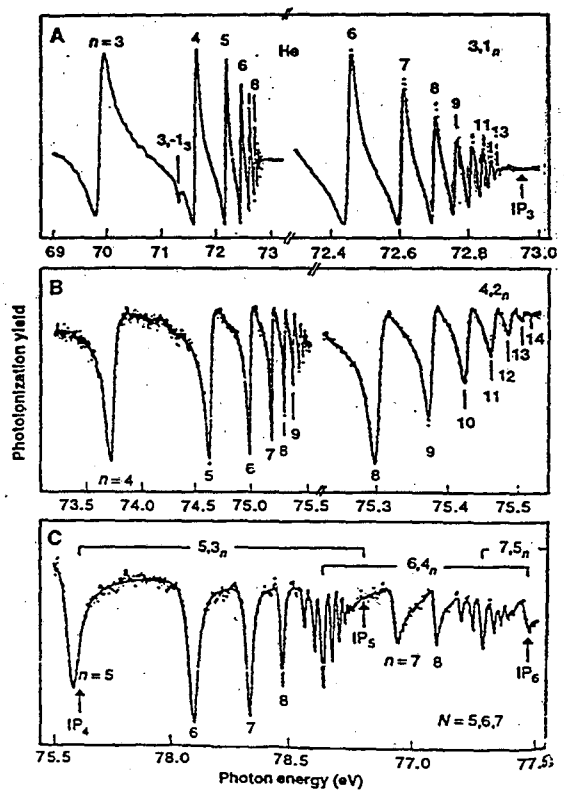

Fig. 3. (A) He($N = 3$, n), (B) He($N = 4$, n), and (C) He($N = 5$, n) and He($N = 6$, n) $^1P^o$ doubly excited states seen in photoabsorption with synchrotron light. Panels (A) and (B) include on the right a magnified high n region. [From (*15*), with permission]

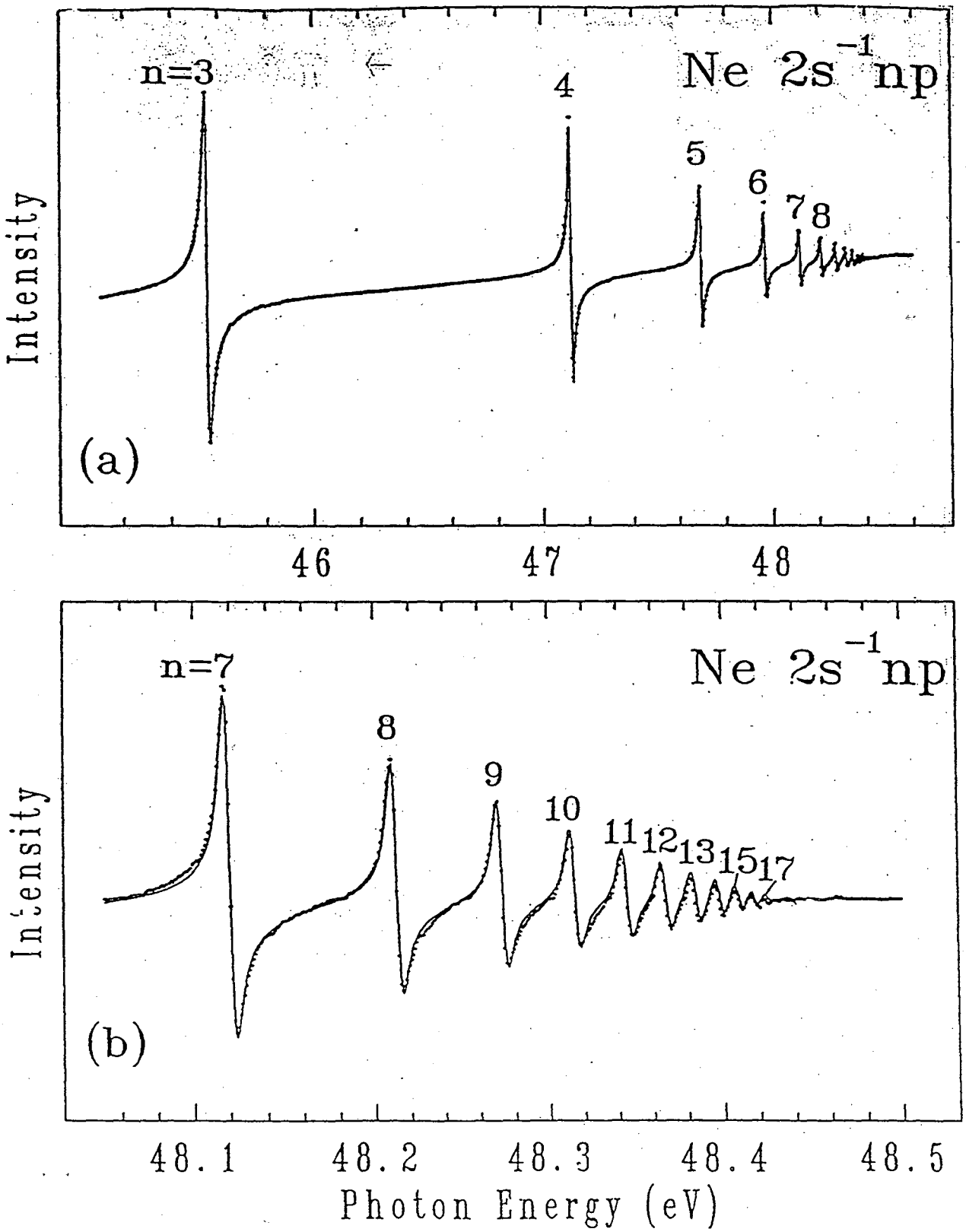
n=3
4
5
6
7
8
Ne 2s^{-1}np
Intensity
(a)
46
47
48
n=7
8
9
10
11
12
13
15
17
Ne 2s^{-1}np
Intensity
(b)
48.1
48.2
48.3
48.4
48.5
Photon Energy (eV)

Fourier Transform Spectroscopy: A Sketch Map to Lyman Alpha and Beyond

Anne Thorne

Imperial College, U.K.

FTS: a sketch map to Lyman α and beyond --

Anne Thorne, Imperial College

Basics of FTS

- resolution & wavenumber accuracy
- sampling & aliasing
- signal to noise ratios

Practical points about interferometers

- tolerances
- sampling accuracy
- field of view
- band limiting

Progress towards Lyman α

- problems & results to date

Beyond Lyman α ??

Fourier transform spectrometry

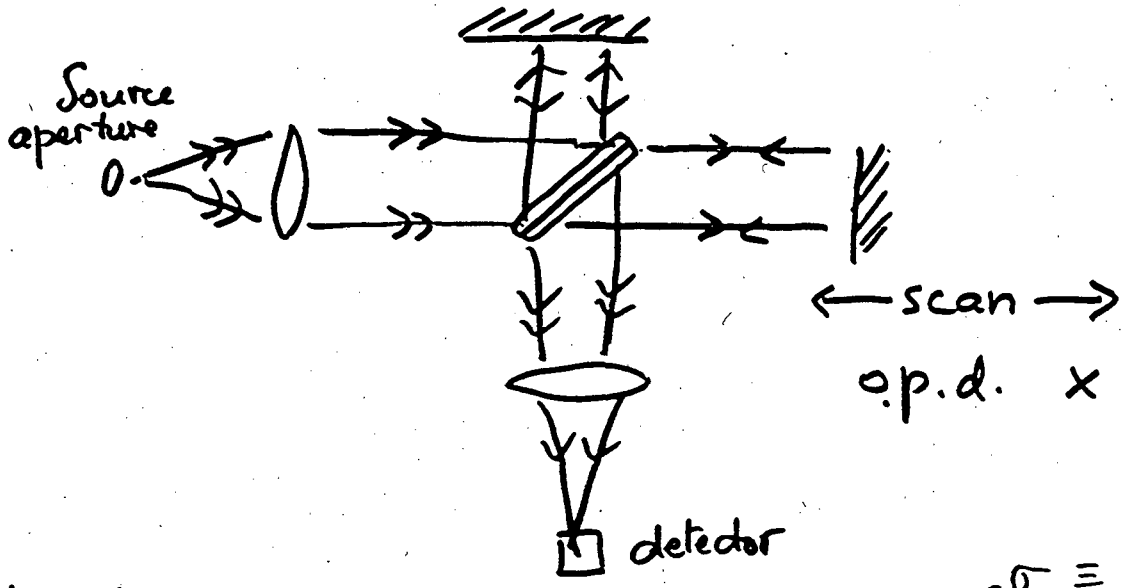

Monochromatic: ($\sigma \equiv 1/\lambda$)

$$I(x) = B(\sigma_0)(1 + \cos 2\pi\sigma_0 x)$$

Source distrib. $B(\sigma)$:

$$I(x) = \int B(\sigma)(1 + \cos 2\pi\sigma x)\, d\sigma$$

Subtract mean $\int B(\sigma)\, d\sigma$:

$$I(x) = \int B(\sigma) \cos 2\pi\sigma x\, d\sigma$$

$\Downarrow$ FFT

$$B(\sigma) = \int I(x) \cos 2\pi\sigma x\, dx$$

Practical modifications

(1) The interferogram is digitally sampled at intervals Δx, so $\int \Rightarrow \sum$

(2) The interferogram is never entirely symmetric, so it is necessary to take the complex F.T.

$$B(\sigma) = \sum_{n=-M}^{n=N} I(n\Delta x)\, e^{-2\pi i \sigma n \Delta x}$$

Note In continuous scanning mode the interferometer converts optical freq. ν to audio frequency f

where $f = \frac{v}{c}\nu$ ($v = \frac{1}{2}$ mirror vel.)

and $f = v\sigma$

Grating vs. F.T. Spectrometer

Grating

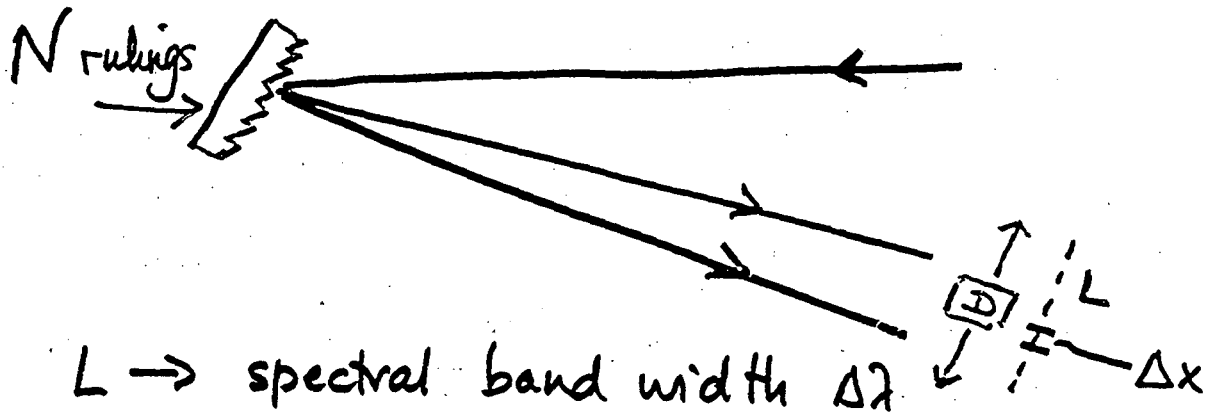

$L \rightarrow$ spectral band width $\Delta\lambda$

$\Delta x \rightarrow$ spectral resolution $\delta\lambda$

$R = N$ (1st order)

FTS

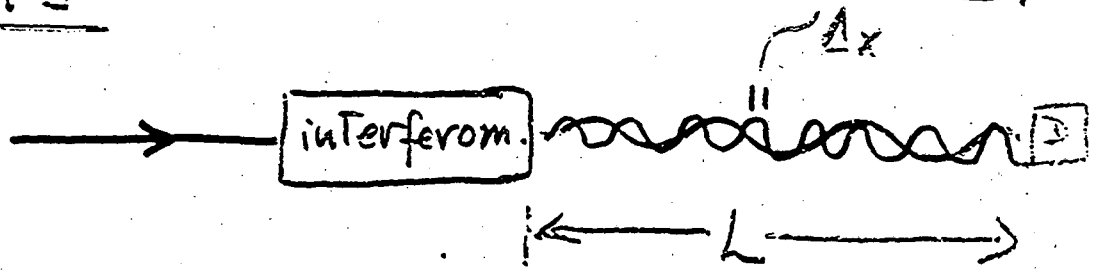

Spatial modulation freq. $\propto \sigma \left(= 1/\lambda\right)$

$L \rightarrow$ spectral resolution

$$\delta\sigma = \frac{1}{2L} \text{ cm}^{-1}$$

$\Delta x \rightarrow$ free spectral range

$$\Delta\sigma = \frac{1}{2\Delta x} \text{ cm}^{-1}$$

N samples $\left(= \frac{L}{\Delta x} = \frac{\Delta\sigma}{\delta\sigma}\right)$

$R = N$ (1st alias)

The principal advantages of FTS

(versus grating spectrometry)

1. Multiplex (Fellgett)

X applies in I.R. where detector noise is independent of signal

gain $\sqrt{N}$ in signal/noise

2. Throughput (Jacquinot)

X applies in vis/UV when noise is photon-limited & also in I.R.

gain ~ 100 in signal/noise IR

~ 10 " " " vis/UV

3. Wavelength (Connes)

always applies

all wavelengths in Terms of reference (He-Ne) laser

4. Resolution

can always be made to exceed grating

$$R = \lambda/\delta\lambda = L/\lambda$$

(±) Spectral coverage

All lines (& background) necessarily recorded.

The principal disadvantages

(±) Spectral coverage
can be disadvantage if only 1 or 2 lines of interest

(±) Noise distribution
Random noise is "white": spectrum has almost uniform noise everywhere

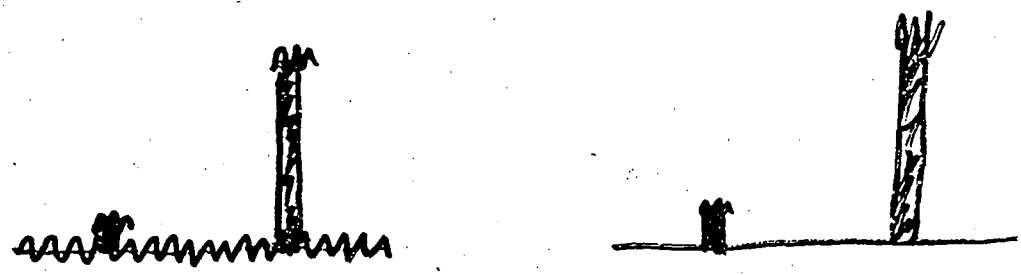

FTS — $\frac{S}{n}$ relatively worse for weak lines

Grating

Conceit of doing a FT of the noise — not the multiplex disadvantage

The wavelength (Connes) advantage

The wavenumber scale in the FT is derived directly from the sampling intervals

— in practice from the wavelength of the reference laser

$\Rightarrow$ accurately <u>linear</u> wavenumber scale

There is still a scaling factor for absolute accuracy of order $1/R$

ie. scaling factor $\frac{\Delta\sigma}{\sigma} \sim 1:10^5 - 10^6$

Calibration

Plot $\frac{\sigma_{meas} - \sigma_{ref}}{\sigma}$ vs. σ

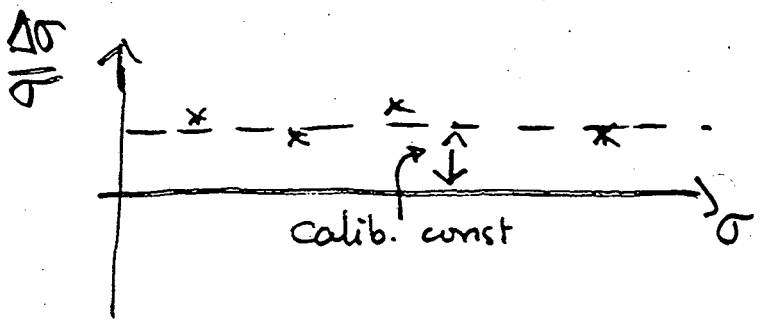

<u>Note</u> in contrast to grating in principle <u>one line</u> required as ref. for whole spectrum.

Resolution — how high?

Doppler width $\frac{\delta\lambda_D}{\lambda} = 7 \times 10^{-7} \sqrt{\frac{T}{M}}$

so for $T \sim 2000$

with $M \sim 60$ $\quad \frac{\lambda}{\Delta\lambda_D} \sim 250\,000$

For negligible instrumental contribution

$$\delta\lambda \leq \frac{1}{2} \Delta\lambda_D$$

$$\Rightarrow R \geq 500\,000$$

For heavy elements or for gases at room temperature

$$R > 1\,000\,000$$

$\Rightarrow$ resolving power

300 000 to 1 500 000

Relation between $\left(\frac{S}{n}\right)_{interf.}$ and $\left(\frac{S}{n}\right)_{spect.}$

For <u>N points</u> (independent) in both interf. and spectrum and for <u>white noise</u> (independent of frequency)

$$\left(\frac{\bar{S}}{n}\right)_{sp} = \frac{1}{\sqrt{N}} \left(\frac{S_0}{n}\right)_{int}$$

$\therefore$ for a local signal s,

$$\frac{S}{n} = \frac{S}{\bar{S}} \frac{1}{\sqrt{N}} \left(\frac{S_0}{n}\right)_{int}$$

$$\frac{S}{\bar{S}} = \frac{\text{peak}}{\text{mean}} = \frac{1}{\text{filling factor}} \equiv \alpha$$

$$1 \leq \alpha \leq N$$

Quasi-continuum: $\alpha = 1$ $\quad \frac{S}{n} = \frac{1}{\sqrt{N}} \left(\frac{S_0}{n}\right)_{int}$

One single unresolved line: $\alpha = N$ $\quad \frac{S}{n} = \sqrt{N} \left(\frac{S_0}{n}\right)_{int}$

Normal "emission spectrum: $\alpha < 1\%$ $\quad \frac{S}{n} \sim \left(\frac{S_0}{n}\right)_{int}$

<u>Noise distribution</u>

<u>Grating</u> noise is where the lines are

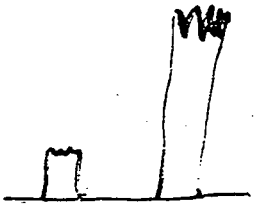

<u>FTS</u> "white" noise – the same everywhere

Sampling & aliasing

Free spectral range σ_{max} determined by sampling interval Δx

$$\sigma_{max} = \frac{1}{2\Delta x} \quad (= FSR\ \Delta\sigma)$$

(cf Nyquist : $\Delta x = \frac{1}{2}\lambda_{min}$)

Discrete FT repeats + & − spectral pairs at intervals $1/\Delta x$, or $2\Delta\sigma$.

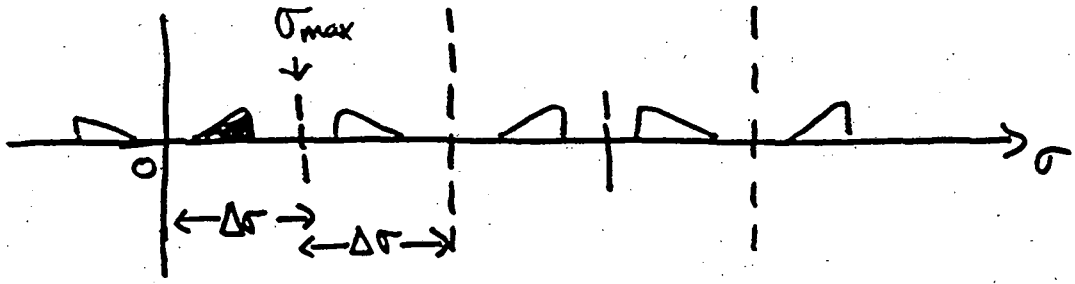

Under sampling ⟹ aliasing

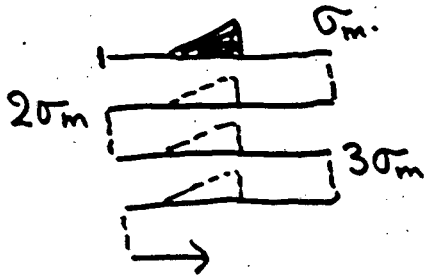

Nyquist sampling

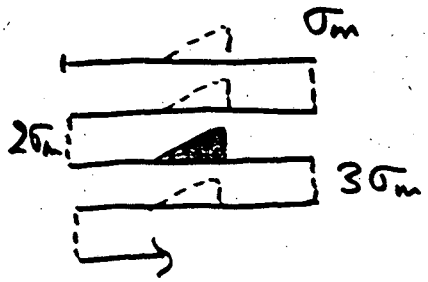

3x undersampled

BEWARE

- Superposition of SIGNALS from other aliases
- Superposition of NOISE from all aliases

Final S/n for the photon-limited case

Emission

resolution $\delta\sigma$ cm^{-1}

modulation m

filter transm. τ

total time T

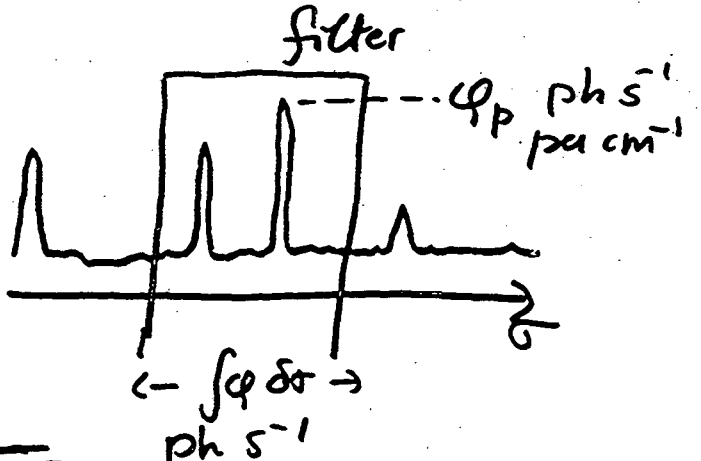

$$\frac{S_p}{n} = m \cdot \delta\sigma \, \varphi_p \sqrt{\frac{\tau T}{\int_{\text{filter}} \varphi \, \delta\sigma}}$$

Absorption

$$\frac{S}{n} = m \, \delta\sigma \sqrt{\frac{\varphi_c \tau T}{w}}$$

$$= m \cdot \delta\sigma \cdot \varphi_c \sqrt{\frac{\tau T \varphi_c}{\varphi_c w}}$$

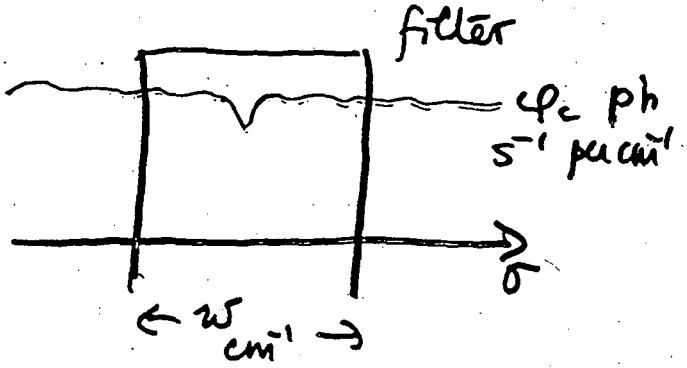

The I.C. VUV FTS

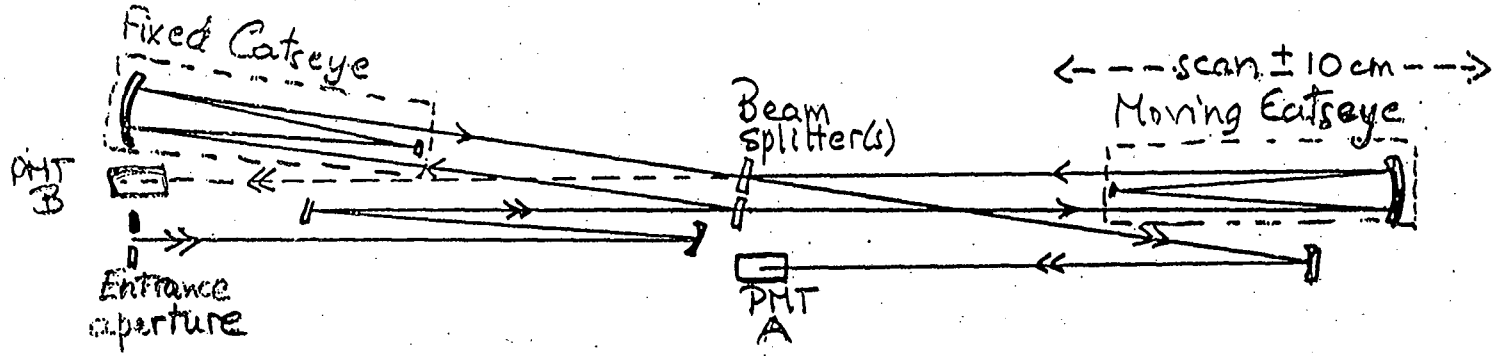

Parameters : rel. aperture f/25
entrance aperture 1·4 mm diam. for $\mathcal{R} \sim 10^6$
max. optical path diff. 20 cm $\Rightarrow \delta\sigma = .025\,cm^{-1}$
dimensions of vacuum tank 1500 x 250 x 250 mm.
present short wavelength limit ~ 1750 Å
(due to spectrosil beam splitter)

Tolerances for UV FTS

(each to give ~80% modulation)

Optical surfaces ($\lambda/8$)

(use of catseyes instead of plane mirrors reduces tilt requirement by ~ 10.)

	500 nm	200 nm	
Surfaces	60 nm	25 nm	≡ 1 micro inch
Catseye focus	100 μm	40 μm	
Drive : tilt	12 ″	5 ″	
shear	25 μm	10 μm	= $\frac{1}{2}$ x 1 thou.
Sample step	.25 nm	.1 nm	

Input focal ratio f/25
Input aperture 1–2 mm diam.
Maximum resolution 0.025 cm^{-1} ($R = 2 \times 10^6$ at 200 nm)

Physical size 1.5 m × 25 cm × 25 cm

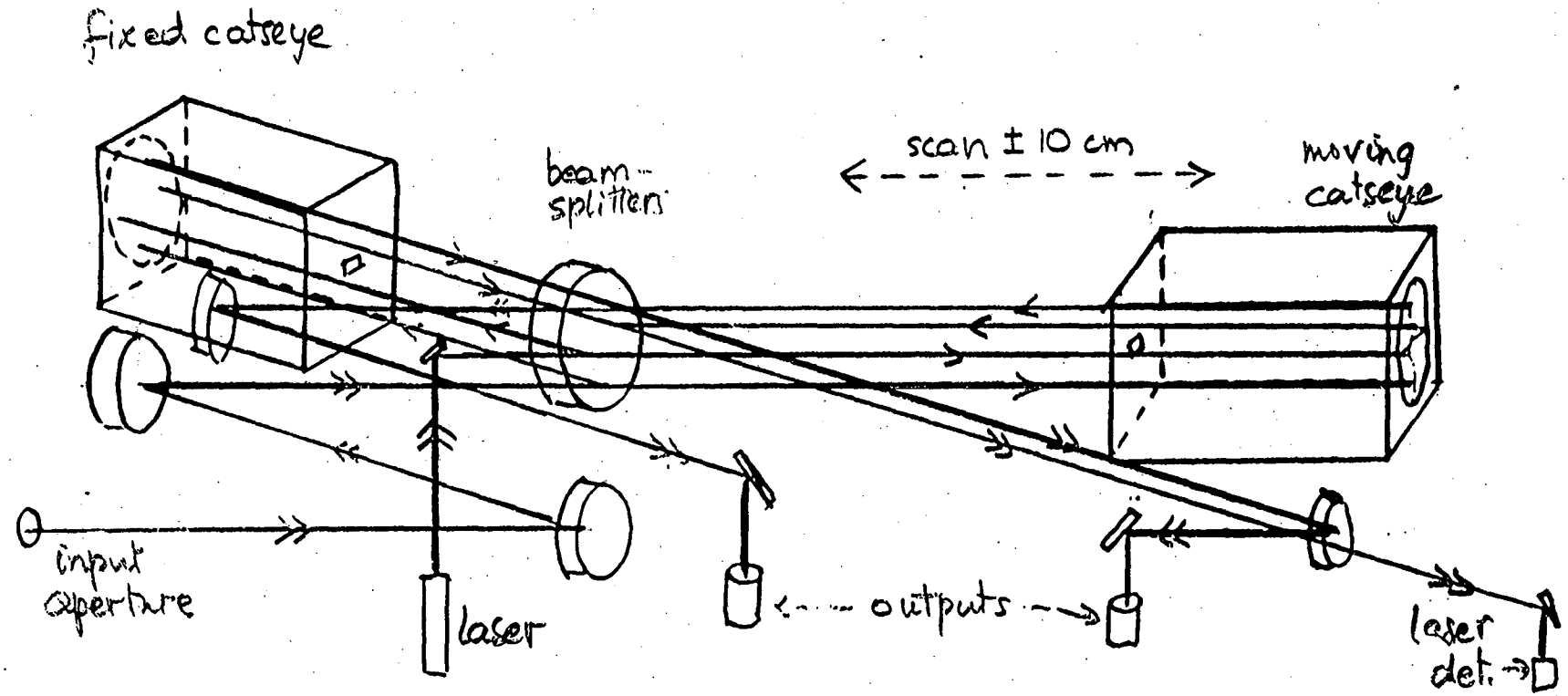

Sampling accuracy

Periodic errors generate ghosts

e.g. for period associated with laser fringes

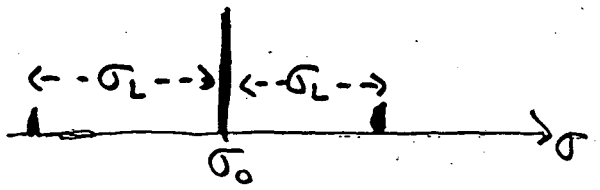

Random errors generate noise

Aim is to keep sampling noise below photon noise.

Criterion depends on type of spectrum & on signal — typically $\lambda/100$

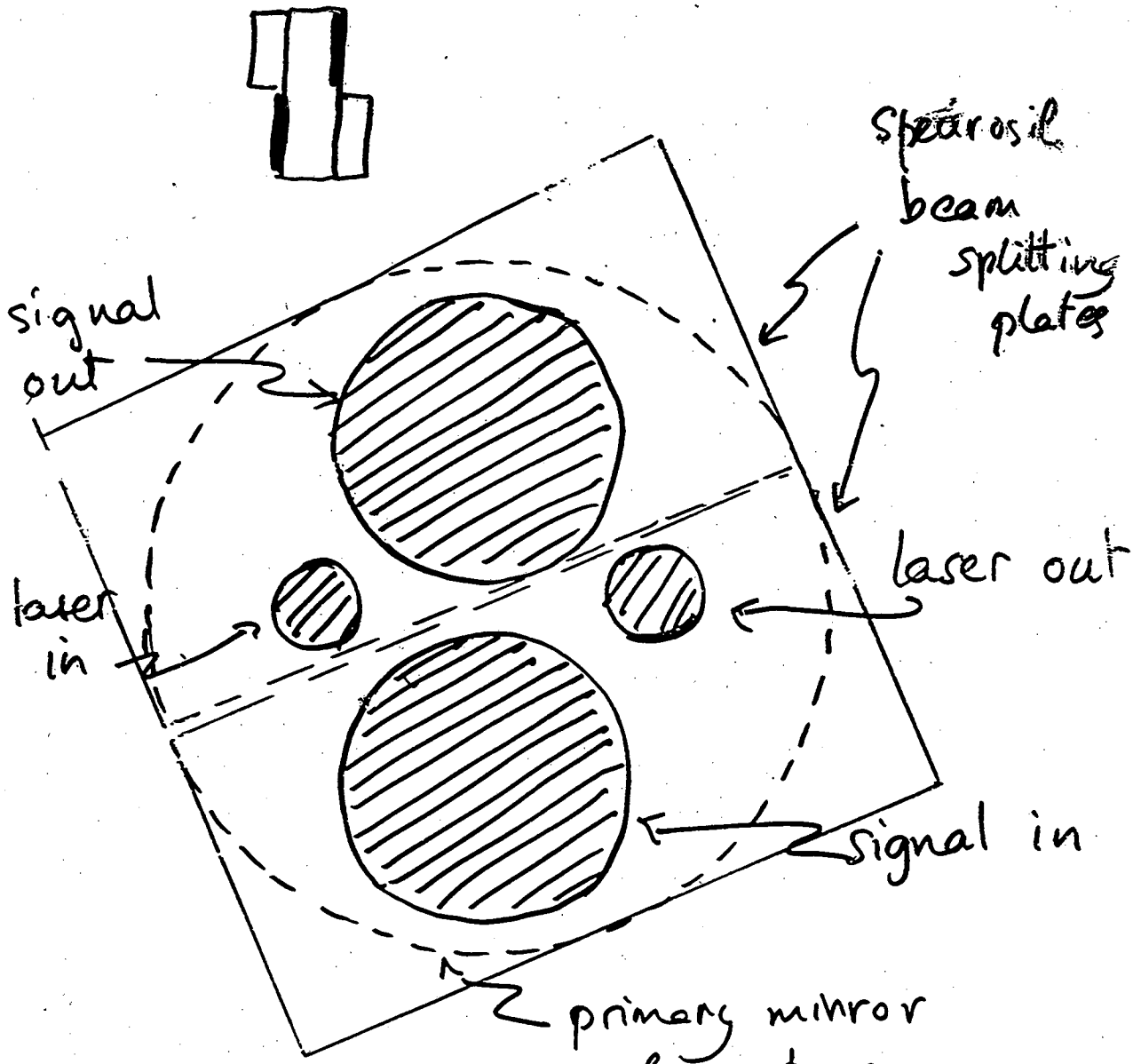

VUV FTS BEAMSPLITTER

Field of view & band-limiting

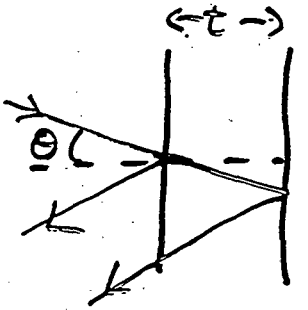

Path diff.

$$x = 2t\cos\theta$$

so phase diff. between normal & extreme rays

$$\delta\varphi = 2\pi\sigma\,\delta x = 2\pi\sigma x_0 \frac{\theta^2}{2}$$

$$\therefore \delta\varphi < \pi \Rightarrow \theta < \sqrt{\frac{2}{R}}$$

$$R = 500\,000 \Rightarrow \theta < 2\ \text{mrad}$$

Michelson Int. — determine size of entrance aperture (circular)

Rayleigh Int — Slit width & determine slit height

Bandpass monochromator

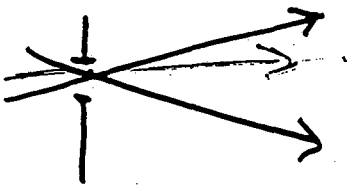

θ depends on λ

$\Rightarrow$ strong phase effects across band pass

$\Rightarrow$ distorted λ scale

Modulation

Modulation vs wavenumber
for silica & MgF_2 beamsplitters
output A only

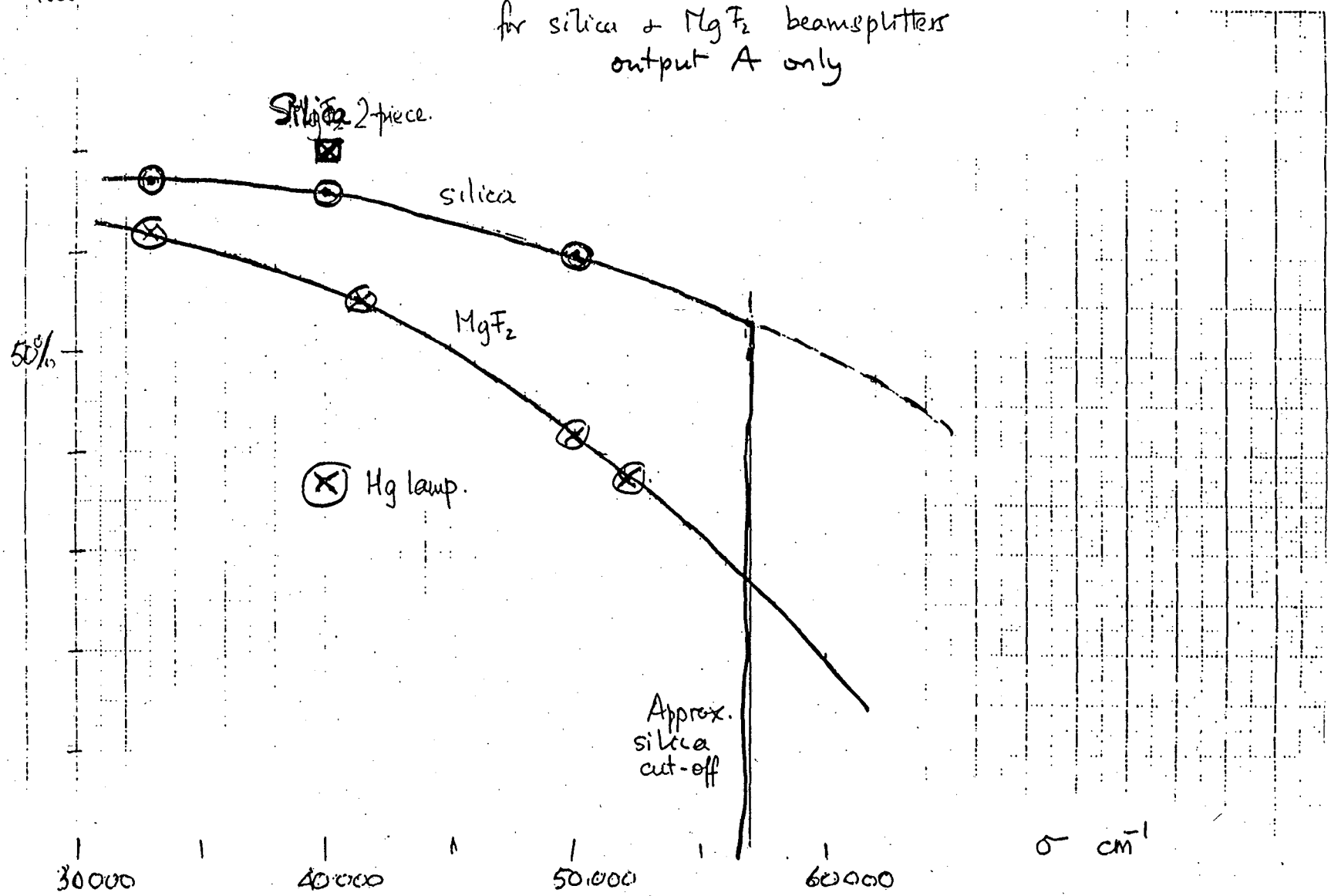

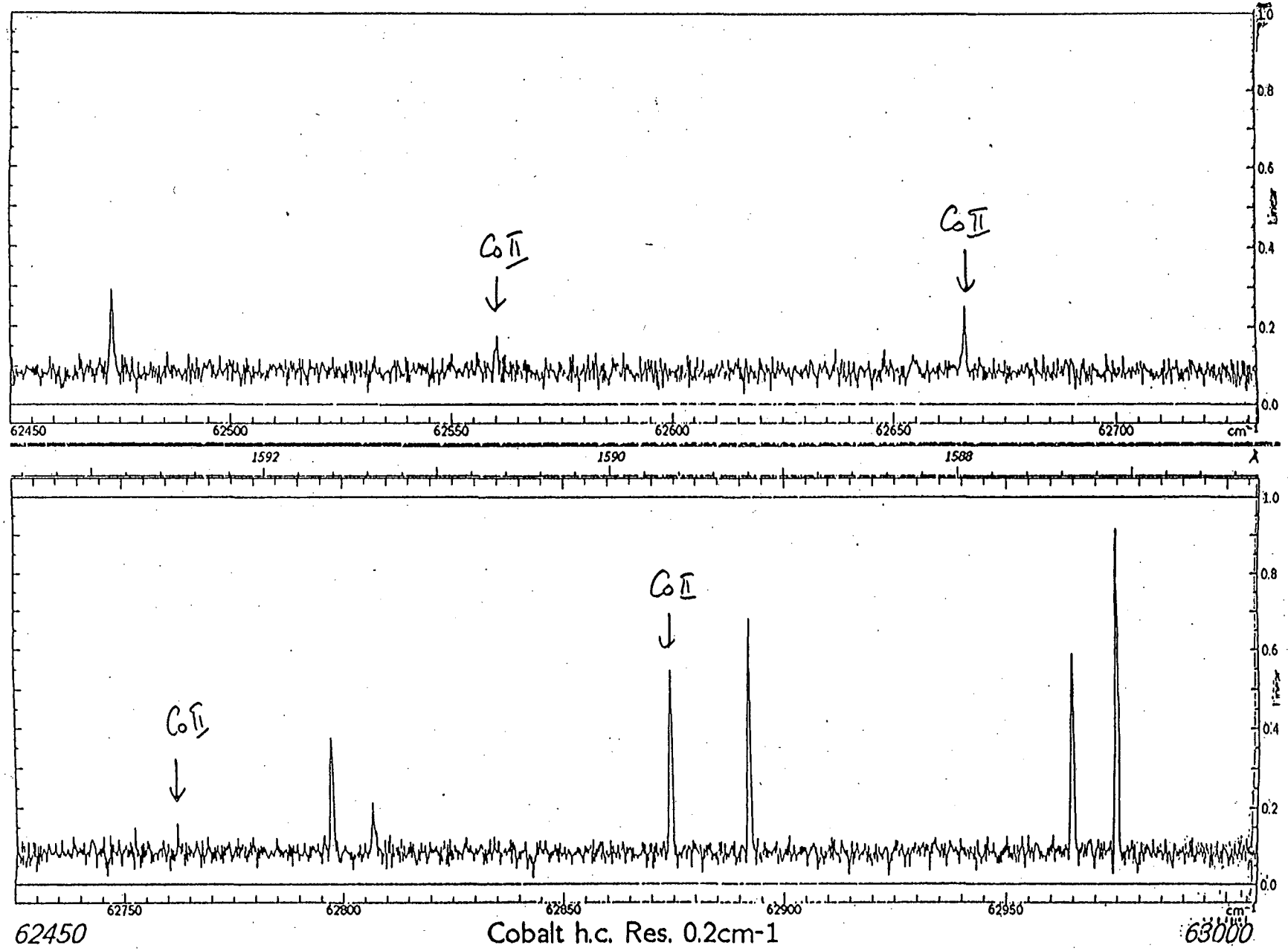

62450 Cobalt h.c. Res. 0.2cm-1 63000

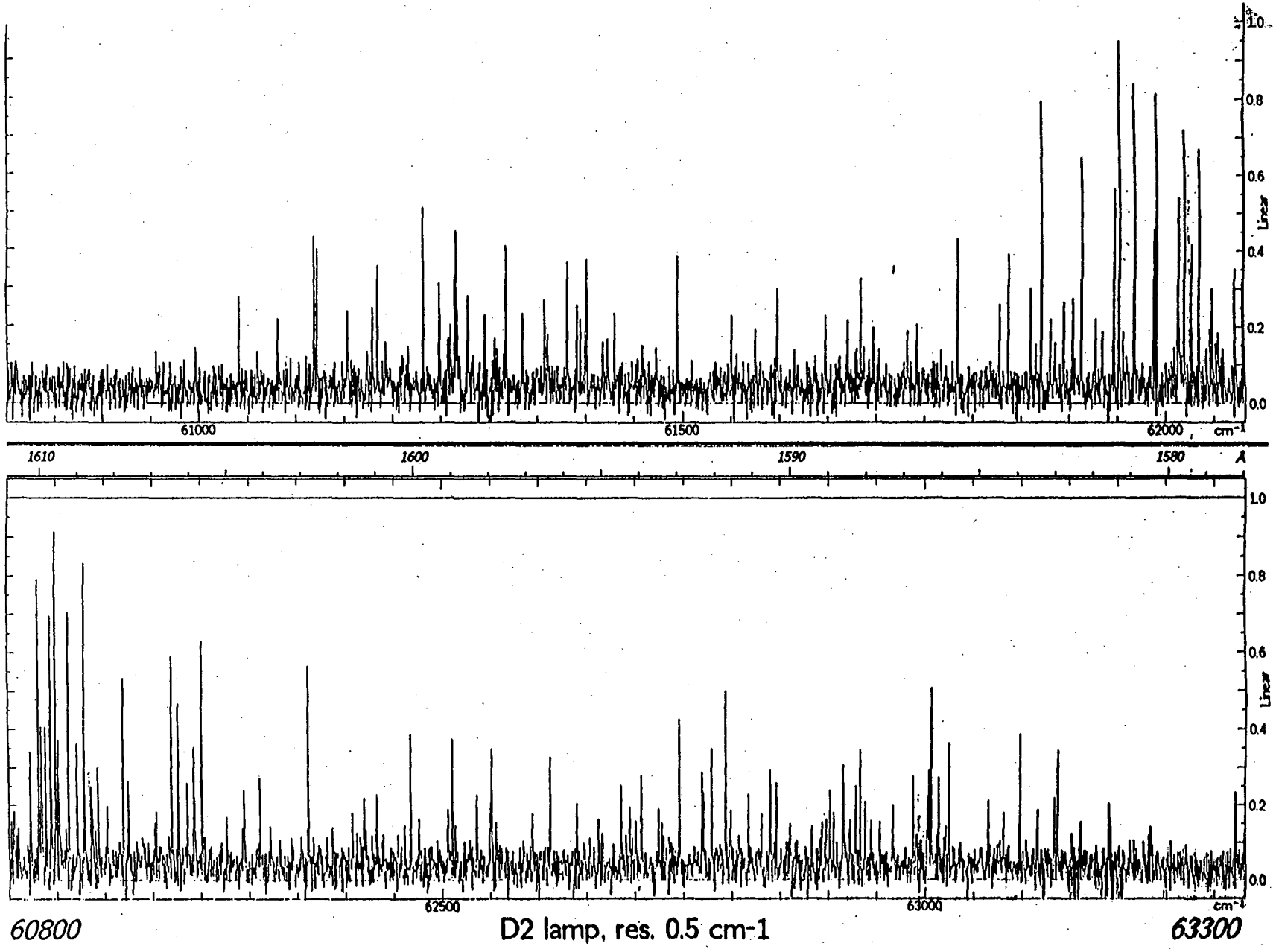

60800 D2 lamp, res. 0.5 cm-1 63300

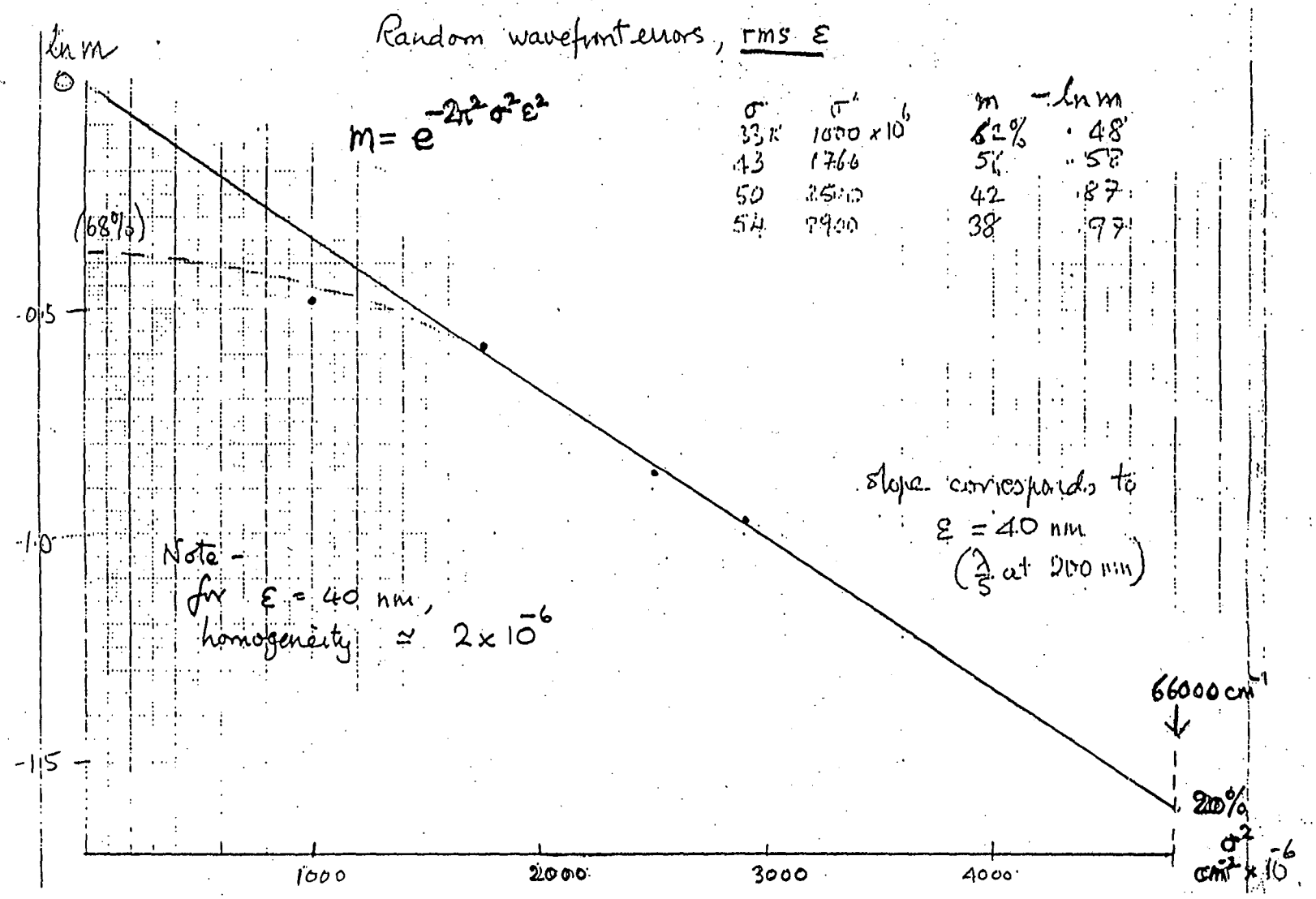
Random wavefront errors, rms ε
ln m
m = e^{-2π²σ²ε²}
σ σ²
33 1000 x 10⁶
43 1766
50 2500
54 2900
m -ln m
82% .48
54 .58
42 .87
38 .97
(68%)
-0.5
-1.0
-1.5
Note -
for ε = 40 nm,
homogeneity ≃ 2 x 10⁻⁶
slope corresponds to
ε = 40 nm
(⅔ at 200 nm)
66000 cm⁻¹
20%
σ² cm⁻² x 10⁻⁶
1000
2000
3000
4000

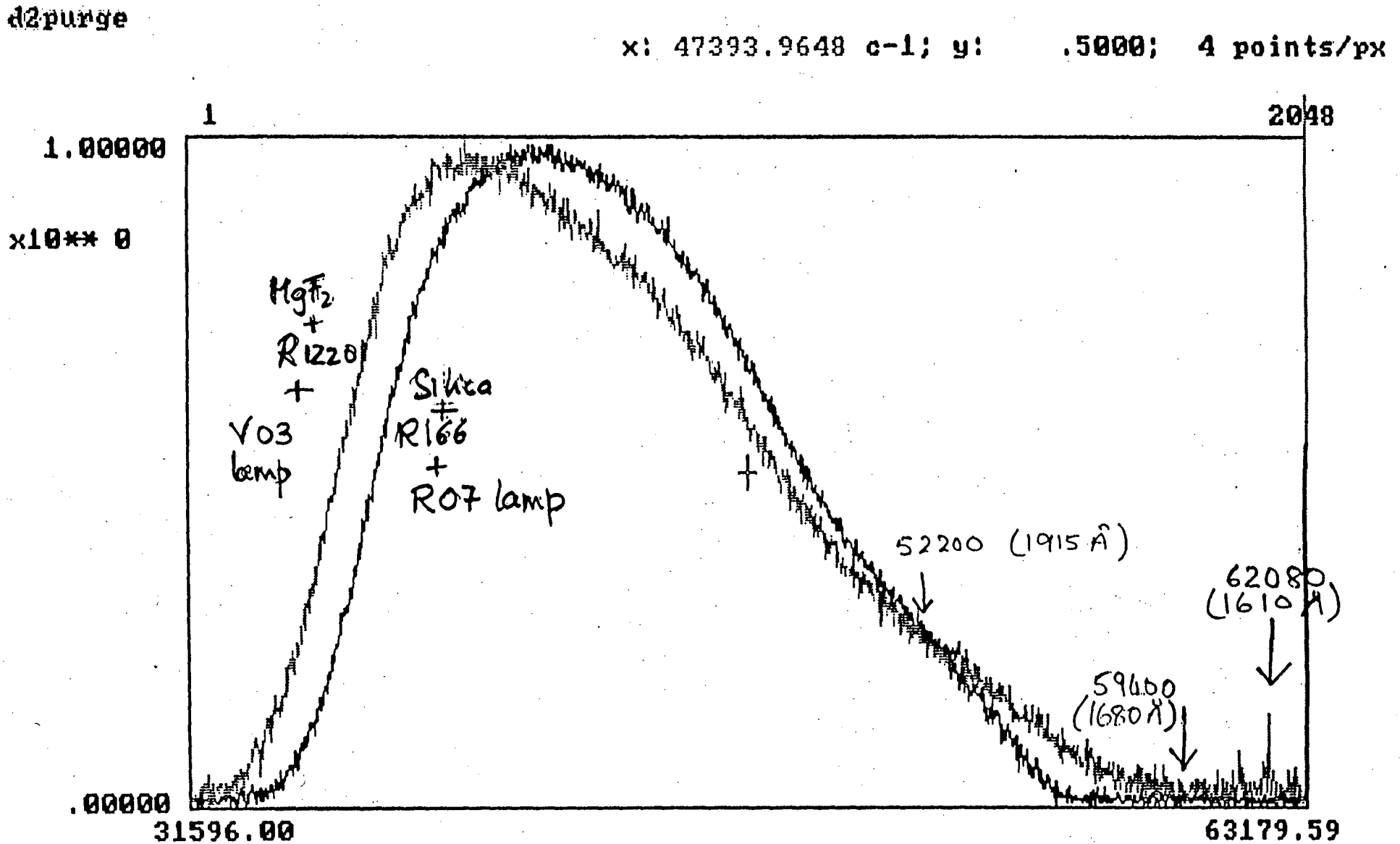
d2purge
x: 47393.9648 c-1; y: .5000; 4 points/px
1
2048
1.00000
x10** 0
.00000
31596.00
63179.59
MgF2 + R1220 + V03 lamp
Silica + R166 + R07 lamp
52200 (1915 Å)
59600 (1680 Å)
62080 (1610 Å)
9 d2mfnew

Fourier Transform Spectroscopy Using Synchrotron Radiation

Dieter Möller

Fairleigh Dickinson University

1) Wavefront Dividing Beamsplitters.

Interferometry in the IR at the Synchrotron at BNL.

Projections for Interferometry in the X-ray region.

2) High Resolution Spectroscopy in the IR.

Folding the spectrum to reduce the number of points.

Errors from unequal sampling intervals.

3) Interferometers without moving parts.

Interferogram displayed in Space.

Michelson and Mach-Zender Array Interferometers.

Array Interferometer with Gratings.

MICHELSON INTERFEROMETER:
AMPLITUDE DIVISION
STANDING WAVE PATTERN

CONSTRUCTIVE INTERFERENCE: MAX. AT DETECTOR
DESTRUCTIVE INTERFERENCE : MAX. AT SOURCE

SPECTRAL RANGE DEPEND ON BEAMSPLITTER
RESOLUTION DEPEND ON DISPLACEMENT OF MIRROR

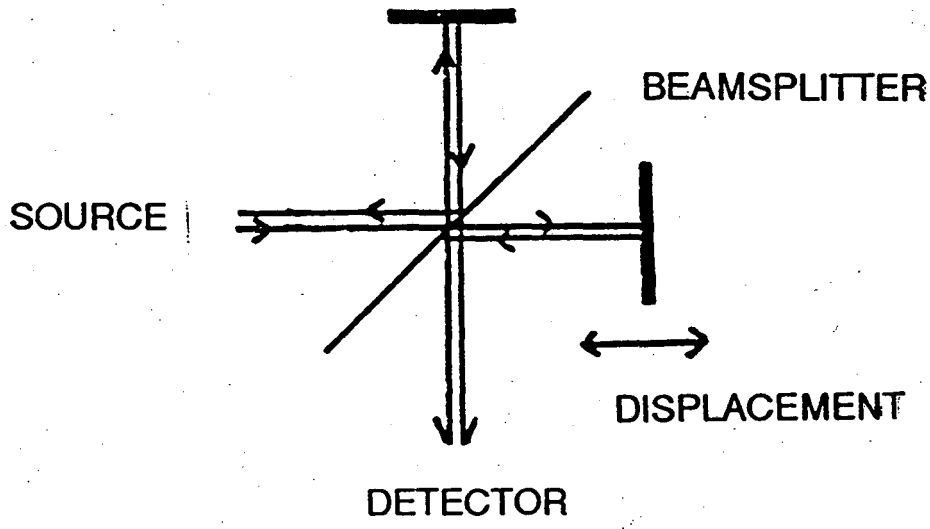

LAMELLAR GRATING INTERFEROMETER
WAVEFRONT DIVISION
DIFFRACTION PATTERN

CONSTRUCTIVE INTERFERENCE: MAX. AT DETECTOR
DESTRUCTIVE INTERFERENCE: MAX. AT FIRST ORDER DIFFRACTION
SPECTRAL RANGE DEPEND ON REFLECTION PROPERTIES OF REFLECTORS.

RESOLUTION DEPEND ON DISPLACEMENT OF MIRROR

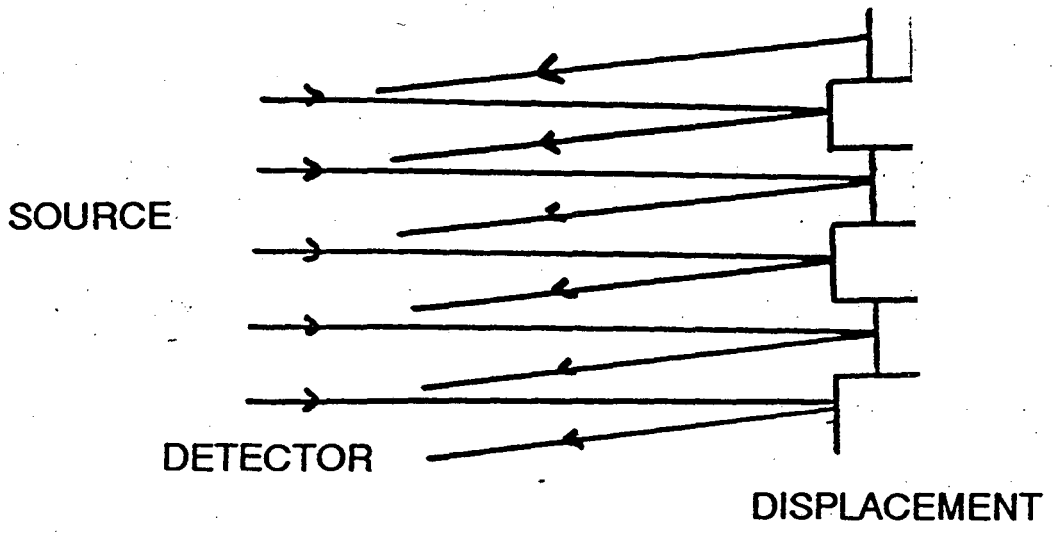

AMPLITUDE DIVISION

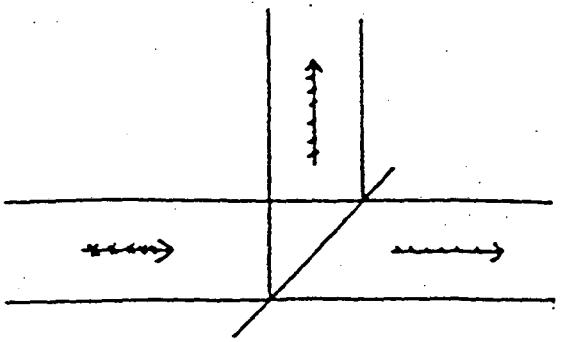

BEAMSPLITTER

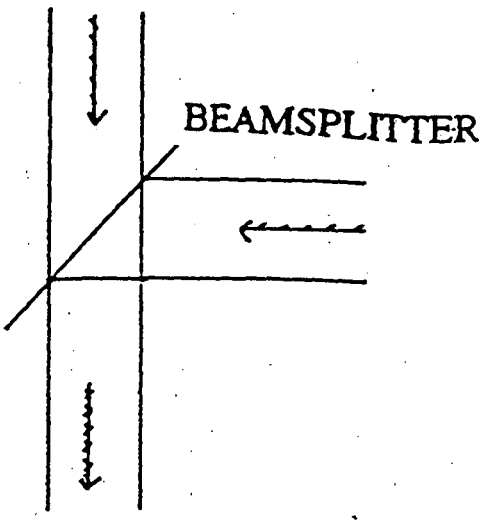

WAVEFRONT DIVISION (FRESNEL DIFFRACTION)

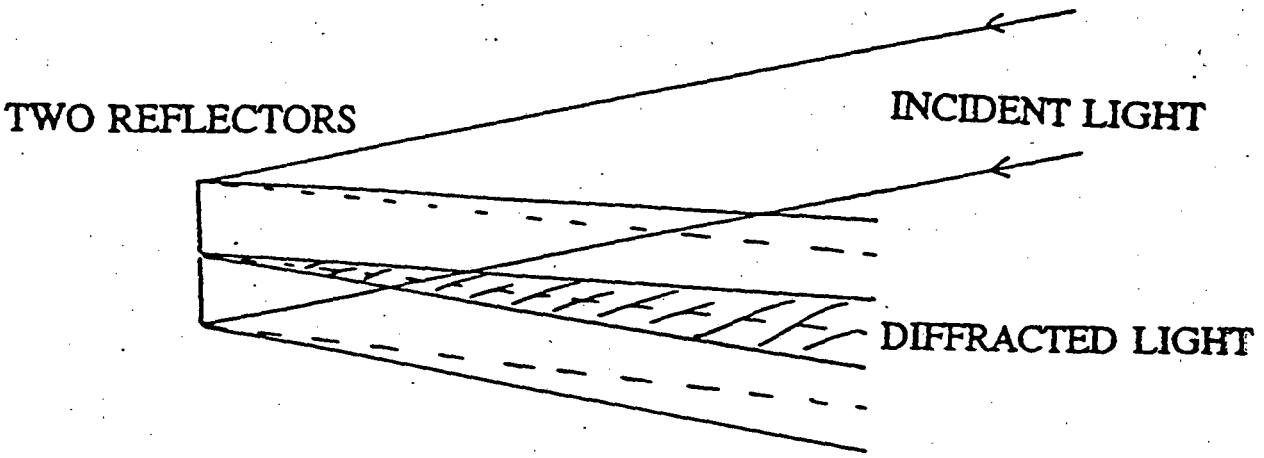

WAVEFRONT DIVISION (FRAUNHOFER DIFFRACTION)

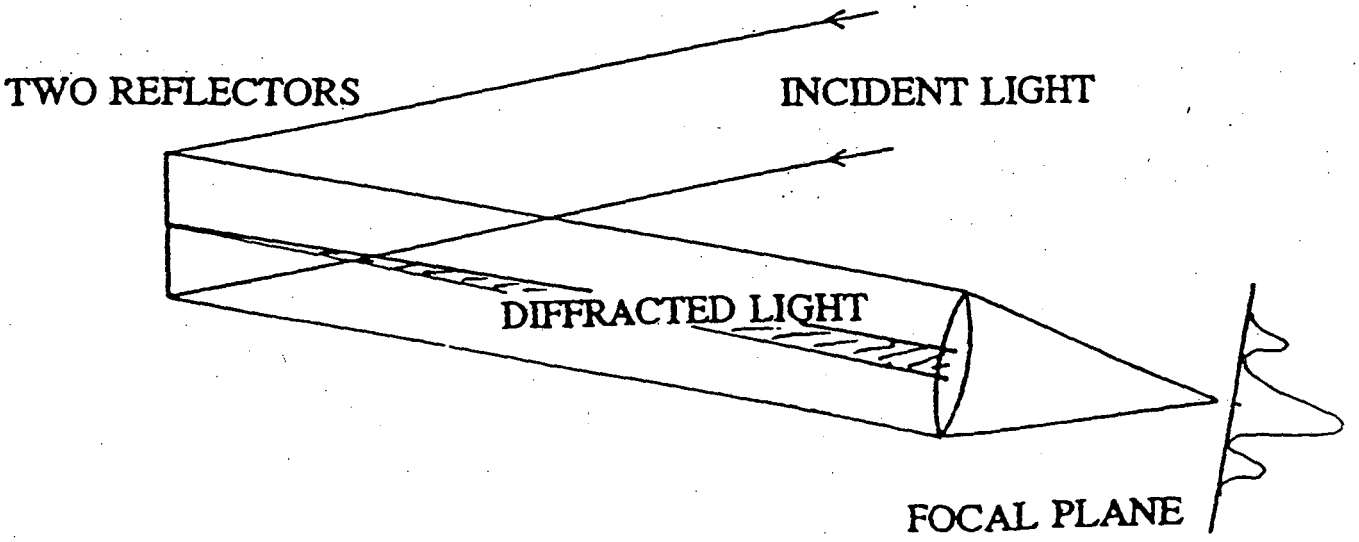

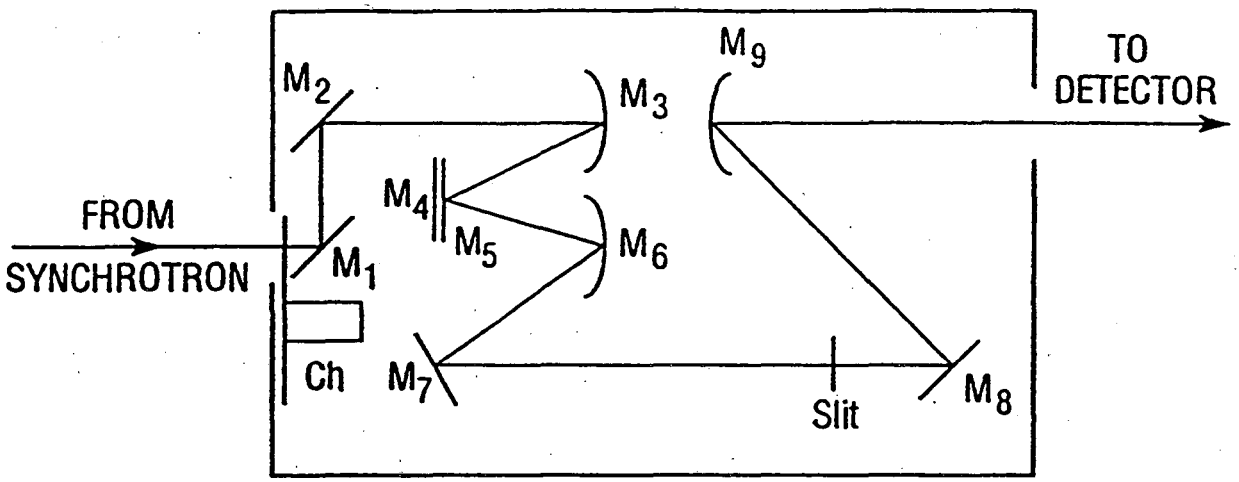

MOST IMPORTANT: THE SLIT

TWO MIRROR WAVEFRONT DIVIDING INTERFEROMETER

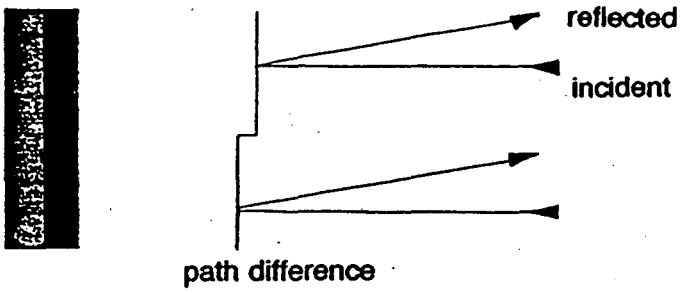

DIFFRACTION PATTERN FOR VARIOUS PATH DIFFERENCES

CONSTRUCTIVE INTERFERENCE

PATH DIFFERENCE $n \cdot \lambda$

DESTRUCTIVE INTERFERENCE

PATH DIFFERENCE $n \cdot \lambda/2$

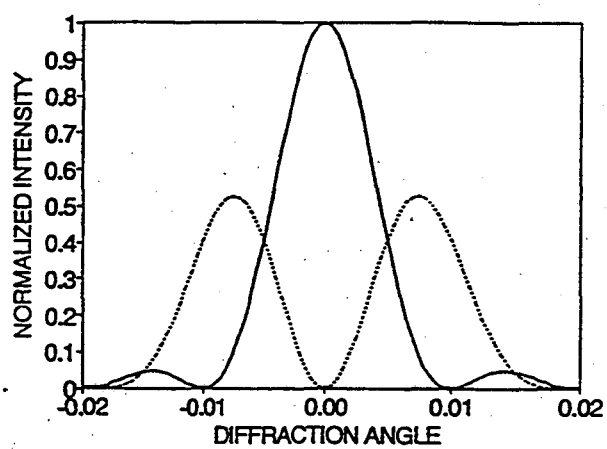

OTHER PATH DIFFERENCES

$\lambda/6$, $2\lambda/6$, $4\lambda/6$, $5\lambda/6$

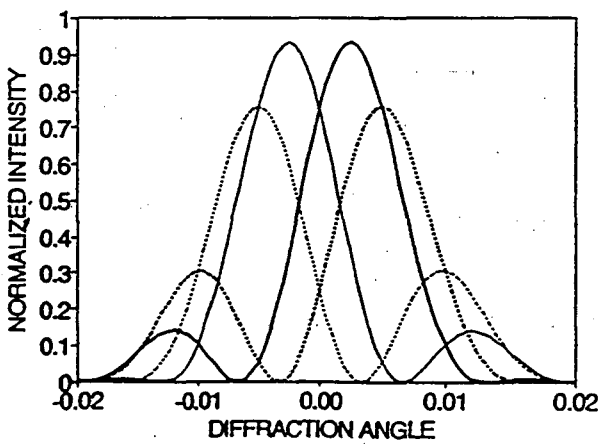

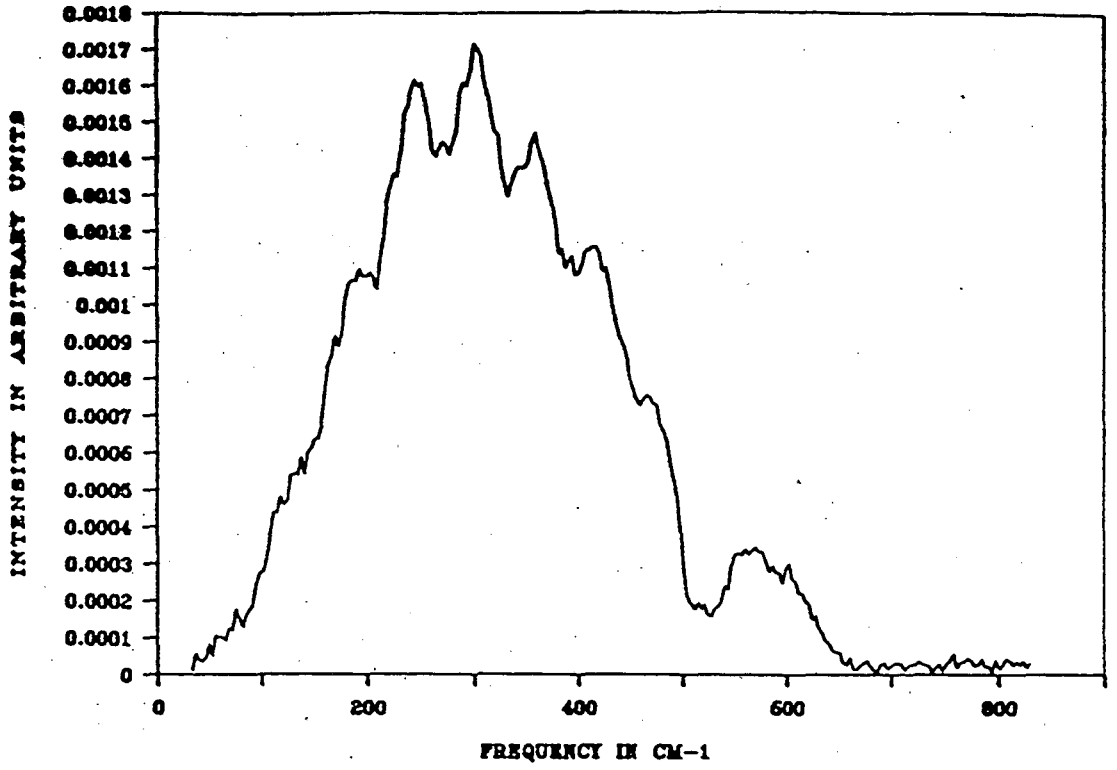
INTENSITY IN ARBITRARY UNITS
0.0018
0.0017
0.0016
0.0015
0.0014
0.0013
0.0012
0.0011
0.001
0.0009
0.0008
0.0007
0.0006
0.0005
0.0004
0.0003
0.0002
0.0001
0
0
200
400
600
800
FREQUENCY IN CM-1

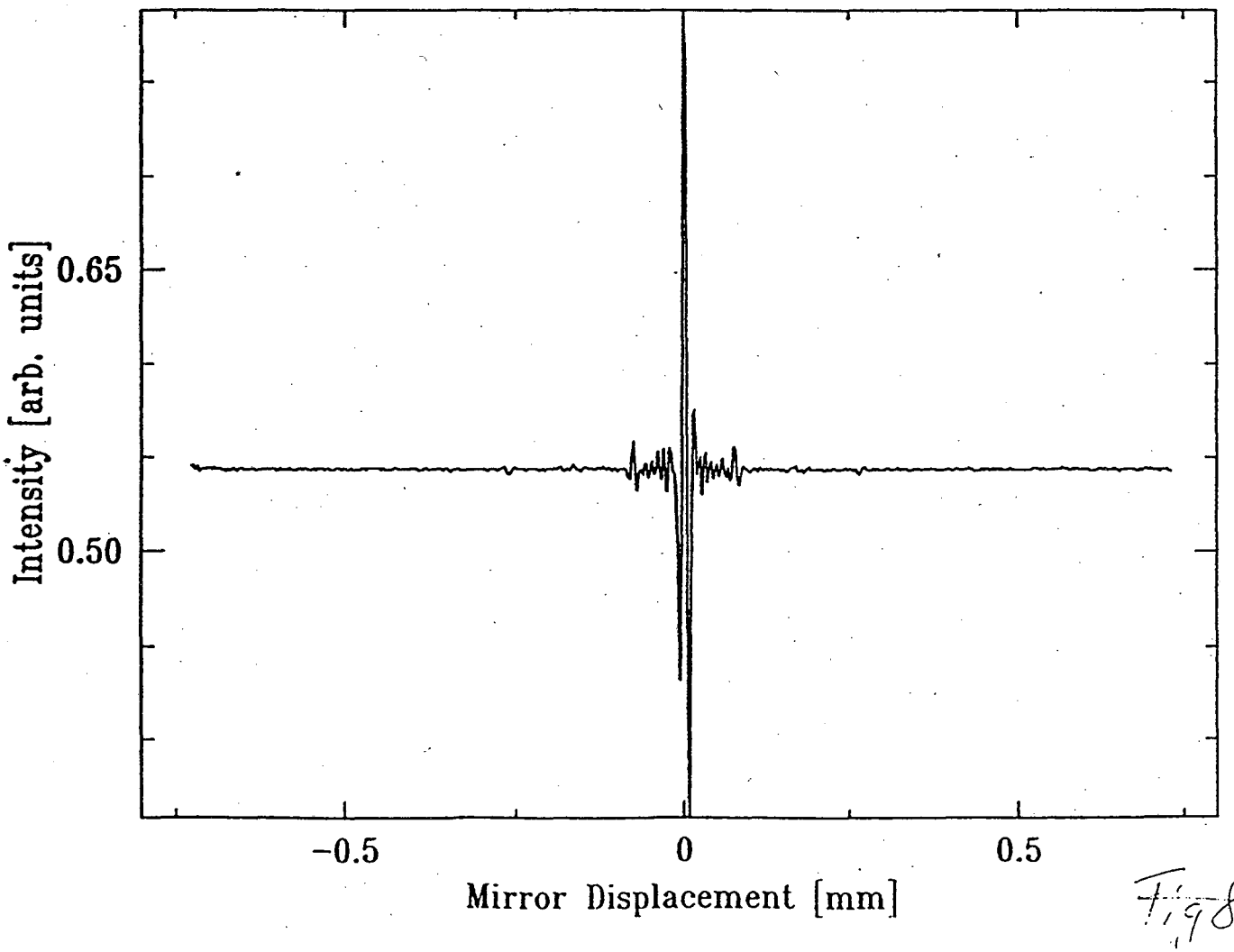
Intensity [arb. units]
0.65
0.50
−0.5
0
0.5
Mirror Displacement [mm]

Fig 8

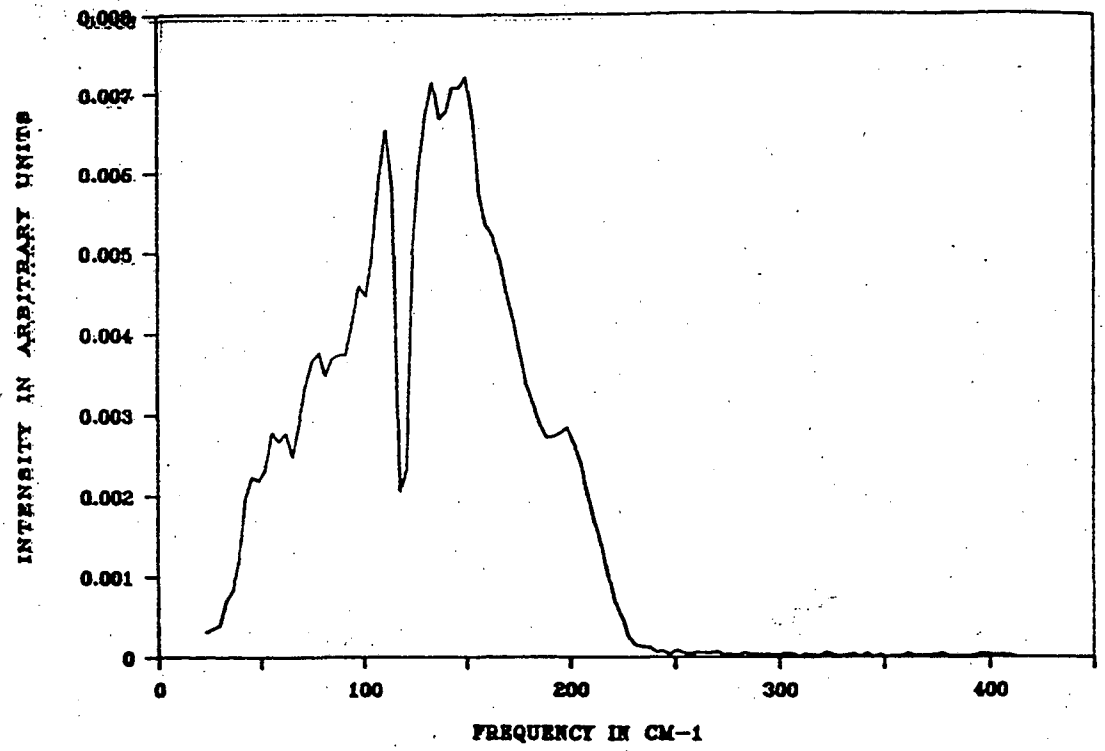
INTENSITY IN ARBITRARY UNITS
0.008
0.007
0.006
0.005
0.004
0.003
0.002
0.001
0
0
100
200
300
400
FREQUENCY IN CM-1

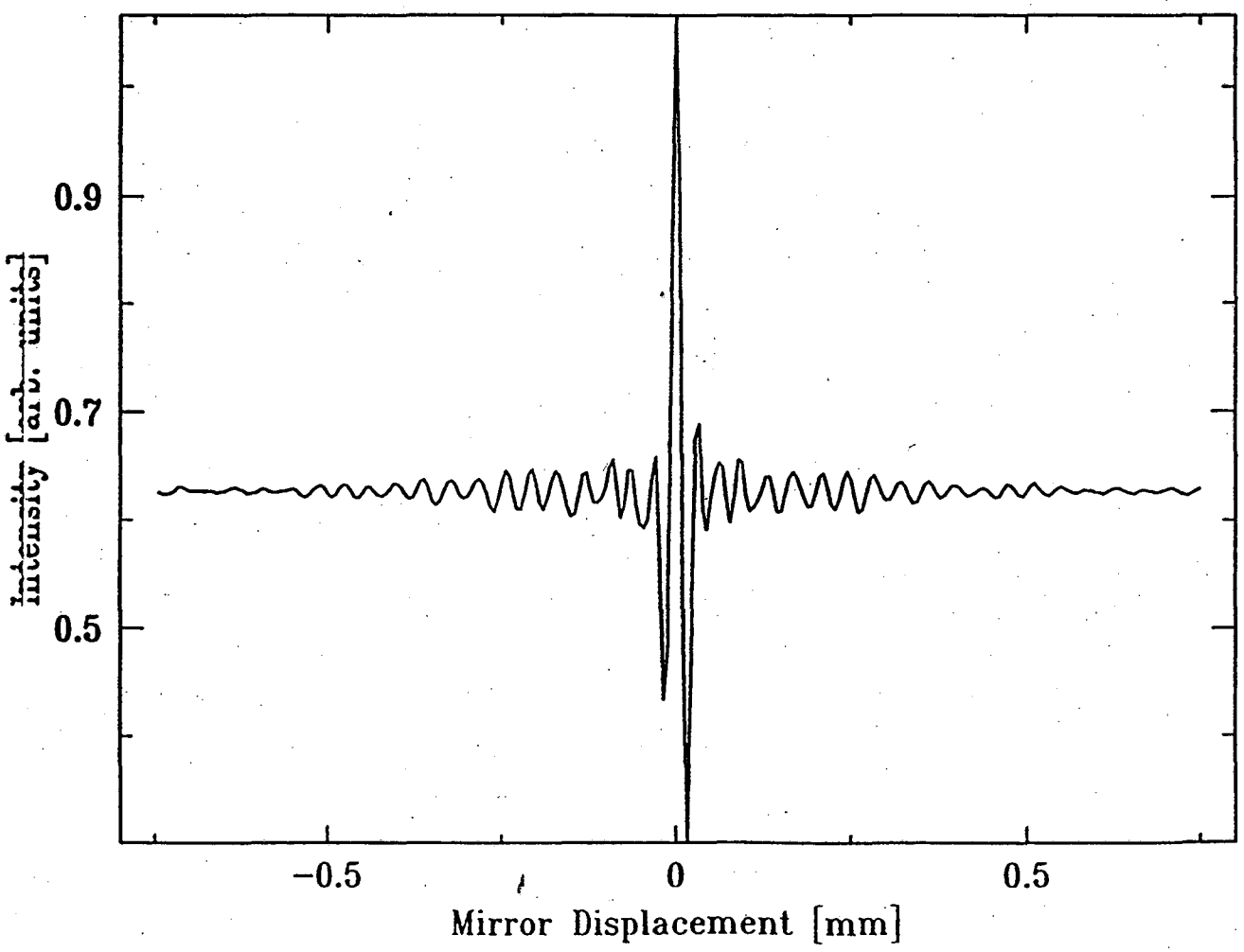
Intensity [arb. units]
0.9
0.7
0.5
−0.5
0
0.5
Mirror Displacement [mm]

UV200INF.XLS

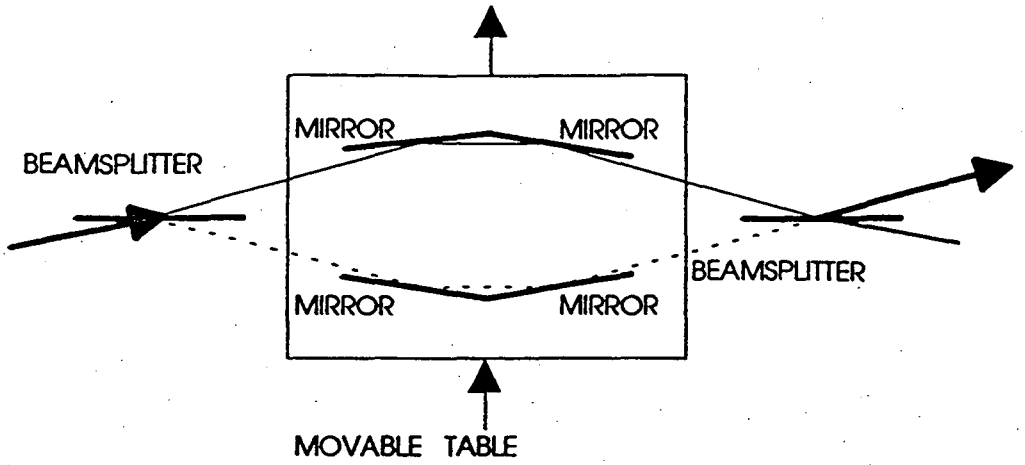

BEAMSPLITTER : WIDTH OF SLOTS 5μ
10μ

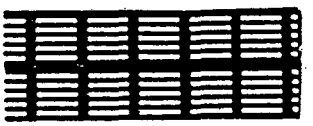

SEPARATION OF ZEROTH AND FIRST ORDER AFTER 1 METER

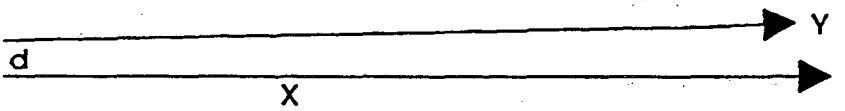

$Y = (X / d)\lambda$
$Y = 4$ mm

WIDTH OF EXIT SLIT OF MONOCHROMATOR IS .6 mm
X-RAYS OF 1 A AT 5 MICRONS GRATING GAVE FRINGES
MOVEMENT OF TABLE WITH VARIOUS METHODS

FOR VERY HIGH RESOLUTION AND NARROW BAND WIDTH SAMPLING OF THE ENVELOPE

FAR INFRARED FOURIER TRANSFORM INTERFEROMETER USING CAPACITIVE GRID BEAMSPLITTER

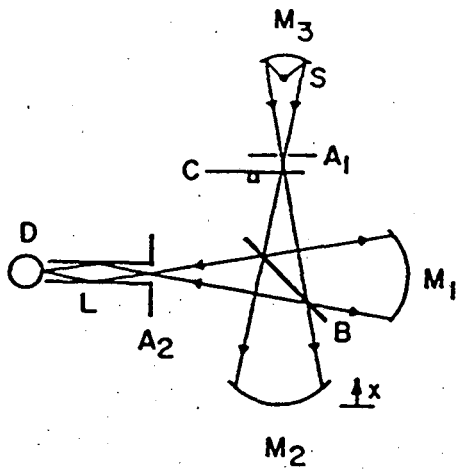

SCHEMATIC

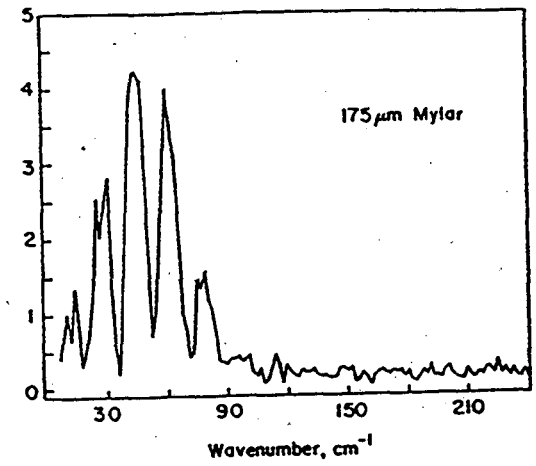

MYLAR BEAMSPLITTER

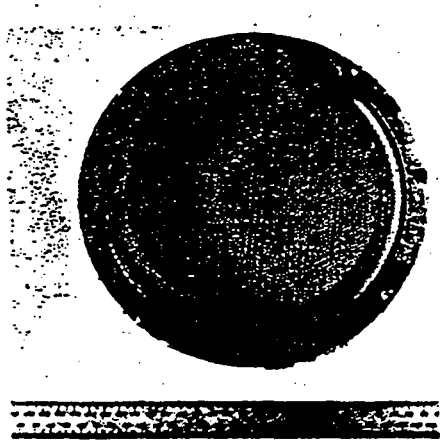

BEAMSPLITTER
CAPACITIVE GRID
WITH 3 mm DOTS

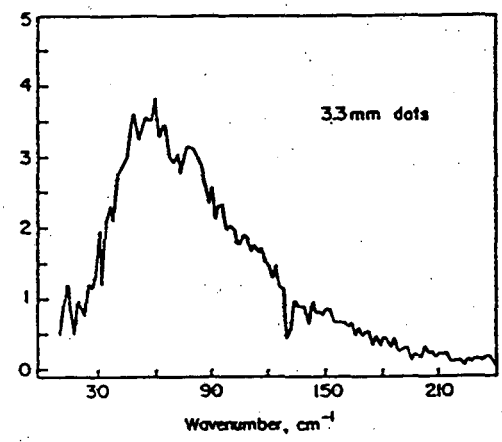

BEAMSPLITTER
SPECTRUM WITH
HAVING 3 mm DOTS

POINT-LIKE SOURCE

EXIT APERTURE DETERMINES SPECTRAL RANGE FOR MODULATION

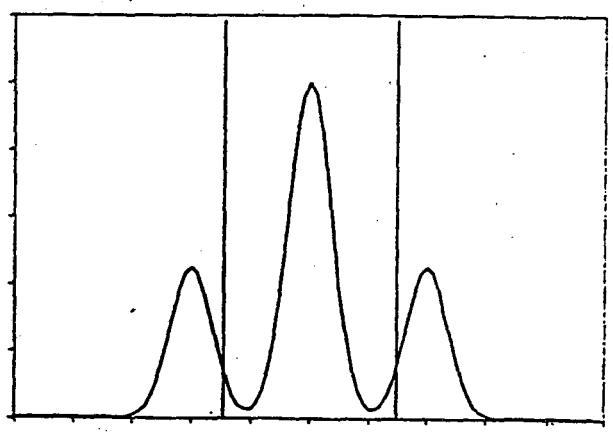

LIGHT OF λ

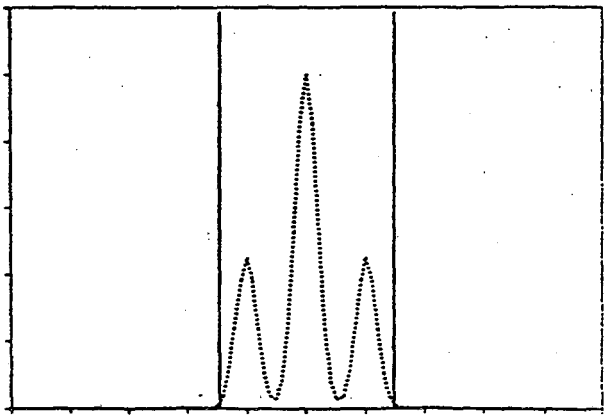

LIGHT OF $\lambda/2$

For shorter wavelength more light of destructive interference enters the exit slit and reduces "modulation".

FOUR REFLECTOR LAMELLAR GRATING "MINIGRATING"

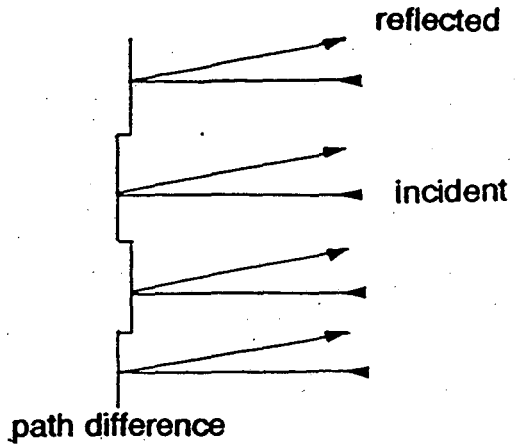

DIFFRACTION PATTERN FOR VARIOUS PATH DIFFERENCES

CONSTRUCTIVE INTERFERENCE

PATH DIFFERENCE $n \cdot \lambda$

DESTRUCTIVE INTERFERENCE

PATH DIFFERENCE $n \cdot \lambda/2$

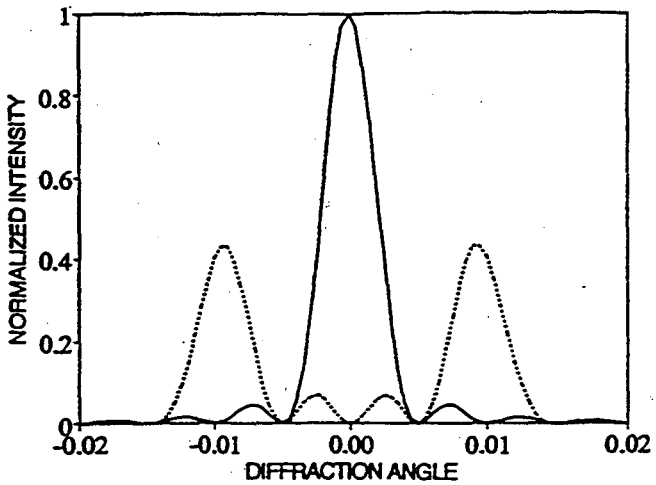

OTHER PATH DIFFERENCES

$\lambda/6, 2\lambda/6, 4\lambda/6, 5\lambda/6$

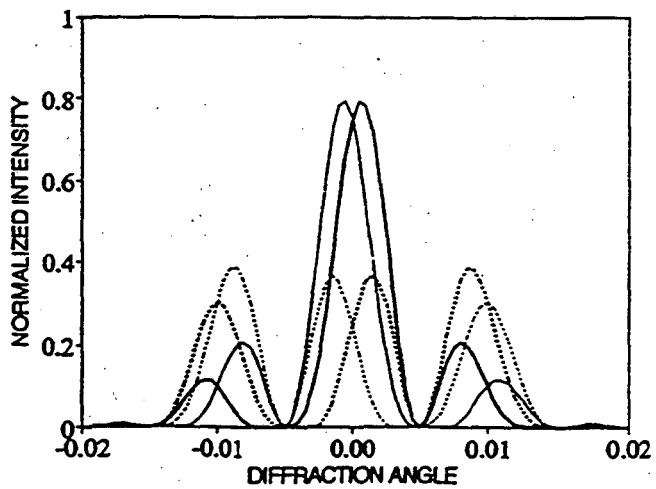

EXTENDED SOURCE

SIZE OF APERTURES LIMIT MODULATION

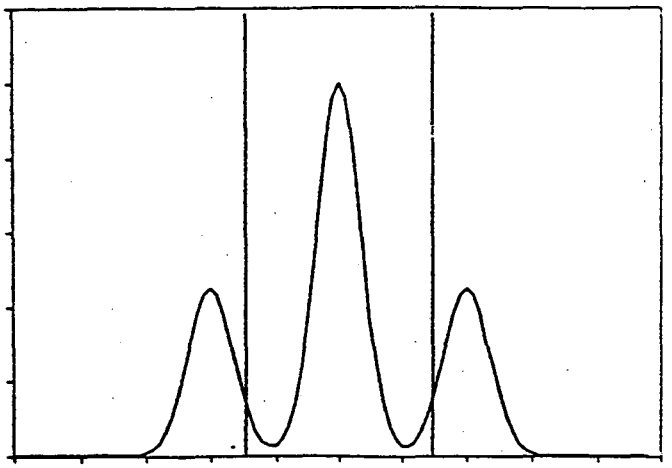

LIGHT OF λ FROM ONE POINT

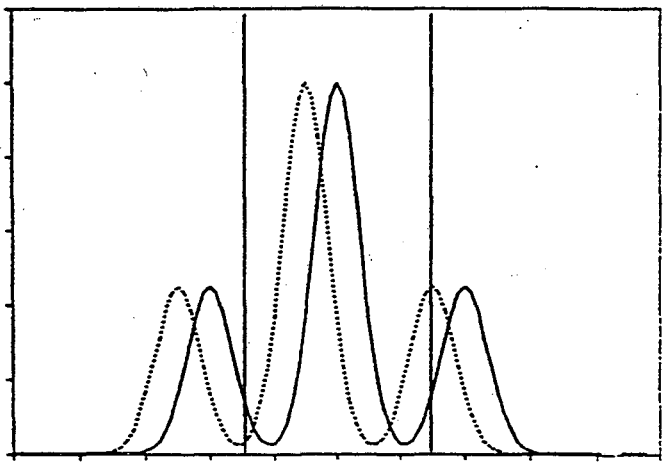

LIGHT OF λ FROM TWO POINTS OF THE SOURCE

When light from two points separated by a distance enter the exit slit, more light of destructive interference arrives at the detector and reduces "modulation".

ZERO ORDER --- FIRST ORDER --- GAP

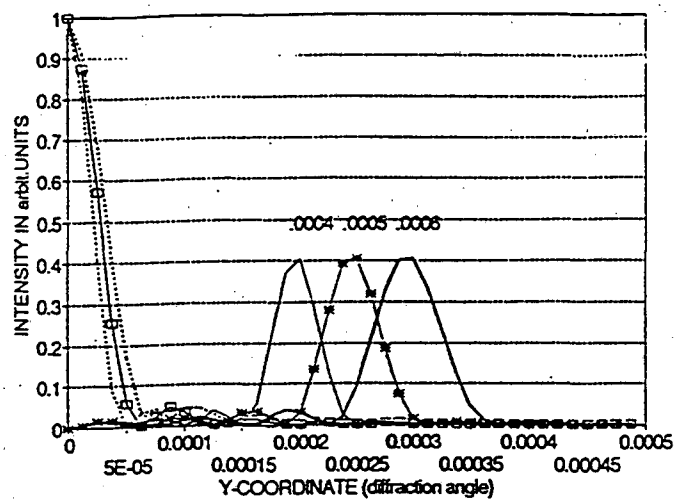

DEPENDING ON WAVELENGTH (D = 1, N = 4, X = 8000)

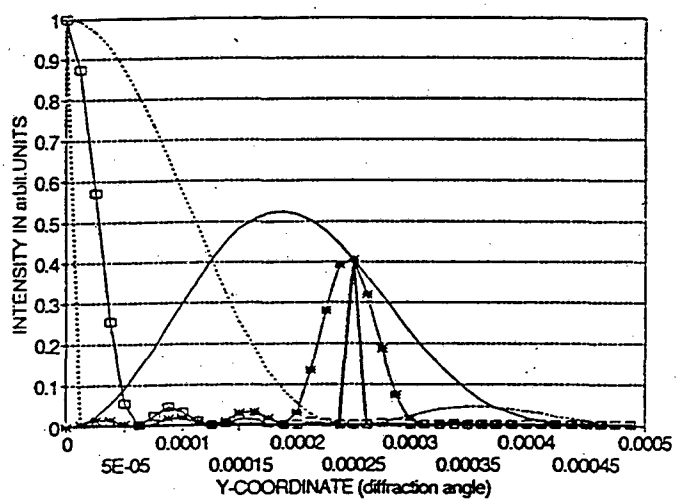

NUMBER OF REFLECTORS: N=1, N=4, N=20

SPACIAL INCOHERENT LIGHT

TO ENLARGE THROUGHPUT AND SPECTRAL RANGE

WE NEED TO DISTRIBUTE THE DIFFRACTED LIGHT OF DESTRUCTIVE INTERFERENCE

NOT AT A SPECIFIC ANGLE

BUT OVER A RANGE OF ANGLES IN SPACE

INTERFERENCE FOR REGULAR AND DECREASING DISTANCES OF SOURCE POINTS

SAME DISTANCE BETWEEN SOURCE POINTS

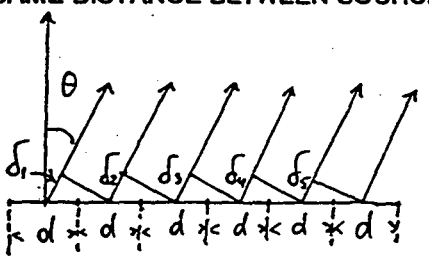

$\delta_1 = \delta_2 = \delta_3 = \delta_4 = \delta_5 = d \sin(\theta)$

PHASE DIFFERENCES ARE ALL EQUAL
SUPERPOSITION WILL ADD UP IN A CONSTRUCTED WAY

DECREASING DISTANCE BETWEEN SOURCE POINTS

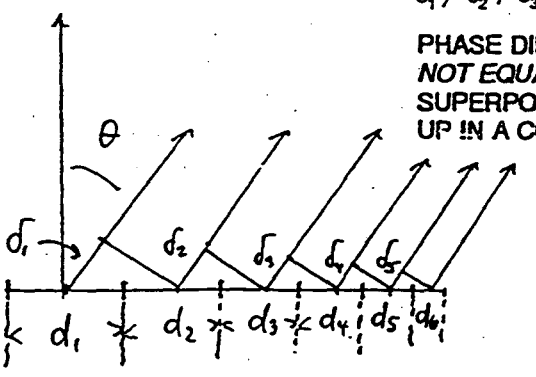

$\delta_1 \neq \delta_2 \neq \delta_3 \neq \delta_4 \neq \delta_5$

PHASE DIFFERENCES ARE *NOT EQUAL*
SUPERPOSTION WILL *NOT* ADD UP IN A CONSTRUCTIVE WAY

DISK AND 3 RINGS

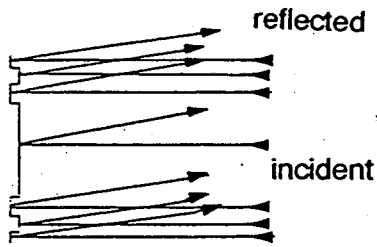

path difference

diffraction pattern
center-symmetric

DIFFRACTION PATTERN FOR VARIOUS PATH DIFFERENCES

CONSTRUCTIVE INTERFERENCE

———————

PATH DIFFERENCE $n \cdot \lambda$

DESTRUCTIVE INTERFERENCE

– – – – – –

PATH DIFFERENCE $n \cdot \lambda/2$

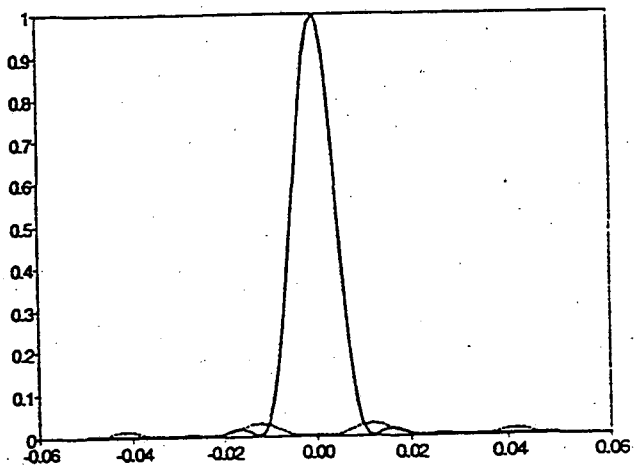

OTHER PATH DIFFERENCES

$\lambda/6$, $2\lambda/6$, $4\lambda/6$, $5\lambda/6$

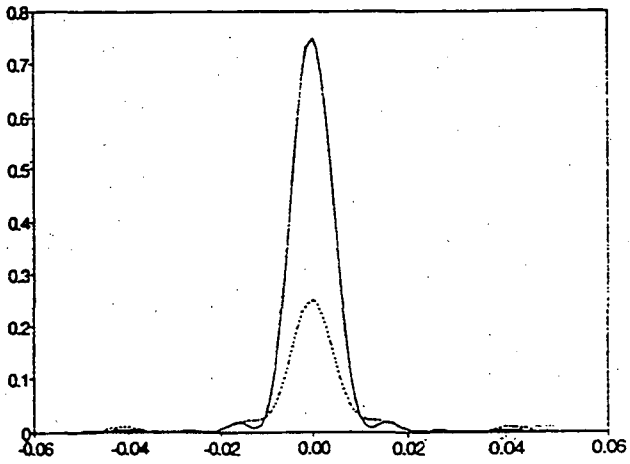

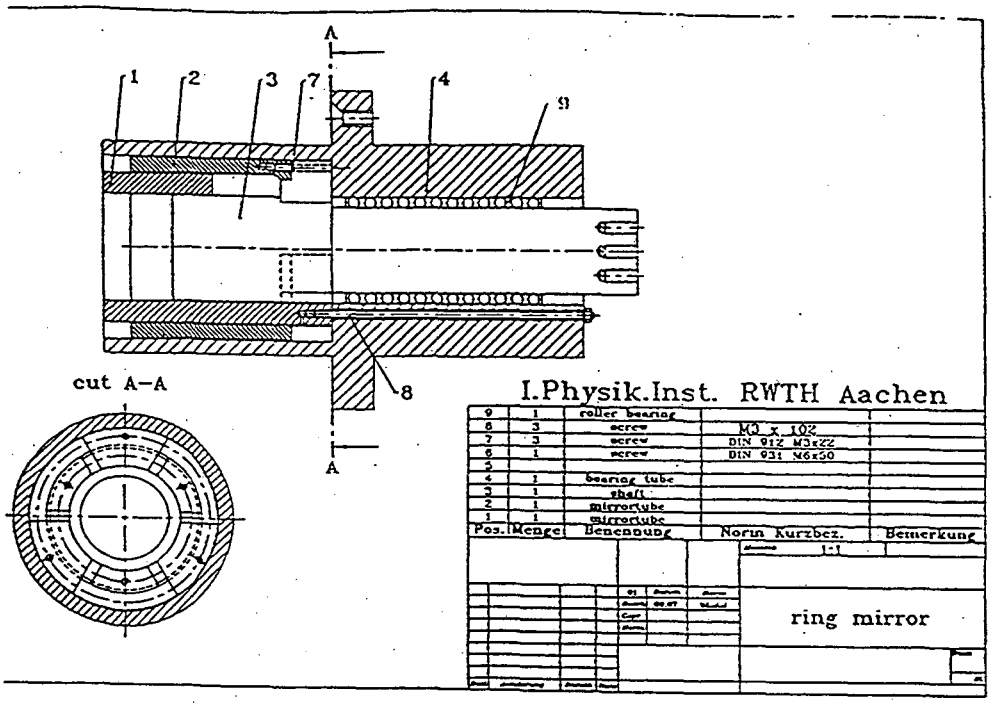
A
1
2
3
7
4
9
8
A
cut A-A
I.Physik.Inst. RWTH Aachen
9 1 roller bearing
8 3 screw M3 x 10?
7 3 screw DIN 912 M3x22
6 1 screw DIN 931 M6x50
5
4 1 bearing tube
3 1 shaft
2 1 mirrortube
1 1 mirrortube
Pos. Menge Benennung Norm Kurzbez. Bemerkung
1:1
ring mirror

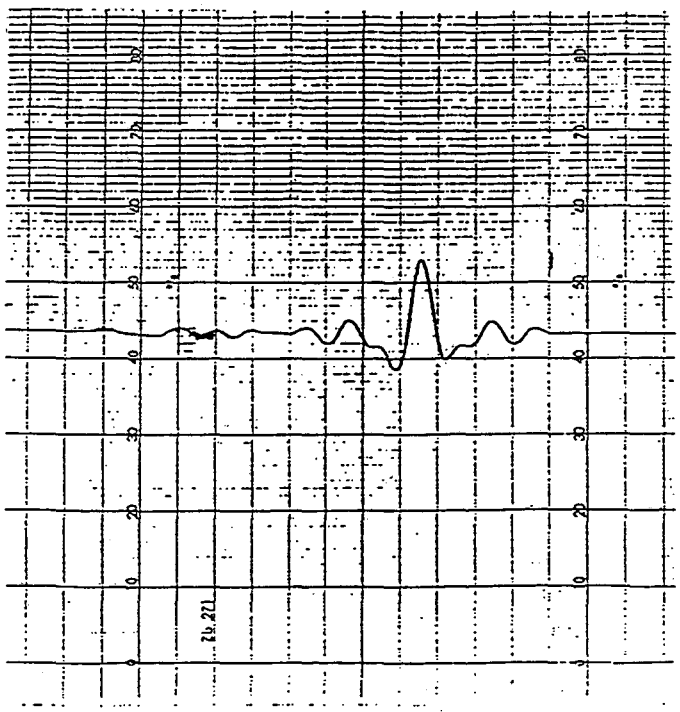

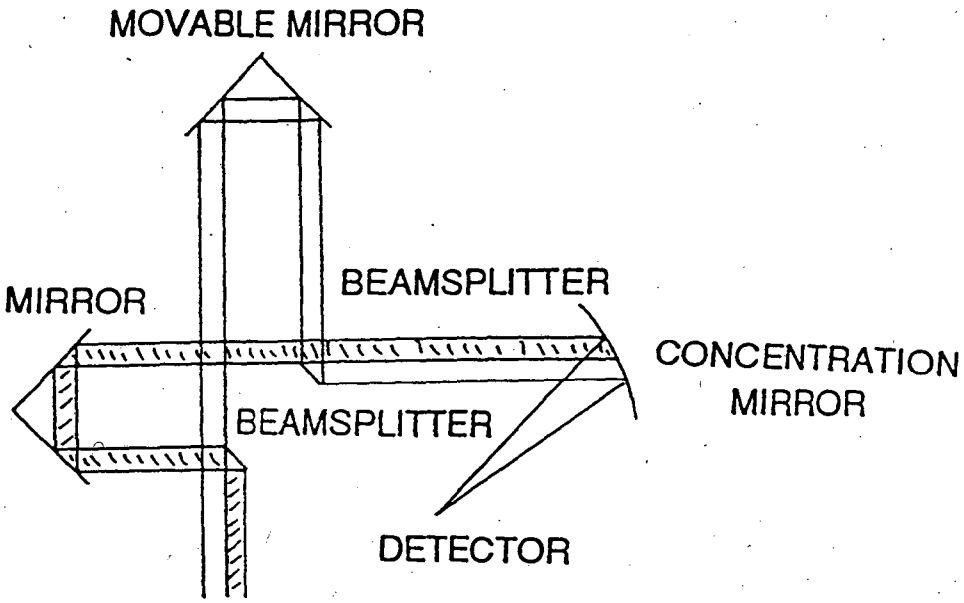

PERIODIC BEAMSPLITTER
DIAMETER OF SECTION
3 TO 5 micron

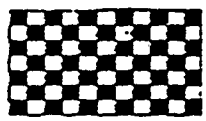

RANDOM PATTERN BEAMSPLITTER
OPENINGS SMALLER OR EQUAL TO
3 TO 5 mm

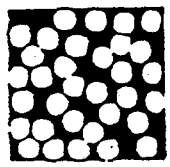

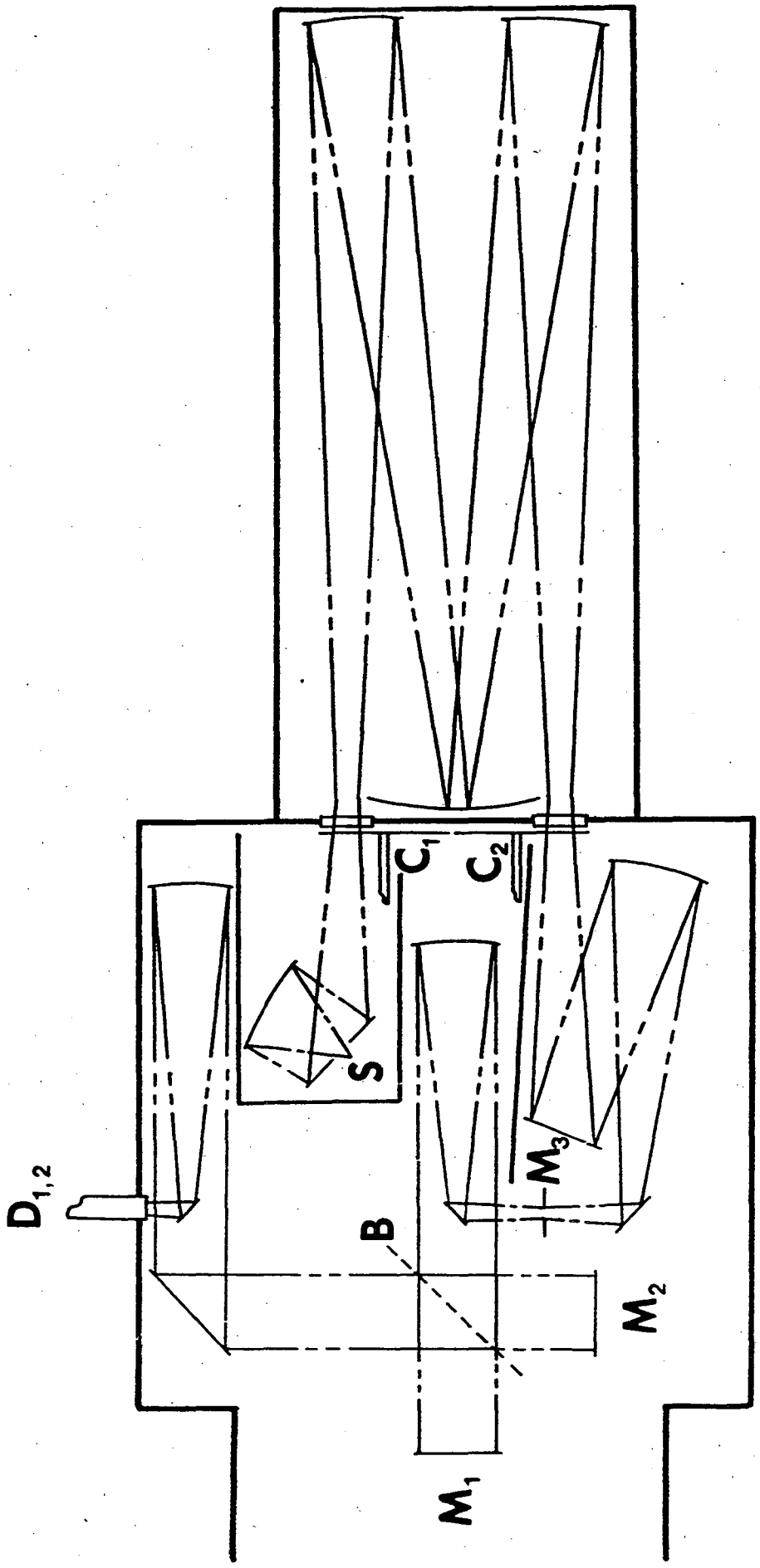
C1
C2
S
M3
D1,2
B
M2
M1

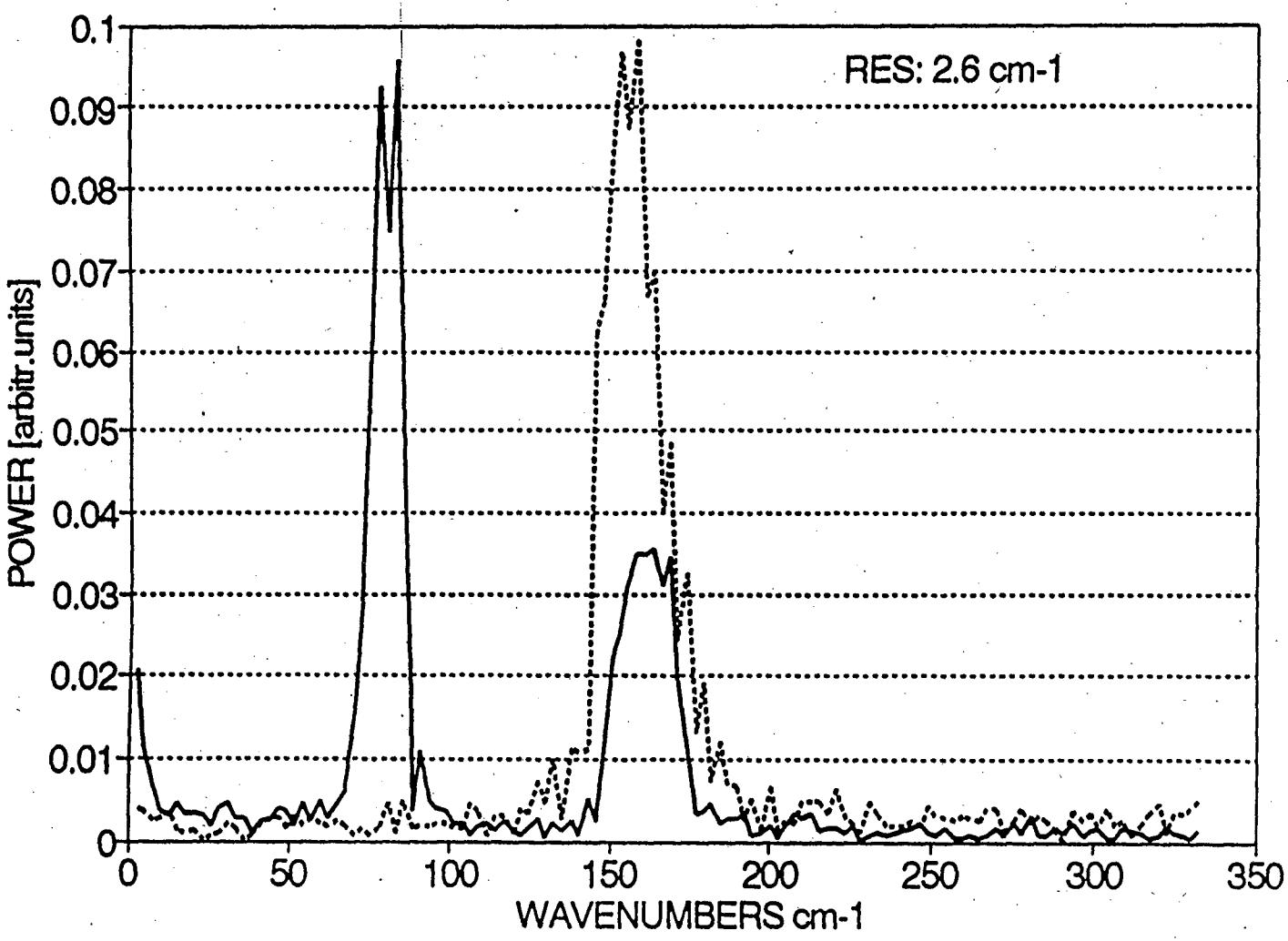
RES: 2.6 cm-1
POWER [arbitr.units]
0.1
0.09
0.08
0.07
0.06
0.05
0.04
0.03
0.02
0.01
0
0
50
100
150
200
250
300
350
WAVENUMBERS cm-1

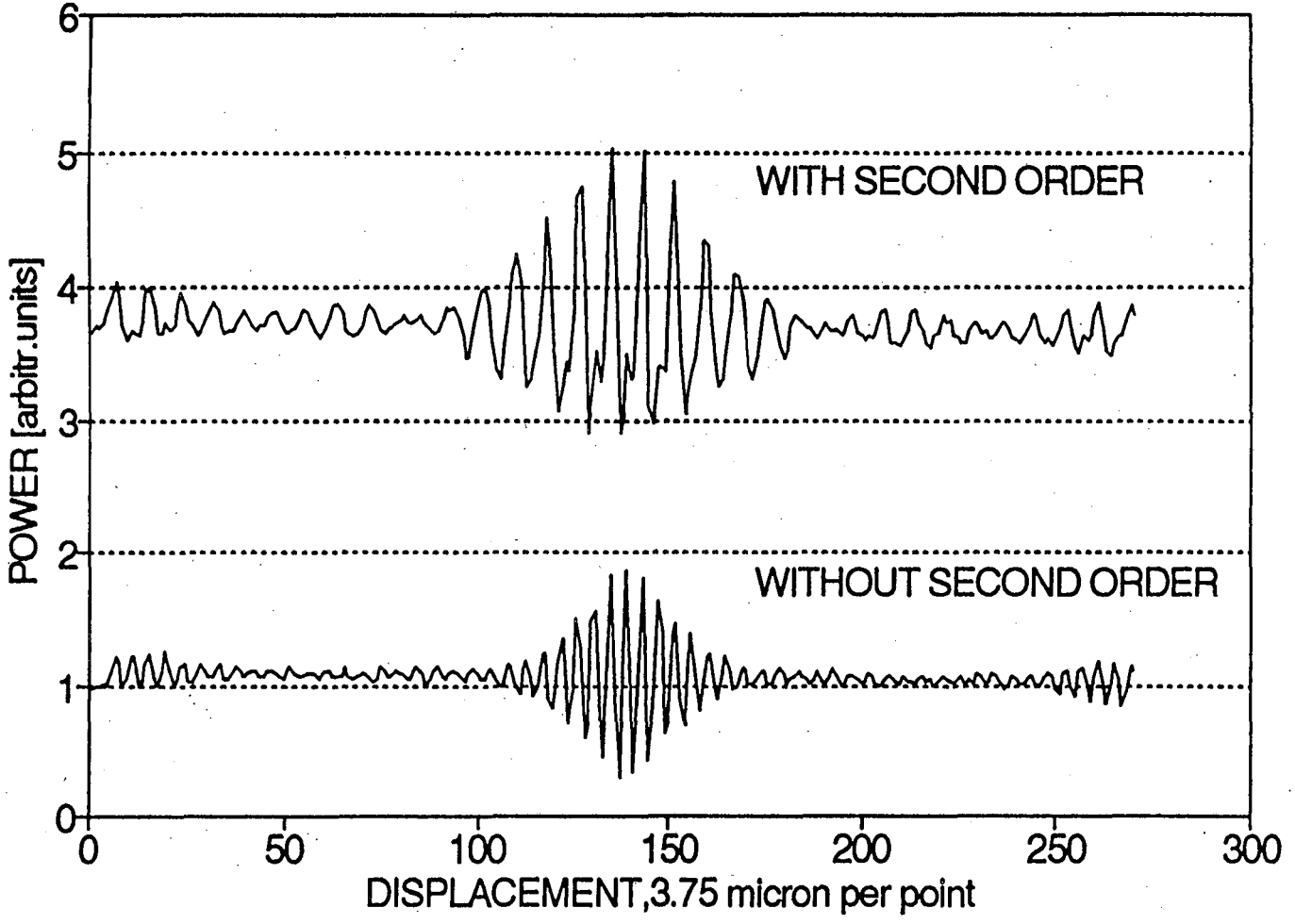
WITH SECOND ORDER
WITHOUT SECOND ORDER
POWER [arbitr.units]
DISPLACEMENT,3.75 micron per point
0
1
2
3
4
5
6
0
50
100
150
200
250
300

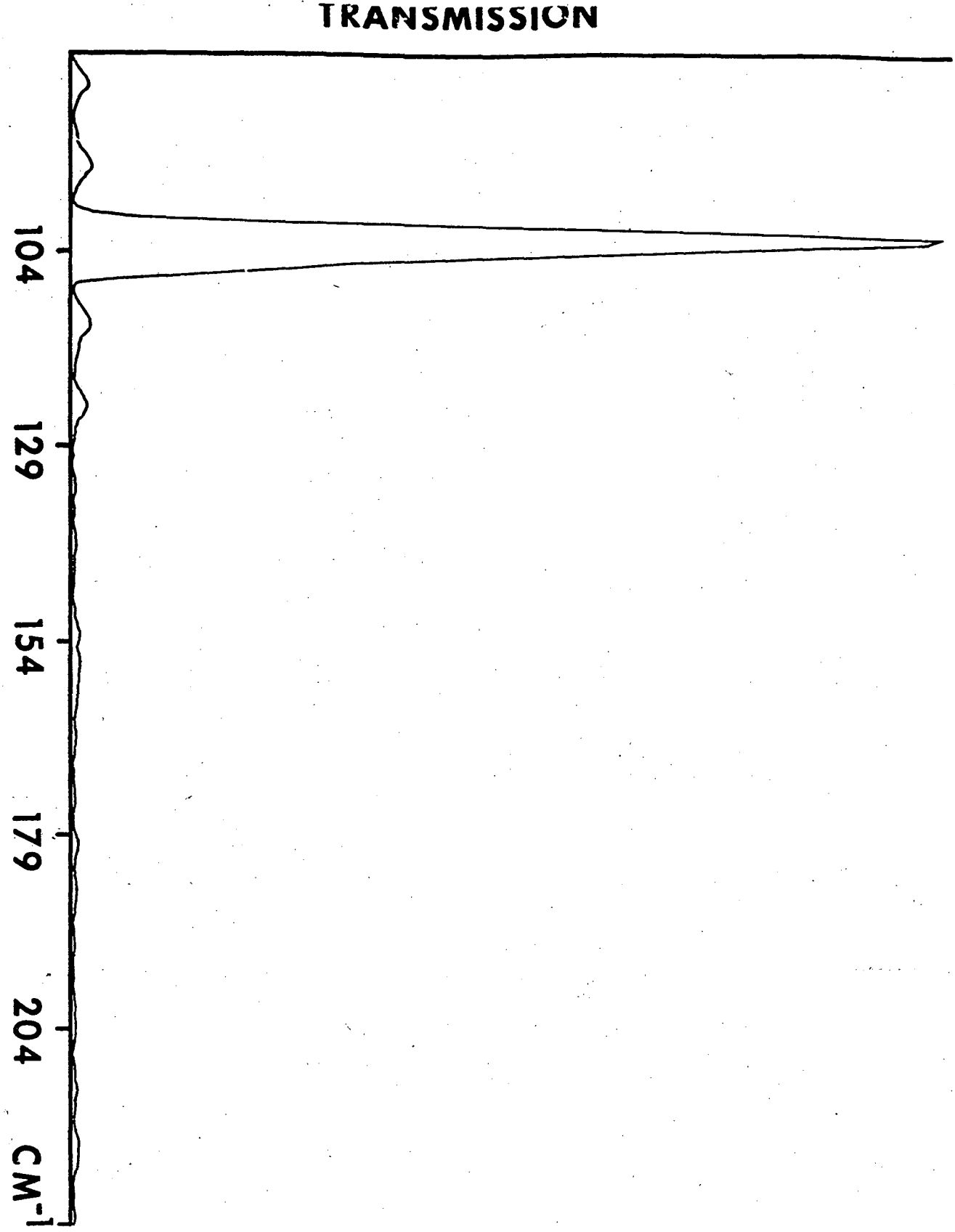
TRANSMISSION
104
129
154
179
204
CM-1

Fourier transform with randomly unequal sampling intervals.

We superimpose two cos-waves with frequencies 13/128 and 17/128:

$$\cos(2*\pi*13*x*\delta/128) + \cos(2*\pi*17*x*\delta/128)$$

where x runs from 1 to 128 (Length) and δ is initially equal 1.

The sampling interval (equal 1) may be multiplied by δ unequal 1 to represent changes of the sampling interval. We take the following different values for δ:

A = (1 - .005)	AA = (1 + .005)
B = (1 - .01)	BB = (1 + .01)
C = (1 - .015)	CC = (1 + .015)
D = (1 - .02)	DD = (1 + .02)
E = (1 - .025)	EE = (1 + .025)
F = (1 - .03)	FF = (1 + .03)
G = (1 - .035)	GG = (1 + .035)
H = (1 - .04)	HH = (1 + .04)

These values have been randomly distributed and how much each was used is given in histogram A.

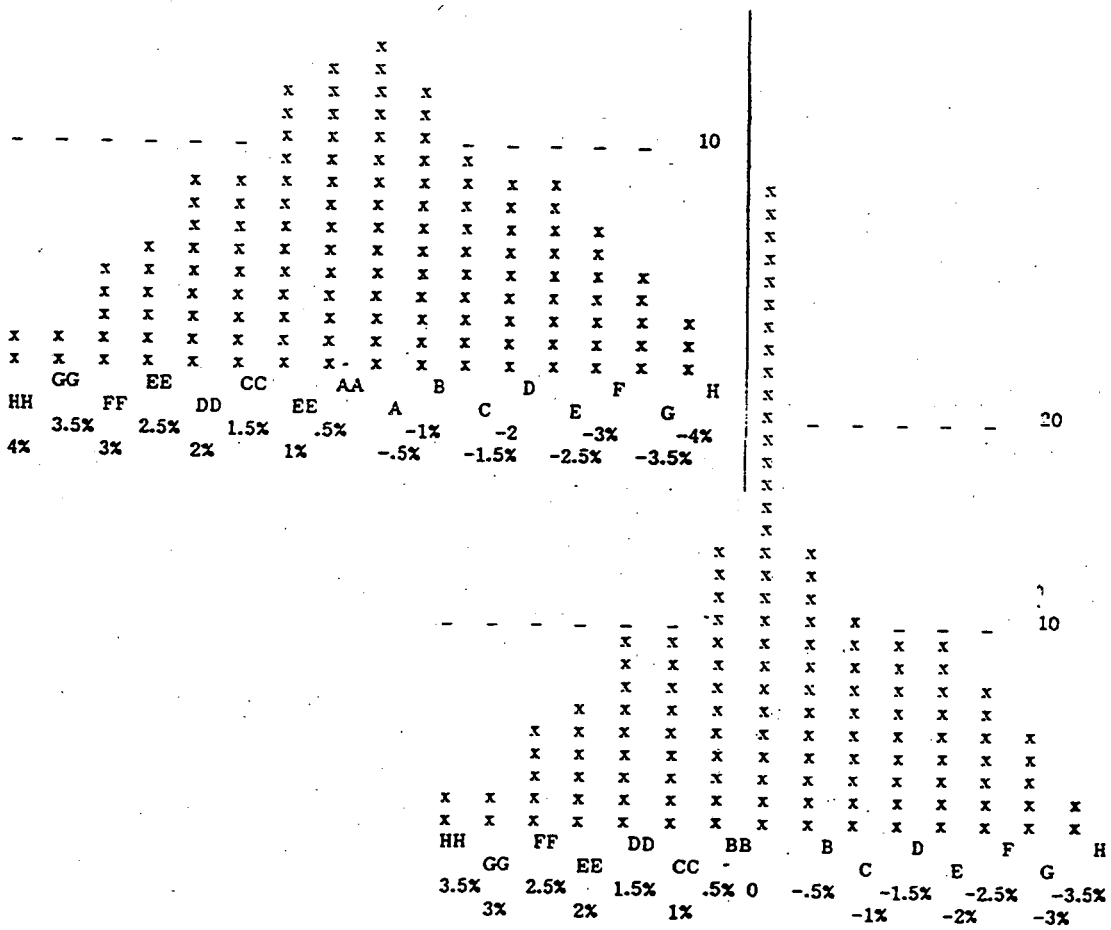

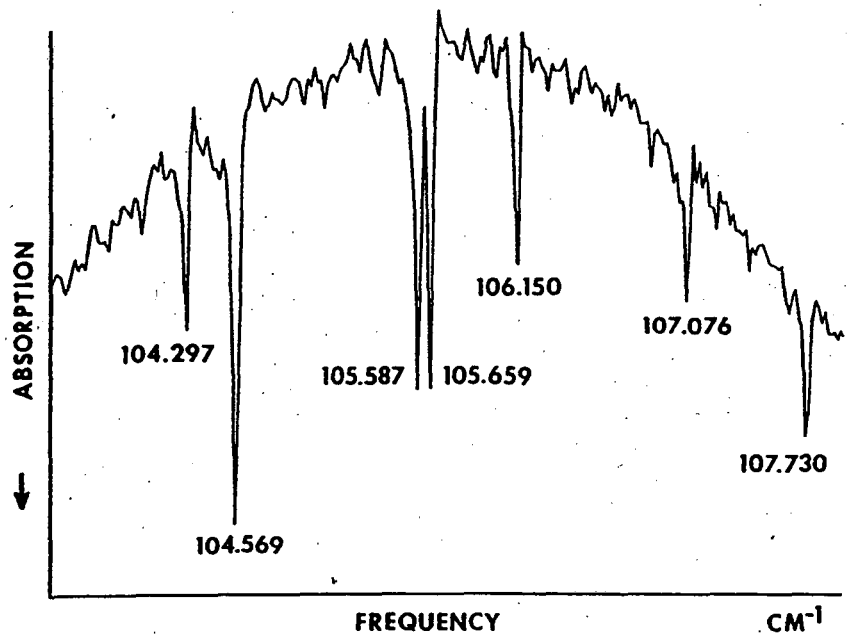

Water:

grating: 10 l/mm

spectrum folded 6 times

1024 points

$\Delta\nu = 0.018\ cm^{-1}$

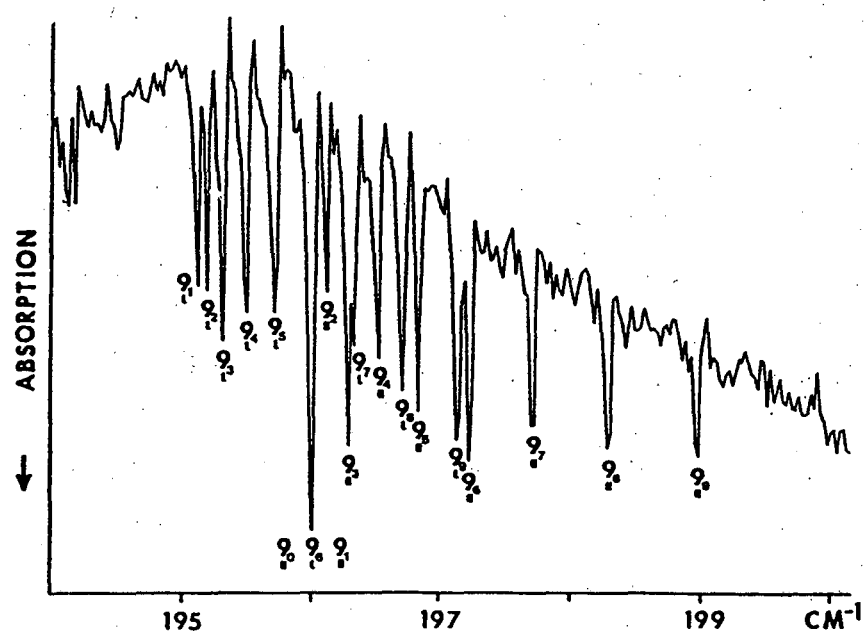

Ammonia

grating: 20 l/mm

spectrum folded 9 times

1024 points

$\Delta\nu = 0.023\ cm^{-1}$

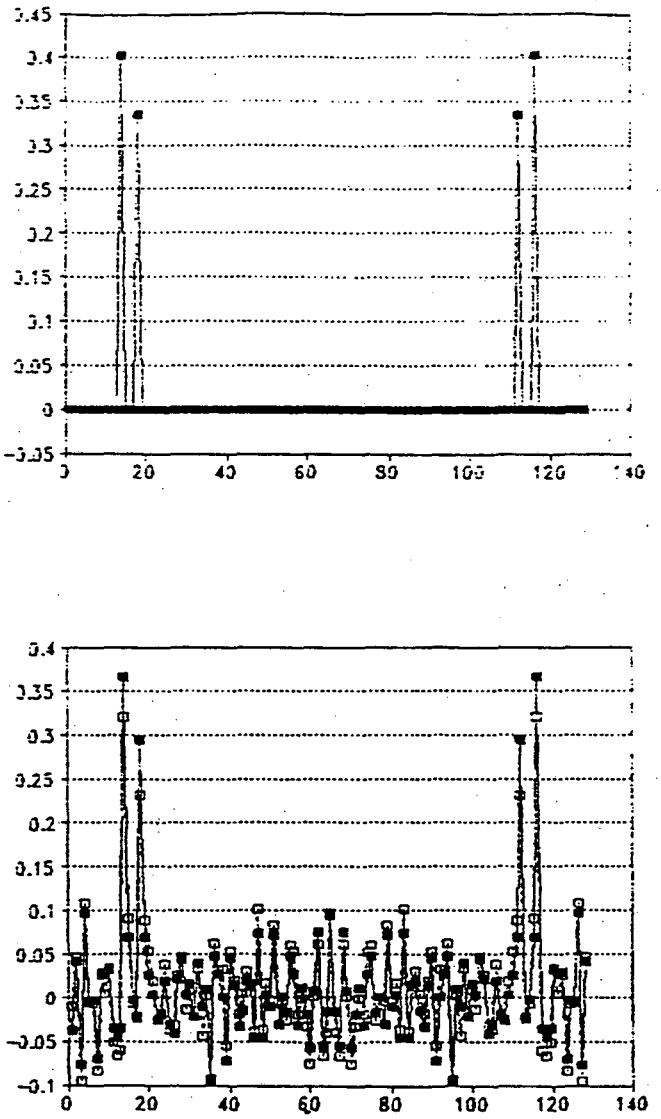

Fig.3 Upper graph: Transformation for $\delta = 1$.
Lower graph: black squares: values of histogram A, white squares: values of histogram B.

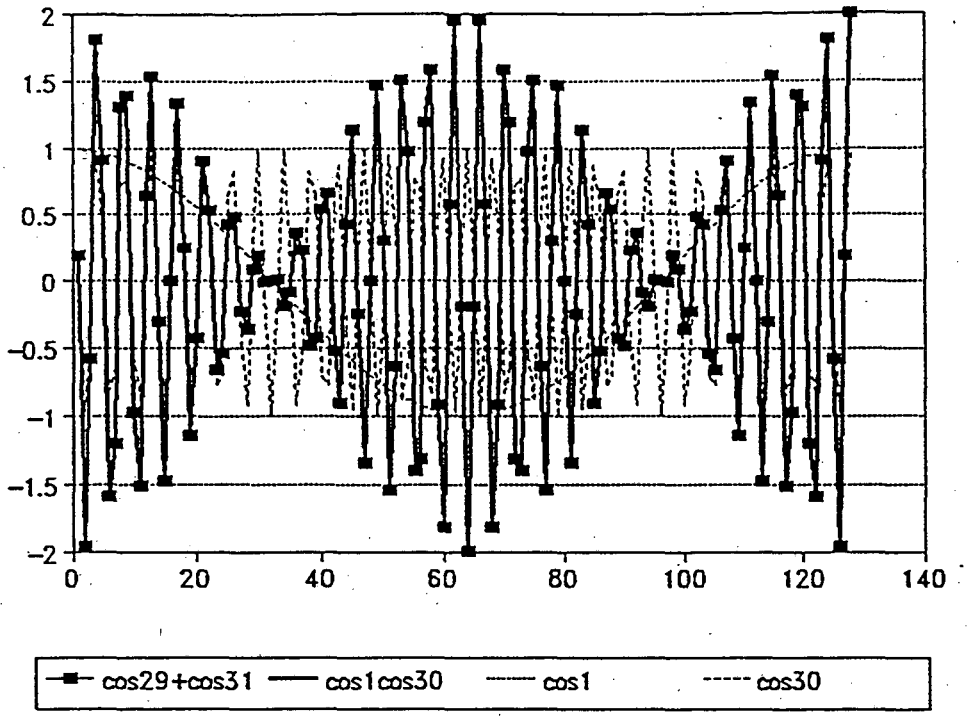
2
1.5
1
0.5
0
-0.5
-1
-1.5
-2
0
20
40
60
80
100
120
140
cos29+cos31
cos1cos30
cos1
cos30

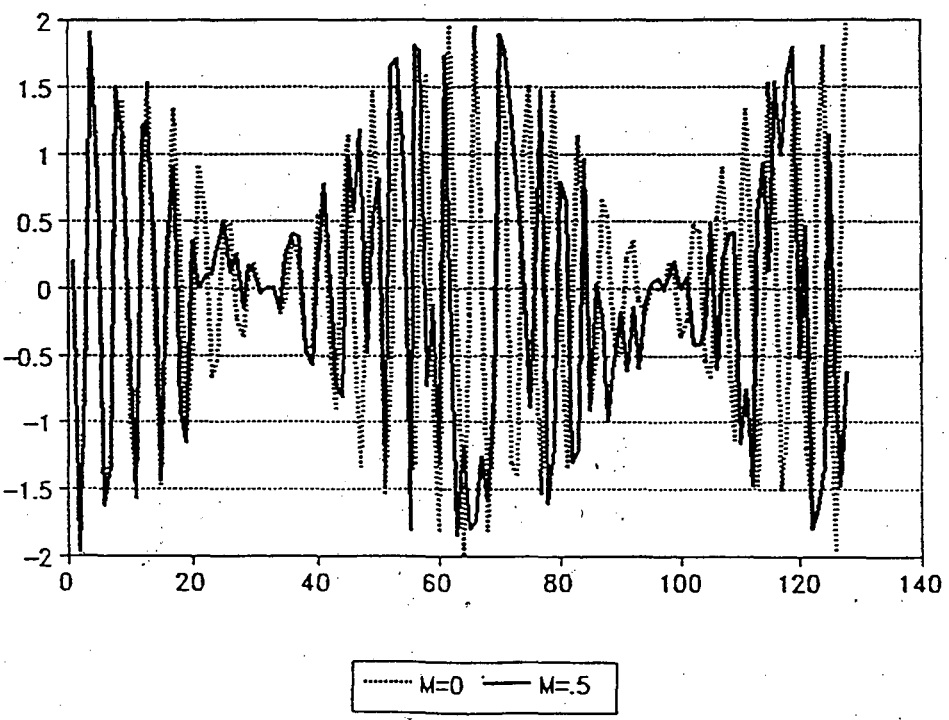
2
1.5
1
0.5
0
-0.5
-1
-1.5
-2
0
20
40
60
80
100
120
140
M=0
M=.5

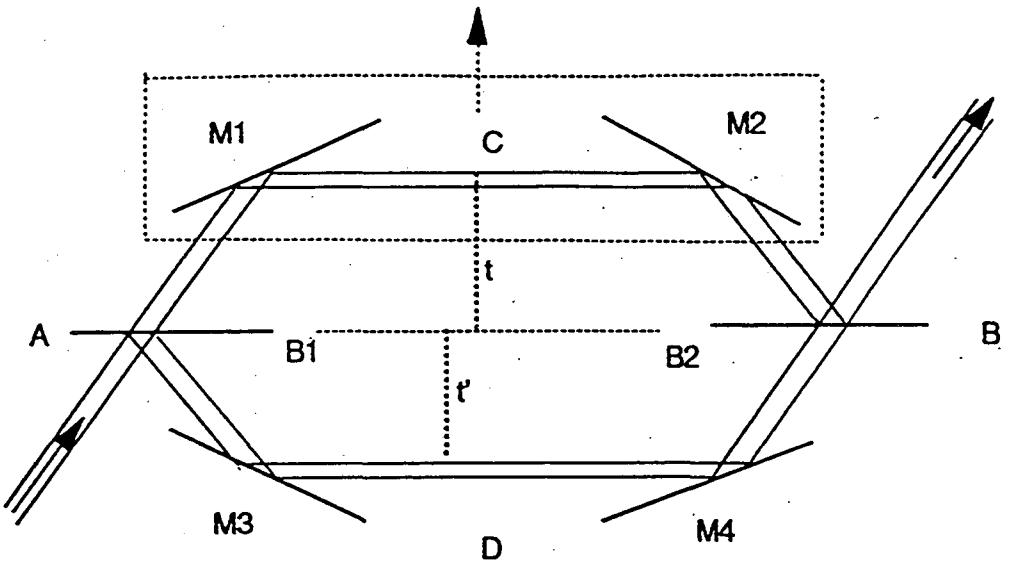

$\delta = 2(t - t') \tan\theta/2$

sampling: $\lambda/2$

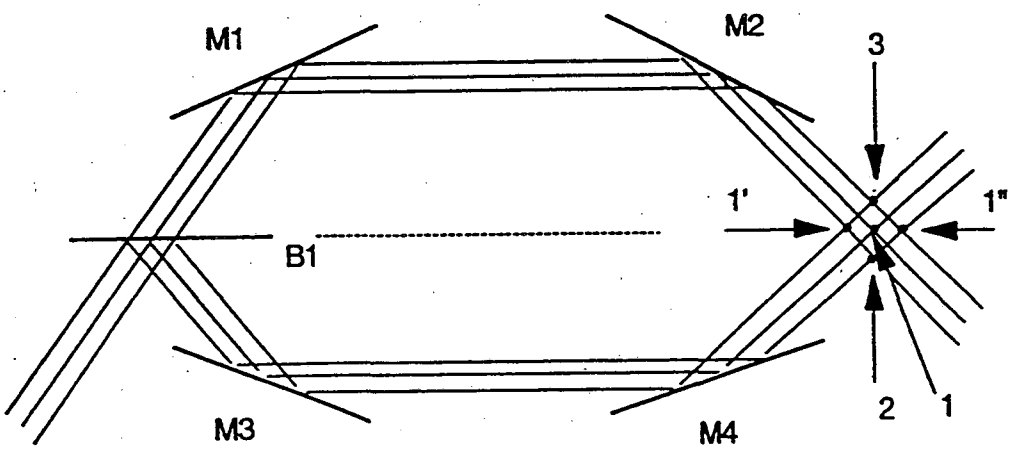

Points 1', 1, 1" have same optical path difference

Points 2, 1, 3 have different optical path differences

At 2 and 3 beams meet which are "counter parts" of splitting at B1.

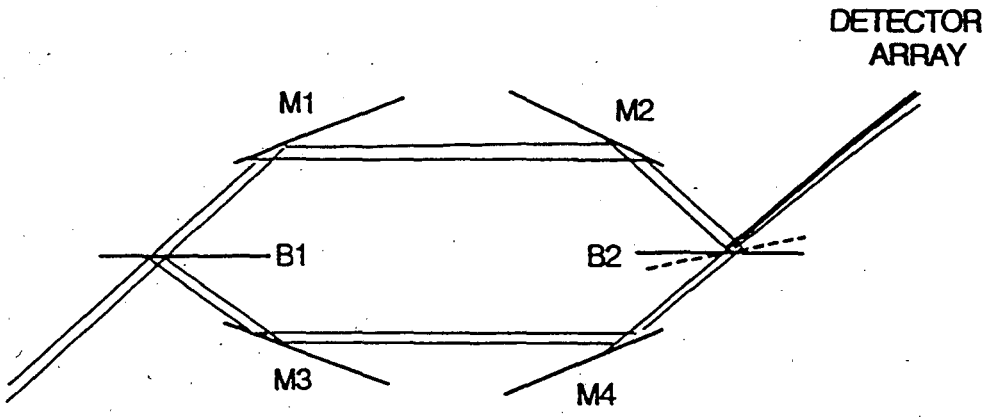

Optical path difference introduced at B2

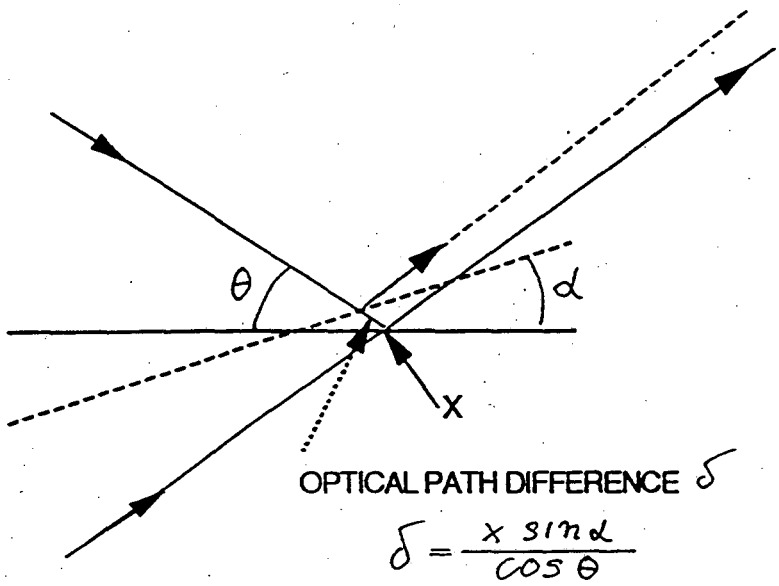

Introduction of optical path difference by tilting

MIRRORS HORIZONTALLY DIVIDED

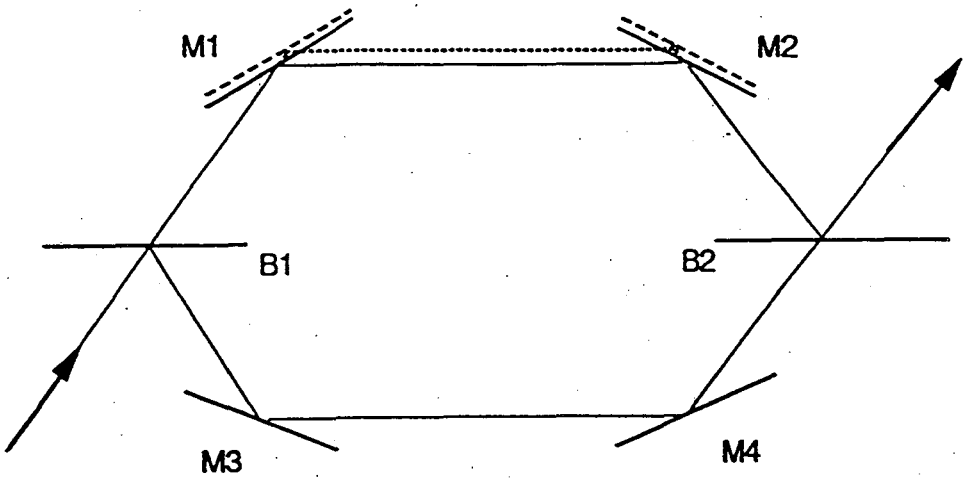

Mirrors with horizontal steps (large)

MIRRORS VERTICALLY DIVIDED

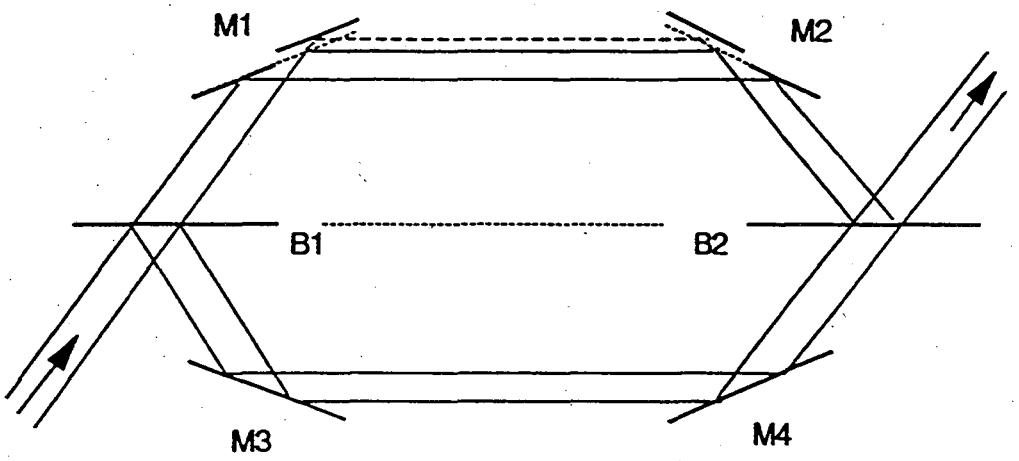

Mirrors with vertical steps (small)

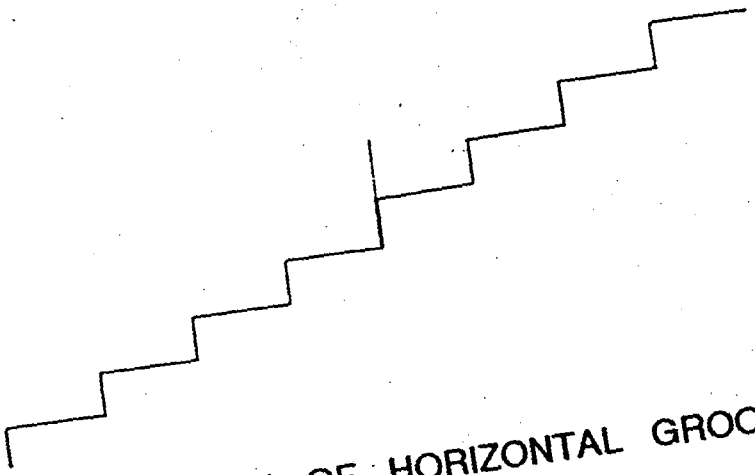

PROFILE OF HORIZONTAL GROOVES

PROFILE OF VERTICAL GROOVES

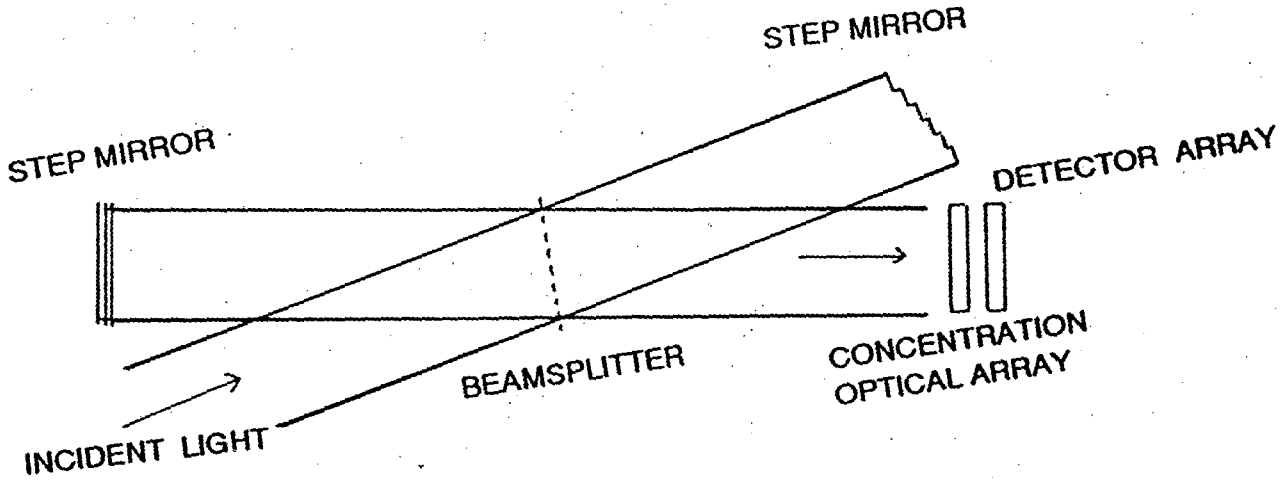

TIME RESOLVED SPECTROSCOPY

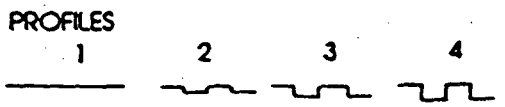
PROFILES
1
2
3
4

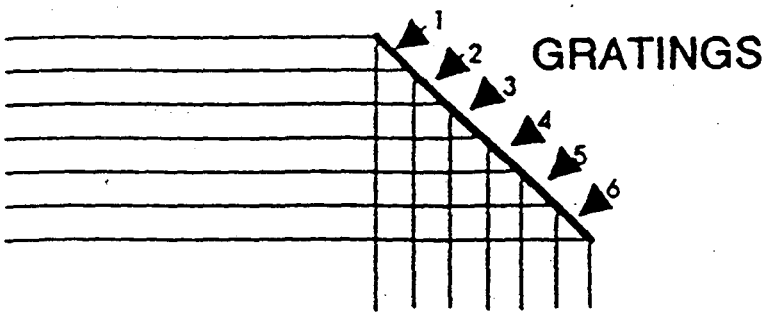
1
2
3
4
5
6
GRATINGS

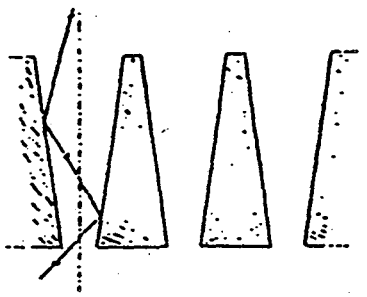

BEAMSPLITTER : WIDTH OF SLOTS 5μ
10μ

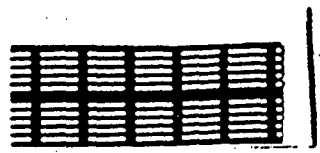

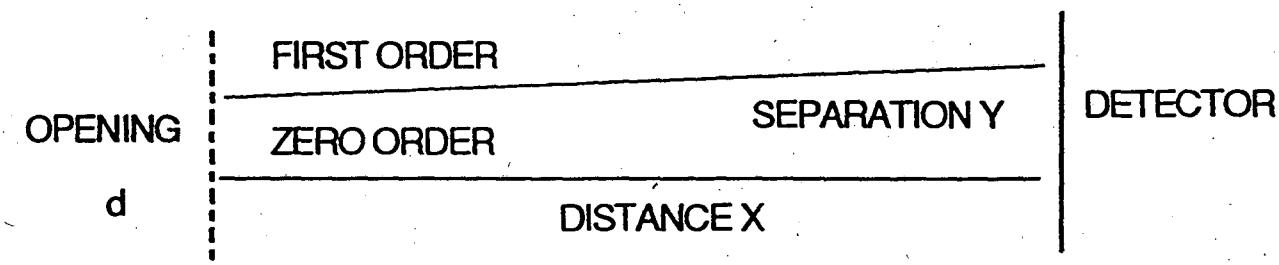

BEAMSPLITTER

$$Y = (X/d)$$

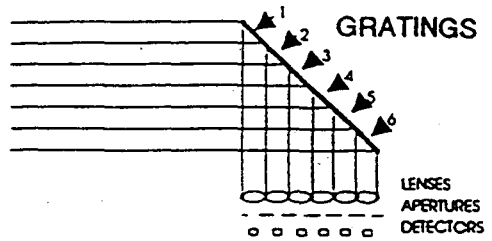
GRATINGS
1
2
3
4
5
6
LENSES
APERTURES
DETECTORS

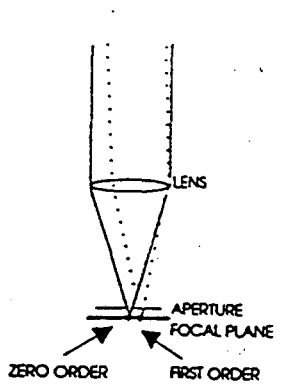
LENS
APERTURE
FOCAL PLANE
ZERO ORDER
FIRST ORDER

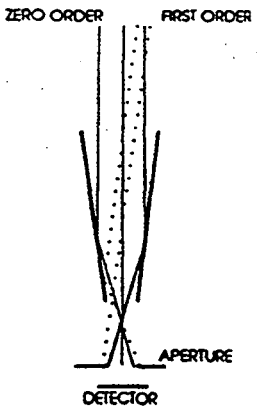
ZERO ORDER
FIRST ORDER
APERTURE
DETECTOR

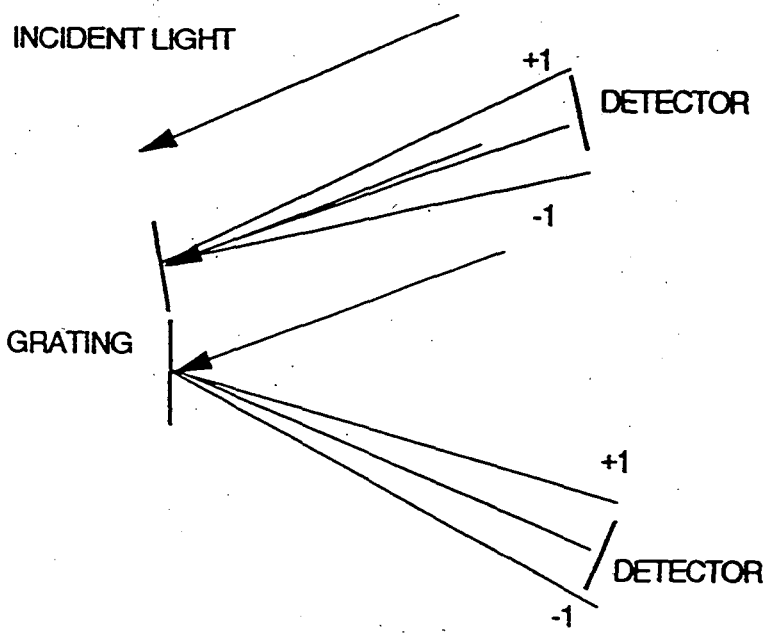
INCIDENT LIGHT
+1
DETECTOR
-1
GRATING
+1
DETECTOR
-1

Toward a Soft X-Ray Fourier Transform Spectrometer

Malcolm Howells

Lawrence Berkeley Laboratory

TOWARD A SOFT X-RAY FOURIER TRANSFORM SPECTROMETER

PARTICIPANTS:

K. Frank	LBL
M.R. Howells	LBL
Z. Hussain	LBL
E. Moler	LBL
D. Möller	Fairleigh Dickenson
T. Reich	LBL
D.A. Shirley	Pennsylvania State

CONTENTS:

TWO-ELECTRON STATES IN HELIUM

Domke et al
PRL 66, 1306 (1991
PRL 69, 1171 (1992

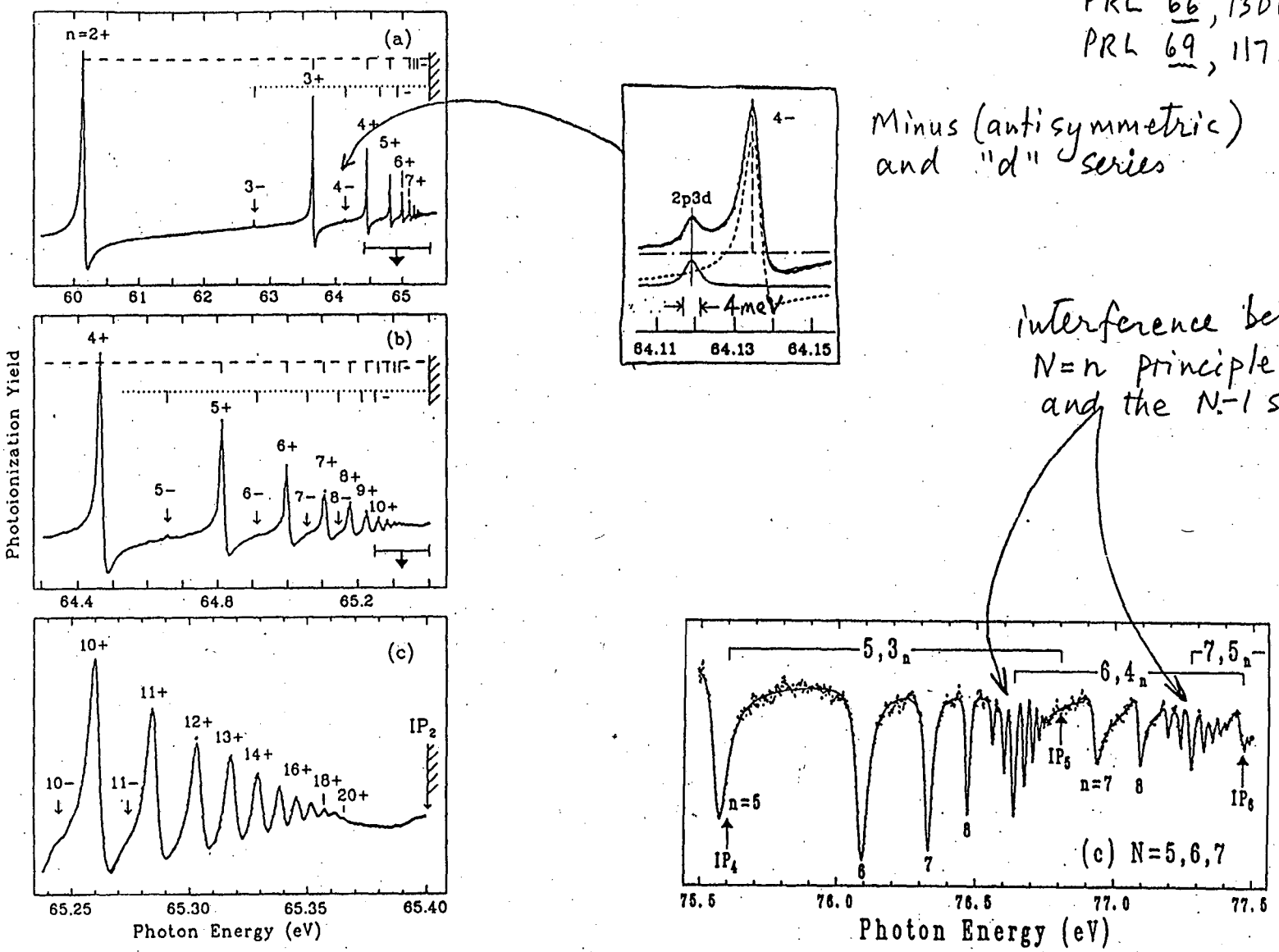

Minus (antisymmetric) and "d" series

interference between N=n principle term and the N-1 series

FIG. 1. Autoionizing resonances of doubly excited He below the $N=2$ threshold (IP_2) of He^+

MOTIVATIONS FOR CONTINUED STUDIES OF HELIUM AND FOR ATTEMPTS AT MUCH HIGHER RESOLUTION

1. THE GENERAL IMPORTANCE OF HELIUM EXPERIMENTS IN STUDIES OF ELECTRON CORRELATION INTERACTIONS

   - Important advances made following the SURF experiments in the 1960's (new quantization scheme and selection rules for two-electron systems)
   - Generally high level of interest and activity following the BESSY experiments in the 1990's

2. PRACTICAL GOALS NOT YET ACHIEVED DUE TO RESOLUTION LIMITATIONS

   - Quantitative measurements on the Rydberg series for higher N and n
   - More detailed study of the interferences between an $N=n$ term and an $N-1$ series
   - Observe and measure Fano parameters for higher members of the antisymmetric series and for the "d" series (not yet done at all)
   - Detection and measurement of parameters for corresponding series for $N>2$ (hardly seen so far)
   - Effects of applied fields

3. DESIRE TO USE MEASUREMENTS OF HIGHER ORDER EFFECTS AS SENSITIVE TESTS OF THEORETICAL TREATMENTS

FOURIER TRANFORM SPECTROSCOPY

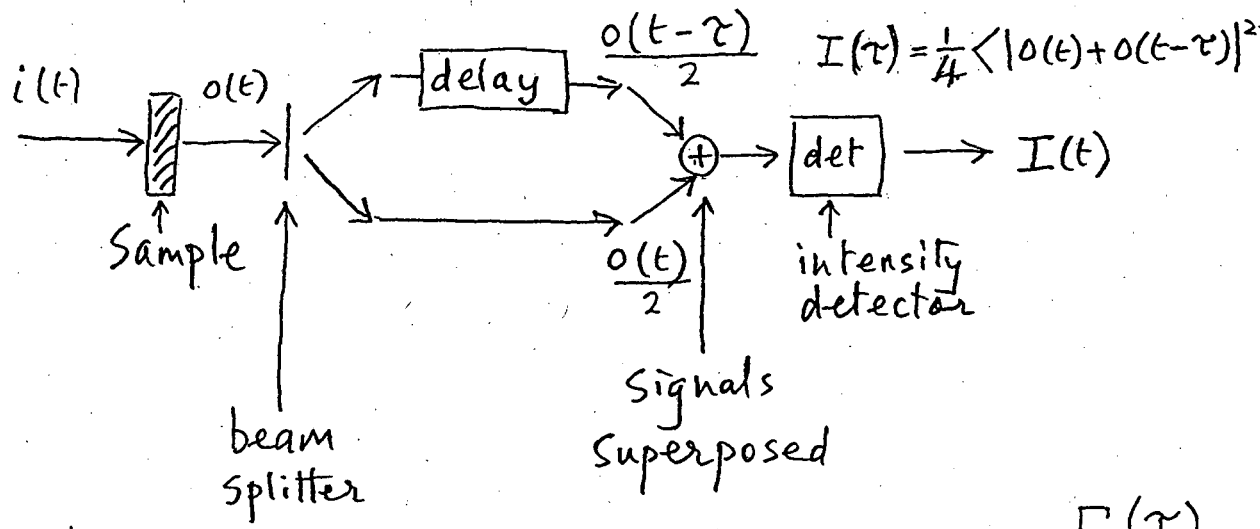

$$I(\tau) = \frac{1}{4}\langle |o(t)+o(t-\tau)|^2 \rangle$$

$$= \frac{1}{2}\langle |o(t)|^2 \rangle + \frac{1}{2}\langle o(t)\, o(t-\tau) \rangle$$

$\Gamma_{11}(\tau)$ — autocorrelation of $o(t)$

By Weiner-Khinchin theorem

$$I(\tau) = \frac{I(0)}{2} + \int_0^\infty B(f)\cos(2\pi f x)\, df$$

$B(f)$ ← desired spectrum

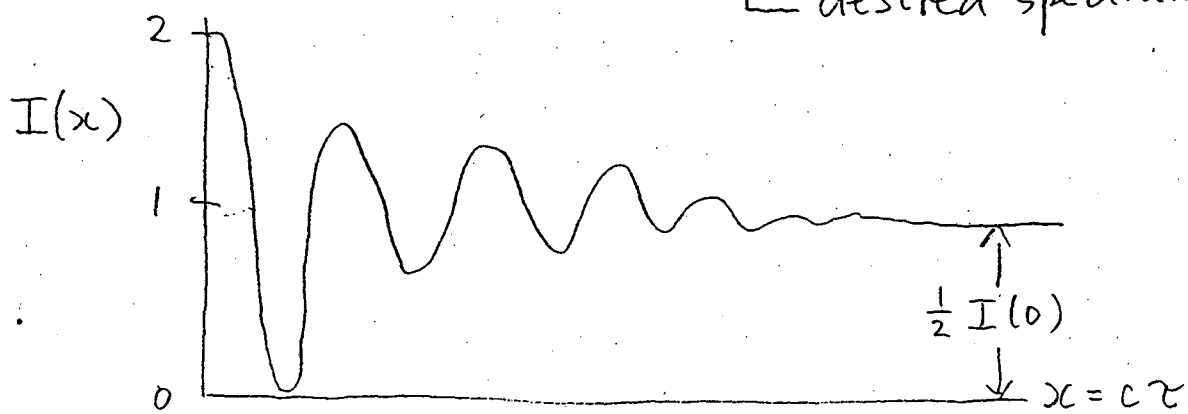

ADVANTAGES OF FOURIER TRANSFORM SPECTROSCOPY

THROUGHPUT:

Jacquinot advantage — doesn't apply for bright sources

MULTIPLEX:

Fellgett advantage — doesn't apply for a shot-noise rather than detector-noise-limited system

RESOLVING POWER:

- Equal to number of waves of path difference between the interfering beams
- Can be very high, but spectral range is normally low — does apply!

FREQUENCY RANGE TRANSFORMATION:

$$I(\tau) = \frac{I_0}{2} + \int_0^\infty B(f) \cos 2\pi f x \, df$$

$$x = v t, \quad f_0 - \Delta < f < f_0 + \Delta$$

$$I(\tau) \sim \cos(2\pi f_0 v t)$$

$$\sim \cos\left(2\pi \nu_0 \frac{v}{c} t\right)$$

$f_0 = \frac{1}{\lambda_0} = \frac{\nu_0}{c}$

optical frequency; reduction factor

$\lambda_0 = 100\ \text{Å}$

$v = 20\ \mu\text{m/s}$

$\downarrow$

1 kHz (optical → audio)

SOFT X-RAY INTERFEROMETER LAYOUT

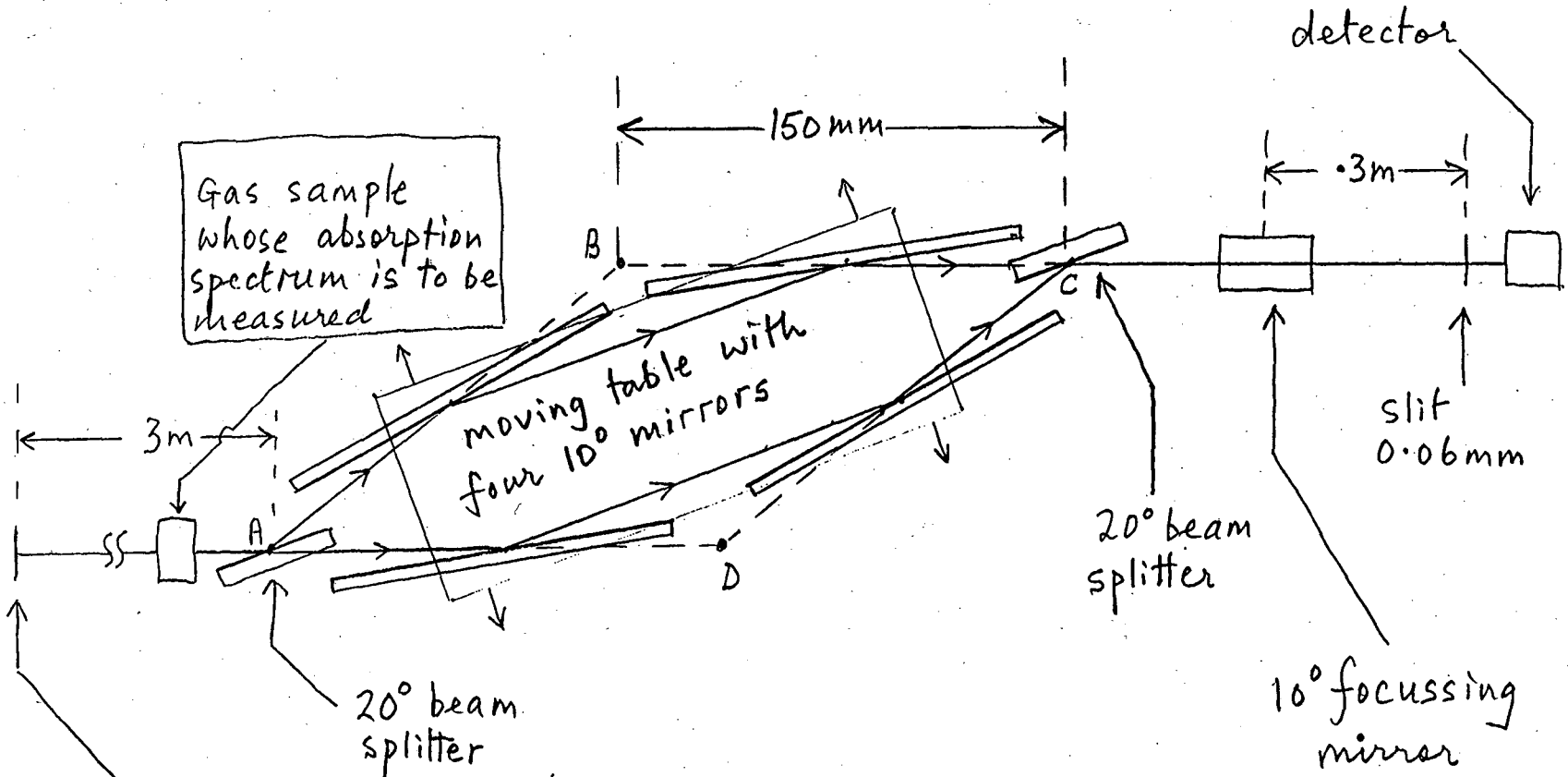

PLAN VIEW WITH SOME DISTORTION OF SCALE

BEAM SPLITTERS

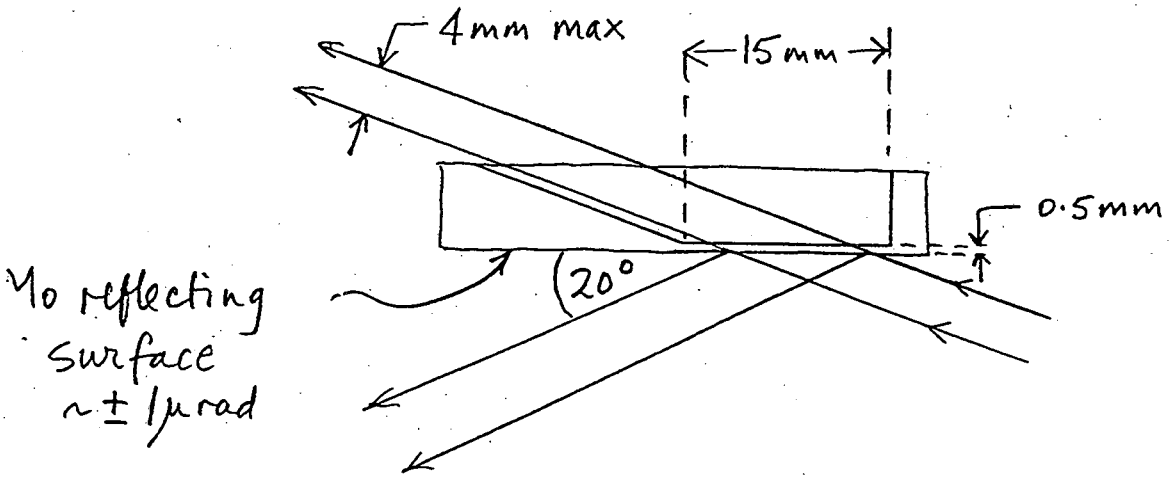

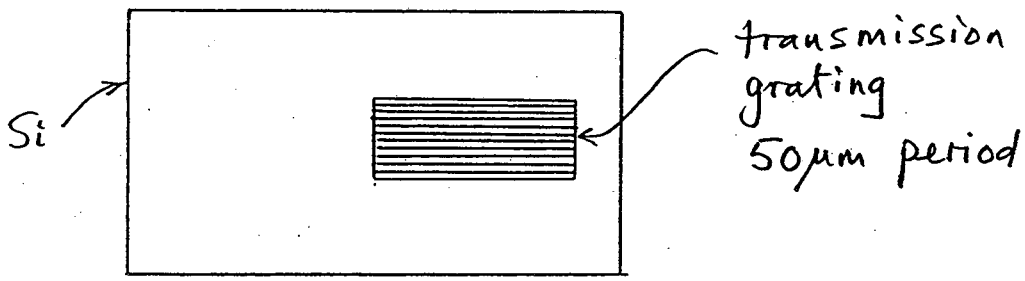

Issues
- manufacture: silicon microfab.
- thermal load
- density driven by order rejection

$\sin\theta = \frac{\lambda}{d} > \frac{s}{r}$

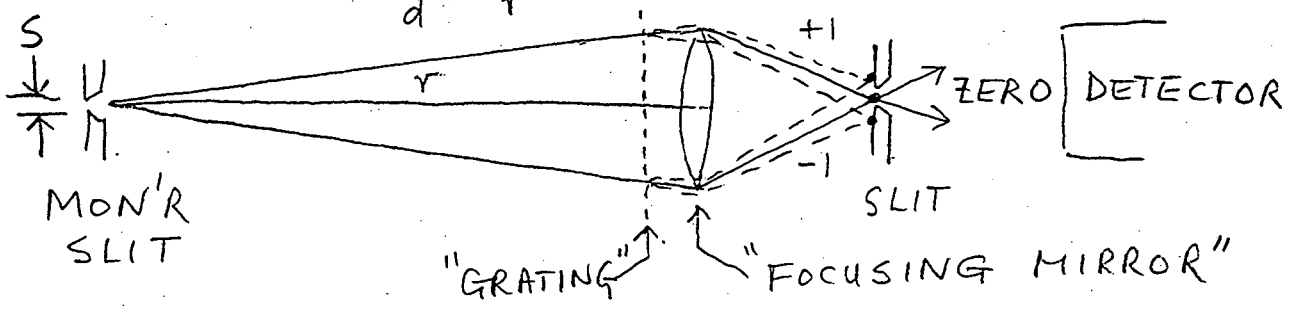

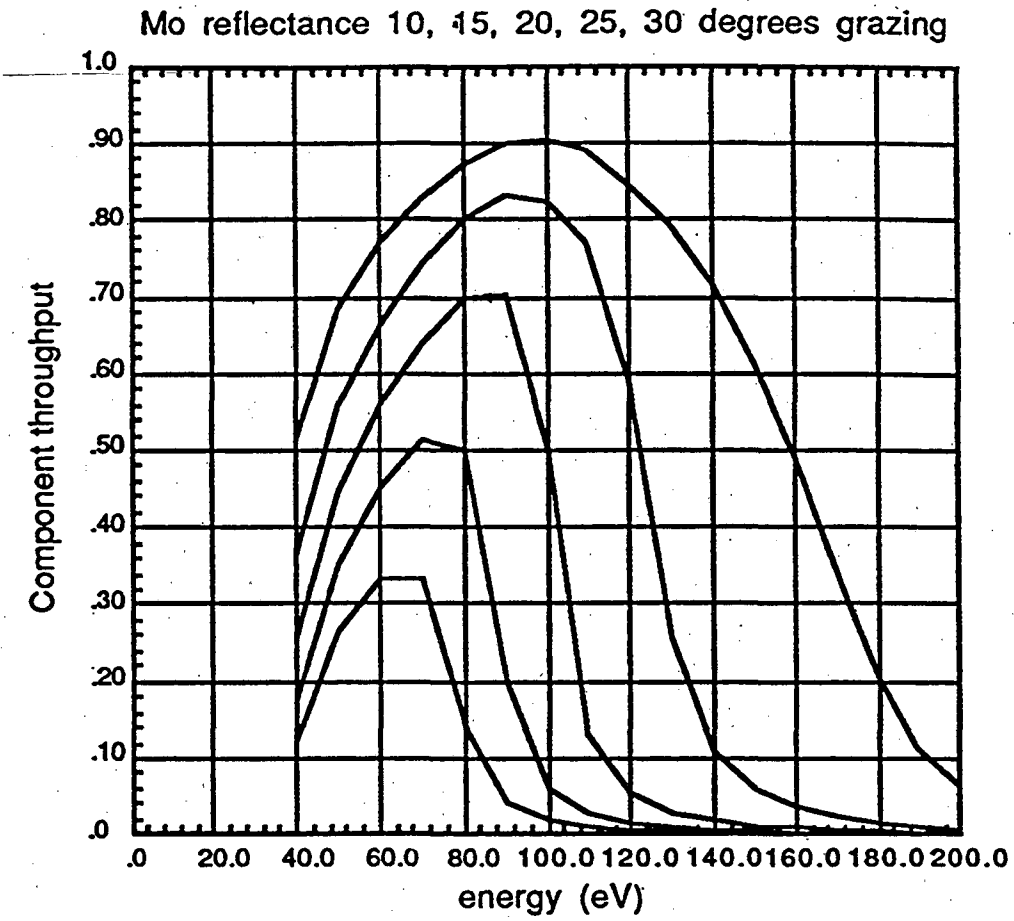
Mo reflectance 10, 15, 20, 25, 30 degrees grazing
Component throughput
1.0
.90
.80
.70
.60
.50
.40
.30
.20
.10
.0
.0
20.0
40.0
60.0
80.0
100.0
120.0
140.0
160.0
180.0
200.0
energy (eV)

STRAIGHT-LINE MECHANISMS

Bonse 1971

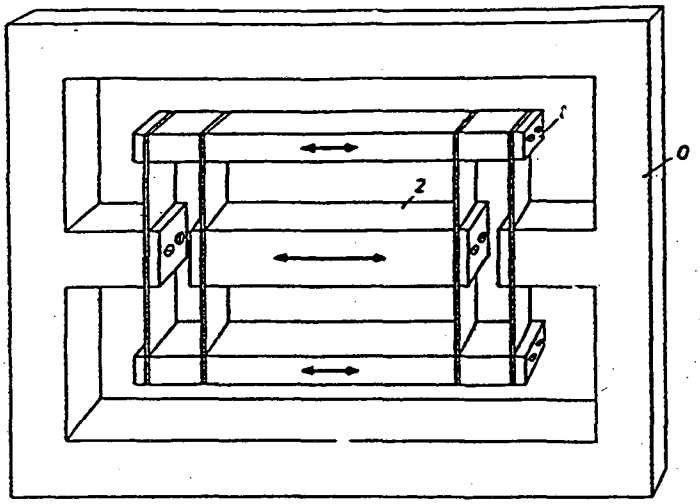

FIGURE 2. ***Construction of traverse units TU used with Δs- and Δx-traverses.***

Hoffrogge 1973

(a)

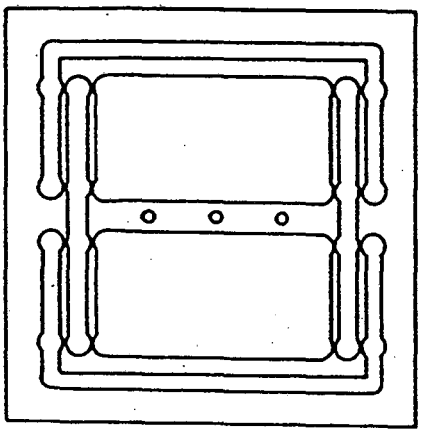

(b)

Deslattes 1969

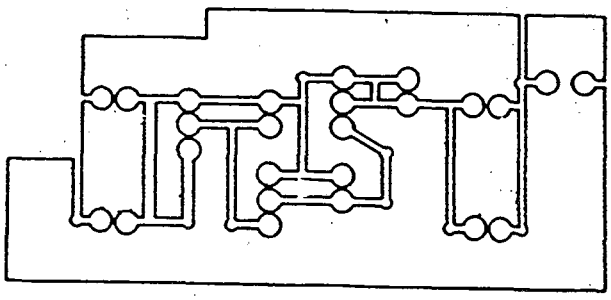

FIGURE 2. *Linear motion devices used in PTB (a) and NBS (b) measurements of Si 220 lattice periods.*

PERFORMANCE OF PTB MECHANISM

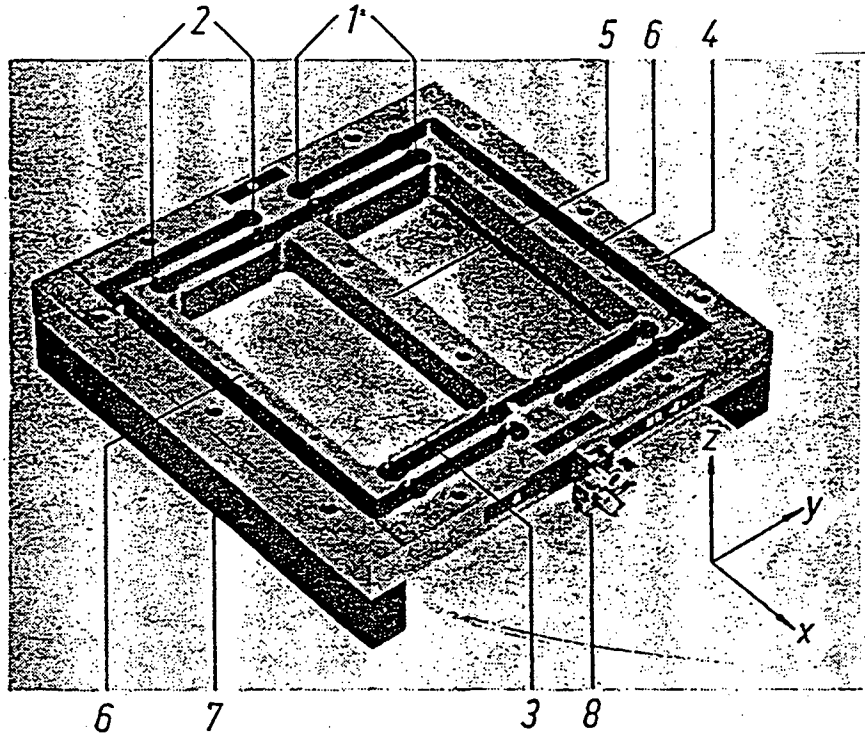

Bild 2. Ansicht der gefertigten Doppelparallelfeder mit Adapter für den Antrieb

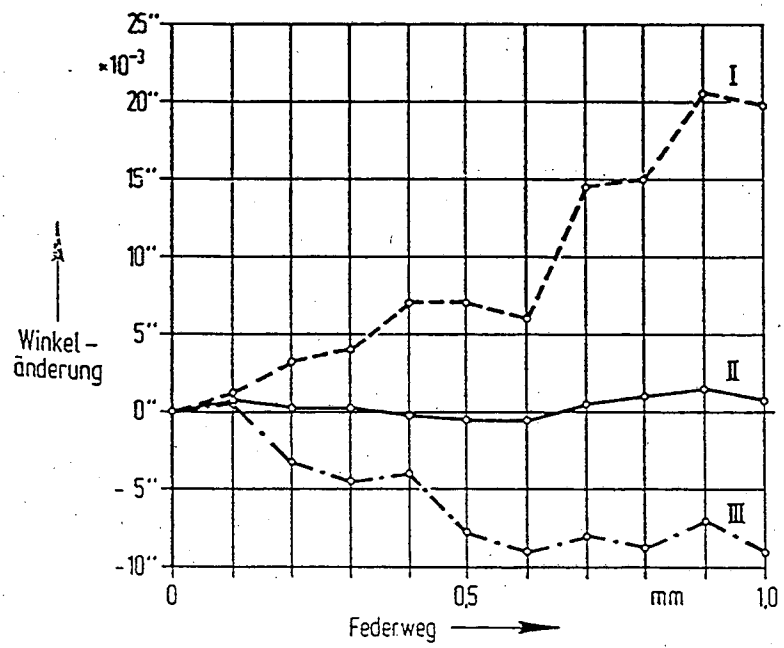

Bild 5. Winkeländerung in Abhängigkeit vom Federweg. Feder in horizontaler Lage, Drehung um die y-Achse

I Kraftangriffspunkt 1,77 mm unterhalb der Mittelachse

II Kraftangriffspunkt 1,47 mm unterhalb der Mittelachse

III Kraftangriffspunkt 1,22 mm unterhalb der Mittel-

FLEXABLE HINGES

better hinge

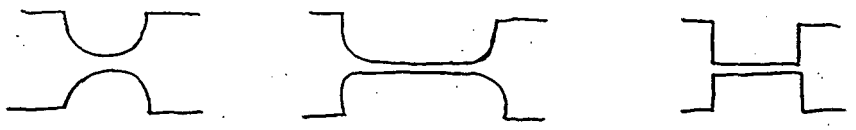

lower stress

$$C(y) = \frac{\tau_{hinge}}{\tau_{beam}} = \frac{2f^2}{\frac{1}{g} + \frac{1}{f^2}\left(g + \frac{8y^2}{g} + \frac{12gy}{f}\tan^{-1} f\right)}$$

$$f = \sqrt{4y+1}$$

$$g = 2y+1 \qquad y = \rho / t$$

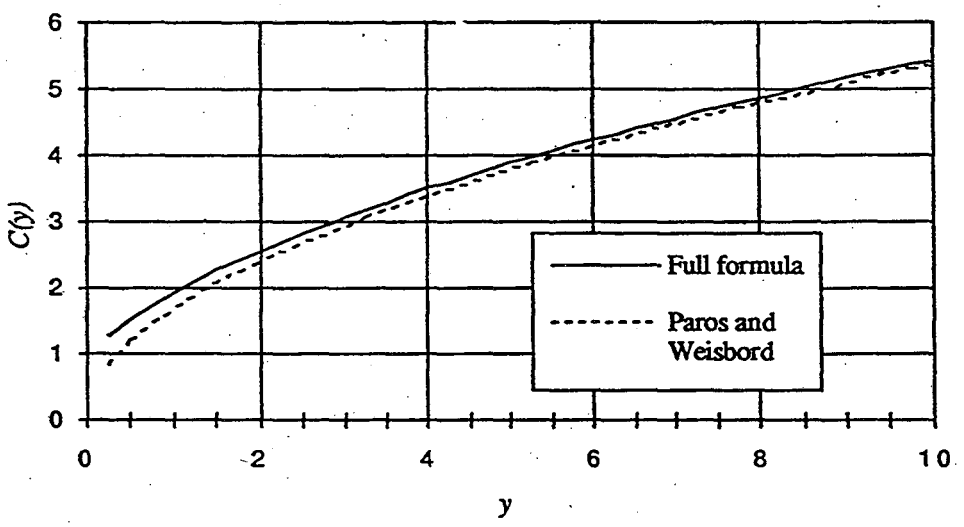

ELEMENT SHAPE	TORSIONAL RIGIDITY	MAXIMUM STRESS
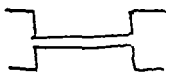	$\tau_{beam} = \frac{Yb\,t^3}{24\rho}$	$\sigma_{beam} = \frac{Yt\,\theta}{4\rho}$
	$C(y)\ \tau_{beam}$	$C(y)\ \sigma_{beam}$
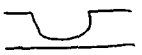	$\frac{C(2y)}{8}\ \tau_{beam}$	$\frac{C(2y)}{8}\ \sigma_{beam}$
	$2C(y)\ \tau_{beam}$	$2C(y)\ \sigma_{beam}$
	$\frac{C(2y)}{4}\ \tau_{beam}$	$\frac{C(2y)}{4}\ \sigma_{beam}$

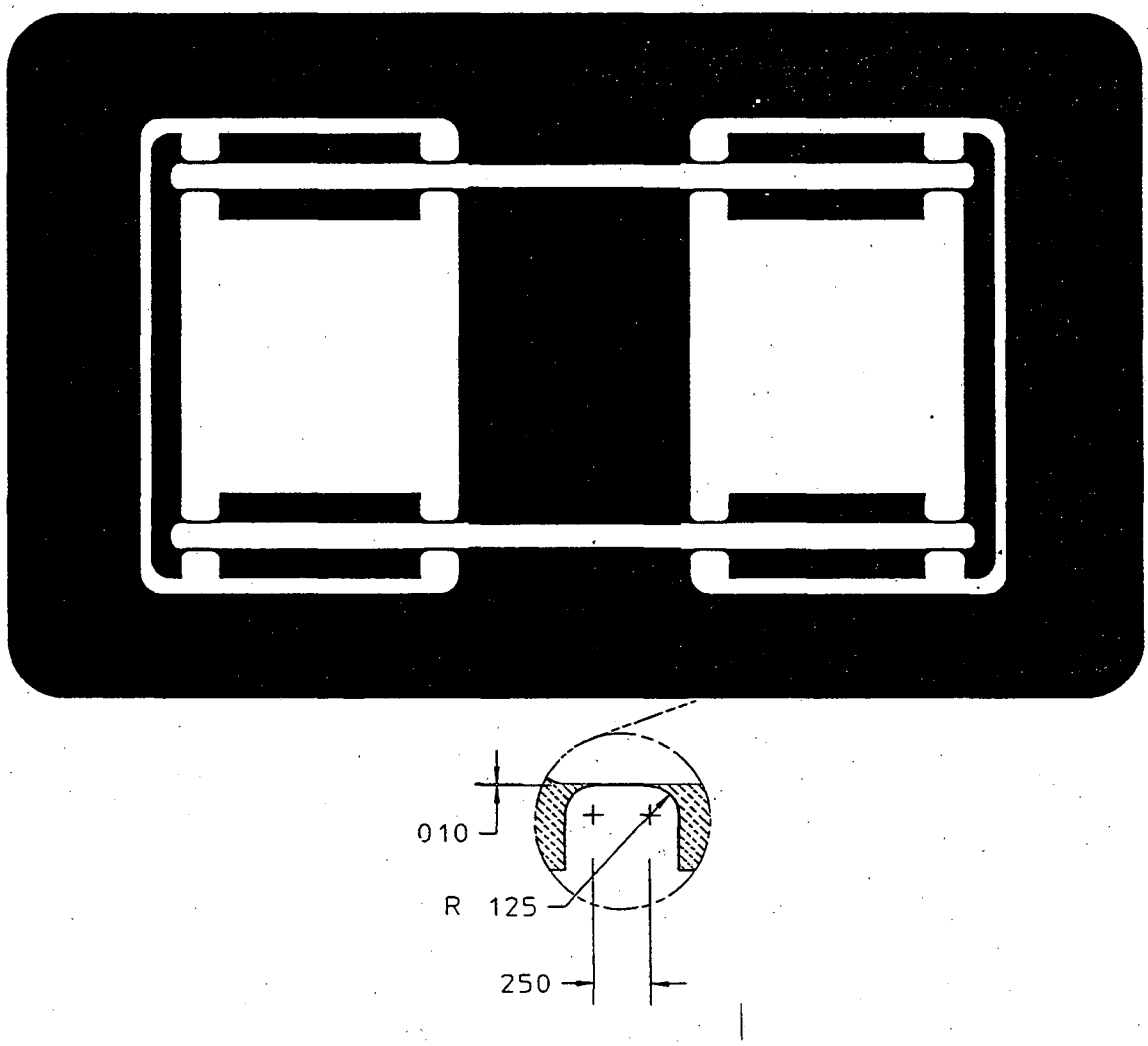
010
R 125
250

FATIGUE PROPERTIES OF CANDIDATE FLEXURE MATERIALS				
Class of material	Tool steel	Alloy steel	Maraging steel (Vascomax)	Aluminum
Type	S7	4340	C-300	7075
Tempering temperature (°F)	1000	200	900	
Temper designation				T651
Tensile strength (ksi)	264	287	294	77
0.2% Yield strength	200	270	287	67
Elongation (%)	10	11	10	6
Reduction in area (%)	33	39	47	12.7
Elastic modulus (Msi)	30	29	27.5	10.3
Strain range(10^5) universal slopes	0.008314	0.009356	0.010160	0.006874
Strain range(10^7) universal slopes	0.004488	0.005048	0.005457	0.003801
Fatigue endurance limit (ksi)		140	125	23

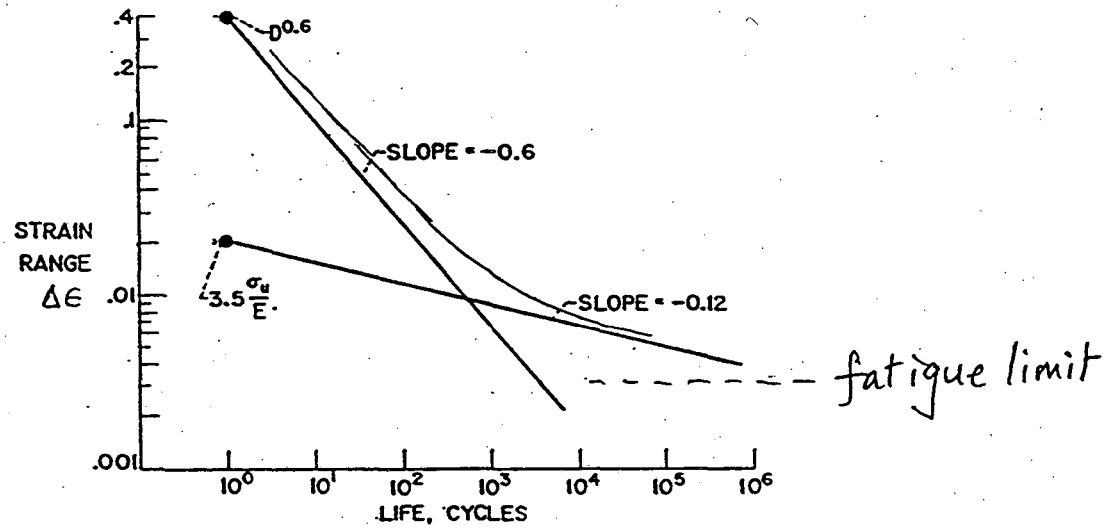

$$\Delta\epsilon = 3.5\,\frac{\sigma_u}{E}\,N_f^{-0.12} + D^{0.6}N_f^{-0.6}$$

where

σ_u = ultimate tensile strength, psi

D = ductility, $\ln \dfrac{1}{1 - RA}$

RA = reduction in area, percent

N_f = number of cycles to failure

$$I(x)=\frac{I(0)}{2}+\int_0^\infty B(\sigma)\cos(2\pi\sigma x)d\sigma$$

Following Chamberlain [2] we represent wavefront errors by allowing x in (2) to be a function of the position (u, v) in the aperture and summing the contributions of all the separate "elementary interferometers" corresponding to each area $dudv$. Thus the total effect when (2) is evaluated is

$$I(x)=\frac{I(0)}{2}+\int_0^\infty d\sigma\frac{B(\sigma)}{A}\iint_A[1+\cos(2\pi\sigma x(u,v))]dudv$$

where $B(\sigma)/A$ is the power per unit area per unit bandwidth in the exiting beam. If we represent $x(u,v)$ as $x+\delta(u, v)$ then (3) can be written

$$I(x)=\frac{I(0)}{2}+\int_0^\infty D(\sigma)B(\sigma)\cos(2\pi\sigma x)d\sigma$$

where

$$D(\sigma)=\frac{1}{A}\iint_A\cos[2\pi\sigma\delta(u,v)]dudv$$

$D(\sigma)$ is called by Chamberlain the "spectral distortion factor": a name which makes sense in view of the first of equations (4).

GENERAL TOLERANCE:

$$D(\sigma)>0.9 \text{ for } \sigma=10^6/\text{cm (same as } \lambda=100\text{Å) and } R=1\text{mm}$$

TILT OF ONE OF THE INTERFERING WAVEFRONTS WITH RESPECT TO THE OTHER:

Consider a wavefront tilt of e so that $\delta(v)=ve$. Substituting again into the second of equations (4) we find

$$\begin{aligned}D(\sigma)&=\frac{1}{A}\int_{-R}^{R}dv\int_{-\sqrt{R^2-v^2}}^{\sqrt{R^2-v^2}}\cos(2\pi\sigma ve)du\\&=\frac{2R}{A}\int_{-R}^{R}\sqrt{\left(1-\left(\frac{v}{R}\right)^2\right)}\cos(2\pi\sigma ve)dv\\&=2\frac{J_1(2\pi\sigma eR)}{(2\pi\sigma eR)}\end{aligned}$$

Where the last line is obtained using a standard integral representation of the Bessel function [3]. Now $2J_1(x)/x$ equals 1 at x=0 and falls to 0.9 at x=0.911 Thus the condition on e is

$$e<\frac{0.911}{2\pi\sigma R}$$

which for our stated tolerance (5) gives e<1.5μradians. This must be respected during initial alignment of the instrument and held during the motion of the table.

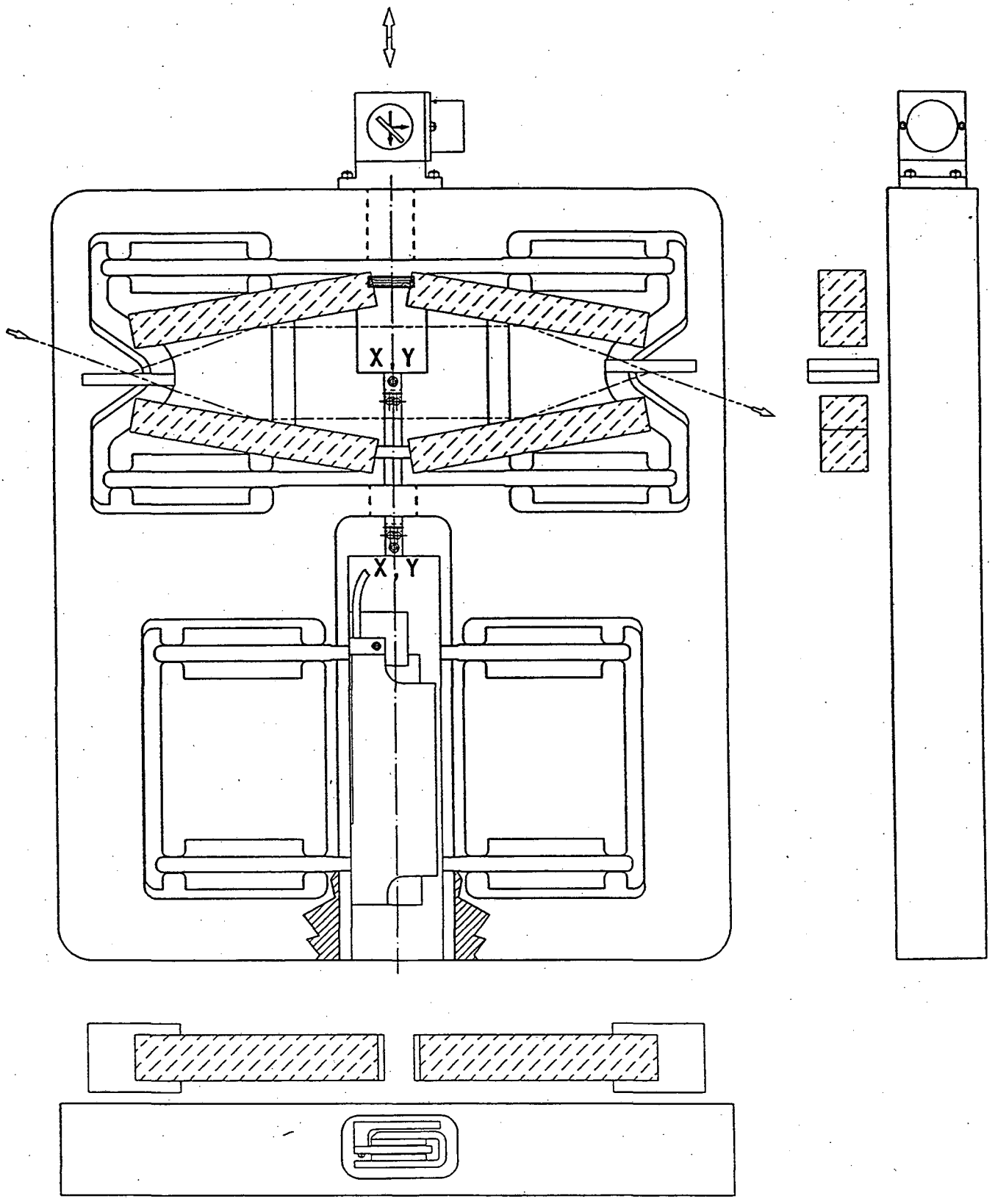
X Y
X Y

QUALITY OF THE TABLE MOTION

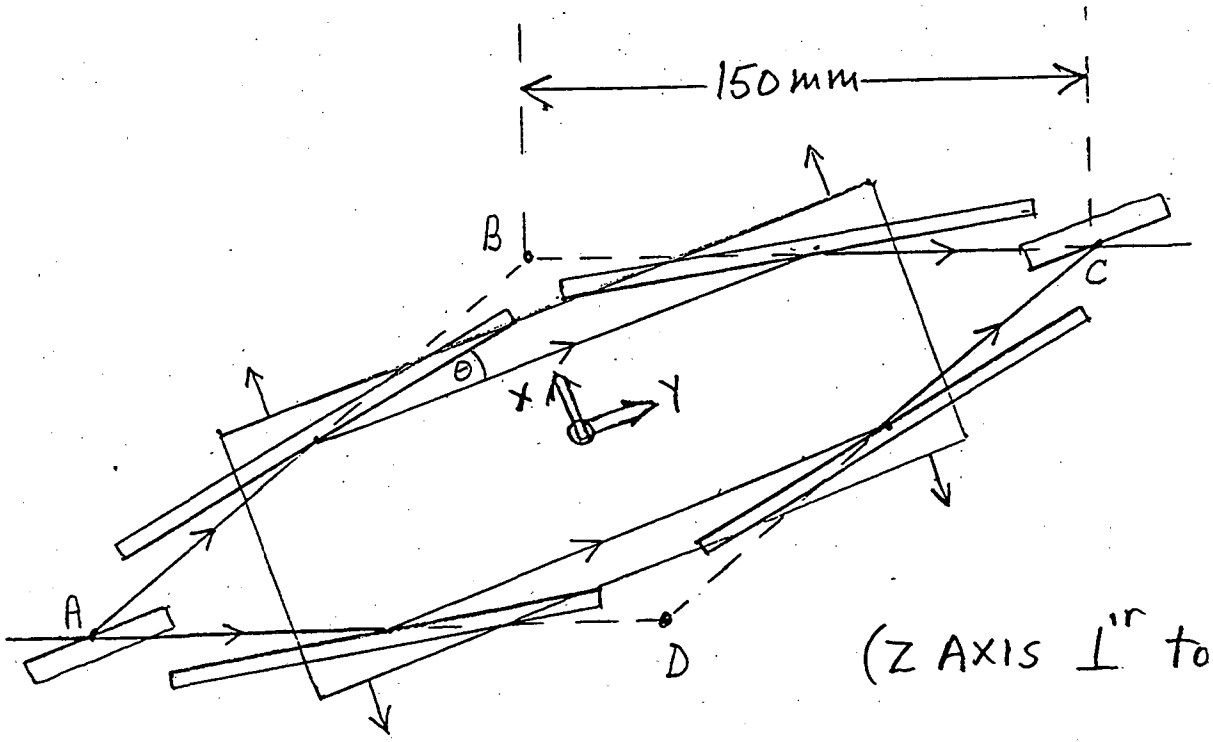

(Z AXIS ⊥^{r} to paper)

ROTATION ABOUT

X AXIS: (ROLL) INITIAL MOTION IS IN THE PLANE OF THE MIRROR → SMALL EFFECT

Y AXIS: (PITCH) ANGLE BETWEEN INTERFERING BEAMS IS FOR PITCH ΔP

$$8\,\Delta P \cos\theta \sin\theta$$

$\therefore \Delta P < 10^{-6}$ RAD FOR BEAM ANGLE $< 1.5\mu$

Z AXIS: (YAW) CANCELS TO FIRST ORDER BECAUSE OF DOUBLE REFLECTION

(COMPARE PENTAPRISM)

SUMMARY OF TOLERANCES

ITEM	TOLERANCE
Incoming beam:	
Angle	±2.2mradian
Width	2mm (full width)
Relative tilt of interfering wavefronts	1.5μradians
Mirror surfaces:	
Slope	±0.5μradian (1.0 peak to valley)
Sphericity	Radius>4.6km
Beamsplitter surfaces:	
Slope	±1.0μradian (2.0 peak to valley)
Sphericity	Radius>2.3km
Moving table:	
Pitch	±1.0μradian
Roll	large
Yaw	large

SAMPLING CONSIDERATIONS

"Shah" $\text{Ш}(x) = \sum_n \delta(x-n)$

$\mathcal{F}[\text{Ш}(x)] = \text{Ш}(f)$

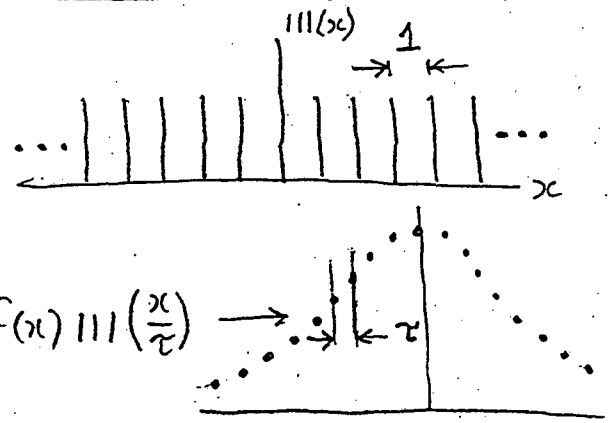

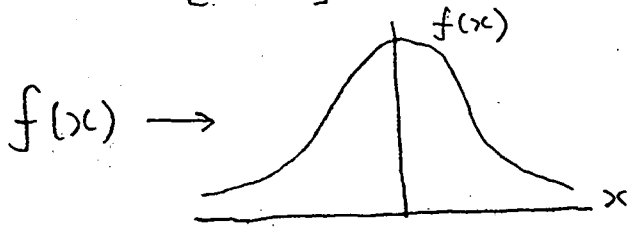

$\mathcal{F}(f(x)) = F(f)$

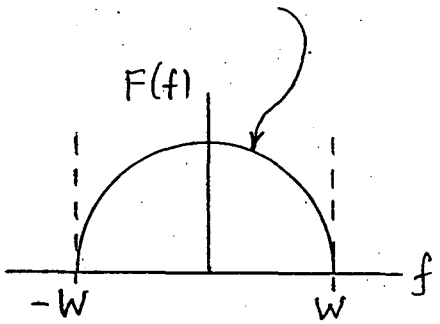

$\mathcal{F}[f(x)\,\text{Ш}(\frac{x}{\tau})] = F(f) * |\tau|\,\text{Ш}(f\tau)$

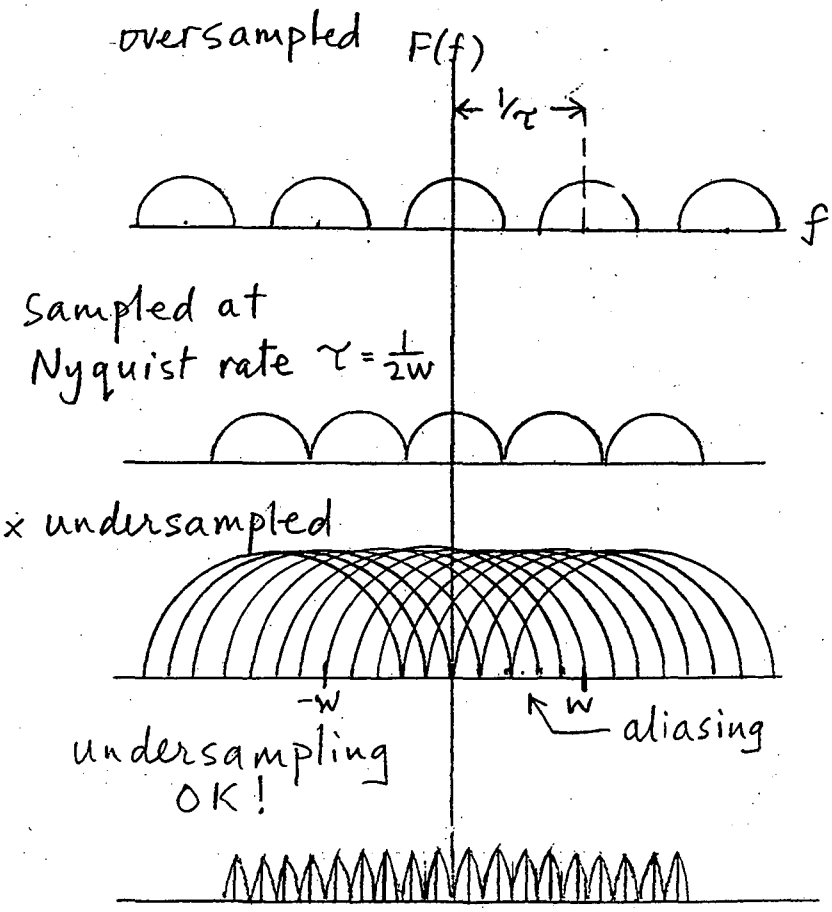

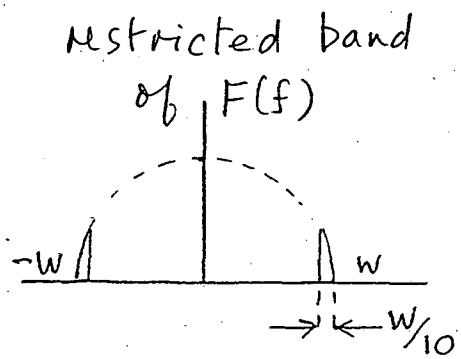

SAMPLING THEOREMS

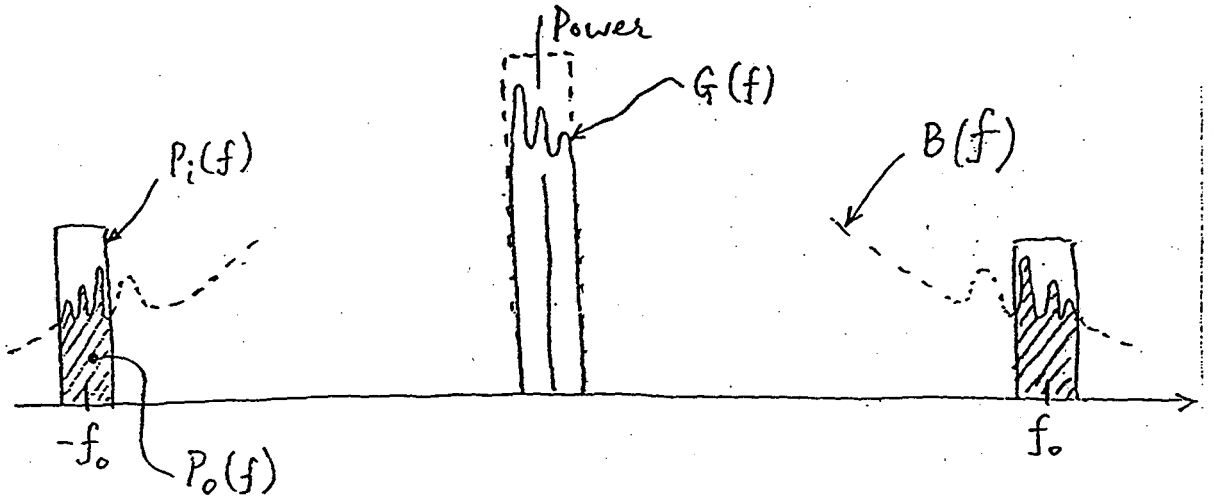

Theorem I:

A function $F(t)$ which is bandwidth-limited within a range $2W$ centered on zero is fully defined by its values $F(t_n)$ at an infinite series of points t_n where n is an integer and

$$t_n = \frac{n}{2W}$$

and

$$F(t) = \sum_{n=-\infty}^{n=+\infty} F(t_n)\,\mathrm{sinc}\left[2W(t-t_n)\right]$$

where $\mathrm{sinc}(x)$ is defined as $\sin(\pi x)/\pi x$.

Theorem II:

A function $F(t)$ which is bandwidth-limited within ranges W centered on f_0 and $-f_0$ is fully defined by its values $F(t_n)$ at an infinite series of points t_n where n is an integer and

$$t_n = \frac{n}{W}$$

and

$$F(t) = \sum_{n=-\infty}^{n=+\infty} \mathrm{sinc}\left[W(t-t_n)\right]\left\{F(t_n)\cos\left[f_0(t-t_n)\right] + \hat{F}(t_n)\sin\left[f_0(t-t_n)\right]\right\}$$

$$= \sum_{n=-\infty}^{n=+\infty} \mathrm{sinc}\left[W(t-t_n)\right]\sqrt{F(t_n)^2 + \hat{F}(t_n)^2}\,\cos\left[f_0(t-t_n) - \phi_n\right]$$

$$\phi_n = \tan^{-1}\left(\frac{\hat{F}(t_n)}{F(t_n)}\right)$$

where $\hat{F}(t)$ is the Hilbert transform of $F(t)$.

THE COMPLEX ENVELOPE FUNCTION

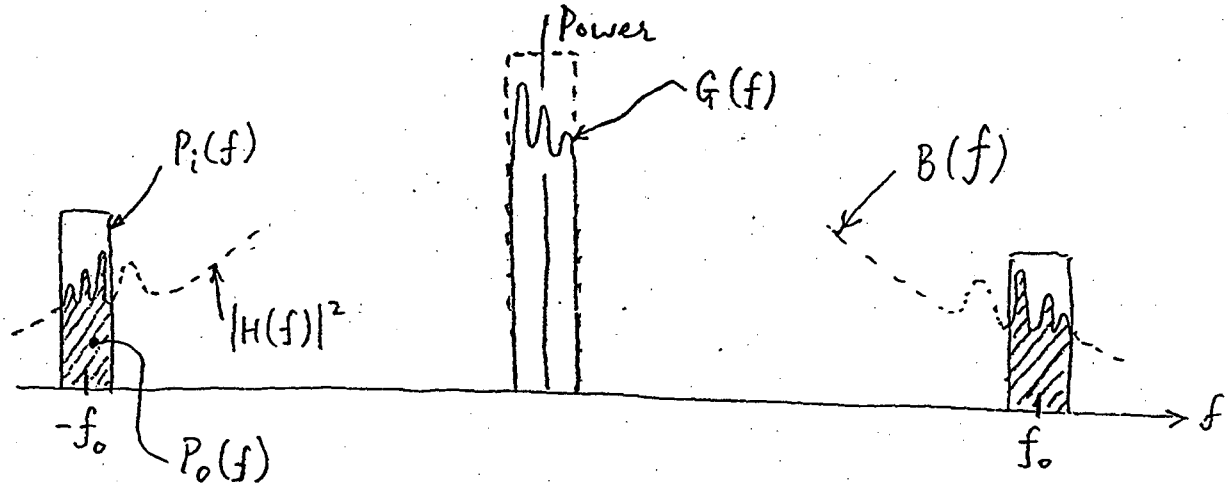

Analytic signal $\longrightarrow \hat{R}(\tau) = e^{2\pi i f_o \tau}\, g(\tau) \longleftarrow$ complex envelope

Measured autocorrelation function

$$R(\tau) = \sqrt{g_R(\tau)^2 + g_I(\tau)^2}\, \cos\left(2\pi f_o \tau + \phi(\tau)\right)$$

$$\phi(\tau) = \tan^{-1} g_I / g_R$$

modulated carrier wave

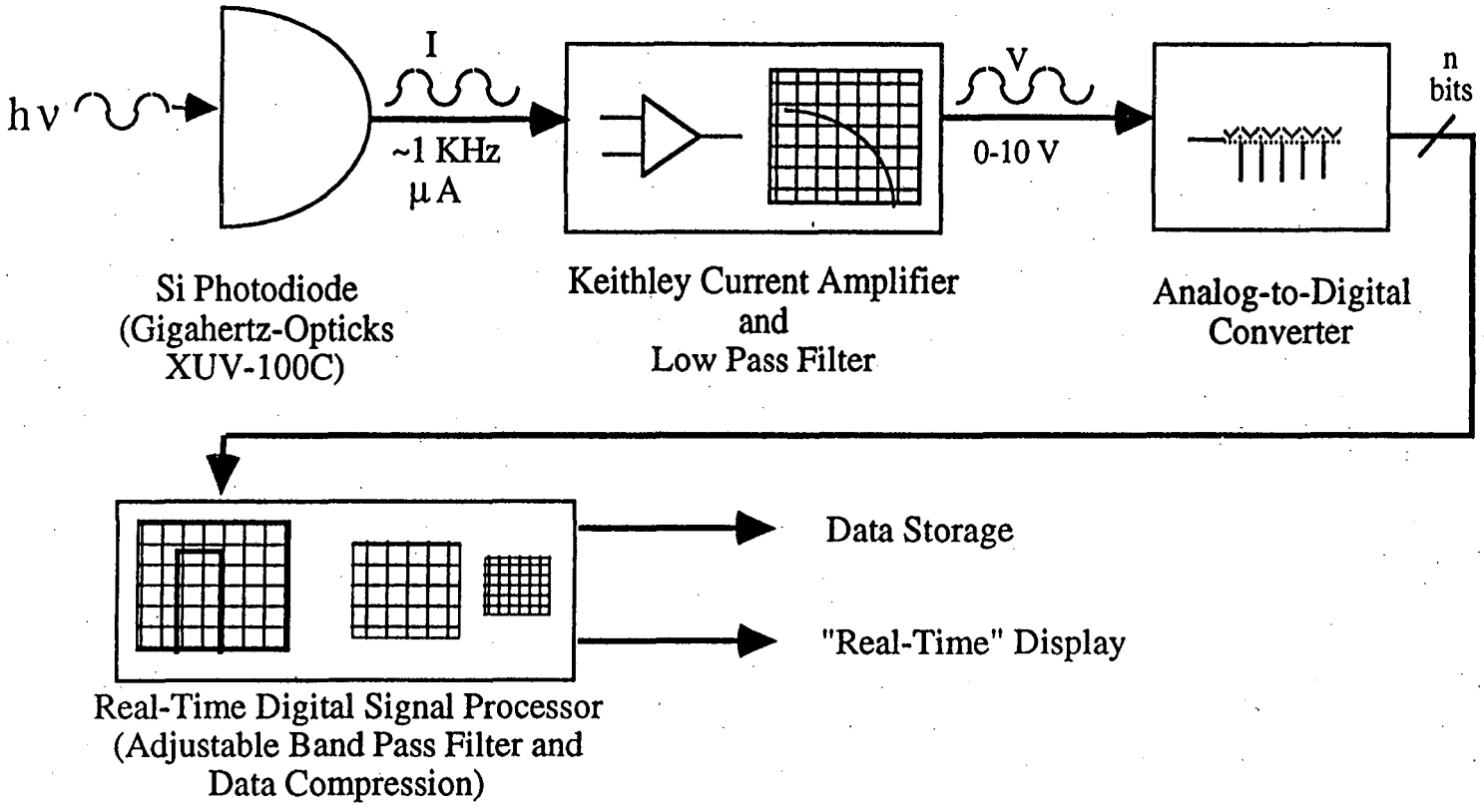
hν
I
~1 KHz
μA
V
0-10 V
n
bits
Si Photodiode
(Gigahertz-Opticks
XUV-100C)
Keithley Current Amplifier
and
Low Pass Filter
Analog-to-Digital
Converter
Data Storage
"Real-Time" Display
Real-Time Digital Signal Processor
(Adjustable Band Pass Filter and
Data Compression)

Gaussian Distribution

@65.35 eV, Sigma=0.05 eV,50 μeV Point Density
With He Resonance Absorptions, 10% absorption
2n+ series, peaks 9+ to 60+

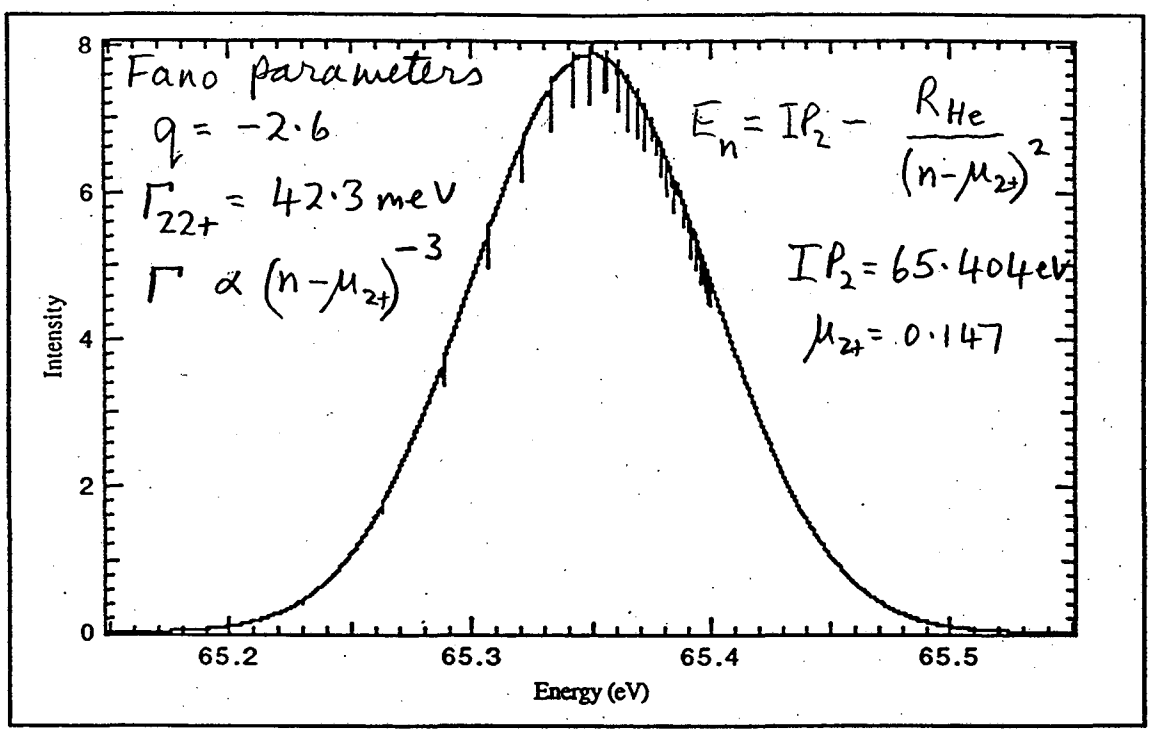

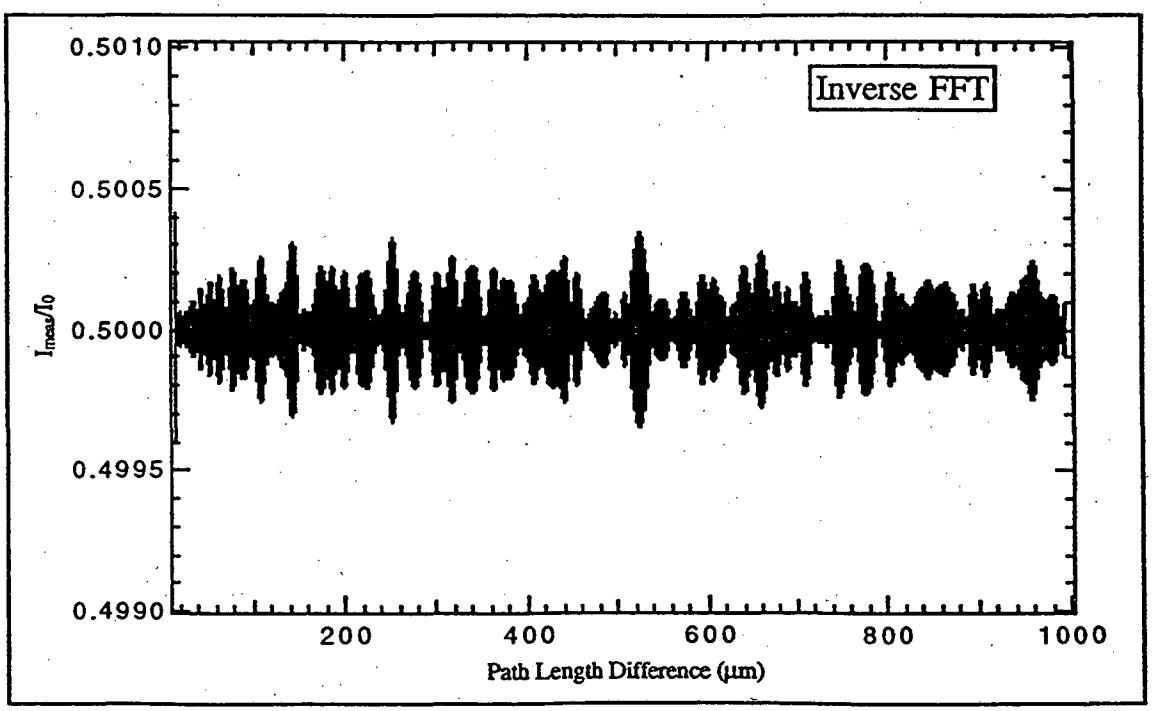

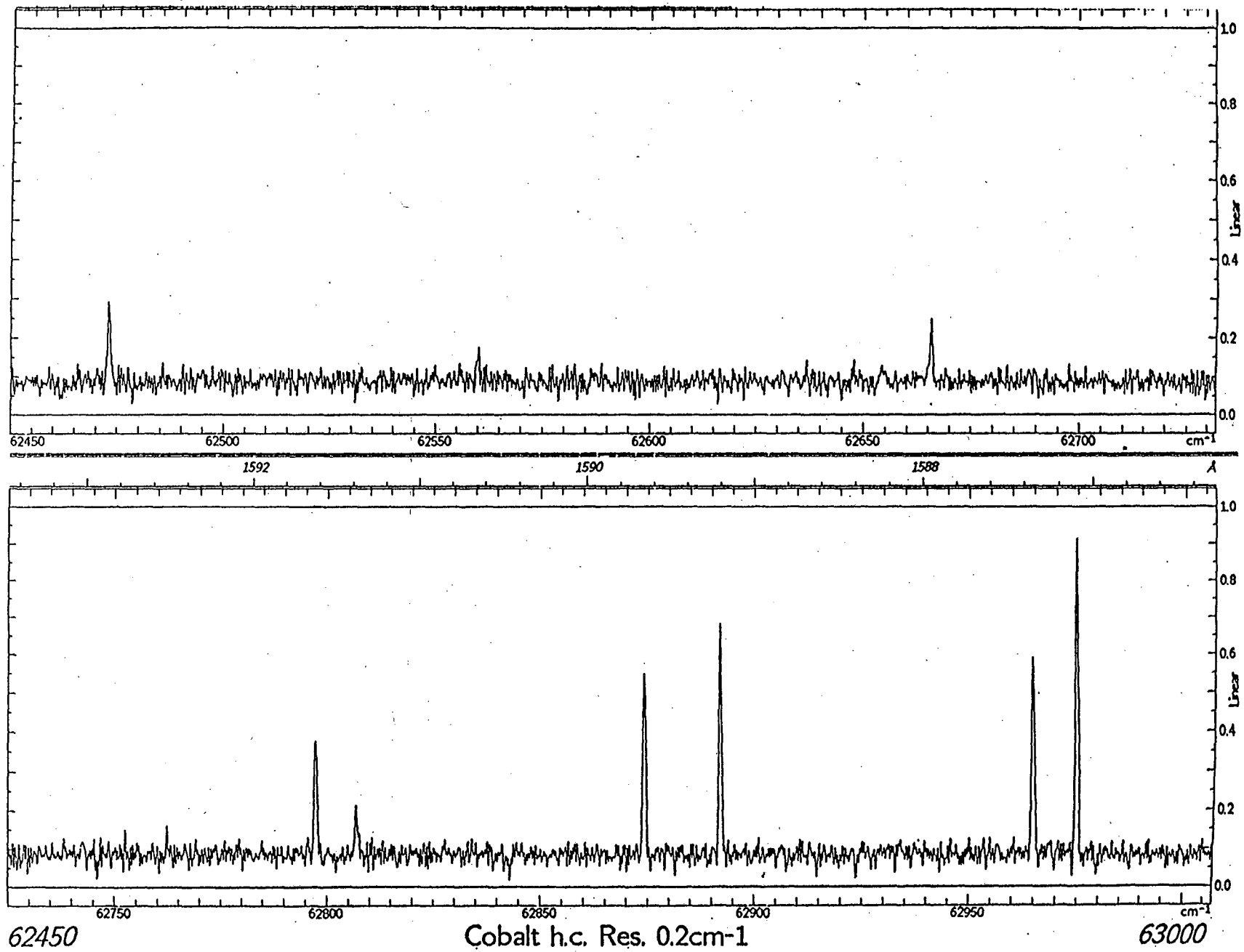

62450 Cobalt h.c. Res. 0.2cm-1 63000

SUMMARY OF MAIN ISSUES

OPTICAL COMPONENT ALIGNMENT

BEAM SPLITTER

MOTION QUALITY

MOTION DRIVER

DETECTOR: SHOT-NOISE LIMITED?

Some Technical Issues in Implementing the ALS Fourier Transform Spectrometer

Zahid Hussain

Lawrence Berkeley Laboratory

VUV/SOFT X-RAY INTERFEROMETER (ENERGY RANGE = 30-120 eV)

- BEAMLINE DESIGN (BL 9.3.2)
- MECHANICAL MOVING STAGE
  FLEXURE HINGES (M H)
- DRIVING MOTOR
  INCHWORM (2 Cm TOTAL TRAVEL) WITH ADDITIONAL HIGH RESOLUTION PZT (12 μ m TRAVEL WITH A RESOLUTION OF BETTER THAN 10 Å)
- INDEXING
  MITUTOYO LASER HOLOSCALE LINEAR ENCODER
  RESOLUTION = 10 nm
  INTERFEROMETER (HP OR ZYGO)
  RESOLUTION = 1.25 nm
- BEAM SPLITTER (GRADING)
  25 μ m REFLECTING AND TRANSMITTED WIDTH
  THICKNESS = 0.5-1.0 mm
- MIRROR
  DIMENSION = 5"x1"x1"
  FLATNESS < 1 μ m
  ROUGHNESS < 5 Å (RMS)
- DETECTOR
  SI BASED VUV/SOFT X-RAY PHOTODIODE
- SIGNAL CHARACTERISTICS (EM)
- MEASURING SCHEME
  LOCK-IN METHODS (EM)
- DATA ANALYSIS
  FT TECHNIQUES (EM)

The figure below shows the layout for Beamline 9.3.2.

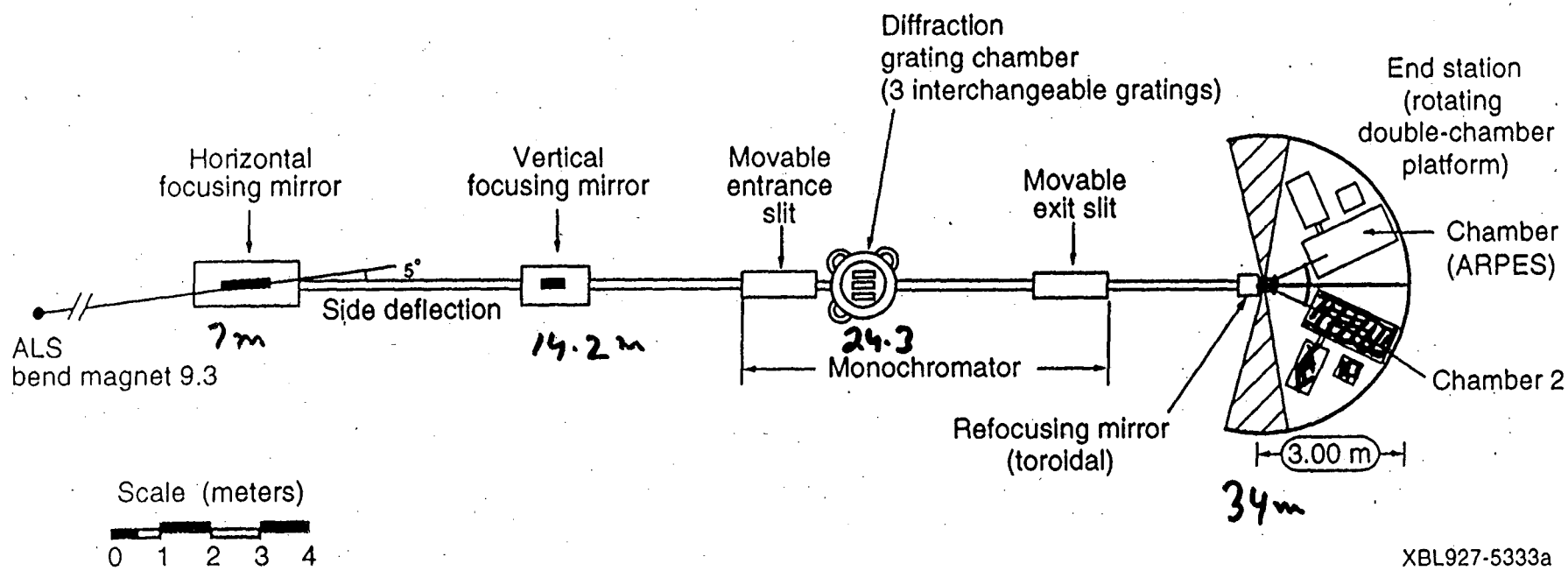

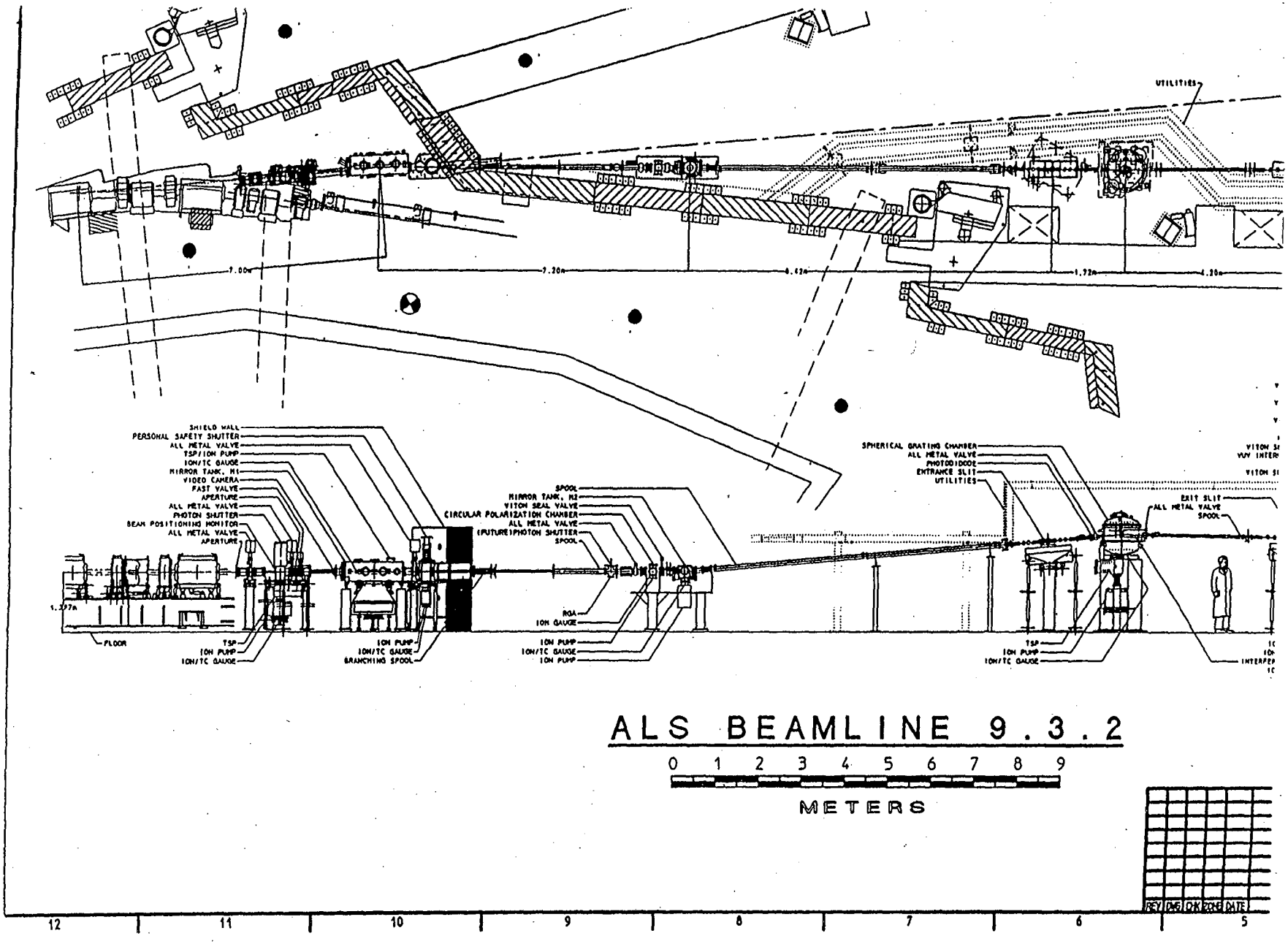
UTILITIES
7.00m
7.20m
0.42m
1.92m
1.38m
SHIELD WALL
PERSONAL SAFETY SHUTTER
ALL METAL VALVE
TSP/ION PUMP
ION/TC GAUGE
MIRROR TANK, H1
VIDEO CAMERA
FAST VALVE
APERTURE
ALL METAL VALVE
PHOTON SHUTTER
BEAM POSITIONING MONITOR
ALL METAL VALVE
APERTURE
1.227m
FLOOR
TSP
ION PUMP
ION/TC GAUGE
ION PUMP
ION/TC GAUGE
BRANCHING SPOOL
SPOOL
MIRROR TANK, H2
VITON SEAL VALVE
CIRCULAR POLARIZATION CHAMBER
ALL METAL VALVE
(FUTURE)PHOTON SHUTTER
SPOOL
RGA
ION GAUGE
ION PUMP
ION/TC GAUGE
ION PUMP
SPHERICAL GRATING CHAMBER
ALL METAL VALVE
PHOTODIODE
ENTRANCE SLIT
UTILITIES
EXIT SLIT
ALL METAL VALVE
SPOOL
TSP
ION PUMP
ION/TC GAUGE
ALS BEAMLINE 9.3.2
0 1 2 3 4 5 6 7 8 9
METERS
REV DES CK ZONE DATE
12 11 10 9 8 7 6 5

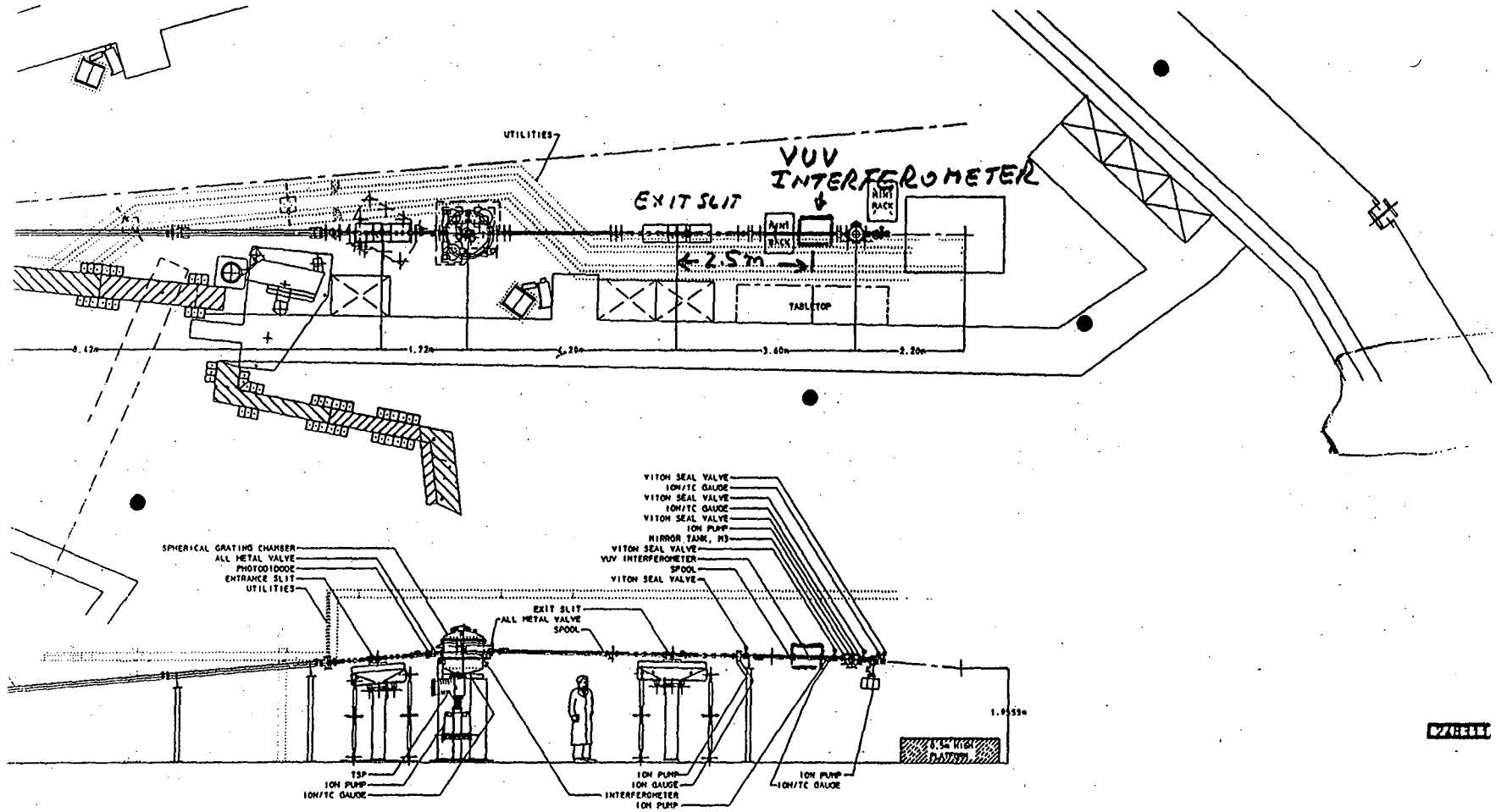

BEAMLINE 9.3.2

2 3 4 5 6 7 8 9

METERS

REV	CHG	CK	ZONE	DATE	CHANGES

UNLESS OTHERWISE SPECIFIED

SHOP ORDERS

DRN: C.L. CUMMINGS 4.7.93

CHK: Z. HUSSAMIN 4.7.93

LAWRENCE BERKELEY LABORATORY
UNIVERSITY OF CALIFORNIA-BERKELEY

ALS - BM BEAMLINES

BEAMLINE 9.3.2

BEAMLINE 9.3.2 - LAYOUT

SCALE: NONE

SIZE: A

CAGE NO. AL6031

DWG. NO. 24B3114

PHOTOIONIZATION GAS CELL
SCHEMATIC

Z. HUSSAIN/T. REICH
8/7/91
Revised 2/18/92

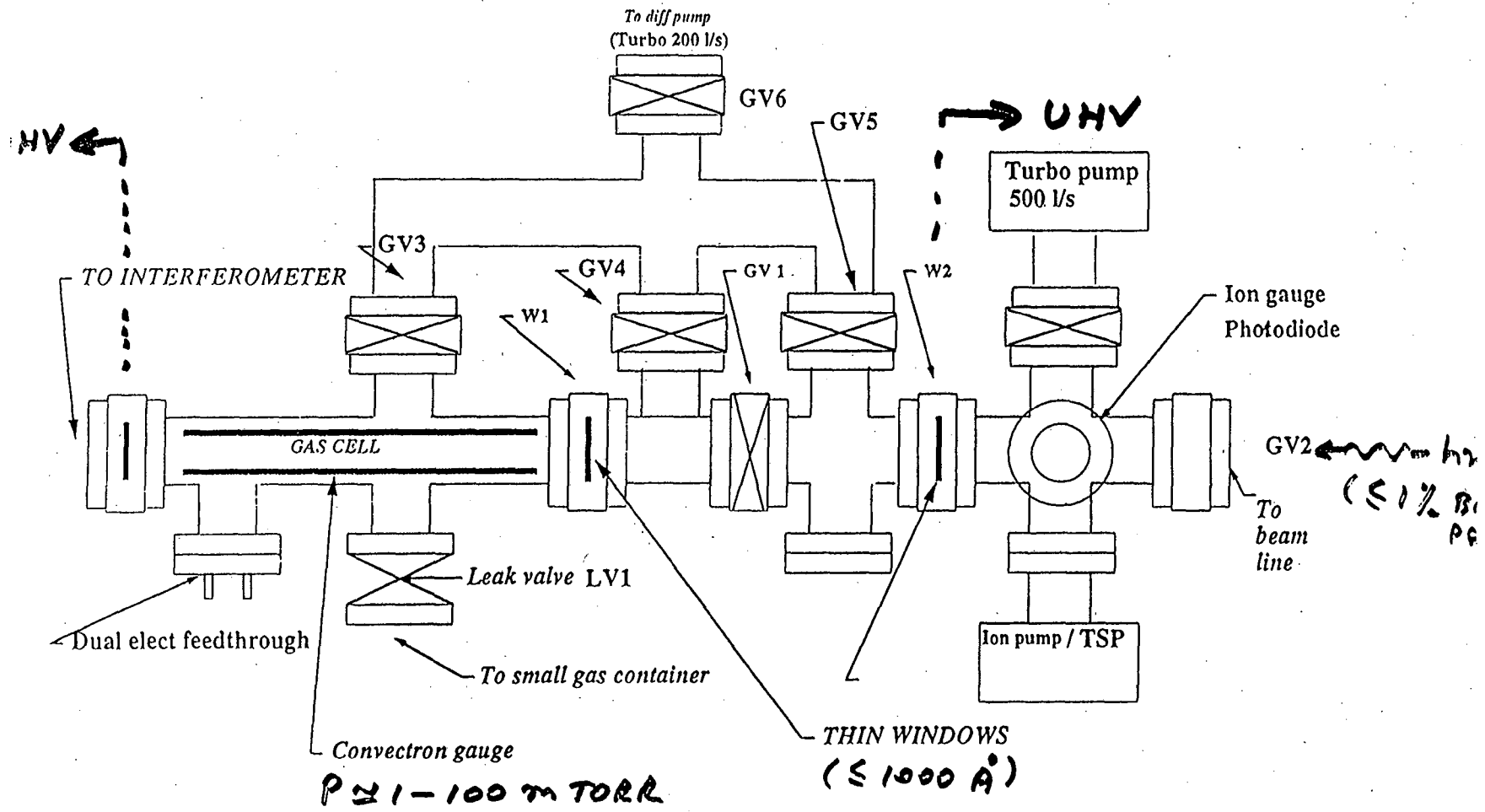

HYSTERESIS AND LINEARITY

PIEZOELECTRIC DEVICES

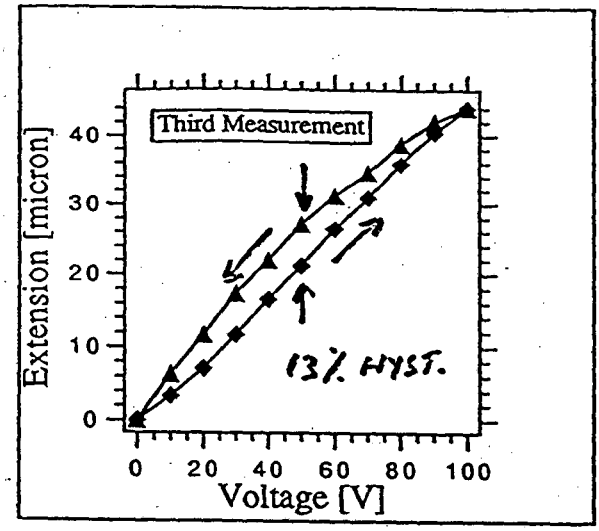

LINEARITY ≈ 1–2%

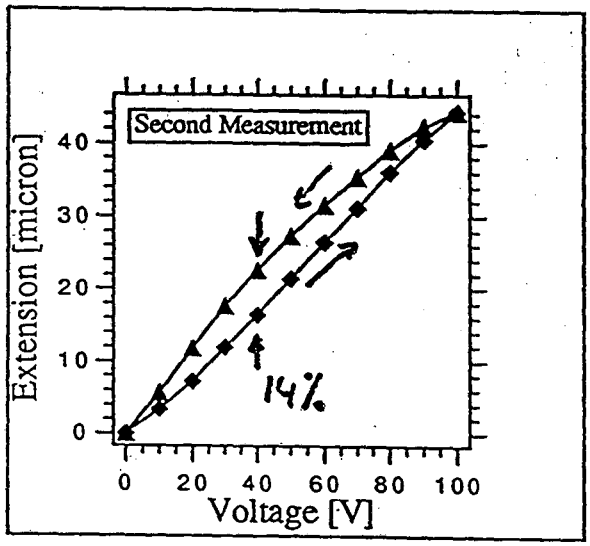

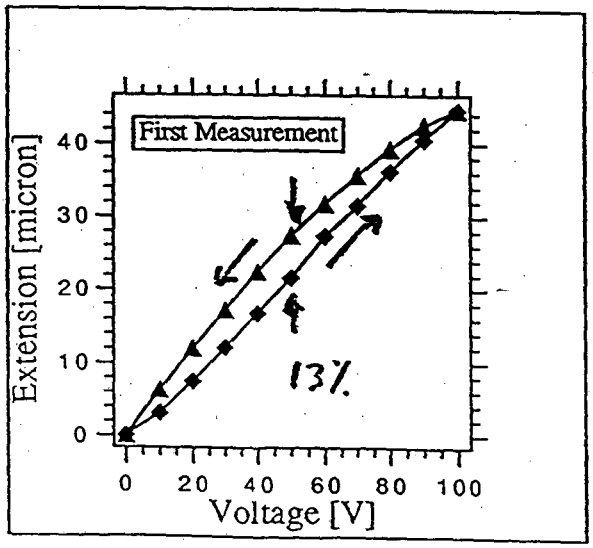

INDEXING OF MOTION

1. LASER HOLOSCALE LINEAR ENCODER

TWO BEAM INTERFEROMETER (MICHELSON-TYPE)

USES HOLOGRAPHIC DIFFRACTION GRATING (2000 ℓ/mm)

HIGH RESOLUTION = 10 nm (100 Å)

PRESENTLY NOT UHV COMPATIBLE

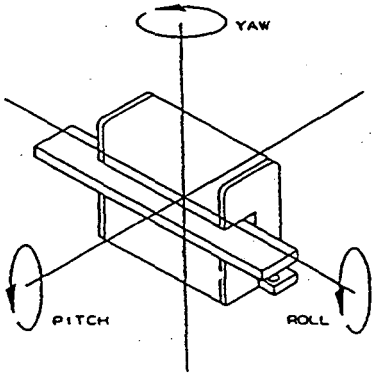

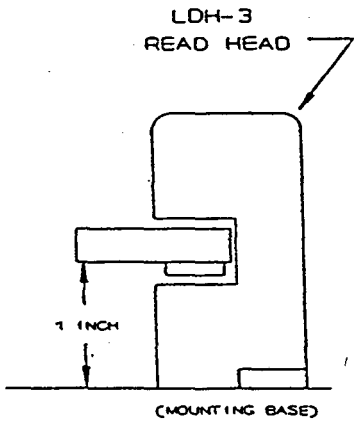

NEED IN SITU ADJUSTME TO ALLIGN.

FIGURE 4. SCALE ALIGNMENT

SCALE VERTICAL POSITION	1 inch from the mounting base ± 150 μinch
PITCH	± 12 arc min
ROLL	± 25 arc min
YAW	± 12 arc min

TABLE 4. POSITIONAL DEVIATION SPECIFICATION

2. HP OR ZYGO INTERFEROMETER

RESOLUTION : 1.25 nm

UHV COMPATIBLE

LINEARITY AND REPRODUCIBILITY

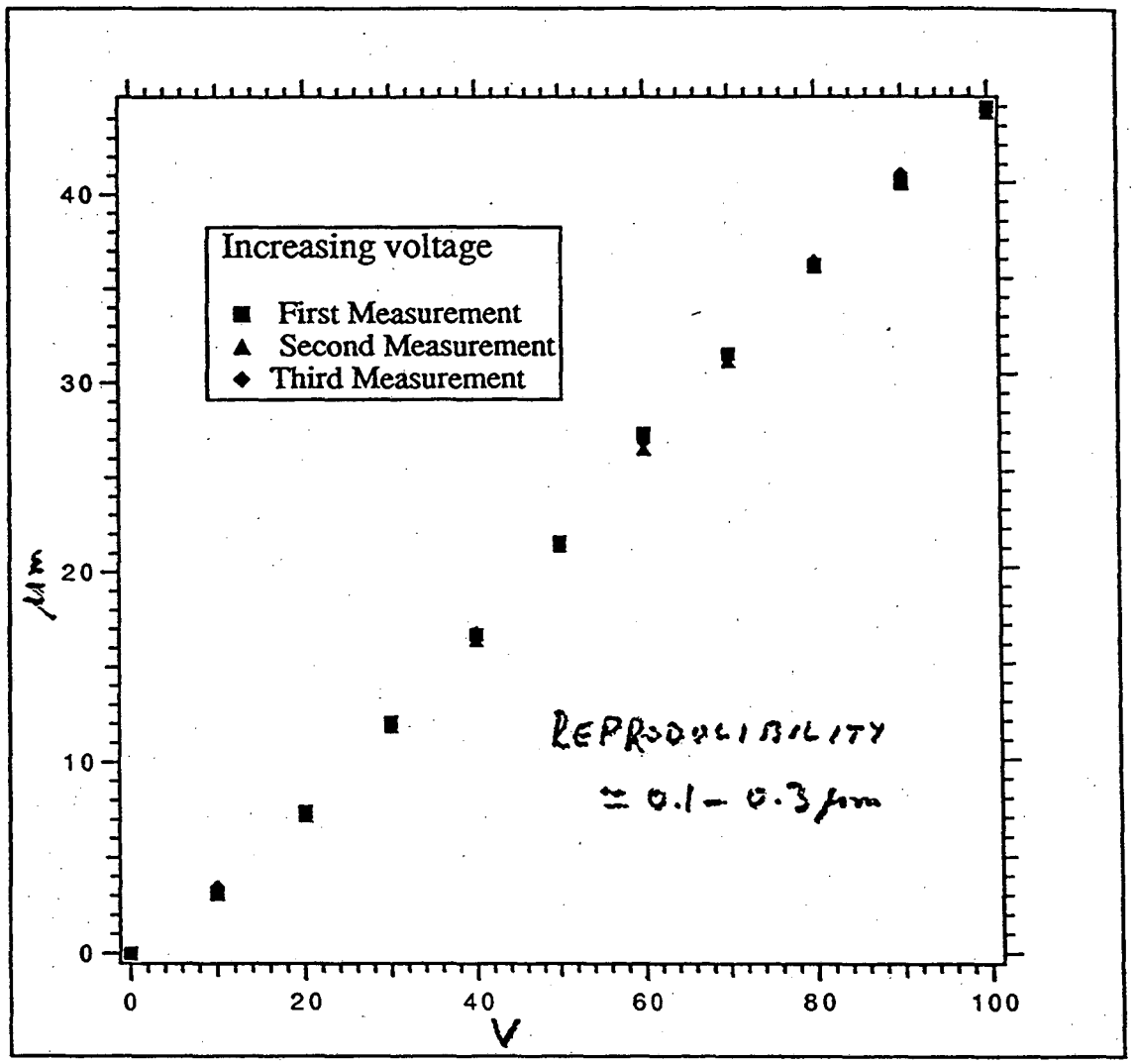

⇒ PZT-8:

EXTENSION ≃ 0 – 12 μm

FOR ≃ 0 – 1000 VOLTS

LINEARITY ~ 2 %

INCHWORM ... (...

BY BURLEIGH

Hammerle et al
RSI, 63, 4308 (1992)

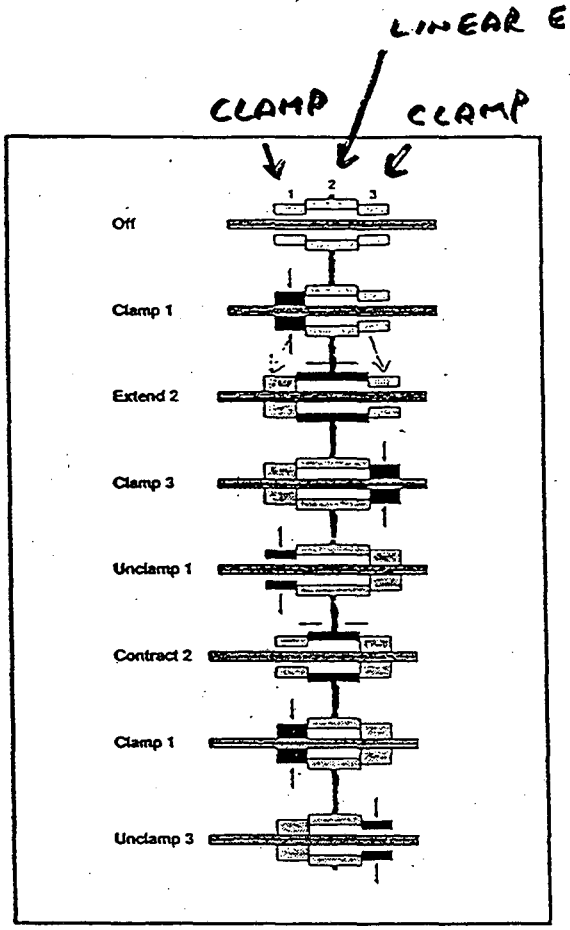

Fig. 1 Inchworm motor operation

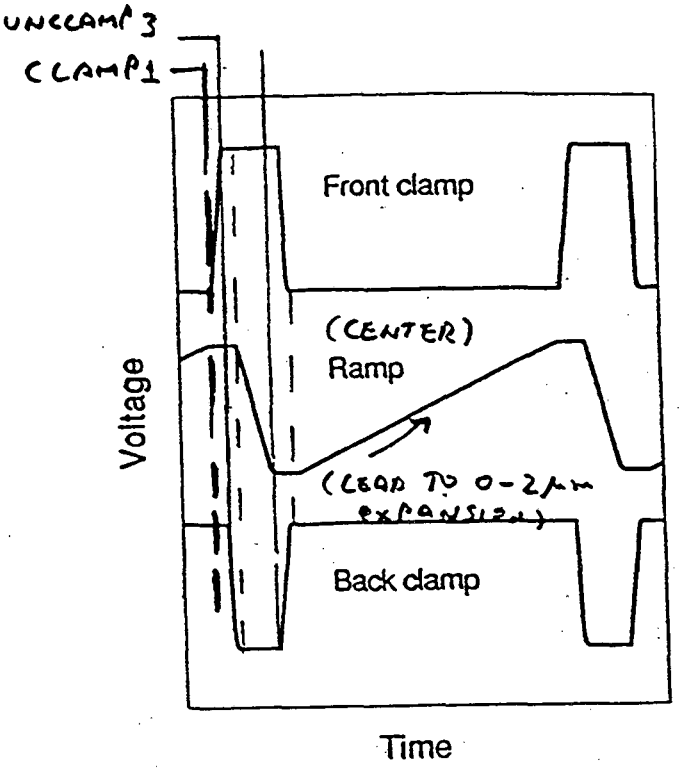

ULTRA LOW NOISE DRIVE SIGNAL

- INCHWORM 3 PZT SECTIONS
- 0-500 VOLTS NOISE LEVEL ≤ 2 mV rms (<0.02Å
  ⇒ STEP SIZE ≥ 0.6 Å (16 BIT DAC
  JERKING OF INCHWORM AVOIDED BY APPLYING RAMPING VOLTA TO CLAMPS INSTEAD OF ON / OFF.
- THREE DISTINCT 0-500 VOLTS WAVEFORM REF. TO COMMON CLEARENCE COMPENSATION AT FIXED POTENTIAL (≠ 0).
- CONTROLLED REVERSE MOTION (~.05μm) WHEN BOTH (ONE AFTER OTHER) CLAMPS GRIP THE SHAFT.

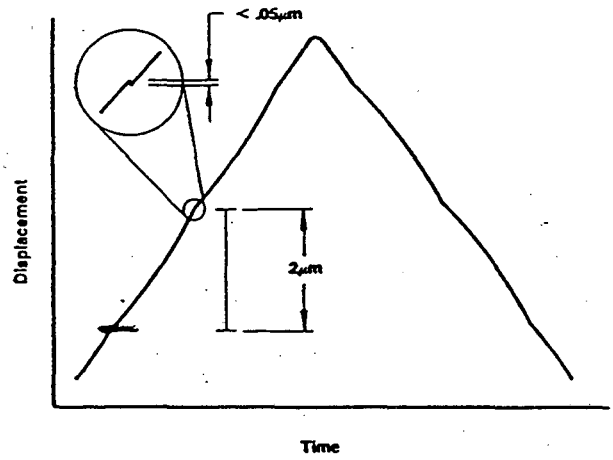

Fig. 5 Inchworm Motion Profile at a Clamp Change

BURLEIGH ARIS-10S

INCHWORM WITH 12 μm TRAVEL P/T
RESOLUTION = 0.5 Å
ULTRA LOW NOISE INCHWORM CONTROLLER

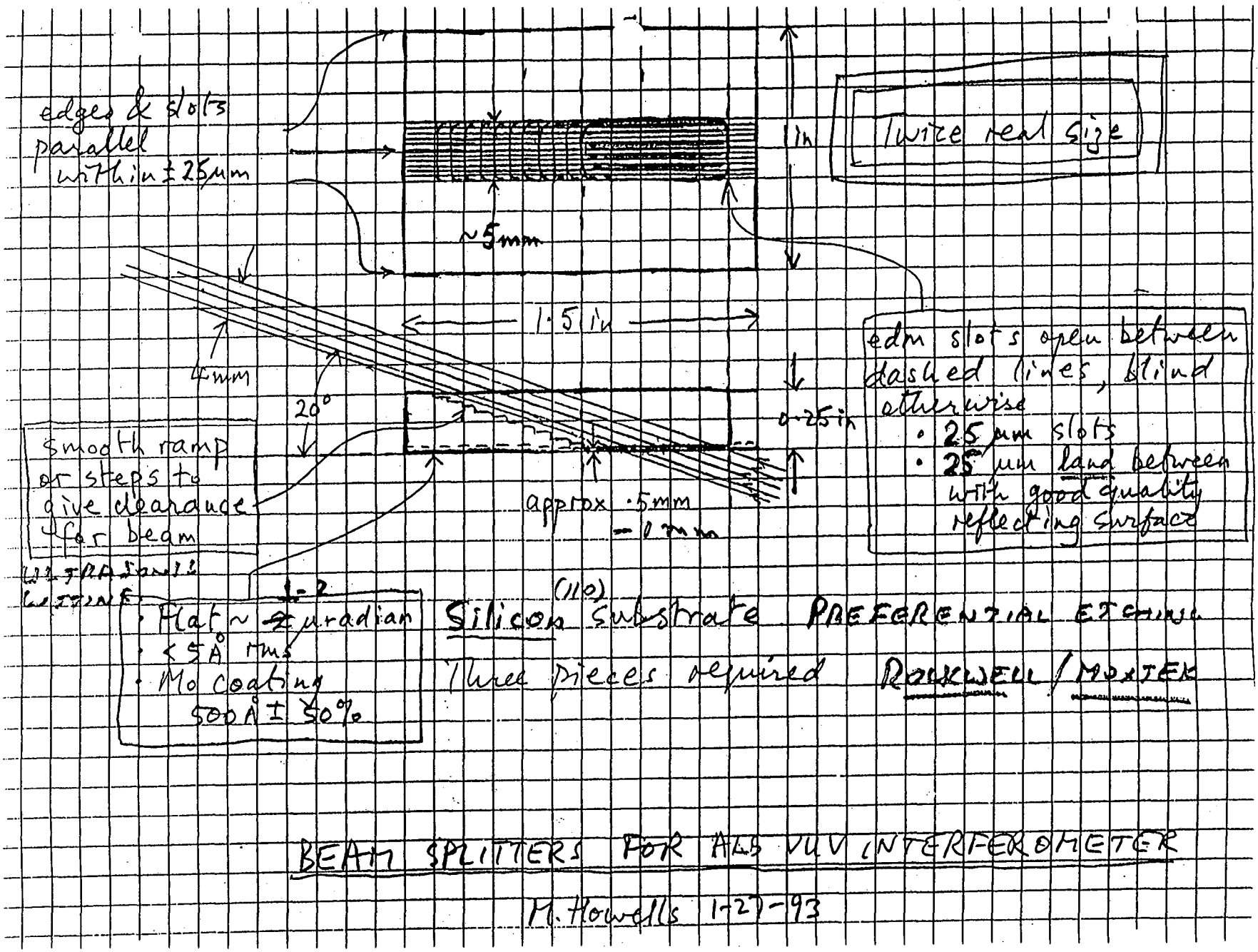
edges & slots parallel within ±25μm
1 in
Twice real size
~5mm
1.5 in
4mm
20°
0.25 in
approx .5mm
~1mm
smooth ramp or steps to give clearance for beam
edm slots open between dashed lines, blind otherwise
• 25 μm slots
• 25 μm land between with good quality reflecting surface
ULTRASMOOTH WINDOWS
• Flat ~ 1/2 μradian
• < 5Å rms
• Mo coating 500Å ± 50%
Silicon (110) Substrate PREFERENTIAL ETCHING
Three pieces required ROCKWELL / MOXTEK
BEAM SPLITTERS FOR ALS VUV INTERFEROMETER
M. Howells 1-27-93

DETECTOR

SANFIELD ET AL (A
APPLIED OPTICS
28, 394

SILICON PHOTODIODE

(HIGHLY SUITABLE IN THE 30-120 eV RANG

(ANTI REFLECTING PASSIVATING LAYER)

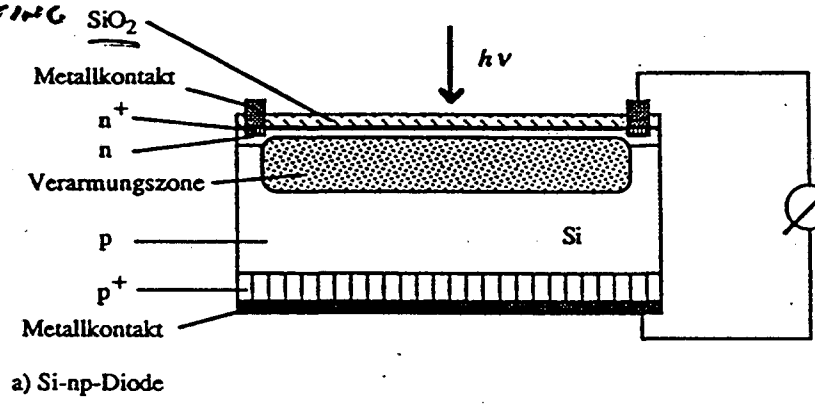

a) Si-np-Diode

- HIGH QUANTUM EFFICIENCY

$$\simeq \frac{E(\text{Photon})}{3.8} \quad \text{e-h pair}$$

- HIGH STABILITY UP TO 2×10^{14} Photon/cm^2
- UHV COMPATIBILITY
- ACTIVE AREA $\simeq 100\ mm^2$

Fourier Transform Soft X-Ray Spectroscopy (FT-SX)

E.J. Moler

Lawrence Berkeley Laboratory

Fourier Transform Soft X-Ray Spectroscopy (FT-SX)

E. J. Moler

Workshop- June 25, 1993

OUTLINE

- **Expected Signal Characteristics**
- **Fundamental Requirements for Absorption Spectroscopy in the 65 eV Region (He N=2 double excitation series & more)**
- **Data Collection & Analysis**
- **Signal Collection Scheme**

Fundamental Requirements

for He N=2 Double Excitation Series
~65.5 eV

Sampling Rate/Energy Range

- "Beat" Envelope Max. Frequency
  $\Delta E = 0.17$ eV (n=9+ to IP2) =>
  $\lambda = 1.24$ eV·μm/0.17 eV = 7.3 μm

- Nyquist Sampling Rate
  7.3 μm/2 = 3.6 μm

Sampling Range/Resolving Power

- 1 cm travel =>

  Res. = 1.24 eV·μm/(2*10,000 μm)
  = 65 μeV
- E/ΔE = 65 μeV/65 eV = 1 million !

  Maybe can double using mirror symmetry

Resolving Power	n_{max} Observable
1,000,000	~71 (21 current max)
750,000	65
500,000	56

- Min # Data Points = 10,000 μm/3.6
  = 2778

Positioning Accuracy and Resolution

- Absolute Positioning Accuracy
  For envelope "peak" w/in 1% =>
  accuracy ~λ/22 = 7.6 μm/22 = 345 nm

- Positioning Precision
  finding average freq. "peak" within 1%
  => 19 nm/22 = 8.6 Å

Data Collection and Analysis

- Measure Envelope Amplitude,
- Use known "average" frequency as set by monochromator band pass,
- Fourier Transform

Question: What are uncertainties introduced by assuming an average frequency which may be incorrect by e.g. 0.15%

Signal Collection Scheme

- Low signal/background ratio implies lock-in technique,

- Noise levels cannot be known in advance, but can be estimated.

- 5500 points in 6 hrs ~ 4 secs/point
  - acquire position,
  - "count"

Gaussian Distribution

@65 eV, Sigma=1.0 eV

2meV Point Density, Normalized

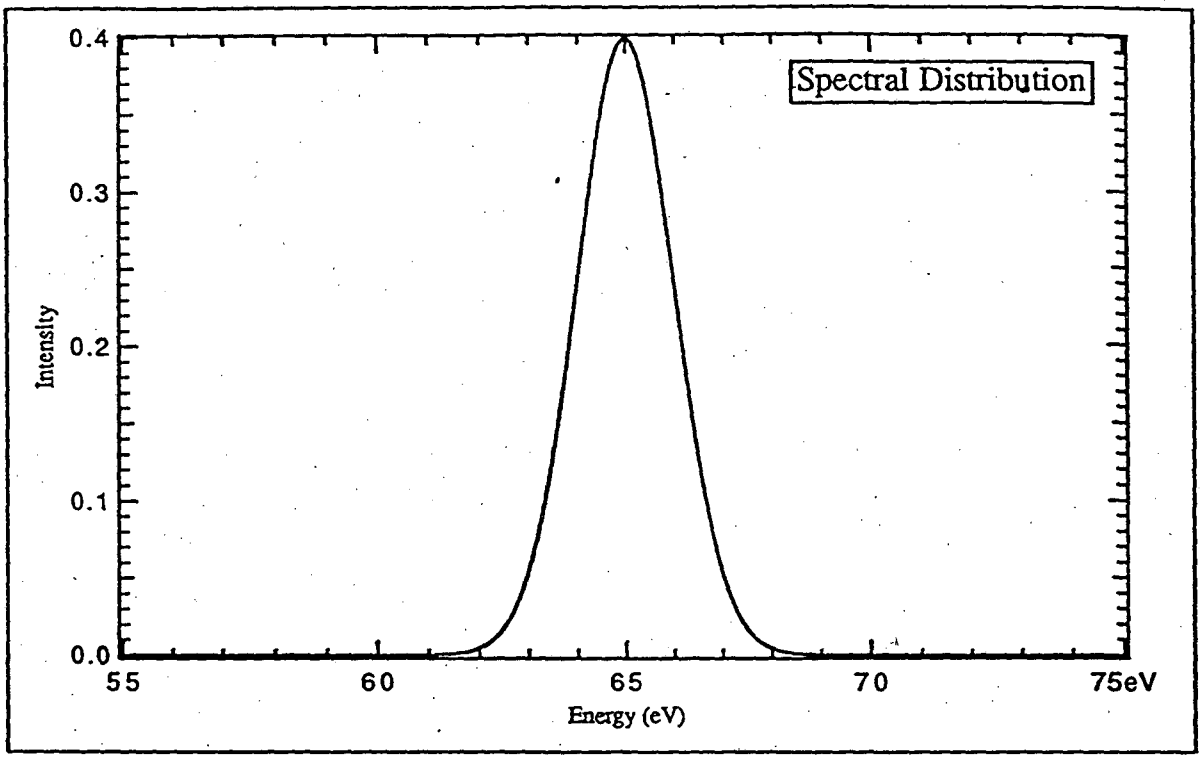

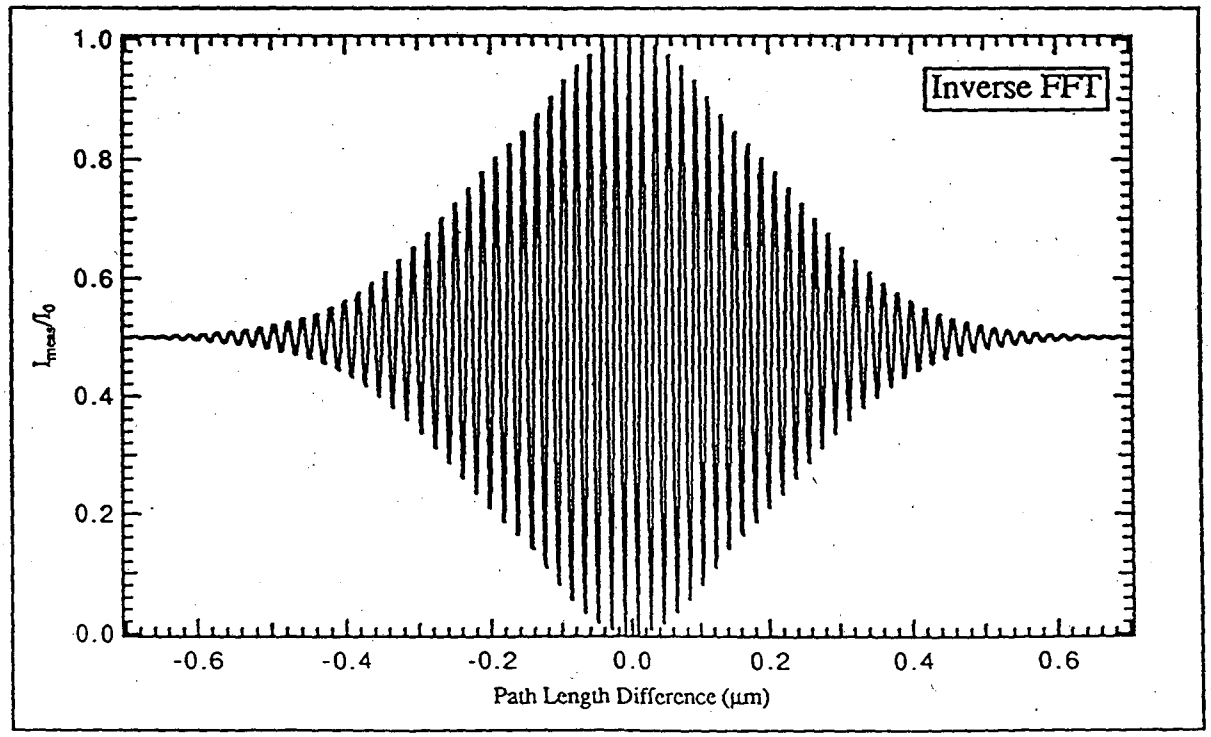

Gaussian Distribution

@65 eV, Sigma=1.0 eV
2meV Point Density, Normalized
With Sharp Absorption
@65 eV, 2 meV Wide (1 channel)

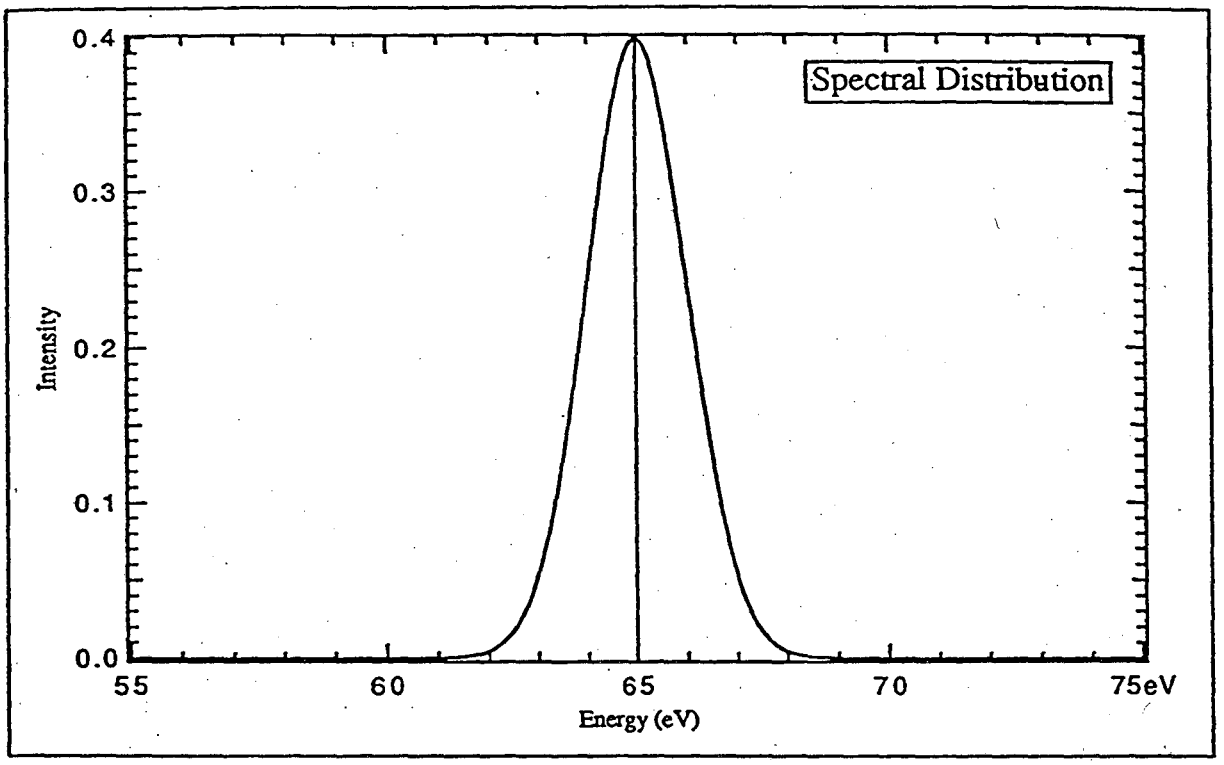

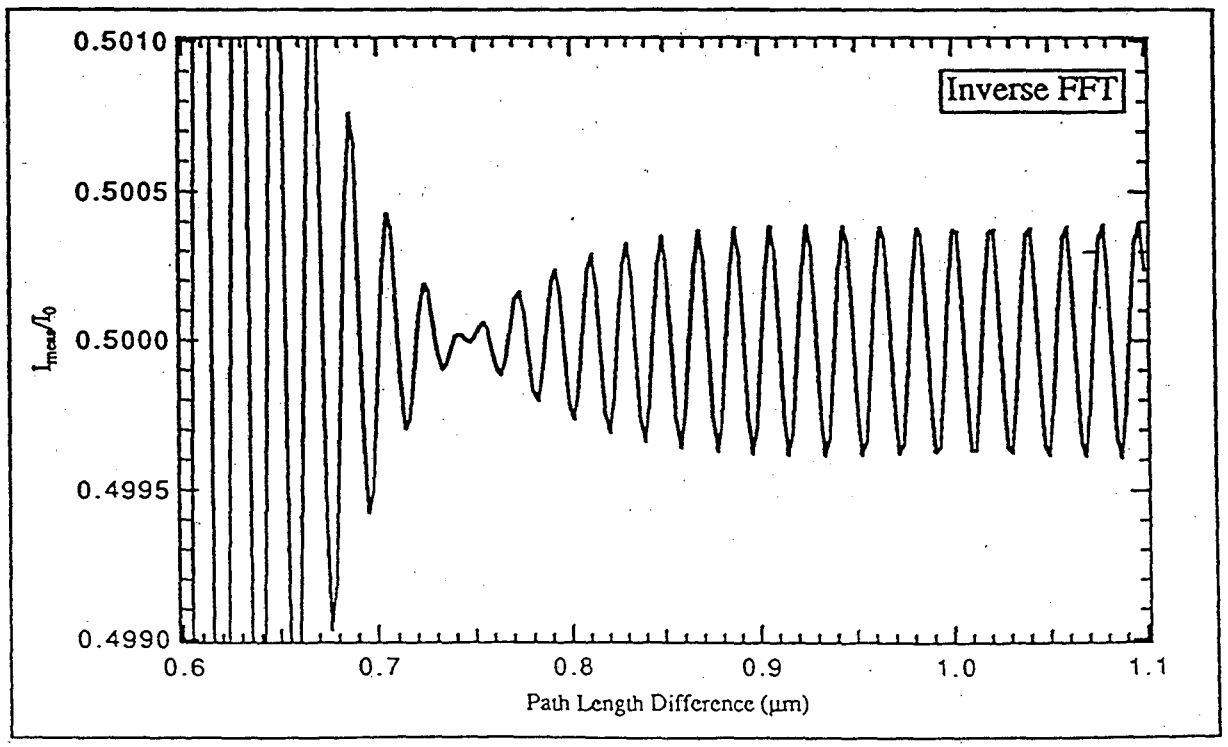

Gaussian Distribution

@65 eV, Sigma=1.0 eV
2meV Point Density, Normalized
With Sharp Absorption
@65 eV, 2 meV Wide (1 channel)

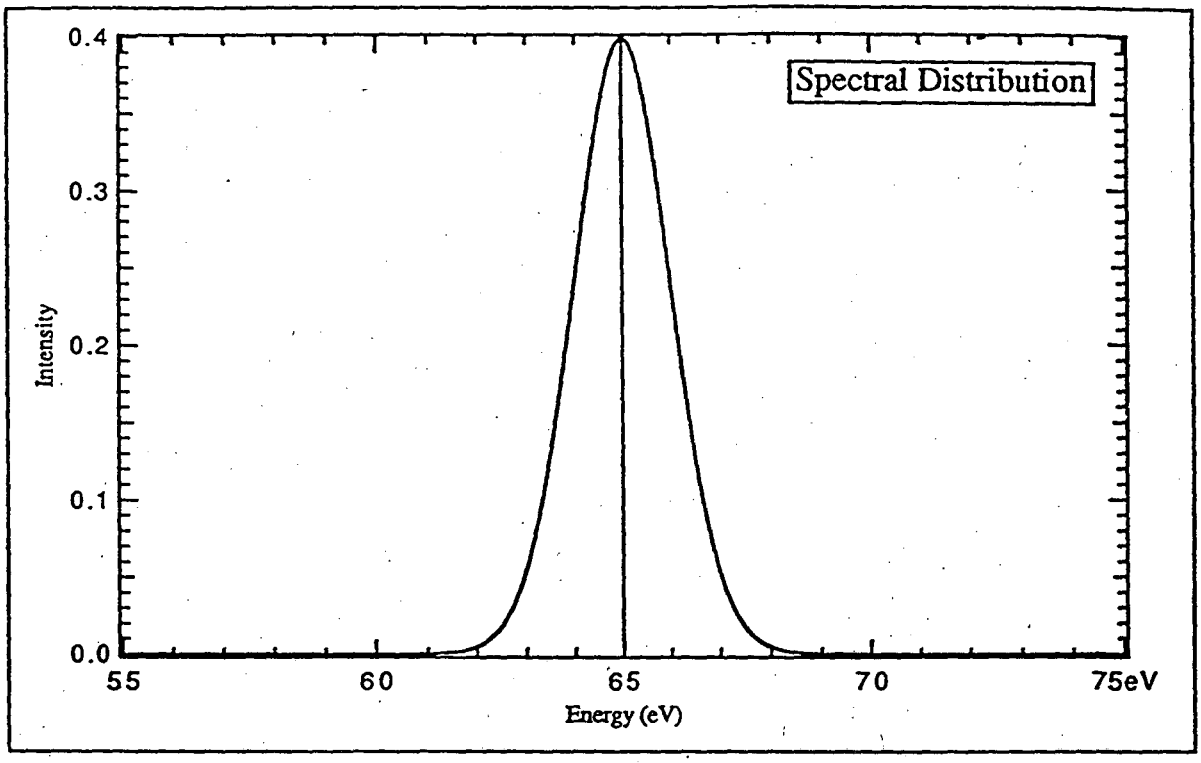

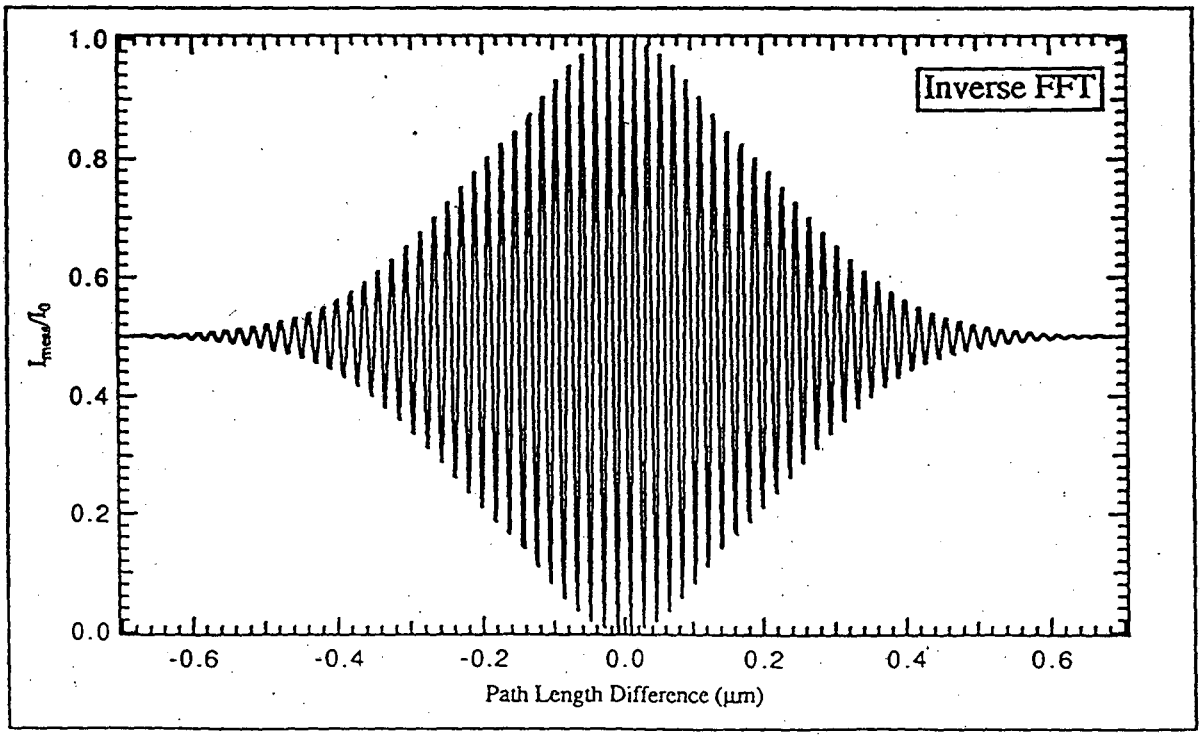

FT-SX Mirror Positioning and Signal Detection

Eddie Moler June, 1993

This note describes the important parameters and requirements for a high resolution (> 300,000) photoabsorption measurement of the He double excitation resonances at ≈ 65 eV using the Fourier Transform - Soft X-ray (FT-SX) spectrometer. A scheme for signal detection and measurement is then proposed which will address the significant problems of signal/noise and signal/background ratios, accuracy and precision of the mirror positioning system, and time limitations for acquiring the full interferogram.

Parameters and Requirements

Two parameters of fundamental importance in FT spectroscopy is the necessary sampling rate (points per unit distance) and range (total path-length-difference introduced) to achieve a given resolution and energy range. These parameters are dictated by the energies and energy differences of the expected spectral features. For interferometry in the X-ray region, the practical aspects of achieving the required accuracy and precision in introducing the path-length-differences and dealing with the expected signal characteristics are also critical in determining the resolution and energy range of the instrument. In this note, I consider the requirements for measuring the helium double excitations below the N=2 ionization threshold.

Sampling Rate / Energy Range

The wavelength of light at the N=2 ionization threshold for helium, 65.4 eV, is ≈ 19 nm. This is the carrier wave of the absorption interferogram whose envelope we wish to measure. We deliberately limit the bandwidth of the light source so that only the envelope of the carrier wave need be measured. There are also advantages in the signal/ background ratios when limiting the band width. Figure 1 shows the Fano resonance profile for N=2, peaks n=9+ to 60+. Note that the intensities of the peaks should all be the same, but in sampling a continuous curve discretely leads to "missing" the peak position. This does not affect the qualitative features of the simulation. Constraints presented by computer memory and computation time prevents a higher resolution simulation. Figure 2 shows the source gaussian and its expected interferogram. Figures 3, 4, and 5 show the interferogram of the source with a 10% peak Fano absorption profile with ranges of 15 to 100, 500, and 1000 μm path length differences, respectively. The envelope consists of the beat frequencies in the absorption lines which can be described by cos[(a-b)x] where "a " and "b" are the frequencies of two absorption lines. This relationship may be used to determine the minimum expected "envelope wavelength" and thus the minimum sampling rate as dictated by the Nyquist theorem. I choose the n=9+ peak as the first peak of interest because it is within the bandwidth of a 100 meV gaussian source peak centered at 65.35 eV, which has significant intensity at the IP2 threshold (65.40 eV). The n=9+ absorption line (in N=2) is approximately 0.17 eV below the IP2 ionization threshold. The higher "n" peaks' energies converge to the ionization threshold. Thus, 0.17 eV is the maximum spacing between the 9+ peak and any other peaks higher in energy. The "wavelength" of the shortest envelope wave is then,

$$\lambda = 1.24\ \text{eV}\cdot\mu\text{m} / 0.17\ \text{eV} = 7.3\ \mu\text{m}.$$

Applying the Nyquist theorem gives a sampling rate of,

Δx_{max}=3.6 μm.

Positioning Accuracy and Precision

To obtain the envelope amplitude peak within 1%, one would like a positioning accuracy of ±1/44 wavelength, or 1/22of the beat wave λ. This corresponds to an accuracy of 332 nm for the n=9+ to IP2 threshold. To include peaks out to the n=2+ (@ ~65.0 eV) would require a sampling rate that is a factor of 30 higher (5.2 eV/.17 eV) and thus would require a positioning accuracy of 11 nm. Relaxing the envelope amplitude determination to within 3% requires an accuracy of ±1/26 wavelength, or 561 nm and 18.7 nm for n=9+ and 2+, respectively. There is the additional problem of the precision of the mirror positioning because the envelope amplitude must be measured across the carrier wave peak. This puts our precision requirements at 1/22 of 19 nm or .86 nm.

Sampling Range / Resolving Power

The energy resolution is determined by the maximum path length difference introduced. A design goal of a resolving power on the order of 1 million was taken as an ideal limit. The currently proposed design allows for a path-length-difference of 6.7 mm (see M. Howells, design note 1-28-93). This gives an energy resolution of,

$$\Delta E = 1.24\ \text{eV}\cdot\mu\text{m}/(2 \cdot 6.7\text{e+3}\ \mu\text{m}) = 92.5\ \mu\text{eV},$$

and a resolving power of,

$$E/\Delta E = 65.4\ \text{eV}/(92.5\text{e-6 eV}) \approx 700{,}000.$$

In principle, the resolving power could be doubled by making use of the mirror symmetry of the interferogram about the zero path-length-difference (ZPD) position, giving a resolution of 1.4 million (!), provided that the ZPD position was at one end of the travel. Based on the tabulations of resolving power and the number of peaks observable in Domke, Shirley, Kaindl, et. al. (PRL march 11,1991, p 1306) and the fact that the peak widths go down as $1/n^3$ I can estimate the number of peaks for N=2 we could expect to see with various resolving powers.
Using,

$$n_{max} \approx (0.360 * \text{resolving power})^{1/3},$$

Resolving Power	n_{max} observed
350,000	50
500,000	56
750,000	65
1,000,000	71

A travel of 6.7 mm, with a sampling rate of 3.6 μm, means acquiring ~2000 data points. To include peaks out to the n=2+ (@ ~65.0 eV) would require 60000 data points at the same resolution.

Requirements Summary

For N=2 double excitations of He^+, considering very high resolution, including peaks n=2+ to IP2 or n=9+ to IP2,

Total Travel	6.7 mm
Sampling Rate	.12 - 3.6 μm
Absolute Positioning Accuracy	11-332 nm
Positioning Resolution	0.86 nm
Total Data Points Measured	2000 - 60,000

The Proposed Mirror Positioning and Signal Detection Scheme

The stringent requirements on the mirror positioning and drive system, along with the extremely small signal/background ratios of the absorption spectra require substantial deviations in design and measurement technique from previous interferometers. Because the signal detection scheme and the mirror drive mechanisms are inherently intertwined, they must be considered together. As we will see, there are ways of taking advantage of these relationships.

The proposed positioning and detection scheme utilizes a modulation of the mirror positions and a lock-in amplifier to extract the resulting amplitude and phase of the time varying signal from the photo-detector. The modulation frequency must be selected to minimize the noise content of the signal while still matching the response characteristics of the photo detector and subsequent amplifiers. In addition to greatly increasing the signal/noise ratio, a problem made apparent by the simulations in figure 5, the phase of the signal can be used as a very precise position monitor. This will be described below. The reader is urged to read the attached analysis of the lock-in technique and expected outputs.

The following sections will address the methods of meeting the requirements inherent in obtaining a high resolution Fourier transform spectrum in the soft X-ray region.

Signal/Noise Ratio Improvement

Noise Sources

The critical aspect of measuring the interferogram signal is the uncertainty associated with each data point. The noise associated with the signal is the source of this uncertainty. The primary sources of noise are:

a) johnson noise, associated with thermal motions of electrons in a resistor,
b) shot noise, associated with the motion of the discreet electrical charges,
c) flicker or 1/f noise, resulting from variations in the electrical characteristics of materials which are proportional to the DC current flowing through them, and
d) interference, from electrical and mechanical pickup of nearby sources of em radiation,
e) inaccuracy in the signal determining parameters, e.g. mirror positions.

Only the first three, the signal noise, will be considered here. The others will be addressed elsewhere in this note.

The frequency spectra of each of these three distributions is interesting. The johnson and shot noise are "white noise", i.e. they have equal noise power at each frequency (up to some very high limit, of course). The 1/f noise has equal power per decade, it is sloped on a log scale and has approximately a 1/f distribution. Below 100 Hz, the 1/f noise dominates over the others except at certain frequencies where the interference from nearby sources can have a very "spiky" nature. The interference signals are typically from the line noise, having frequencies of 60 Hz and the first few harmonics. These signals are particularly important to avoid and filter.

Band-width Reduction

The method of dealing with these uncertainties in practice can be all placed under the strategy of "band-width narrowing". The simplest of band-width narrowing techniques is signal integration. Basically, the longer you count, the better your signal/noise ratio because while the signal grows with counts, the noise grows with $\sqrt{}$counts. Counting for a time t means reducing the band-width Δf to 1/t. The band-width begins at zero frequency, thus the most intense portion of the noise spectrum accompanies the signal for even very long counting times. Ideally, one would want to 1) shift the signal of interest up in frequency away from the 1/f and interference noise, and 2) impose a band-width that is centered on the signal and thus excludes all of the noise in the signal except for a very small contribution that is "beneath" the signal.

The Lock-in Technique

The lock-in technique is a sophisticated form of band-width limiting. The lock-in amplifier multiplies the incoming signal with a reference signal and passes the result through a low pass filter. This results in a rejection of very large portions of the noise spectrum without integrating for impractically long times, mainly by avoiding the lower frequency noise, where most of the noise power is. The band pass is determined by the time constant in the low pass filter, $\Delta f = 1/2\pi RC$ and the time for the filter to get within 99.3% of its final value is 5RC. Thus, the expected noise characteristics and the required accuracy of the signal determines the desired time constant and the "acquisition" time for one data point. A selectable time-constant range of 1ms to 100 s is common in commercial lock-in amplifiers. In addition, the phase of the signal relative to the reference can be measured quite accurately.

Signal Collection

The proposed method to acquire one data point is as follows (assuming one begins within 1 wave of the desired position. How to get there is described later):

• Impose a triangular modulation on the mirror position via the linear piezo actuator. The displacement of the piezo is assumed for now to be known exactly and set to 1/4 λ. The correct phase factor in the lock-in is also assumed to be known. The modulation signal is also the reference signal for the lock-in amplifier,

• Using a lock-in amplifier in 2f mode, move the mirrors to where the output of the lock-in is zero,

• Using a lock-in in 1f mode, wait 5 RC and measure the output signal. This signal is within 0.7% of the final output value. The positioning accuracy also places the output within 1% of the true maximum (see mirror positioning discussion, below). This method is far superior to the proposal to integrate the signal at several points across the wave to find the peak. In addition to the signal/noise ratio improvement, it also has the added benefit of allowing rapid determination of the carrier wave peak position by using the zero crossing of the 2f mode lock-in amp as described in the mirror positioning section.

Finding the correct values for the phase and peak-to-peak displacement involve maximizing the lock-in output by searching the phase-displacement-position parameter space. This need only be done once unless the voltage/expansion characteristics of the linear piezo actuator change drastically. It may be necessary to avoid large expansions of the piezo to prevent hysterisis. The search can proceed rather quickly if one is judicious in selection of the search method. The reader is referred to the output surfaces in the back of the lock-in analysis attachment.

Mirror Positioning

The requirements of length of travel and accuracy of positioning have been solved in the past, for IR and visible FT spectroscopy, by using a continuous drive lead-screw or gearing mechanisms. The relatively long wavelengths of visible and infra-red light are easily handled with a precision machined screw. However, the short wavelengths of X-rays demand accuracy and resolution in positioning that are not amenable to current machining technology. Thus, we have selected piezo-electric "inchworm" motors to drive our translation stage. These are readily available as they are the same drives used in STM for allowing the metal tip to approach the sample. Still, the position measurement is critical and is addressed below.

Absolute Accuracy

By absolute accuracy, I mean how closely to a desired absolute position can the mirror be placed. The current solution to this is to use a Mitutoyo holoscale linear encoder fixed to the translation stage of the interferometer. The resolution of the encoder is claimed to be 10 nm and the linearity is _____. For the currently proposed translation stage, 10 nm travel corresponds to ~ 7 nm of path length difference. This easily meets the accuracy requirements of 332 nm for the N=2 resonances starting with n=9+. For including peaks down to n=2+ the required accuracy still is sufficient. The consequence of the encoder linearity errors on the measured spectrum will be to introduce an uncertainty in the energy calibration of the spectrum of the same magnitude. The inchworm motor drives are capable of 4 nm steps, thus allowing the desired encoder position to be achieved.

Positioning Resolution

Resolution refers to the smallest amount of motion we can move the mirror by reliably. The resolution is important because we wish to measure the amplitude of the peak of the carrier wave with a wavelength of 19 nm. The linear encoder gets us to within 1/2 of a wavelength of the desired position. To allow high resolution positioning of the mirrors, we will use a piezo actuator with very good linear expansion characteristics. The above mentioned inchworm motor can clamp and hold it's position while the piezo crystal is used for high resolution motion. With and expansion of 12 nm/Volt, a stability of sub-angstrom position is achievable. In addition, the position modulations will be easily implemented with high precision with a standard laboratory wave form generator.

The signal output from the lock-in amplifier is extremely sensitive to the average position of the mirrors, as seen from the lock-in "output surfaces" in the attached analysis

of the lock-in technique. I proposed that we use the zero crossing of the output of the lock-in in 2f mode to find the exact position of the carrier wave with very high precision. The slope of the output with position is highest at the zero crossing, thus providing the most precision in maintaining that position. At the zero crossing in 2f mode, the 1f mode output is the amplitude of the carrier wave. This is a direct consequence of the fact that the 2f output is the derivative of the 1f signal. A lock-in output at 0.0±3.5% of the maximum output amplitude results in a (average X0) position within $\pm\lambda/44$ or 4.3Å. This meets the precision criteria quite well and I believe is realistically possible. It is also possible to use this system in a closed-loop positioning mode, maintaining the position despite creep in the piezo actuators real position.

The Data Acquisition Algorithm

The question of how to acquire the entire interferogram depends on the number of data points and the time scale of acquiring one data point. There are two possible methods, the continuos-pickoff and the step-creep-sit methods. A schematic of the data acquisition system is shown in figure 6.

The Continuos-Pickoff method

The basic idea here is to slowly scan the mirror position and when there is a zero-crossing in the 2f lock-in read the output of the 1f lock-in amplifier. Of course, there must be breaks in the scan every 10 μm as the end of the piezo travel is reached. The linear encoder can allow repositioning within 1/2 a wave, so this should not be critical. The main concern with this method is the trade-off between scanning rate and the low-pass filter time constant. A larger time constant gives a better accuracy of the output, but also limits the rate at which the amplifier can adapt to changing signals. For a scan of 7 mm to be done in 6 hrs determines a scan rate of 324 nm/sec or 1 wave/61 msecs. If we wish to find the peak amplitude within 1% we can average the signal as it passes over the top 2% of the peak. This corresponds to 1/15 of a wave and thus sets the time constant of the low pass filter to

$$\lambda/(15 * 5RC) = \text{scan rate},$$

$$RC = \lambda/(75 * \text{scan rate}) = 0.82 \text{ msecs}$$

which give a band width of

$$\Delta f = 1/2\pi RC = 203 \text{ Hz}.$$

This is not acceptable, so this method does not seem feasible in this "pure" continuous form for the high resolution measurements. This method could have advantages where the required resolution is less by a factor of 50 or more, particularly if the signal is not band-limited as it is for the He absorption experiment. Of course, the noise power per unit root band-width must always be taken into account in determining an acceptable time constant. It should be noted that a time constant of 637 msecs gives a band width of 1 Hz.

This method has the advantage of avoiding the uncertainties in energy position

associated with the properties of the linear encoder. This may not be critical, though, anyway. In addition, this "fringe-counting" method may be very useful in measuring the linearity and resolution of the encoder as well as the piezo actuator. If the linearity of the encoder is known, this can be accounted for. The calibration and hysterisis measurement of the piezo actuator is also useful information to have.

The Step-Creep-Sit Method

By taking advantage of the band-limited light source, we do not have to measure every peak (positive and negative) amplitude, but need only sample the envelope, which substantially reduces the required sampling rate. The acquisition algorithm here, then, would be to take a large step using the inchworm motor, and then creeping to the 2f zero-crossover to take the signal measurement by waiting 5 RC. If we wanted to measure 4000 data points over 6 hrs, this allows 5.4 secs/point to find and measure it. This should give very accurate results. Assuming that the peak position could be found in 1.5 secs, the allowable time constant of 4/5 gives a band width of 0.2 Hz, probably more than enough. Conversely, if we wish to have a band-width limit of 1 Hz -> RC=.64 secs, the entire high resolution interferogram would take under 4.5 hrs. This seems reasonable. Depending on the noise characteristics of the signal, larger band-widths may be usable, allowing more data points to be collected in the reasonable time frame of 6 hrs. 60,000 data points would mean .36 secs/point to find the peak and make the measurement. This may be very difficult to do with high accuracy in the measurements.

It should be noted that while positioning using the carrier wave as a reference is necessary and desirable, the exact frequency of the carrier wave is only known to within certain limits, since it is the weighted average of the frequency of each absorption line. This is where the narrow band-width of the source is particularly important. For 100 meV FWHM at 65.5 eV, the uncertainty in the possible frequency of the carrier wave is .1/65.5 = .15%. This is not too bad, as that is then the uncertainty in the energy calibration of the transformed spectrum. For a 5.00 eV FWHM, the uncertainty is 7.6%. Some prior knowledge of the peak spacing and widths can be used to reduce the uncertainty in this case, though. The linearity of the linear encoder can also affect this uncertainty if the error in a single step is greater than the wavelength of the carrier wave. For a step size of 3.6 um and a carrier wave of 20 nm a linearity of 0.5% or better is required to get to the exact wave we want. For measuring the n=9+ and above peaks, the positioning accuracy required is 332 nm. This is a linearity of better than 9%, which is far worse than the encoder's claimed value. In general, one would like to have a linearity better than 1/22 of twice the sampling rate to measure an envelope peak amplitude within 1% of the "true" amplitude.

Conclusion

The very high resolution measurement of the He double excitation resonances are feasible using the proposed positioning and measurement scheme. The lock-in amplifiers' outputs provides a high signal/noise ratio in measuring the amplitude of the signal while the phase information allows very precise positioning of the mirrors, with real-time feedback if necessary. The data collection time is reasonable when making use of the band-width limited source to reduce the sampling rate and allowing a longer signal averaging of the lock-in output.

Fano Resonance Simulation

N=2+, n=9-60, 50 μeV/chan

65.15 eV to 65.55 eV Range

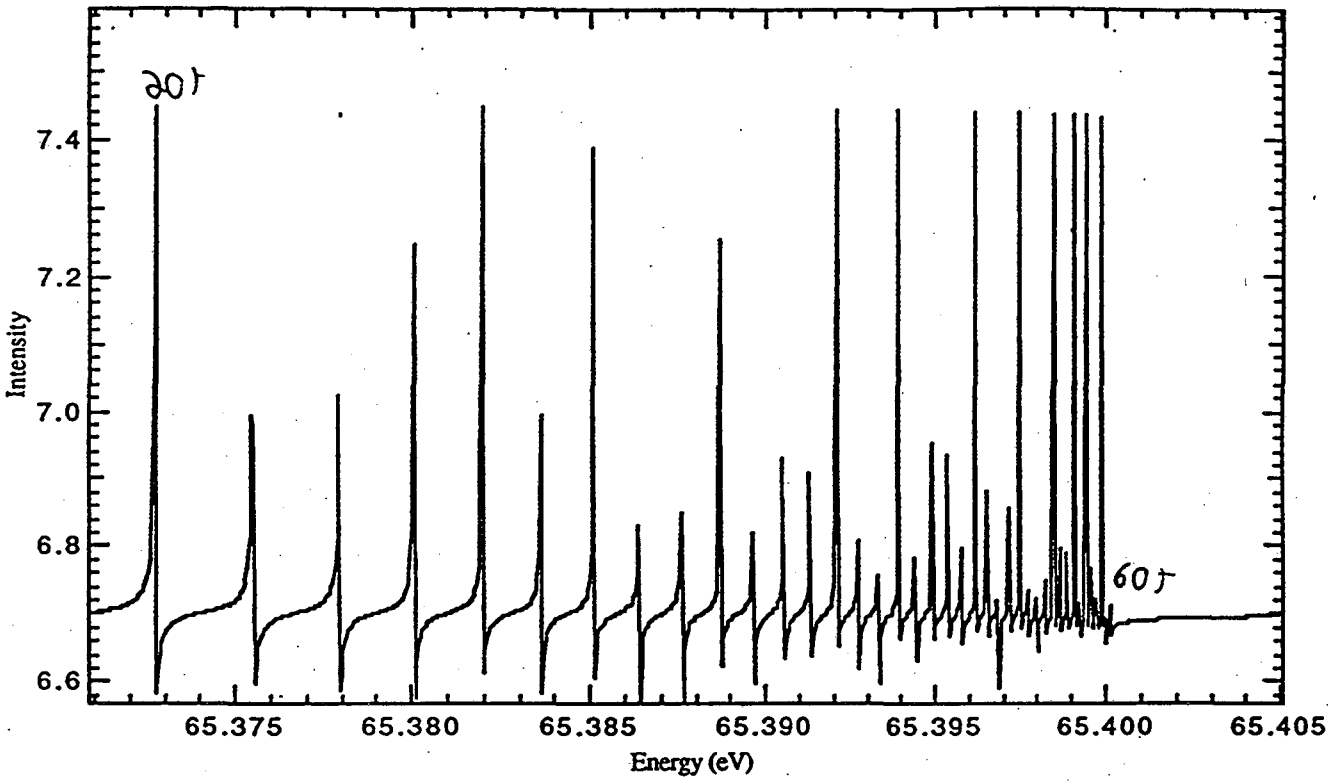

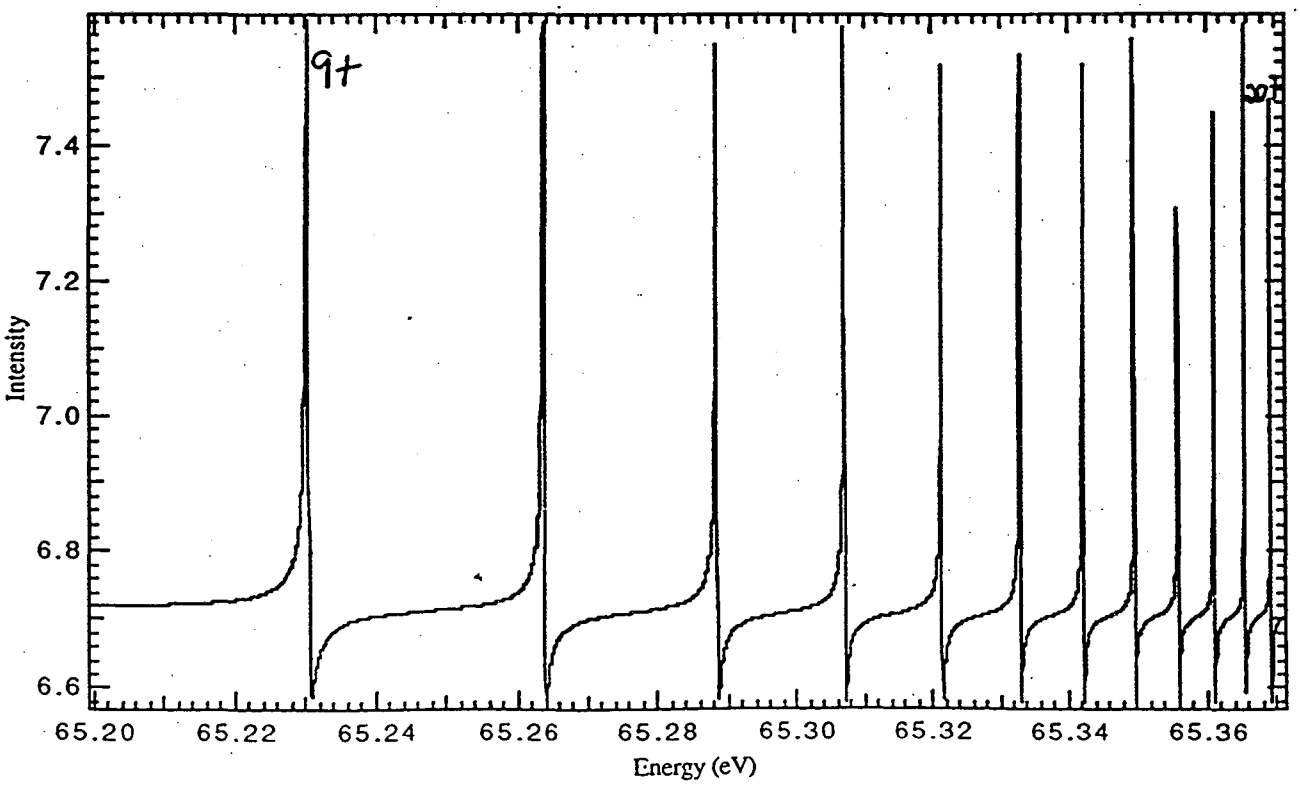

Some issues still left to consider (wrt mirror positioning and signal detection) are:

• Detector selection: we must keep in mind the time response characteristics of both the detector and any amplifiers subsequent to it necessary for the modulation technique to work and the noise characteristics which in part determine the required low-pass filter time constants, thus the acquisition time per data point,

• Minimizing the external noise interference by use of short, low noise cables, etc.,

Gaussian Distribution

@65.35 eV, Sigma=0.05 eV,60 μeV Point Density

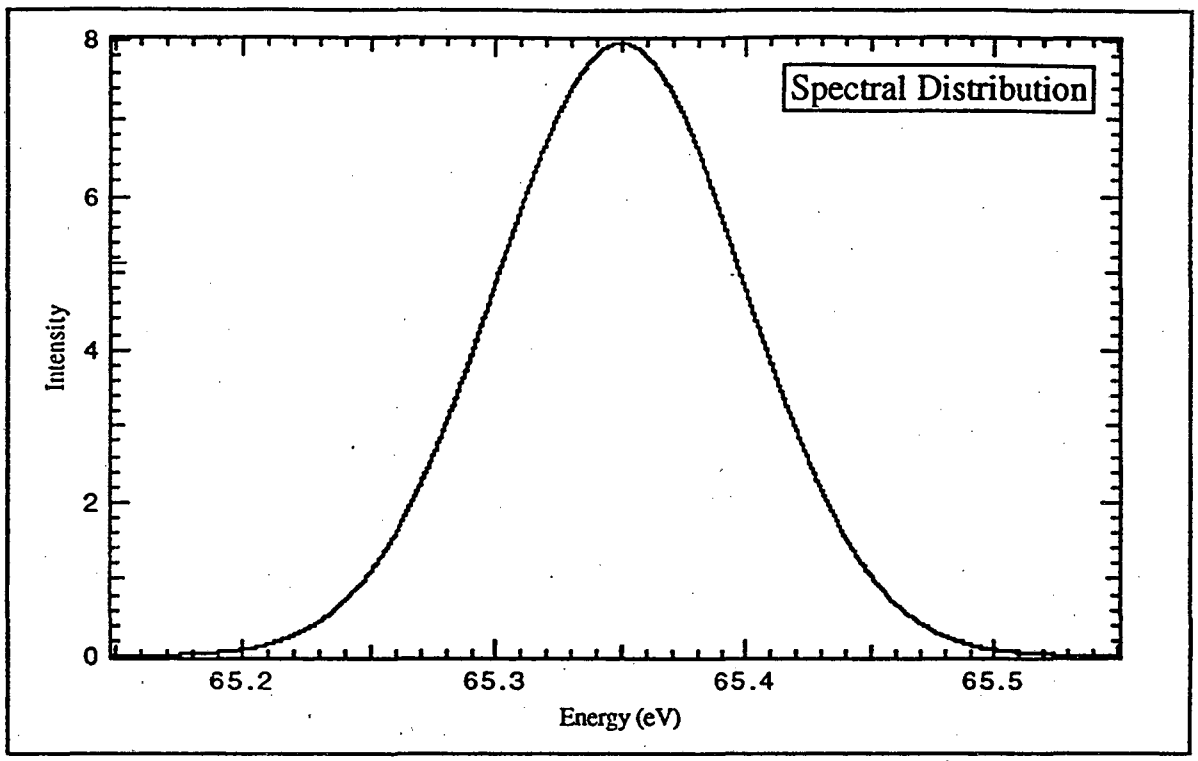

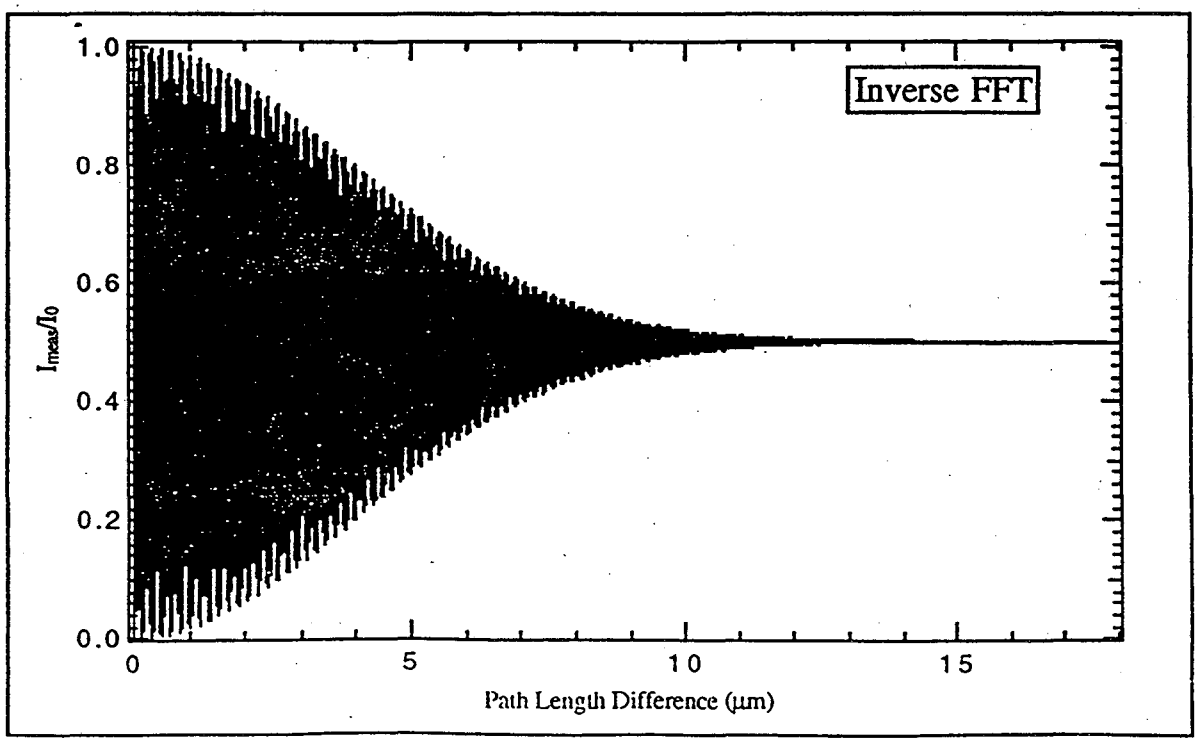

Gaussian Distribution

@65.35 eV, Sigma=0.05 eV,50 μeV Point Density
With He Resonance Absorptions, 10% absorption
2n+ series, peaks 9+ to 60+

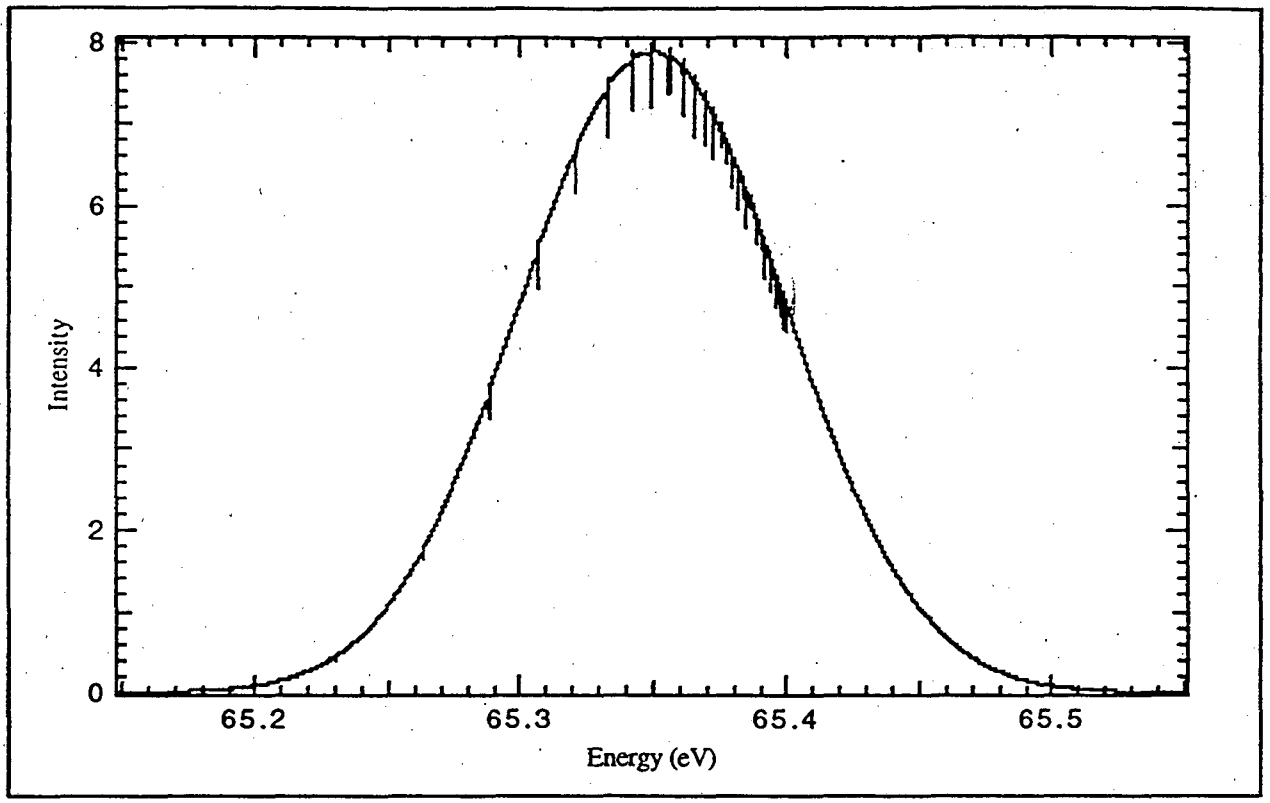

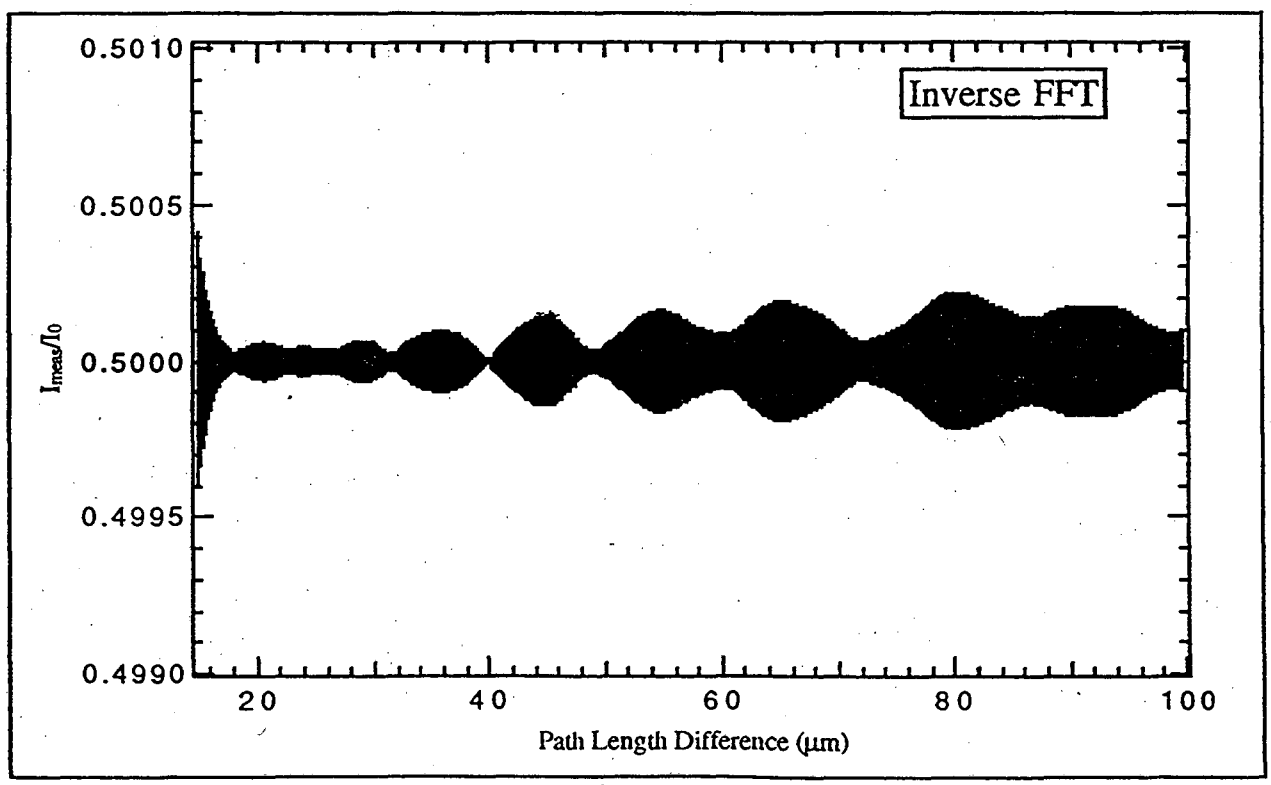

Gaussian Distribution

@65.35 eV, Sigma=0.05 eV,50 μeV Point Density
With He Resonance Absorptions, 10% absorption
2n+ series, peaks 9+ to 60+

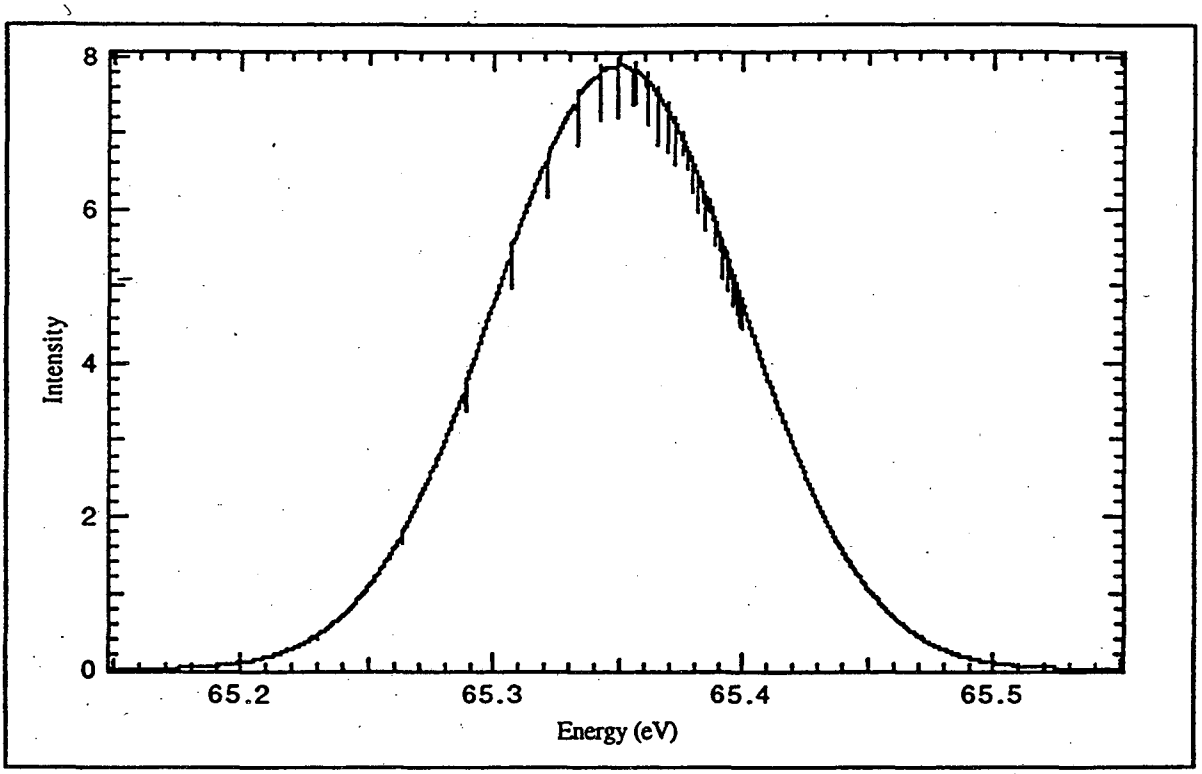

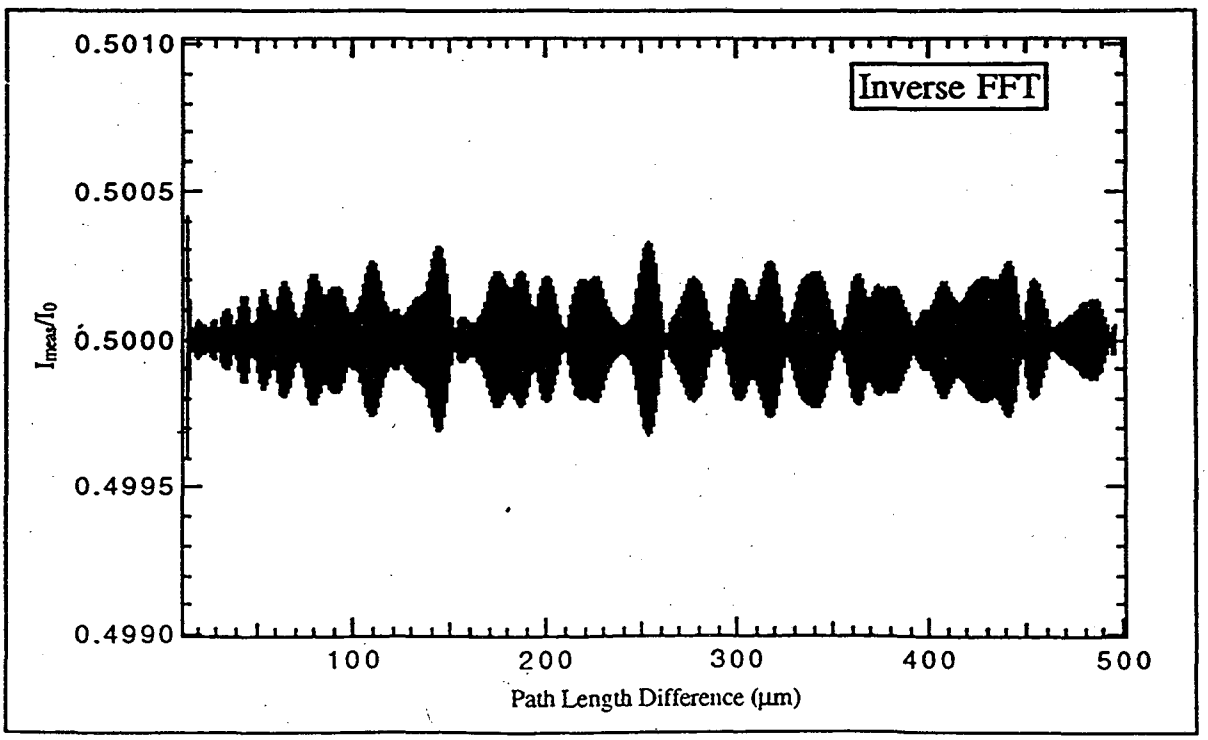

Gaussian Distribution

@65.35 eV, Sigma=0.05 eV,50 μeV Point Density
With He Resonance Absorptions, 10% absorption
2n+ series, peaks 9+ to 60+

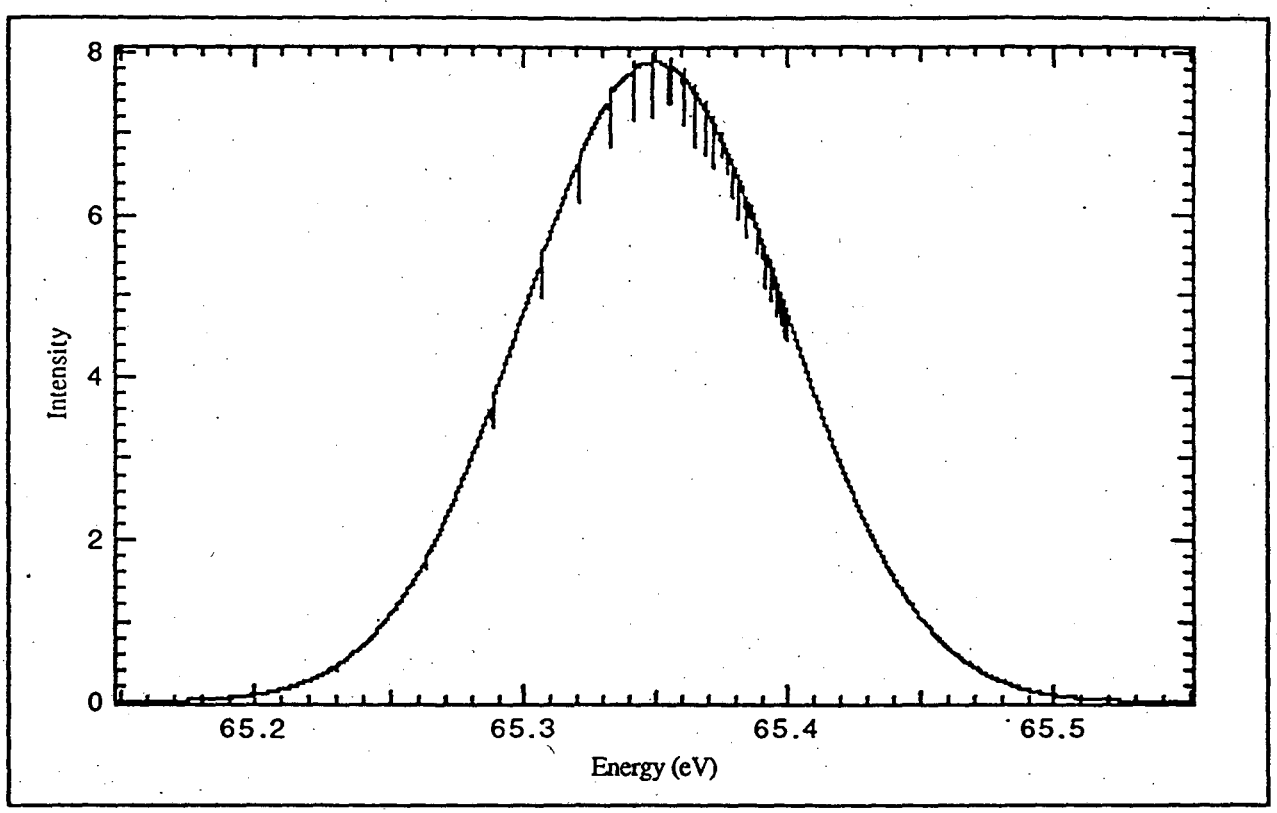

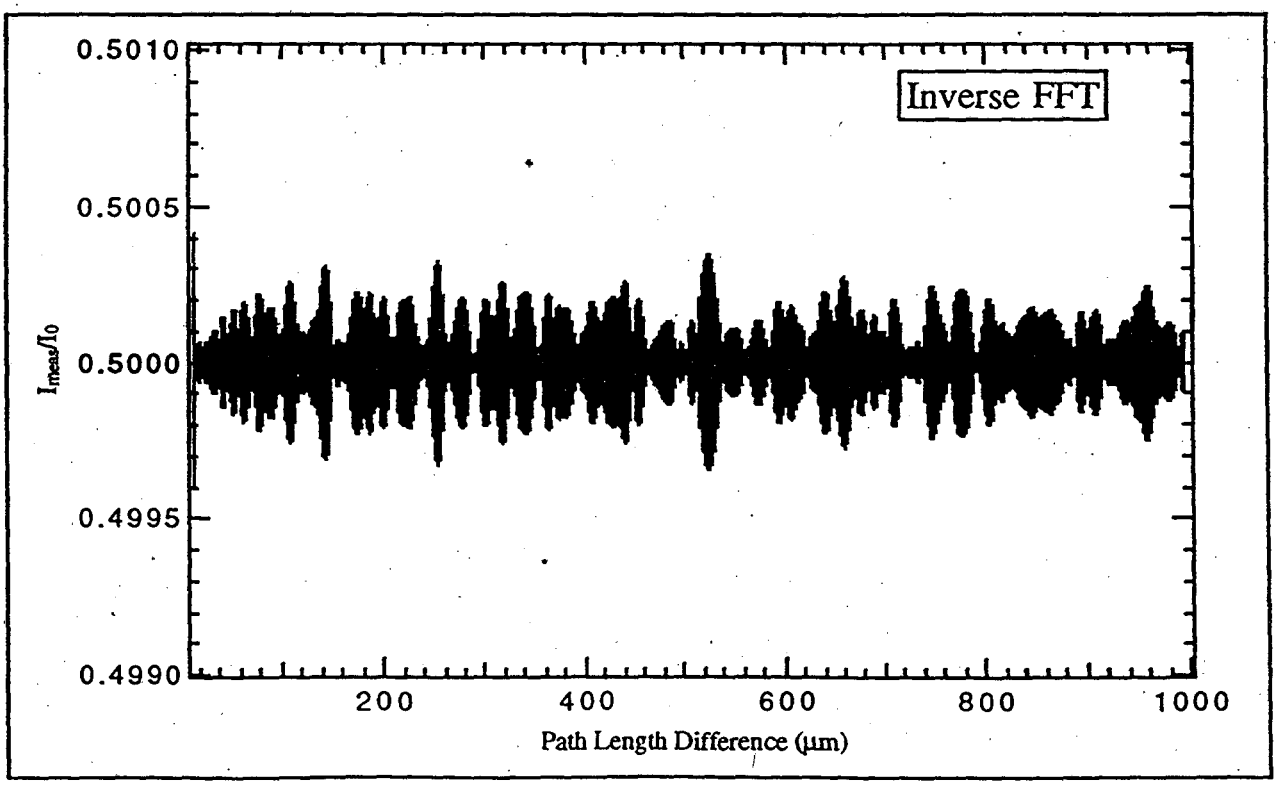

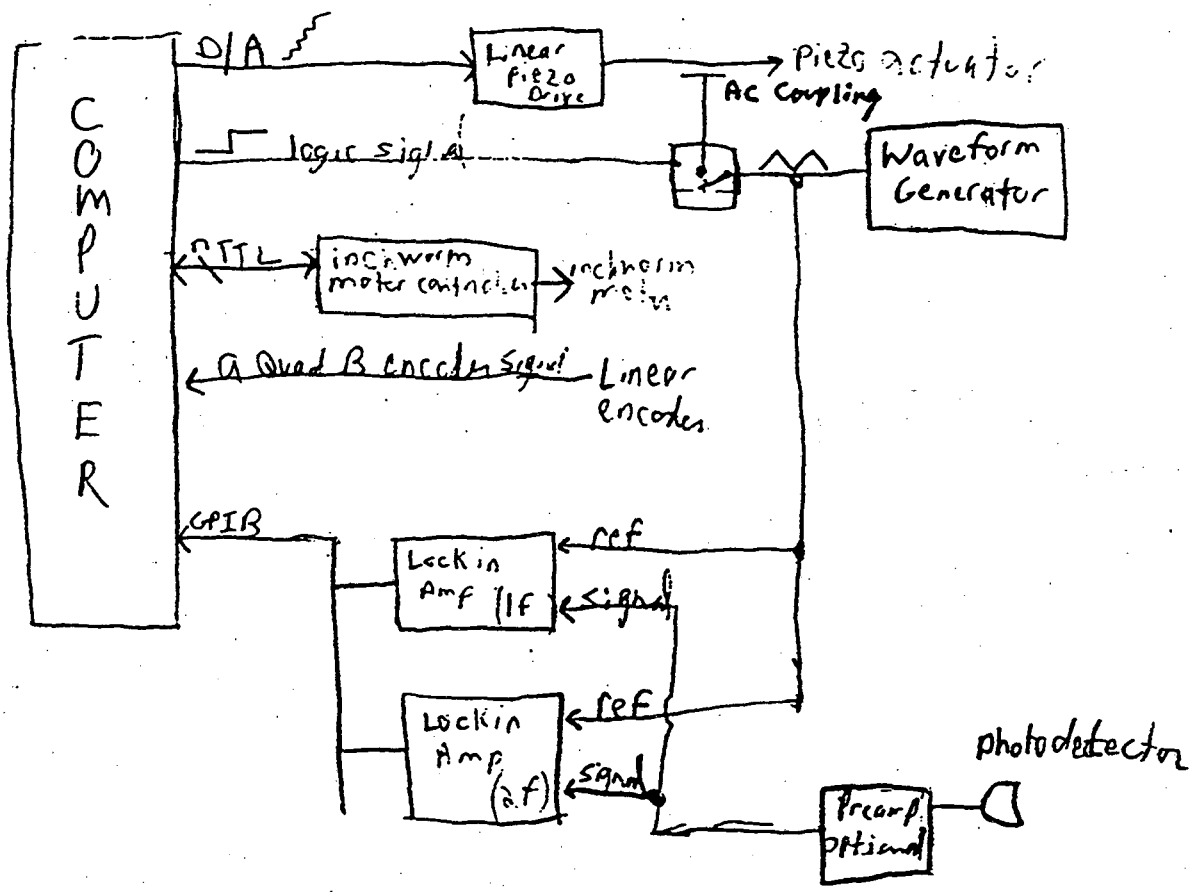
COMPUTER
D/A
Linear Piezo Drive
Piezo actuator
AC Coupling
Waveform Generator
logic sig.
TTL
inchworm motor controller
inchworm motor
Quad B encoder signal
Linear encoder
GPIB
Lock in Amp (1f)
ref
signal
Lock in Amp (2f)
ref
signal
photodetector
Preamp optional

Lock-in Analysis for FT-SX

Edward Moler June, 1993

First, the modulation signal and interferogram signal will be considered. Then, the resulting modulated interferogram signal and lock-in output will be analyzed.

The Modulation Signal

We modulate the mirror position with a triangle function which varies from +1 to -1 over t = 1. The time and frequency units are arbitrary.

$$\mathrm{Tri}(f,t) := 1 - 4\cdot f\cdot \mathrm{if}\left(\mathrm{mod}\left(t,\frac{1}{f}\right) < \frac{1}{2\cdot f}, \mathrm{mod}\left(t,\frac{1}{2\cdot f}\right), \frac{1}{2\cdot f} - \mathrm{mod}\left(t,\frac{1}{2\cdot f}\right)\right)$$

For example, $f := 1$ $t := 0, .01 .. 2$

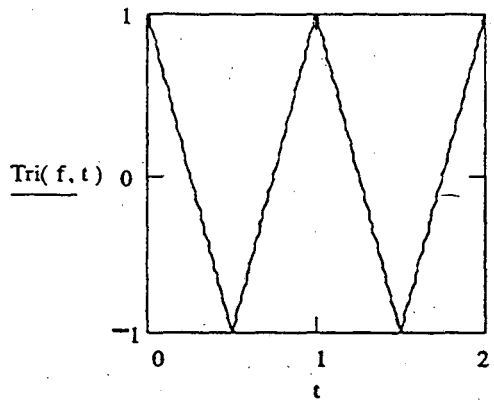

The Interferometer Signal

The interferometer signal as a function of path length displacement is a small cosine like function on a large background. The cosine-like function is the carrier wave and we are interested in the amplitude of the carrier wave across one peak. As an example,

$$I_0 := 1 \quad x := -2, -1.99 .. 2 \quad A := 1$$

$$I_s(x) := A\cdot\cos\left(2\cdot\pi\cdot x\right) + I_0$$

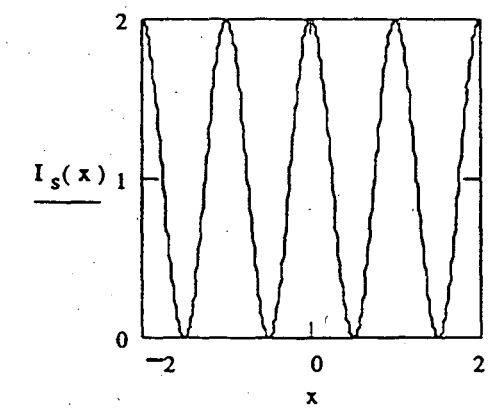

The amplitude A is what we are interested in ultimately extracting. One should note that the signal/background ratio in the real system will be typically < 0.1%.

The signal is AC coupled to the electronics and thus the time-averaged signal is subtracted out. This means that if the mirrors are stationary, only transient noise will be recorded with time. If the mirrors are moving in an oscillatory mode, the time averaged signal across the oscillation amplitude (delta-x) will drop out.

The Modulated Interferometer Signal

We next explore the effect of applying the modulation to the interferometer position to get a time varying output from the photo-detector. There are two parameters of interest here, the average X position of the mirrors,X0 , and the peak-to-peak maximum displacement induced by the modulation,D. We can define the position as a function of time by,

$$X(D, X0, T) := X0 + \frac{D}{2} \cdot Tri(f, T)$$

We assume that $f := 1$ for the following.

The time varying output of the detector can now be expressed as a function of time, position, and displacement as,

$$I0(D, X0) := \int_0^{\frac{1}{f}} I_s(X(D, X0, T))\, dT$$

$$I_{mod}(D, X0, T) := I_s(X(D, X0, T)) - I0(D, X0)$$

Where I0 is the DC baseline of the detector signal over which the oscillation takes place. To understand where the time varying signal comes from, refer to the picture of the interferometer signal as a function of "X" below. If X0, the average position of the mirrors, is centered at the 1/4 period point, and the total displacement, D is +-1/8, then the time varying signal will oscillate back and forth between the points marked D/2 and -D/2.

$D := .25$

$X0 := 0.25$

$T := 0, .05 .. 2$

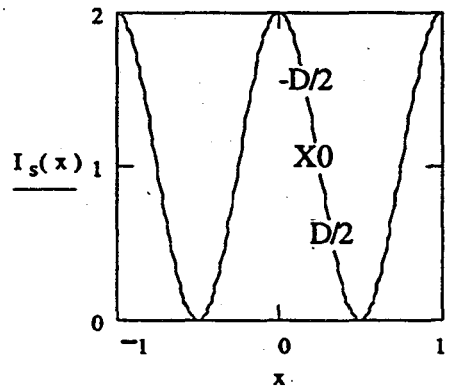

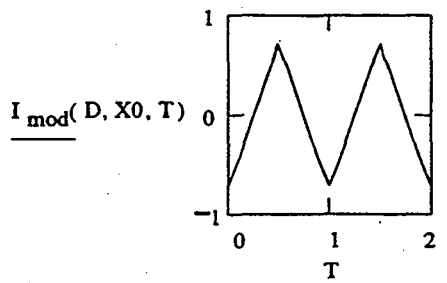

Increasing the peak to peak displacement of the modulation to exactly 1/2 of a wave gives a perfect cosinusoidal signal output with time.

$D := .5$

$X0 := 0.25$

$T := 0, .05 .. 2$

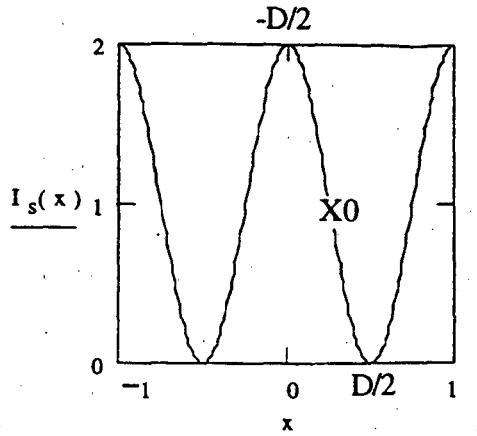

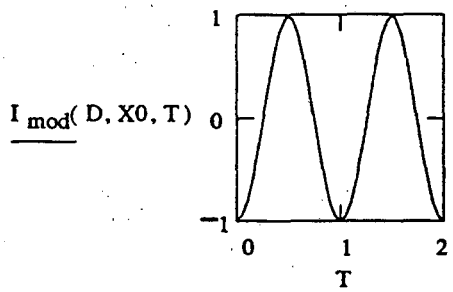

Shifting X0 over to center on the top of the carrier wave peak gives a time varying output that is twice the modulation frequency as it traces back and forth over the "hump" for each period of the modulating signal.

$D := .5$

$X0 := 0.0$

$T := 0, .05 .. 2$

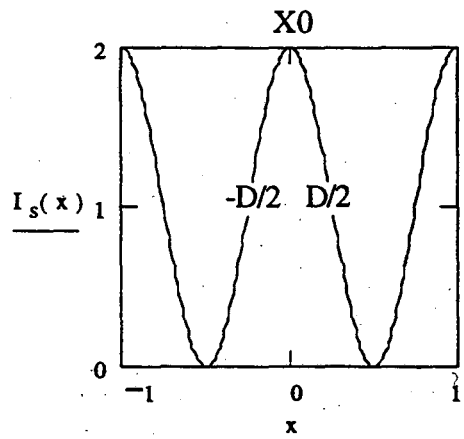

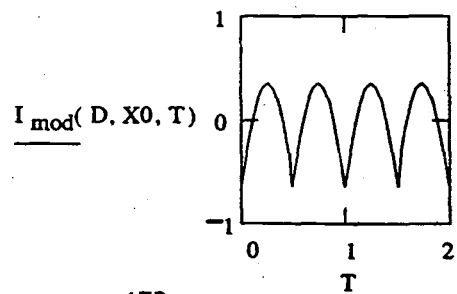

The Lock-in Technique and Output

The lock-in amplifier multiplies a reference cosine-wave, I-ref, and the AC coupled signal, I-s, and gives as an output the time-averaged product. Typically, the reference cosine-wave is locked with great precision to the periodic modulation wave imposed upon the experiment. A phase shift between the modulation signal and the reference wave can also be introduced with great accuracy. The signal wave is AC coupled to a high gain, low noise AC amplifier and several different filters before multiplication. The lock-in technique can be extremely sensitive to small signals and can reject very large signals that are not of the frequency of interest, thus greatly enhancing the signal/background and signal/noise ratios.

We can write the output of the lock-in amplifier as the time average of the product of the phase-shifted reference cosine-wave and the modulated input signal,

$$O(ff, nf, phi, D, X0) := \frac{\int_0^{nf} \cos(2\cdot\pi\cdot ff\cdot T + phi)\cdot I_{mod}(D, X0, T)\, dT}{nf}$$

where ff is the reference frequency, nf is the integration limit, and phi is the phase shift of the reference relative to the modulation signal after adjusting for the phase delays of the detector amplifiers, piezo amplifiers, and any other intervening electronics. It is assumed here that any frequencies close to but not exactly ff will be properly averaged after nf periods of the reference frequency. For all calculations and examples below, ff will be set to f, the modulation frequency, since this is the point of introducing the modulation in the first place, to use the lock-in amp to extract the signal intensity. It is useful to note that

$$O = A*\sin(phi)/2,$$

for I-mod =A*cos(2*π*f*T). Thus, the output is proportional to the amplitude of the peak and the sin of the phase angle between the two waves.

It is interesting to see the lock-in output as a function of relative phase angle phi for the optimum case of an exact cosine signal from the modulated interferometer signal, i.e. a displacement of 1/2 a wave (peak to peak) and an average position 1/4 of a wave from the top of the "hump".

$D := .5 \qquad X0 := 0.25 \qquad T := 0, .05 .. 2 \qquad phi := 0, .5 .. 2\cdot\pi$

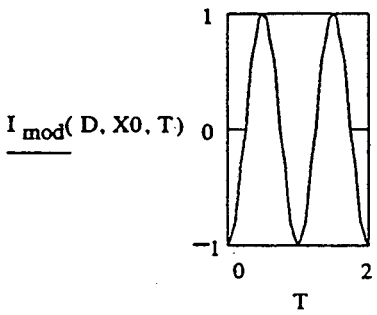

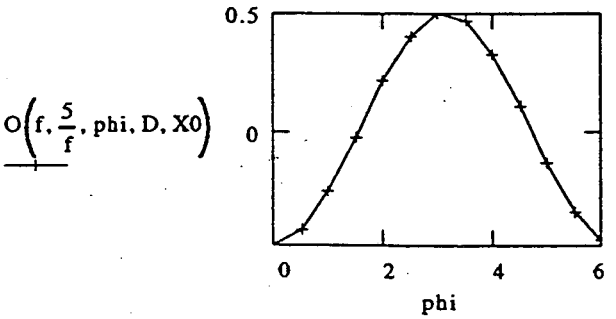

As expected, the output looks like sin(phi).

It is more interesting to observe the lock-in output as a function of average position, X0, since this is how it is proposed that the precise positioning of X0 is done. Here we assume ideal phase adjustment and displacement.

D := .5 X0 := 0, .1 .. 1 T := 0 phi := π

$O\left(f, \frac{5}{f}, phi, D, X0\right)$

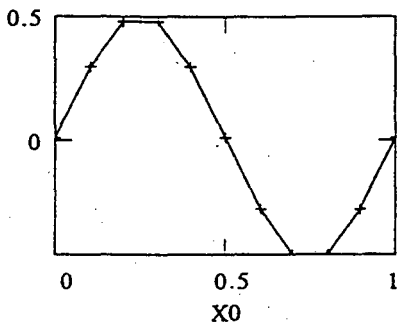

Not surprisingly, the X0 also produces a sin (2*π*d) output in the lock-in, where d is the fraction of a wavelength of the carrier wave.

If the lock-in reference wave phase is shifted 90 degrees from optimum, the output is zero.

D := .5 X0 := 0, .1 .. 1 T := 0 phi := $\frac{\pi}{2}$

$O\left(f, \frac{5}{f}, phi, D, X0\right)$

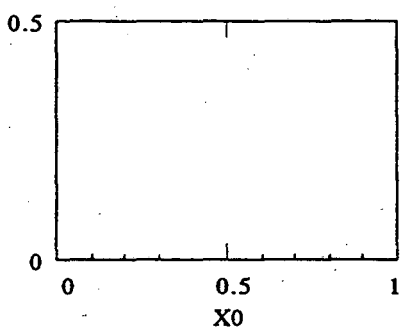

With the hope of finding an algorithm for precise positioning of the mirrors on the carrier wave, below is shown the lock-in output as a function of reference wave phase shift, phi =0..2π, and center position, X0 = 0..1 wavelengths.

$$N := 10 \quad i := 0..N \qquad j := 0..N \qquad x_i := \frac{1}{N}\cdot i \qquad p_j := 2\cdot\frac{\pi}{N}\cdot j$$

$$x0\_phi_{(i,j)} := O\left(f, \frac{3}{f}, p_j, D, x_i\right)$$

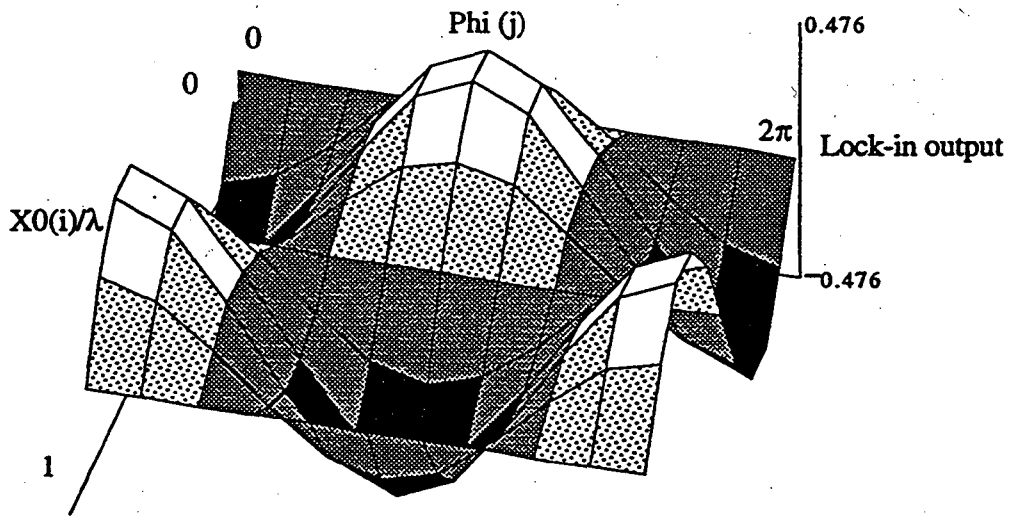

x0_phi

There are four nodal lines on this "output surface" where the output is zero. Two are along the constant lines X0=0 and X0=0.5, corresponding to sitting at the extrema of the carrier wave. The other two are along lines of constant phi, at phi=π/2 and phi=3π/2. There are also four lines of maximum fluctuation, X0=0.25,0.75, and phi =0,π.

Next consider the lock-in output surface again vs. X0 and phi, but with doubling the reference frequency relative to the modulation frequency

$$x0\_phi\_2f_{(i,j)} := O\left(2\cdot f, \frac{3}{f}, p_j, D, x_i\right)$$

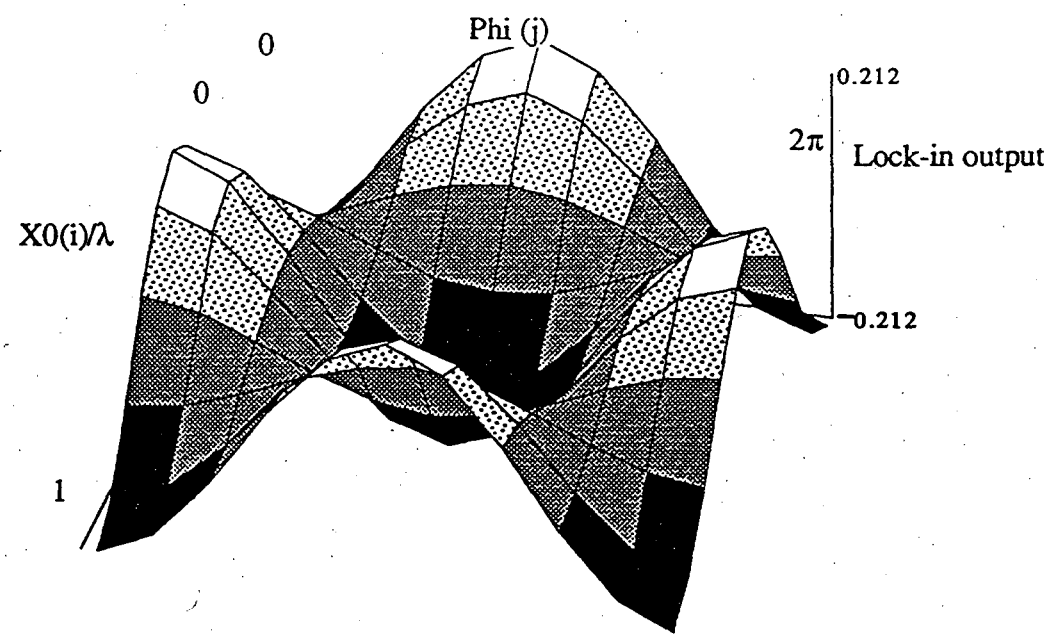

x0_phi_2f

Are there nodal lines on this surface?

$D := .5$ $\quad X0 := 0, .1 .. 1$ $\quad T := 0$ $\quad phi := \frac{\pi}{2}$

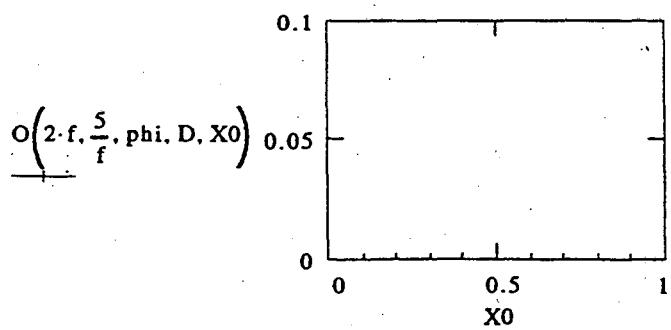

Yes, there are nodal lines along the constants X0=0.25,0.75, and phi=$\pi/2,3\pi/2$.

The four lines of maximum amplitude are X0=0,0.5, and phi=0,π. It is useful to recall that using the 2f reference frequency in the lock-in gives the derivative of the 1f output. Thus, the 2f surface is still harmonic, but shifted by 90 degrees from the 1f surface, along each axis. This means that where there is a peak in the 1f surface, there is maximum slope in the 2f, and vice versa. This will contribute greatly to the positioning precision and signal detection scheme

Next we consider the lock-in output surface as a function of position, X0, and displacement, D. We assume optimum phase for maximum output signal at D=1/2.

$$d_j := \frac{2.0}{N} \cdot j \qquad phi := \pi$$

$$x0\_D\_1f_{(i,j)} := O\left(f, \frac{3}{f}, phi, d_j, x_i\right)$$

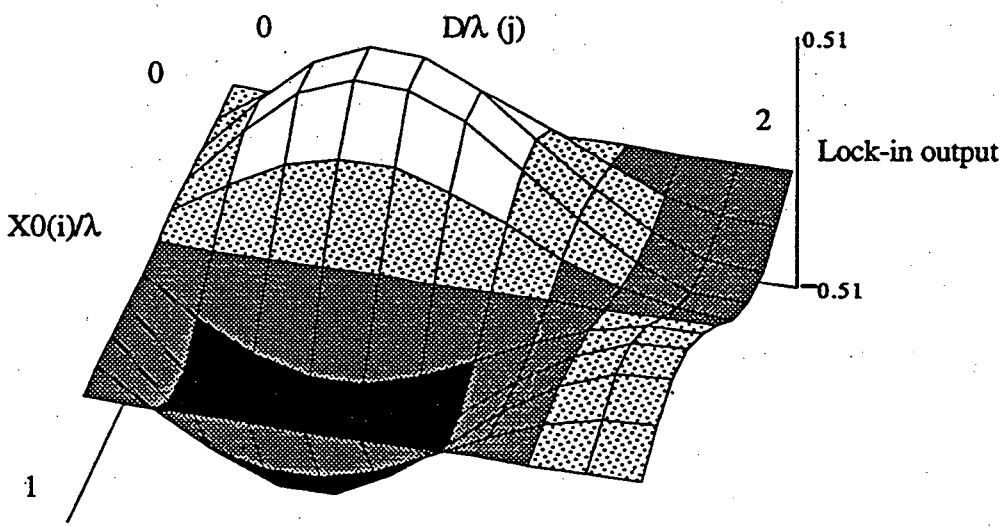

x0_D_1f

Also, look at output surface for 2f lock-in reference mode, for X0 and D

$$x0\_D\_2f_{(i,j)} := O\left(2\cdot f, \frac{3}{f}, phi, d_j, x_i\right)$$

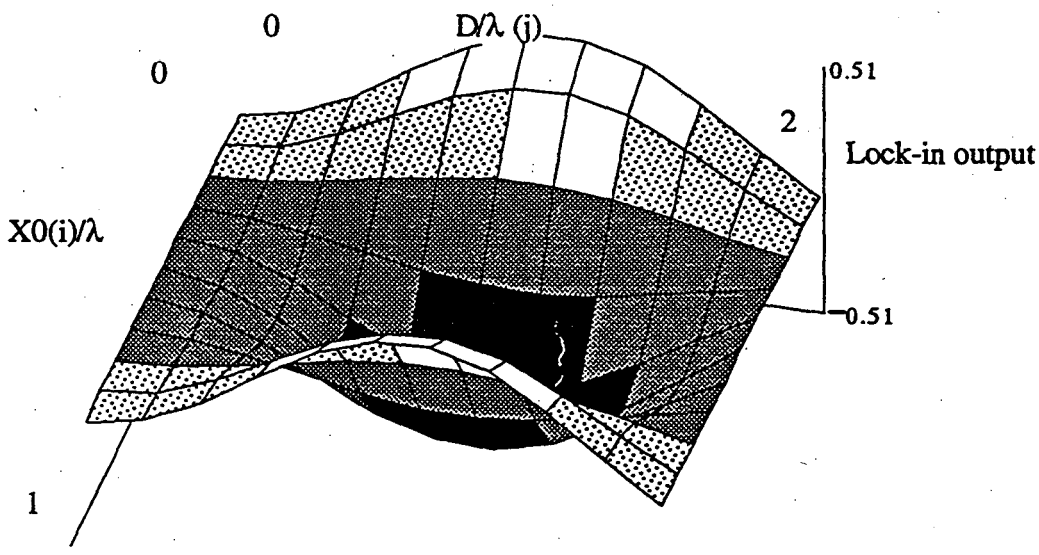

x0_D_2f

Application of Hard X-Ray Interferometry

Wenbling Yun

Argonne National Laboratory

The ANL/APS Effort in Hard X-Ray Fourier Transform Techniques

1: Scientific Applications:

Fourier transform spectroscopy

Fourier transform imaging of surfaces and interfaces

Real-time spectroscopy

Real-time imaging of surfaces and interfaces

2: Fourier transform spectrometers:

Amplitude-division

Wavefront-division

Basic principle of x-ray reflectivity technique

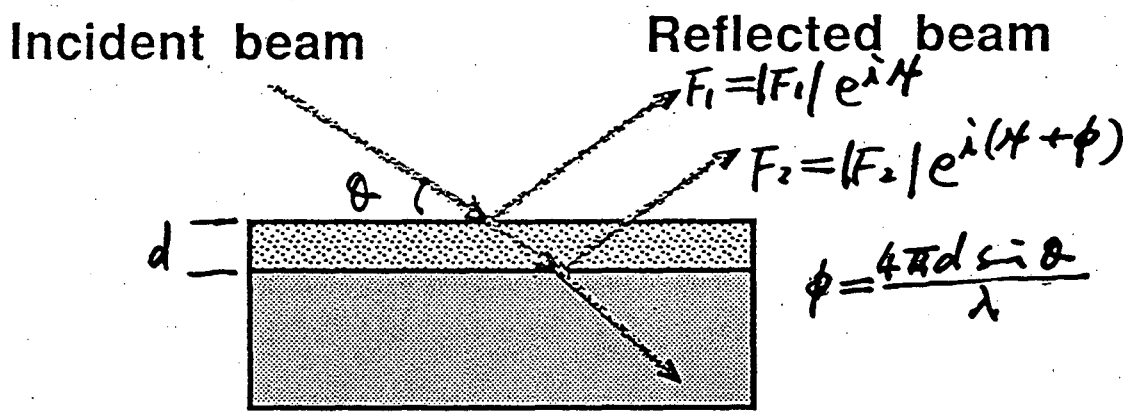

Reflected intensity is dependent on the interference of the amplitudes reflected from the interfaces (two here).

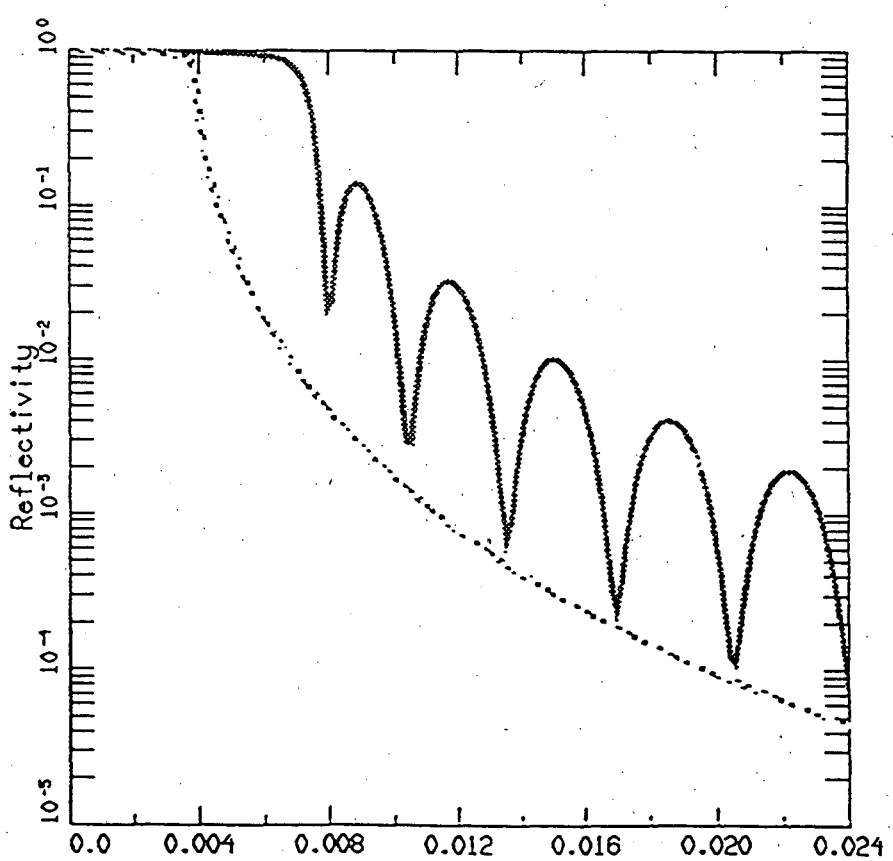

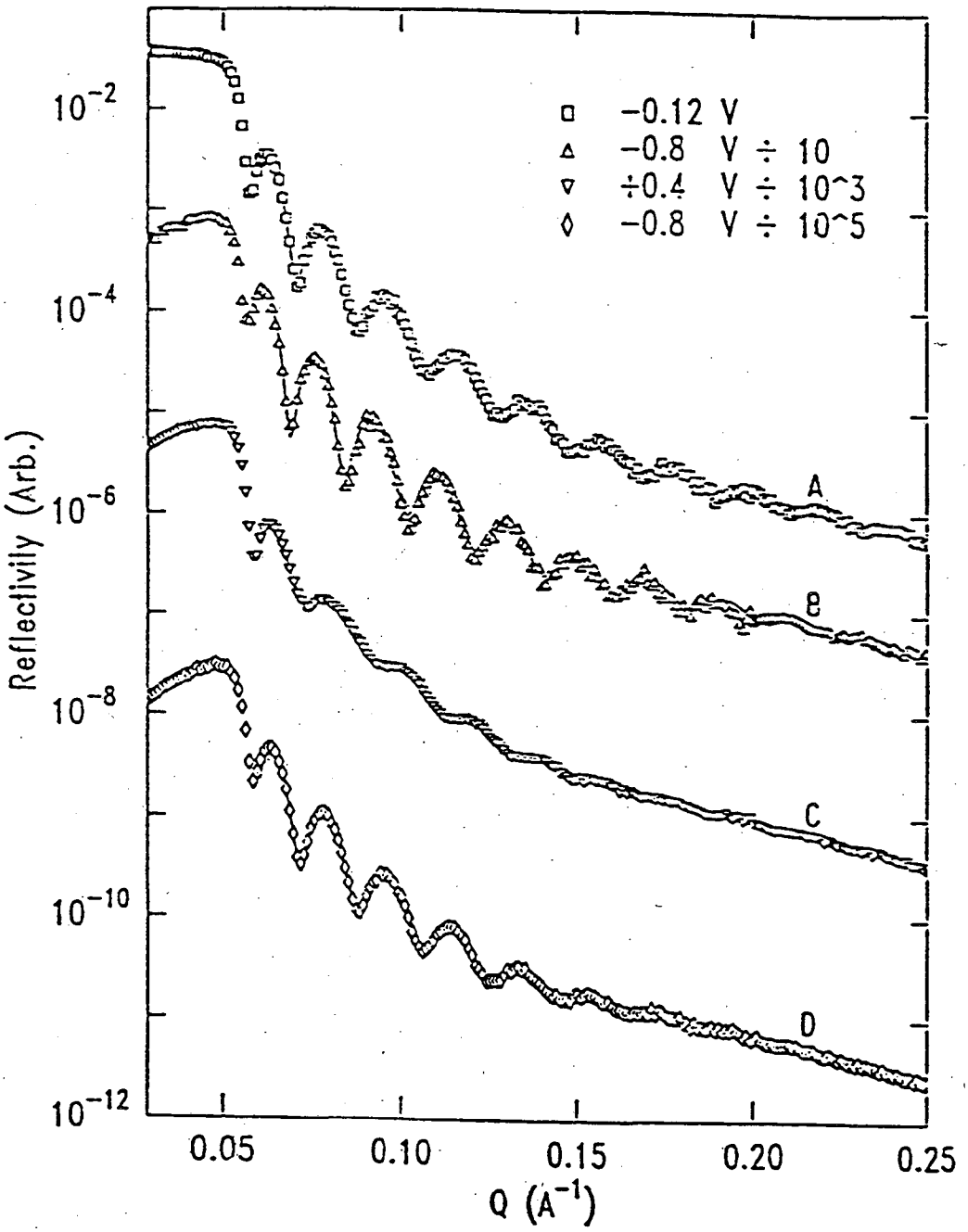

Fig. 3. Reflectivity of Cu-on-Si electrode at various potentials in borate buffer solution (pH 8.4). A, B, C, D correspond to potentials indicated in cyclic voltammogram of Fig. 2.

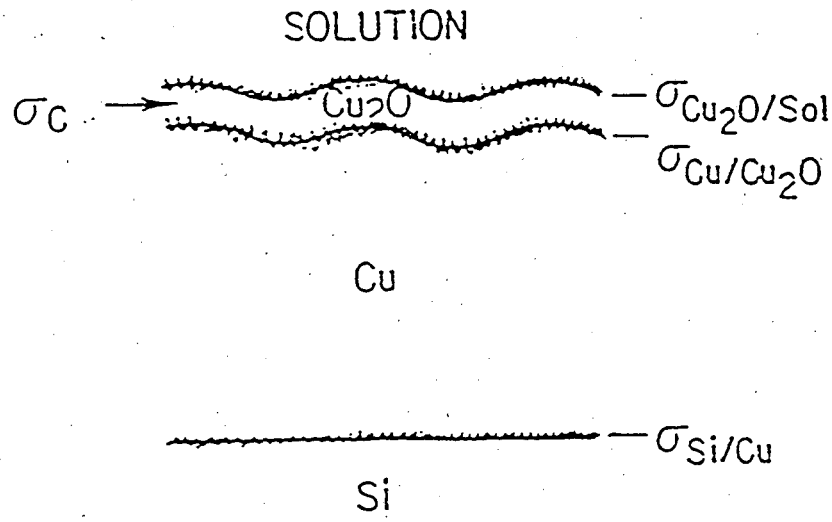

Fig. 4. Schematic of multi-layer model for Cu-on-Si electrode (not to scale). The oxide film has been represented as Cu_2O.

Table I. Parameters Derived from Least Squares Fit to Experimental Data.

E(V)	d_{Cu}(Å)	d_{Cu_2O}(Å)	ρ_{Cu_2O}(g/cc)	σ_c(Å)	$\sigma_{Cu_2O/Cu}$ (Å)	$\sigma_{Cu_2O/sol}$ (Å)
-0.12	268	24	6	17	8.3	3.4
-0.8	284	--	--	--	--	--
+0.4	250	26	5.5	26	9.4	2.2
-0.8	275	--	--	--	--	--

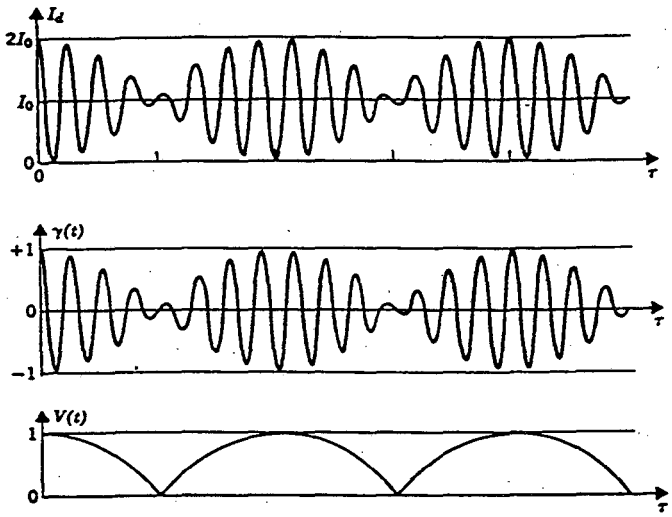

Fig. 6.8

different frequencies. Reinforcement occurs whenever $|\nu_2 - \nu_1|\tau$ is an even integer; then for a limited range of τ both cosines oscillate together between ± 1, giving a γ that also oscillates between ± 1. Cancellation occurs whenever $|\nu_2 - \nu_1|\tau$ is an odd integer and is complete if $P_1 = P_2$; otherwise the fringes are still present but with reduced strength.

The interference fringes in Figs. 6.7–6.9 continue periodically for all values of the retardation time τ. This behavior is unreal and is a property of the discrete nature of the distribution functions that we have used thus far.

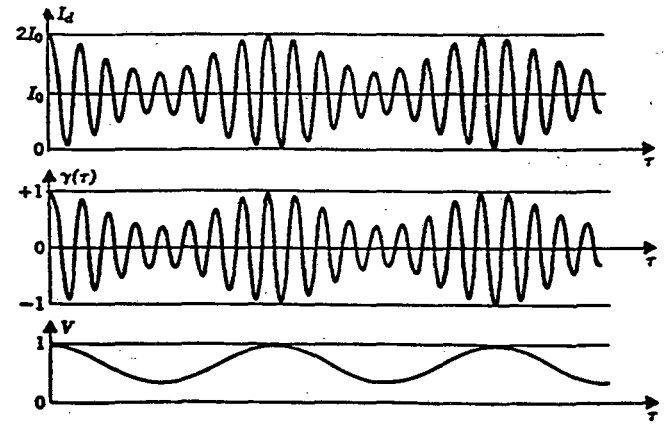

Fig. 6.9

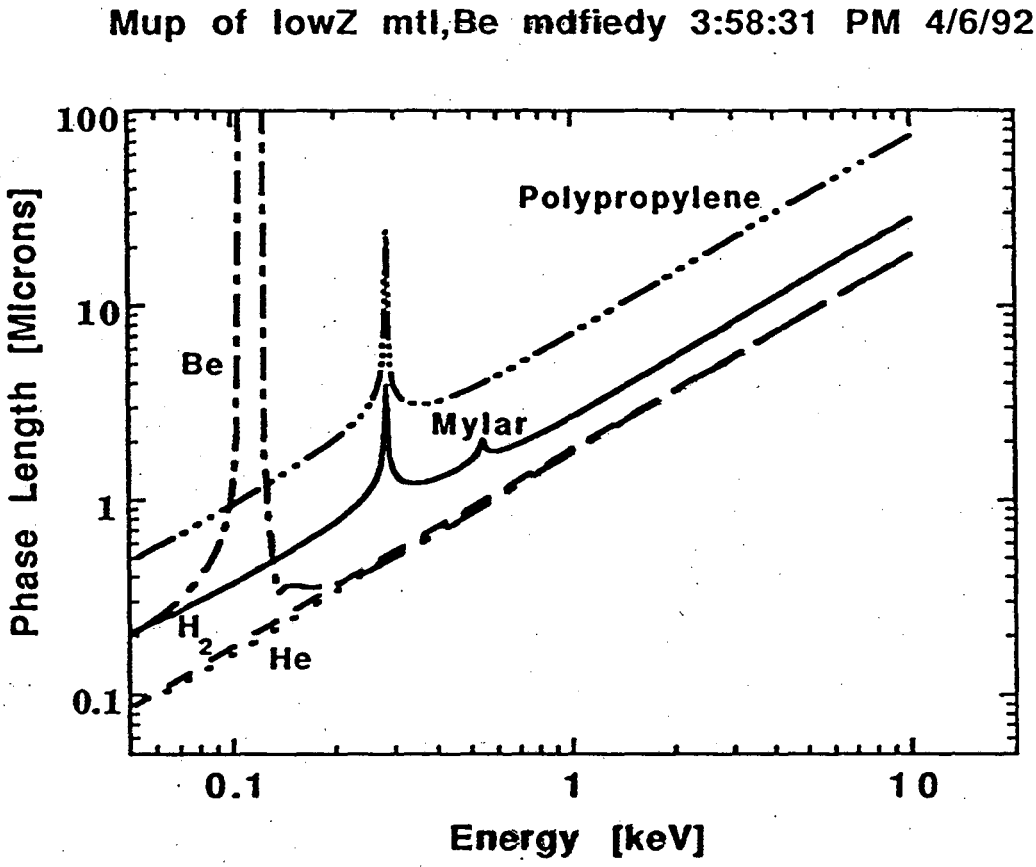
Mup of lowZ mtl,Be mdfiedy 3:58:31 PM 4/6/92
100
10
1
0.1
Phase Length [Microns]
Polypropylene
Be
Mylar
H2
He
0.1
1
10
Energy [keV]

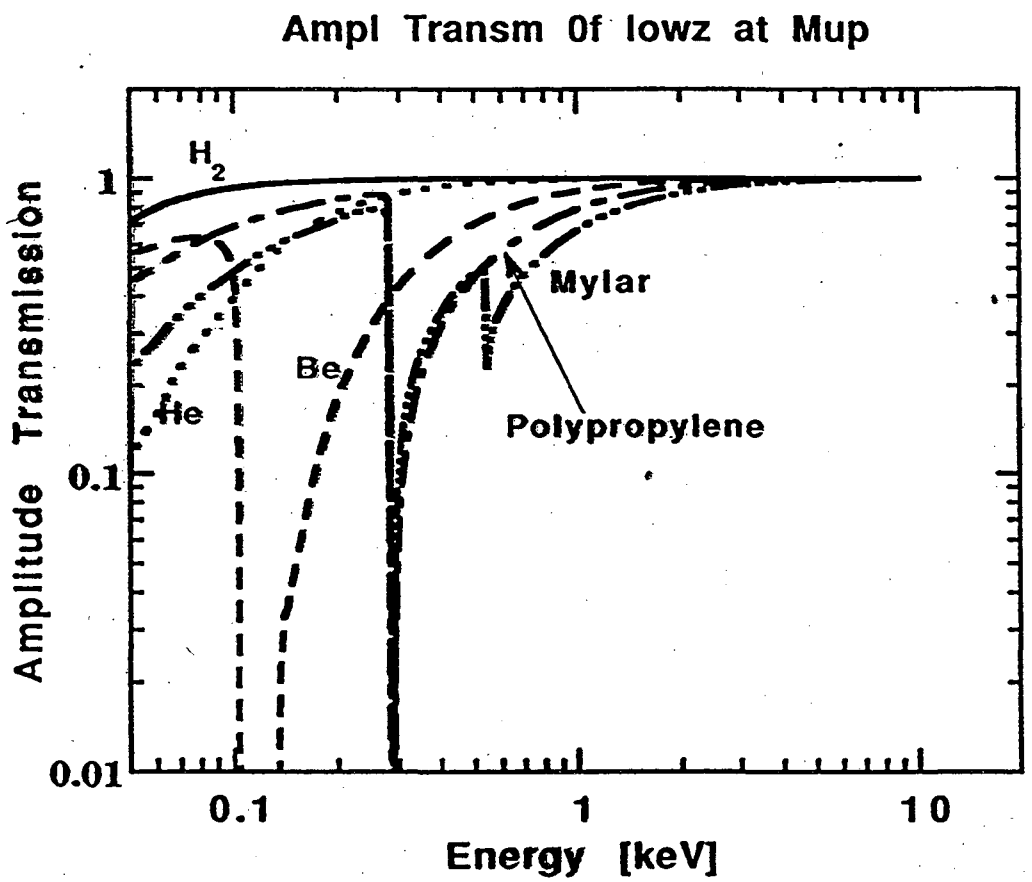
Ampl Transm 0f lowz at Mup
Amplitude Transmission
1
0.1
0.01
0.1
1
10
Energy [keV]
H2
He
Be
Mylar
Polypropylene

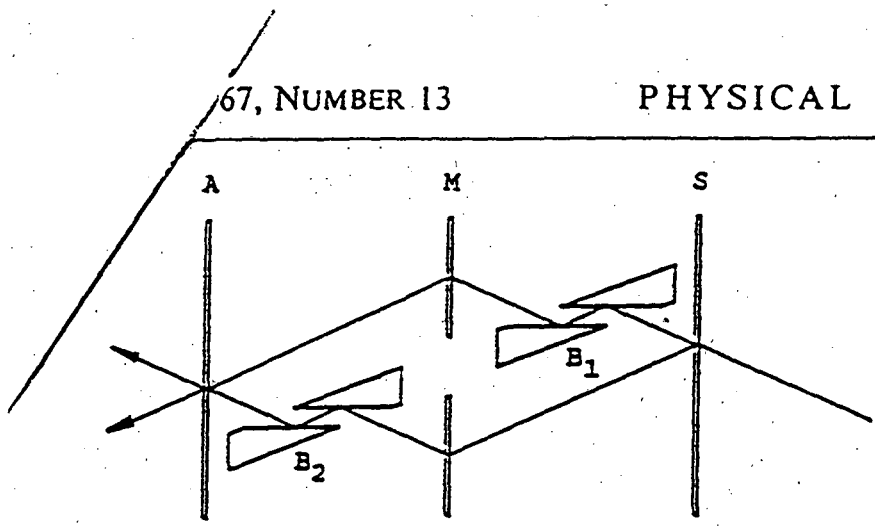

FIG. 2. Beam-path geometry of the Michelson interferometer for x rays and thermal neutrons. *S*: splitter; *M*: mirror; *A*: analyzer components of a LLL interferometer generating Laue-case waves by Bragg transmission. B_1, B_2: grooved crystals generating Bragg-case waves by surface Bragg reflection.

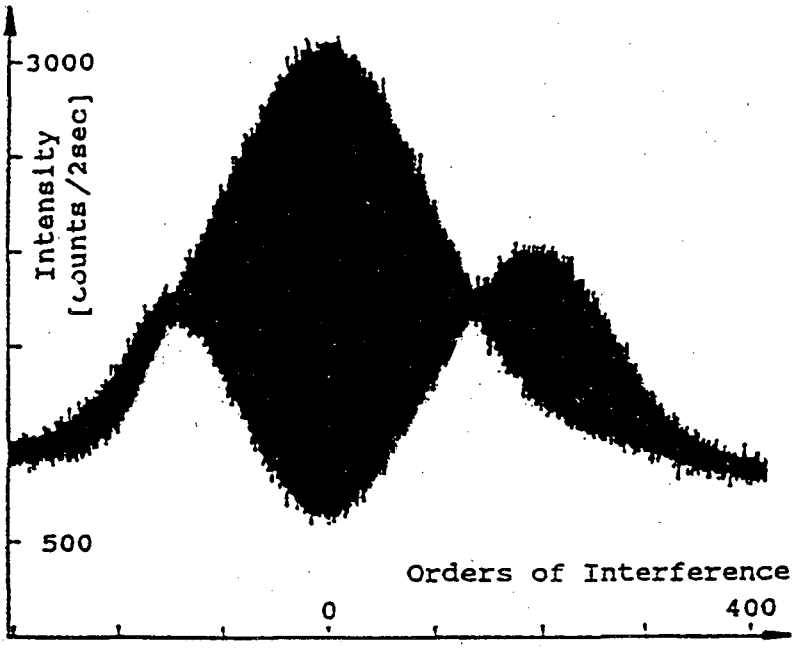

FIG. 5. Spectrum measured with the new interferometer for the copper $K\alpha_1 K\alpha_2$ doublet. Clearly visible are the nodes occurring due to the slightly different wavelengths. The approximately 630 orders of interference appearing as fast oscillations in the spectrum cannot be resolved in this representation (see Fig. 6).

Spatially Resolved X-Ray Microspectroscopy:

microprobe + Real time Fourier transform Spectrometer.

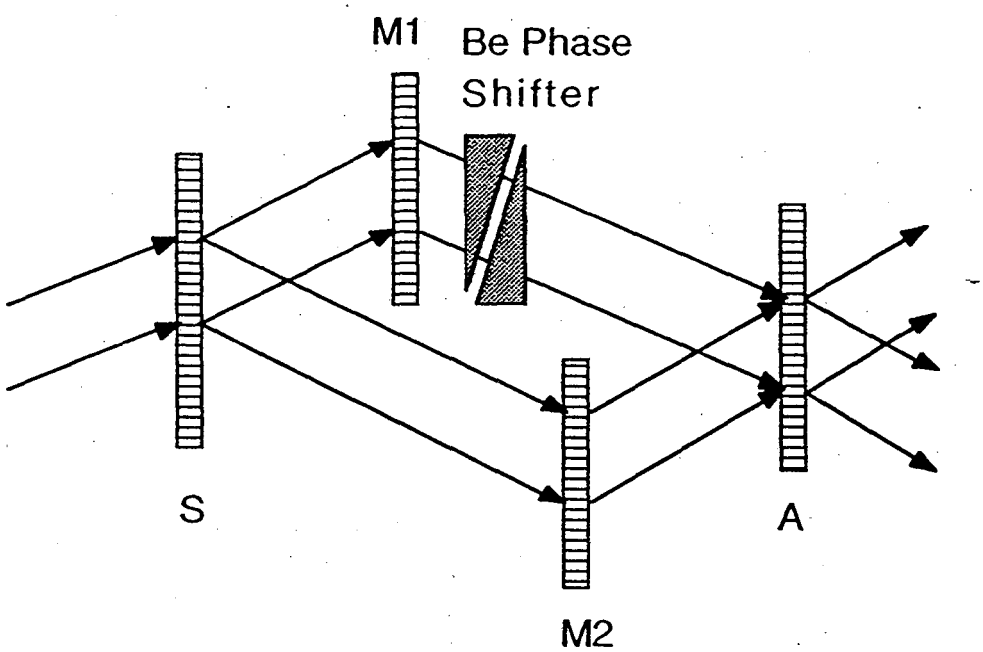

Fig. 2. Schematic illustration of the amplitude-division Fourier transform interferometer to be developed. This interferometer consists of a skew symmetry LLL interferometer and a phase shifter. The LLL interferometer consists of a beam splitter S, two transmission mirrors/crystals M1 and M2, and an analyzer A. The relative phase difference between the two interfering beams split by S is obtained by adjusting the thickness of the phase shifter. Real-time Fourier transform spectroscopy or Fourier transform imaging of surfaces and interfaces may be obtained by using a single wedge rotated 90 degrees from that shown above. A position sensitive detector is required to record the intensity distribution behind the analyzer crystal A.

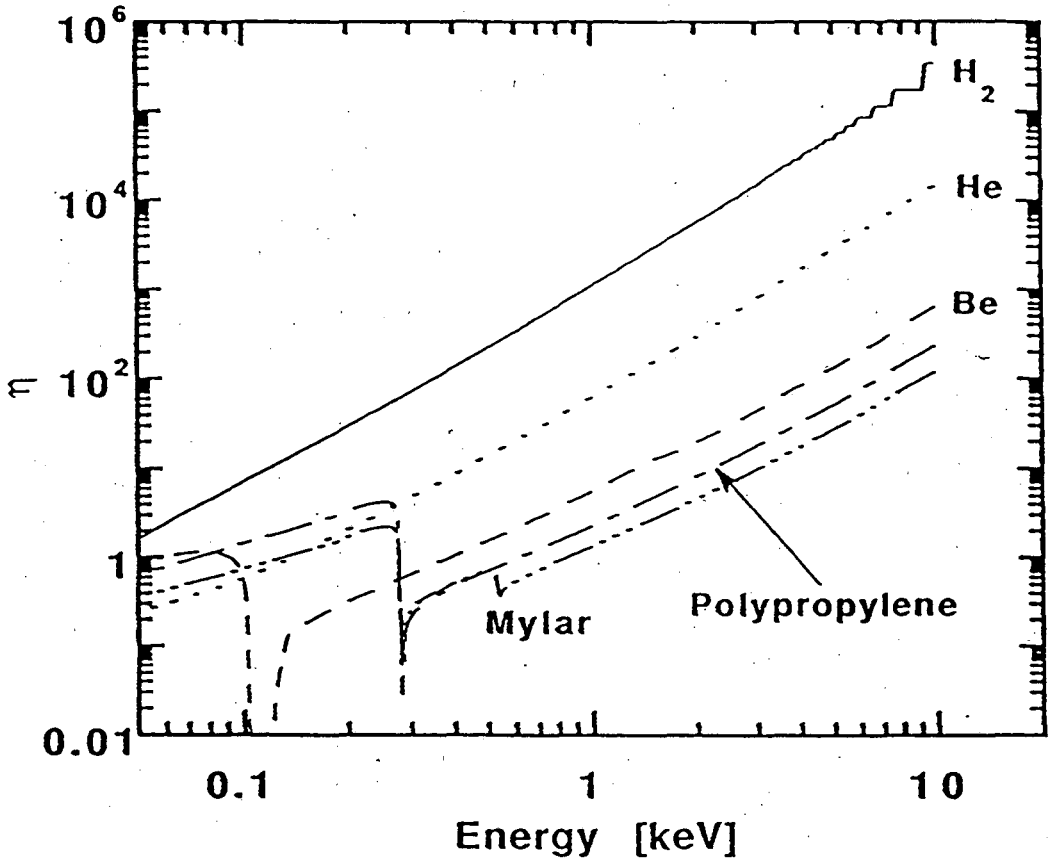

Fig. 3 Calculated phase change η introduced to x-rays when they travel through a slab of material of thickness equal to the amplitude linear absorption length of the material. Calculated results for several low-Z materials are presented here.

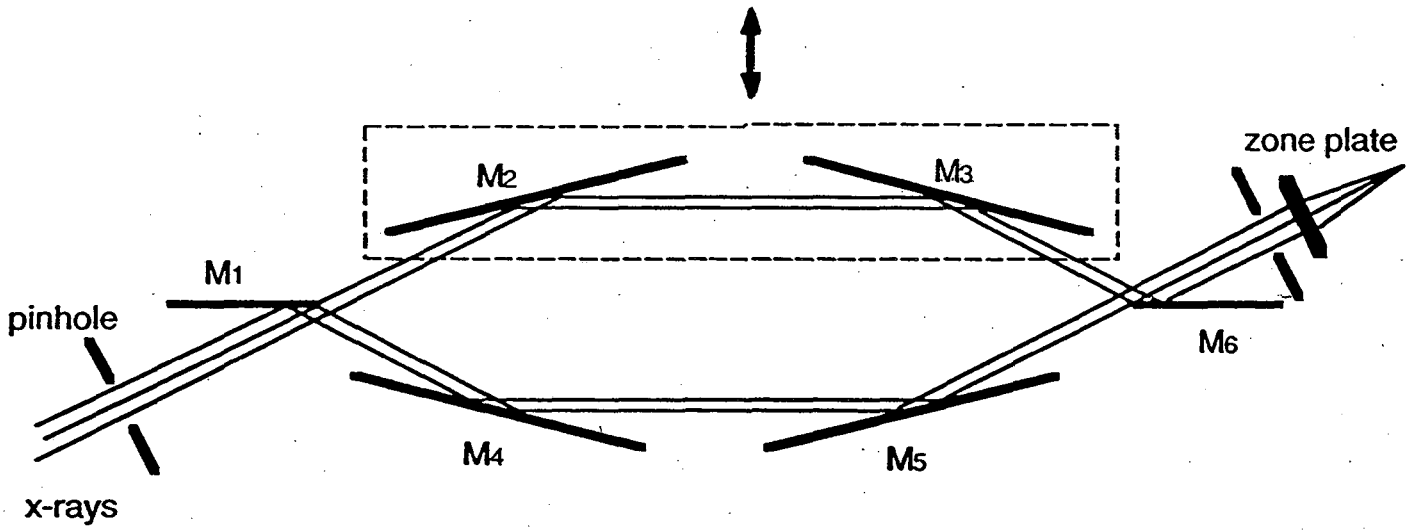

Fig. 1 Schmatic diagram of a wavefront-division Fourier transform x-ray interferometer. A spatially coherent x-ray beam is incident on and physically split into two beams at mirror M_1. Each of the two beams is reflected by a two-mirror optics. When the six mirrors are properly arranged and aligned, the two beams combine into one after the mirror M6. A variable phase delay of one beam relative to the other can be introduced by moving one of the mirror sets along the direction normal to the beamsplitter. While the spatial coherence of either beam is reserved, the two beams are recombined after a linear zone plate and the resultant power of the interference of the two beams is recorded as a function of the phase delay

LAWRENCE BERKELEY LABORATORY
UNIVERSITY OF CALIFORNIA
TECHNICAL INFORMATION DEPARTMENT
BERKELEY, CALIFORNIA 94720